

We thank the reviewer for the careful reading of the manuscript and the insightful comments. Please find below our point-by-point replies:

General comments:

GC1. I have multiple concerns on how the model is described within this manuscript. Very little general information on the TM5 model is provided, except for a long list of citations. For a non TM5 community member it is impossible to understand the key features of this model without opening another publication. A general description of the model needs to be provided, especially since many discrepancies in the model comparison are attributed to transport processes. A summary on how transport processes are simulated needs to be added. An additional evaluation of these transport processes would be useful to justify the later claims.

- Indeed, our point is not to present the whole model, nor to reevaluate each part of it. This has been already presented in detail in numerous publications. Instead, our focus here is to present the new chemistry developments as stated in Sect.1. The model and specifically the transport of TM5 has been successfully evaluated in the past, e.g., see (Koffi et al., 2016; Krol et al., 2005; Peters et al., 2004; Williams et al., 2017). For this, we provide references for each major release of the model that can guide the reader for further reading. Following the reviewer's comment, however, a statement on the reference of the transport processes in TM5 is added in Model Description (Sect. 2.1): *"The advection scheme used in TM5 is based on the slopes scheme (Russell and Lerner, 1981) and the deep and shallow cumulus convection scheme is parameterized according to Tiedtke (1989). The performance of the transport in the model has been evaluated by (Peters et al., 2004) using sulphur hexafluoride simulations and by analyzing the vertical and horizontal distribution of radon (^{222}Rn) to simulate the boundary layer dynamics (Koffi et al., 2016; Williams et al., 2017). More recently, global transport features, such as the transport times associated with inter-hemispheric transport, vertical mixing in the troposphere, transport to and in the stratosphere, and transport of air masses between land and ocean, were evaluated via an inter-comparison of six global transport models (Krol et al., 2018)."*

GC2. Additionally, some information that should be included in the model description can be found in later sections (e.g. how the tropopause altitude is calculated between the different simulations). The manuscript should be harmonised such that all this information is included in the model description.

- All information related to model description has been moved to the model description as suggested by the reviewer in the specific and technical comments (please see also our replies to respective comments).

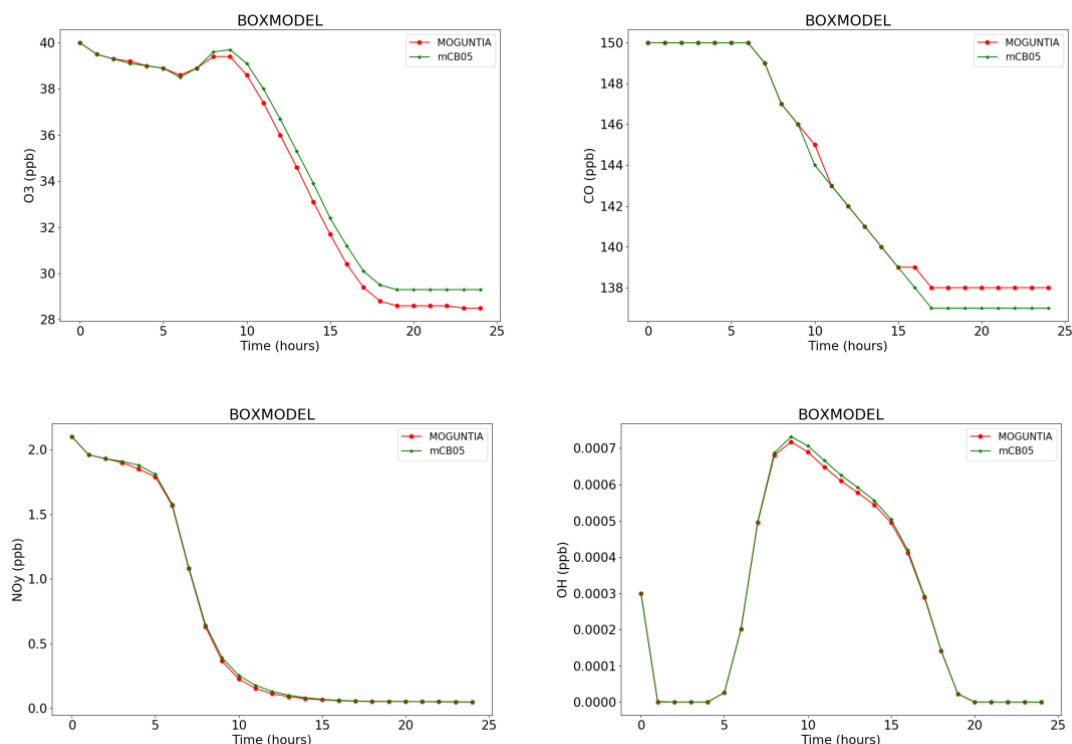
GC3. Within this study, two different chemical mechanisms are used but the manuscript only includes information on the newly developed one. A short description on the "standard" TM5 mechanism should be included and a list of all reactions of this mechanism needs to be added to the supplemental material. A box model comparison of all mechanisms (i.e. MOGUNTIA, CB05 and MCM) would be useful to understand the mechanistic differences.

- CB05 is a well-established mechanism that already presented in numerous publications. Specifically, the modified version of the CB05 mechanism used in the standard configuration of the model (i.e., mCB05) is already described in several publications of the TM5 community, such as the publications by (Williams et al., 2013, 2017); the full table of reactions is freely available for the reader, i.e., see Table A1 and A2 there, <https://www.atmos-chem-phys.net/13/2857/2013/>. For this, we believe that it is needless to repeat here the same tables. However, to make it more clear we now state that for the mechanism we refer to *"Williams et al. (2013), along with updates presented in Williams et al. (2017)."*

- We present below an example of the box model comparison for O₃, CO, NO_y (=NO+NO₂+NO₃+2*N₂O₅+HNO₄) and OH, between the mCB05 and MOGUNTIA mechanisms, using the KPP files from the TM5-MP model of this study. Note that, to our knowledge, MCM does not exist in a KPP format (e.g., see Sommariva et al., 2020), and our comparison is therefore limited to the comparison of mCB05 and MOGUNTIA.
 - Initial conditions:
 - O₃: 40 ppb
 - HO₂: 1ppb
 - H₂O₂: 1 ppb
 - OH: 0.003 ppb
 - NO: 0.6 ppb
 - NO₂: 1.5 ppb
 - NO₃: 9x10⁻⁷
 - N₂O₅: 4x10⁻⁹ ppb
 - HCHO: 0.5 ppb
 - CH₃O₂: 0.025 ppb
 - CH₃O₂H: 5 ppb
 - CH₄: 1700 ppb
 - CO: 150 ppb
 - HCOOH: 0.1 ppb
 - ISOPRENE: 0.1 ppb
 - Temperature: 298.15 K
 - Pressure: 1023 hPa
 - Relative humidity: 45%
 - Emissions: None
 - Deposition: None
 - Photolysis rates; represent equator, noontime, in s⁻¹ based on (Lim et al., 2005) box modelling study. Note that a prescribed diurnal cycle of radiation is applied.
 - JO₃ = 1.36E-5
 - JNO₂ = 4.65E-3
 - JH₂O₂ = 7.65E-6
 - JNO_{3a} = 1.10E-1
 - JNO_{3b} = 1.30E-1
 - JHONO = 3.05E-3
 - JHNO₃ = 2.69E-7
 - JHNO₄ = JHNO₃
 - JN₂O₅ = 2.54E-5
 - JCH₂O_a = 2.54E-5
 - JCH₂O_b = 1.31E-5
 - JCH₃O₂H = 3.63E-6
 - JPAN = 1.47E-6
 - JORGNTR = 1.47E-6
 - JALD = 6.71E-6
 - JGLY_a = 6.82E-5
 - JGLY_b = 7.08E-5
 - JGLYAL = 1.30E-5
 - JMGLY = 2.02E-4
 - JACETONE = 1.40E-6

For all organic hydroperoxides the photolysis rate of CH₃O₂H is used.

For all organic nitrates, the photolysis rates of the lumped species (ORGNTR) is used



Although we studied both mechanisms in detail in box models to understand the differences, we feel that a box-model addition to the paper would be of limited value. Reasons are the heterogeneous conditions that are encountered in the atmosphere in terms of emissions, radiation, and temperature.

GC4. Within the text, it becomes evident that different emission data sets are used for the different mechanisms. However, this information is not at all included in Section 2.4. The emissions for the standard mechanism need to be provided (e.g. table in the supplementary material).

- We could not find evidence for this in the text. Both mechanisms use the same emission data sets and boundary conditions (see Sect. 2). This choice is made in order to specifically focus only on the differences between the two mechanisms in the model as explicitly presented in Sect. 3. The only difference is on how the two mechanisms distribute the VOC emissions to the species considered in the mechanisms: the more lumped mCB05 does not resolve all of the NMVOCs provided by the emission datasets, whereas MOGUNTIA explicitly simulates the NMVOCs (C1-3) and isoprene. To make this point clearer, however, we changed the word “speciation” with “*representation*” when we refer here to the differences between the two chemical schemes (see also our reply to SC17) and we now clearly state in the manuscript that both mechanisms use the same emission datasets.

GC5. Scientifically, many claims on what causes the differences between the model and the observations are not supported by the provided data and not enough evidence is given. In one particular case, too low upward transport is given as a reason and one page afterwards it is claimed that the model simulates a too high transport in the same region. The manuscript therefore needs to be checked if the claims are supported by the results. If so, more justification must be provided (e.g. presenting differences in O₃ precursors). Otherwise these statements should be removed.

- We thank the reviewer for attracting our attention to this issue. Particularly, we removed the sentence: “The negative model bias in the tropical UTLS points at a weak convective uplift in tropical Africa in April.” from the discussion of ozone comparison with the

MOZAIC data. The discussion of both the O₃ and CO evaluation with the MOZAIC observations is now rewritten in the manuscript (see our reply in SC35).

GC6. All in all, the model tends to underestimate VOCs, which is mainly attributed to too low emission sources. Higher emission strengths of VOCs will lead to higher VOC concentrations in low-NO_x regime, influencing the O₃ production. I therefore strongly suggest to perform a sensitivity simulation with up-scaled emission sources to investigate the impact on O₃ and HO_x.

- Indeed, the model tends to underestimate the C₂H₆ and C₃H₈ atmospheric mixing ratios in most of the cases. For C₂H₄ and C₃H₆, however, the model presents mixed results depending on the location of the climatological data as already mentioned by other modelling studies (e.g., Huijnen et al., 2010).

Recently, Dalsøren et al. (2018) showed that an increase of natural (geologic) and anthropogenic fossil fuel emissions by a factor of two to three (compared to current inventories), may significantly improve the simulated C₂H₆ and C₃H₈ mixing ratios compared to observations. Additionally, applying enhanced ethane and propane emissions results in an increase of the simulated surface ozone concentrations by 5-13%, particularly in polluted regions. Since our paper is already lengthy, we prefer to refer to that study instead of performing additional sensitivity simulations.

GC7. Another major concern I have is the overuse of citations when referring to earlier work. A good example is page 4 line 17-20: This sentence has 12 citations but only 18 words with providing no important information about the model at all. It feels as if every paper that used the model is cited here (without evidence why this is necessary), which should not be the goal of the model description. It should be sufficient to cite e.g. Huijnen et al., 2010 since they focus on the chemical modelling in TM5. The same holds when referring to earlier studies using parts of the mechanism (e.g. page 6 line 6-7, page 6 line 32, page 7 line 3-4), especially if they are not further used in the manuscript. It would be scientifically more profound to only cite publications, in which the approach was novel or were it was used first and not every publication using this part of the mechanism or model development. I therefore strongly advise you to recheck every citation in the manuscript and limit citations to a minimum.

- We present the main (not all) publications that show how the model evolved over time, which we believe can be very useful for a reader who wants to understand each step of the model development, offering also a source for further reading. Also, this is common practice in model description papers (e.g., in GMD) that provide the reader the opportunity to search in-depth the literature for more information about the model.

GC8. Last but not least, when reading the manuscript, it does not feel like a coherent story and each section feels like an isolated section. Additionally, the manuscript suffers from grammatical mistakes. I therefore suggest sweeping through the document focusing on simpler sentence structures.

- Strong structural changes and grammatical corrections will be provided in the revised manuscript.

Specific Comments:

- SC1.** Page 1, Line 31-33: Not much information is given about other global models in your manuscript. Therefore, you should only focus this statement on TM5.
- We agree with the reviewer. This part now reads as: “Overall, the MOGUNTIA scheme simulates a large suite of oxygenated VOCs that are observed in the atmosphere at significant levels. This significantly expands the possible applications of TM5-MP”
- SC2.** Page 4, Line 28-29: What influence does this approach have on the stratospheric-tropospheric exchange in your budget analysis?
- TM5-MP is a chemistry-transport model that focusses on the troposphere and no explicit stratospheric chemistry is considered. The stratospheric O₃ concentrations are nudged to ozone datasets to ensure realistic stratospheric O₃ overhead concentrations and thus a realistic chemical tropopause level (i.e., 150 ppb O₃ mixing ratio) for the budget analysis. A free running simulation without nudging stratospheric conditions of O₃ (as well as for HNO₃, CH₄) would lead to great discrepancies in tropospheric mixing ratios due to the omission of explicit stratospheric chemistry that is a source of O₃ (and HNO₃ and a sink of CH₄). Also, the chemical tropopause level used for the budget analysis would significantly change.
- SC3.** Page 5, Line 4-5: When using 150 ppb as definition, the tropopause altitude will differ when using different chemical mechanisms or integrators. Do you use the same tropopause altitude for each simulation? And if so, on which simulation is this definition based? Is the tropopause altitude calculated for each time step or is it based on mean data? What impact do you expect from this?
- As a reference for this study we use the monthly mean O₃ concentrations from the mCB05-EBI configuration of the model, since the EBI configuration of the model has been already published multiple times in the literature. As stated in the manuscript, the differences of O₃ mixing ratios close to the chemical tropopause considered for this study are, however, negligible, and in all model configurations the same tropopause height is calculated. This is, we believe, due to the strong influence of nudging at these altitudes.
- SC4.** Page 5, Line 7: The only O₃ chemical aqueous-phase sink considered here is SO₂. However, the major aqueous-phase sink of O₃ is the reaction with O₂⁻ (Liang and Jacob, 1997). By not taking this sink into account, what impact do you expect this has on the O₃ budget and the O₃ burden in your analysis?
- We do not expect significant differences on a global scale. Even though aqueous phase chemistry may impact the oxidative capacity of the troposphere, this is expected to be minor compared to gas-phase sinks. Liang and Jacob (1997) clearly indicated that including aqueous phase HO_x chemistry in regional and global models of tropospheric O₃, is less than 3%. In contrast, hydrolysis of NO₃ and N₂O₅ on aerosols and clouds that is included in our model is, indirectly, far more important for the O₃ budget. Note also the relatively low Henry constant of O₃ (e.g., $\sim 1 \times 10^{-4}$ mol/m³/Pa @ 273.15 K; see Sander, 2015) For clarity, we note that when a detailed aqueous-phase chemistry scheme (unpublished results; work in progress) is considered in our model, a global O₃ sink on clouds is roughly 20 Tg/yr, thus very low compared to the gas-phase sinks.
- SC5.** Page 7, Line 13-15: Due to the citation style used, it is not at all obvious in which publication each of the advances have been published.
- The citation style we use is the recommended by the GMD journal. Moreover, the reference(s) for each reaction are also presented in detail in Tables 1 and 2 as clearly stated in the manuscript.

- SC6.** Page 7, Line 26: How are meteorological conditions simulated in TM5? This needs to be discussed in the general description of the model (Section 2.1).
- TM5-MP is an offline CTM that reads the meteorological data from the ERA-Interim database. By default, offline CTMs do not simulate meteorology but are driven by meteorological fields. In Sect. 3 we clearly state that TM5-MP is driven by meteorological fields from the ECMWF ERA-Interim reanalysis (Dee et al., 2011) with an update frequency of 3 hours. For clarity we included this description in Sect. 2.1 where we now clearly state that TM5MP is an “*offline*” CTM.
- SC7.** Page 8, Line 23-26: This information is useful to understand why KPP was implemented into TM5. I would suggest you mention this first (i.e. page 8 line 8 and in the introduction).
- We agree with the referee. This information has been moved to the beginning of Sect. 2.3 and the introduction.
- SC8.** Page 10, Line 12: What complexity has the chemical mechanism used for mCB05? Provide more information about this mechanism.
- mCB05 is a chemistry scheme which is based on the structural lumping of atmospheric species. CB05 has already been published in numerous papers in the literature (e.g., Flemming et al., 2015; Houweling et al., 1998; Luecken et al., 2008; Yarwood et al., 2005; Zaveri and Peters, 1999) and the specific implementation of this chemistry scheme in the TM5-MP mode has been recently published by Williams et al. (2017). We have a separate paragraph in the introduction focusing specifically on this mechanism in Sect. 1.
- SC9.** Page 11, Line 1-15: How is this model performance analysis performed (e.g. which software)? What are the expected limitations?
- The model performance calculations are based on the timings of each procedure in the model. There is no specific software for this, but the analysis is based on the on-line calculations of the time spent per procedure as the model runs (see Table S3). The limitations for the model performance may, however, depend on the hardware.
- SC10.** Page 11, Line 2-4: This information should be included in Section 2.5.
- This part is now moved to Sect. 2.5.
- SC11.** Page 11, Line 8-9: The transport of tracers seems to be important for the model performance. How is it decided which tracer is transported and which not? This should be discussed in the model/mechanism description.
- The transport of a tracer in the model domain is mainly dependent on its lifetime relative to the applied timestep of the transport. In TM5-MP, as in most offline CTMs, all species are considered as transported except for the radicals due to their extremely short lifetime. This has already been discussed in previous publications of the model, such as by Huijnen et al. (2010) and references therein.
- SC12.** Page 12, Line 7-9: This is not clear. Why is the chemical destruction higher due to changes in the O₃ precursors?
- We thank the reviewer for attracting our attention to this. Indeed, we think that, given the differences in the chemical scheme, chemical destruction is rather similar. Moreover, switching from EBI to the KPP-based solver has a larger influence. So, we propose: “*Chemical destruction in the troposphere is similar in the MOGUNTIA and mCB05(KPP) chemistry configurations.*”
- SC13.** Page 12, Line 8-9: How do the changes in the O₃ precursors look like? This is a nice example where a statement is given without providing any results or argument why this must be the case (see general comments).

- This remark links to the previous one (i.e., SC12). In the manuscript we present the changes due to the different model configurations for NO_x, OH and CO, which play an important role in the O₃ budget. However, ozone formation and destruction are non-linear processes that critically depend on the NO_x/VOC ratio. A complete analysis of the ozone budget is, however, beyond the scope of this manuscript. Following the reviewer recommendation, we now provide in the Supplement the changes of the organic nitrates (ORGNTR) concentrations that represent an important pool of NO_x in the model (see also our reply in SC27).

SC14. Page 12, Line 12: Why is it necessary to used NO_y mass fixing when using EBI? This needs to be discussed in the model description since this is a major difference between EBI and KPP!

- The NO_y mass fixing in case of intense NO_x photochemistry, is applied due to the approach of the EBI solver. To save computational resources, EBI employs a fixed time step with a restricted number of iterations. In some grid boxes this approach leads to incomplete convergence. This is not, however, a major difference between EBI and KPP, but a way not to miscalculate the N-budget when EBI is used. For the KPP configurations this is not needed, since the KPP-based solver (Rosenbrock) uses a variable sub-time step which ensures absolute mass conservation of N. These numerical issues are, of course, a major reason to investigate the implementation of KPP-based solvers.

SC15. Page 12, Line 19: This is unclear. By referring to table 3 it implies that different emission datasets are used for the different simulations. If so, why is that the case? This needs to be elaborated in Section 2.4.

- We thank the reviewer for pointing this out. Indeed, this is a typo and Table 3 should be “Table 4”.

SC16. Page 13, Line 4: With the 150 ppb definition your simulation are already up to 15% higher. How does your model compare to Lamarque et al. (2012) when using 100 ppb as tropopause definition? It would be best to provide both budgets (i.e. in Table 4) for the 100 and 150 ppb definition to allow a fair comparison.

- The relative difference when accounting for the 100 ppb O₃ tropopause definition is added in the respective Tables within parenthesis.

Table 1. Tropospheric budgets of O₃ for the year 2006 in Tg(O₃) yr⁻¹ and burden in Tg(O₃), using the 150 ppb O₃ mixing ratio to define tropopause level. In parenthesis the relative differences using the 100 ppb O₃ mixing ratios are also presented, calculated by reference to the 150 ppb O₃ definition of tropopause level.

Production terms	mCB05 (EBI)		mCB05 (KPP)		MOGUNTIA		Loss terms	mCB05 (EBI)		mCB05 (KPP)		MOGUNTIA	
Stratospheric inflow*	632	(10%)	429	(32%)	424	(30%)	Deposition	955	(0%)	932	(0%)	913	(0%)
Trop. chem. production	5589	(-3%)	5719	(-3%)	5709	(-3%)	Trop. chem. loss	5192	(-1%)	5216	(-1%)	5219	(-1%)
Trop. burden	385	(-8%)	384	(-8%)	375	(-8%)	Trop. lifetime (days)	22.8	(-8%)	22.8	(-8%)	22.3	(-6%)

*sum of the deposition and the tropospheric chemical loss minus the production

Table 2. Tropospheric chemical budget of OH for the year 2006 in Tg(OH) yr⁻¹, using the 150 ppb O₃ mixing ratio to define tropopause level. In parenthesis the relative differences using the 100 ppb O₃ mixing ratios are also presented, calculated by reference to the 150 ppb O₃ definition of tropopause level.

Production terms	mCB05 (EBI)		mCB05 (KPP)		MOGUNTIA		Loss terms	mCB05 (EBI)		mCB05 (KPP)		MOGUNTIA	
O(¹ D) + H ₂ O	1960	(0%)	1953	(0%)	1878	(0%)	OH + CO	1665	(-2%)	1671	(-2%)	1775	(-2%)
NO + HO ₂	1268	(-4%)	1312	(-4%)	1426	(-4%)	OH + CH ₄	613	(0%)	626	(0%)	644	(-1%)
O ₃ + HO ₂	560	(-1%)	566	(-1%)	561	(-1%)	OH + O ₃	254	(-2%)	260	(-2%)	262	(-3%)
H ₂ O ₂ + <i>hν</i>	262	(-1%)	265	(-1%)	303	(-1%)	OH + ISOP	114	(-1%)	115	(-1%)	120	(0%)
Other	203	(-2%)	201	(-2%)	120	(-1%)	Other	1606	(-1%)	1626	(-1%)	1487	(-1%)

Table 3. Global budgets of CO for the year 2006 in Tg(CO) yr⁻¹ and burden in Tg(CO), using the 150 ppb O₃ mixing ratio to define tropopause level. In parenthesis the relative differences using the 100 ppb O₃ mixing ratios are also presented, calculated by reference to the 150 ppb O₃ definition of tropopause level.

Production terms	mCB05 (EBI)		mCB05 (KPP)		MOGUNTIA		Loss terms	mCB05 (EBI)		mCB05 (KPP)		MOGUNTIA	
Emissions	1097	(0%)	1097	(0%)	1097	(0%)	Deposition	98	(0%)	97	(0%)	99	(0%)
Trop. chem. production	1809	(-1%)	1818	(-1%)	1992	(-1%)	Trop. chem. loss	2840	(-6%)	2849	(-6%)	2924	(-2%)
Strat. chem. production	26	(69%)	26	(73%)	26	(65%)	Strat. chem. loss	87	(68%)	89	(69%)	90	(68%)
Atmos. burden	370	(0%)	360	(0%)	361	(0%)	Lifetime (days)	47.5	(2%)	46.2	(2%)	43.6	(3%)

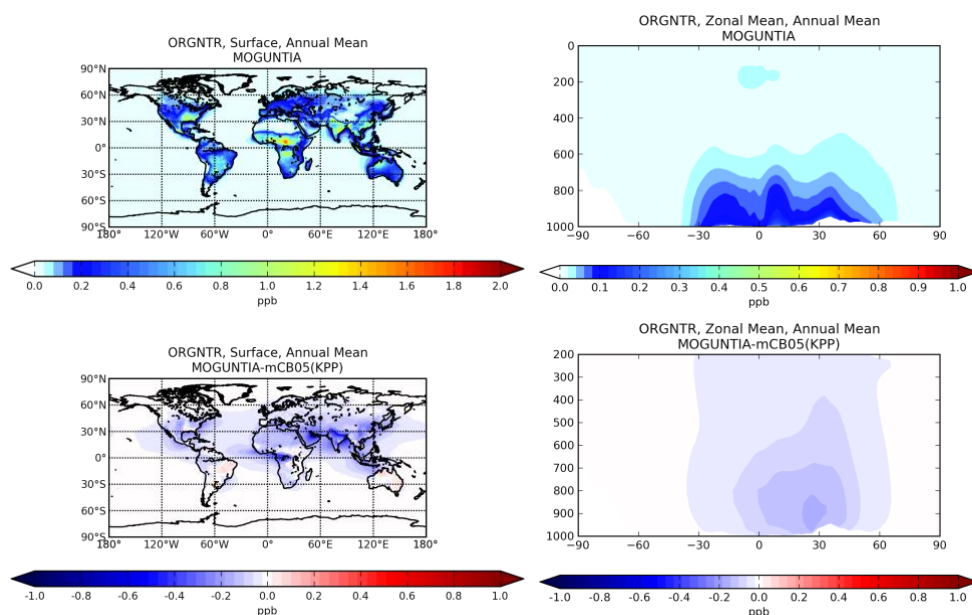
SC17. Page 13, Line 13: It is not at all clear in Section 2.4 that different emissions are used. What is the impact of using different emissions?

- As clarified above we use the same emission datasets for the different chemistry configurations of the model. We here refer to the different “speciation” of the emitted species due to the required lumping, i.e., how the same VOC emissions are represented in each mechanism. To avoid confusion, we changed the word “speciation” to “representation”.

SC18. Page 13, Line 30-31: This is a good argument for the model description to justify why this approach is used.

- We agree with the reviewer. We moved this part to *Sect. 2.1*.

- SC19.** Page 14, Line 4: The contribution of the “other reactions” changes from about 200 to 120 Tg/yr. What causes these changes and what is included in this category?
- This category includes the rest of the reactions in the chemical scheme. However, due to the different representation of the VOC species in mCB05 and MOGUNTIA, there is not one way to exactly match the VOC oxidation reactions, and for this reason they are added in the same pool. More details are explicitly presented in Tables 1 and 2.
- SC20.** Page 14, Line 9-10: This should be mentioned in the model description.
- We moved this part to *Sect. 2.1*.
- SC21.** Page 14, Line 12: Which tropopause definition did van Noije et al. (2014) use?
- “150 ppb O₃ level for the tropopause definition” is added in the text.
- SC22.** Page 14, Line 27: The difference is about 15%, so using “somewhat shorter” is a slight underestimation.
- “somewhat shorter” is changed to “*roughly 15% shorter*”
- SC23.** Page 14, Line 34: What lifetime do you get when using 100 ppb as tropopause definition?
- The lifetime of CH₄ changes only marginally (i.e., from 7.18 yr to 7.22 yr). This is, however, expected due to the relative low differences (i.e., -1%) of tropospheric CH₄ oxidation by OH radicals (see the new Table 5).
- SC24.** Page 15, Line 9: To what else can these differences be attributed to?
- Differences can be also attributed to differences in the general model set-up, the chemistry scheme used, the meteorology, etc.
- SC25.** Page 17, Line 18-19: This is a bit confusing. The dataset used to compare 2006 is published in 2000? What are the limitations of this comparison when using different years?
- Aircraft observations are used as climatological data, as we clearly stated in the manuscript. Some small differences are of course expected due to annual variation of emission and local meteorology changes. However, since no large differences are expected, these observations can be safely used to determine the state of model simulations.
- SC26.** Page 18, Line 21-22: Due to the lack of specific details on mCB05 in the manuscript, it is impossible to identify why this must be the case. More details are necessary here.
- The mCB05 mechanism is well documented and we deem it not necessary to repeat the tables in the manuscript (see also our reply to SC8). Moreover, the two mechanisms are presented in detail online on Zenodo. In general, the more explicit a chemical scheme, the more formation pathways are considered.
- SC27.** Page 18, Line 24: Provide more details on how NO_x reservoir species differ in their concentration and spatial distribution between both mechanisms.
- The simulated annual mean surface and zonal mean organic nitrates mixing ratios for the MOGUNTIA chemistry scheme for the year 2006 and the respective differences compared to mCB05(KPP) are now added in the Sup. Material:
“Simulated annual mean surface (left columns) and zonal mean (right columns) mixing ratios (ppb) of organic nitrates (ORGNTR) for the MOGUNTIA chemistry scheme for the year 2006 (a,b), and the respective differences compared to mCB05(KPP) (c,d).”



where, for the MOGUNTIA configuration ORGNTR represents the sum of CH_3ONO_2 , $\text{C}_2\text{H}_5\text{ONO}_2$, $\text{OHCH}_2\text{CH}_2\text{ONO}_2$, $\text{CH}_3\text{CH}_2\text{CH}_2\text{ONO}_2$, $\text{CH}_3\text{CH}(\text{ONO}_2)\text{CH}_3$, $\text{CH}_3\text{CH}_2\text{CH}(\text{ONO}_2)\text{CH}_3$, nitrates from isoprene (ISOPNO_3), nitrates from methyl-ethyl ketone (MEKNO_3), nitrates from methyl vinyl ketone (MVKNO_3) and nitrates from methacrolein (MACRNO_3).

Table S4. Tropospheric chemical budget of ORGNTR for the year 2006 in $\text{Tg}(\text{N}) \text{ yr}^{-1}$, using the 150 ppb O_3 mixing ratio to define tropopause level. Tropospheric burdens in $\text{Gg}(\text{N}) \text{ yr}^{-1}$.

Production terms	mCB05 (EBI)	mCB05 (KPP)	MOGUNTIA*	Loss terms	mCB05 (EBI)	mCB05 (KPP)	MOGUNTIA*
$\text{XO}_2\text{N}/\text{RO}_2 + \text{NO}$	8.586	8.122	7.030	ORGNTR + hv	4.077	4.037	2.621
$\text{RH} + \text{NO}_3$	4.336	4.190	6.732	ORGNTR + OH	1.315	1.377	5.848
Tropospheric Burden	159.579	159.822	63.054	Deposition	7.424	7.627	5.132

*For the MOGUNTIA configuration ORGNTR represents the sum of CH_3ONO_2 , $\text{C}_2\text{H}_5\text{ONO}_2$, $\text{OHCH}_2\text{CH}_2\text{ONO}_2$, $\text{CH}_3\text{CH}_2\text{CH}_2\text{ONO}_2$, $\text{CH}_3\text{CH}(\text{ONO}_2)\text{CH}_3$, $\text{CH}_3\text{CH}_2\text{CH}(\text{ONO}_2)\text{CH}_3$, nitrates from isoprene (ISOPNO_3), nitrates from methyl-ethyl ketone (MEKNO_3), nitrates from methyl vinyl ketone (MVKNO_3) and nitrates from methacrolein (MACRNO_3)

This part now reads as: “Overall, since deep convection may efficiently transport ORGNTRs to the upper troposphere, the more explicit representation of VOC chemistry in the MOGUNTIA chemistry scheme alters the distribution of ORGNTR compared to the more lumped chemistry of mCB05. Although production of ORGNTR is about 10% larger in the MOGUNTIA scheme, the ORGNTR burden is dominated by the loss term (Table S4). Due to the more detailed speciation of the ORGNTR species in the MOGUNTIA scheme, the destruction becomes significantly more efficient compared to the mCB05 configuration. As a result, the global ORGNTR burden calculated using the MOGUNTIA scheme in the model is about 60% smaller”.

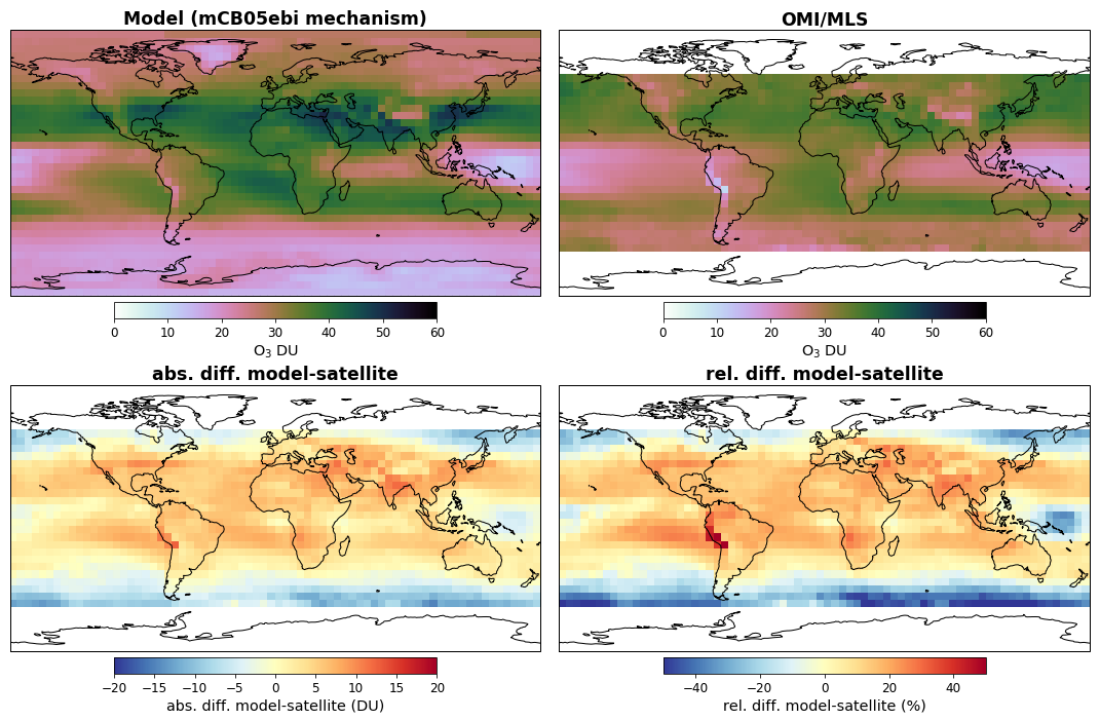
- SC28.** Page 19, Line 2-3: How well does your model compare when using 7.9 Tg-N/yr ?
- The dataset with the 7.9 Tg-N yr^{-1} is not available to us. Increasing the soil emissions to 7.9 Tg-N yr^{-1} will not match the data from field observations.
- SC29.** Page 19, Line 14-17: Provide evidence why this is the case.

- As we stated in our reply in SC27, a more efficient removal of the organic nitrogen is simulated for the MOGUNTIA compared to the mCB05 mechanism. This is due to the more detailed representation of these NO_x reservoir species in the more explicit MOGUNTIA scheme. Organic nitrogen in the MOGUNTIA mechanism includes several species (i.e., CH₃ONO₂, C₂H₅ONO₂, HOCH₂CH₂ONO₂, CH₃CH₂CH₂ONO₂, CH₃CH(ONO₂)CH₃, CH₃CH₂CH(ONO₂)CH₃, nitrates from isoprene (ISOPNO₃), nitrates from methyl-ethyl ketone (MEKNO₃), nitrates from methyl vinyl ketone (MVKNO₃) and nitrates from methacrolein (MACRNO₃)), while in the mCB05 mechanism, all these species are represented by one lumped ORGNTR species. Budget calculations show that although the production of ORGNTR is roughly 10% higher for the MOGUNTIA configurations compared to mCB05, the destruction is significantly more efficient (~56%) in MOGUNTIA. Therefore, the reactivity of the mixture of organic nitrogen species in MOGUNTIA mechanism is higher than that of the lumped species in mCB05 as shown in Table S4, with chemical loss of organic nitrogen by reaction with OH in the MOGUNTIA mechanism which largely compensates for the faster photolysis of these compounds in mCB05. Overall, this results in a lower tropospheric burden of ORGNTR of about 60% for the MOGUNTIA compared to mCB05 configuration. Thus, we conclude that the MOGUNTIA speciation leads to increased destruction of the organic nitrates and consequently to lower mixing ratios at higher altitudes. Concerning the impact of organic NO_x reservoir species on troposphere OH mixing ratios, we note that due to the NO_x release upon the destruction of ORGNTR, O₃ will be formed in remote locations, and thus OH recycling will be stimulated. However, a more detailed analysis would be needed to examine how the ORGNTR destruction affects NO_x, O₃, and finally OH mixing ratios. This would be out of the scope of this paper that is focused on model development. Overall, the developments presented in this work further indicates the benefits of using the MOGUNTIA configuration in the model, since we can have a more accurate representation of ORGNTRs, and can overall predict better their distribution. This part now reads as: *“These relatively small differences in OH mixing ratios are mainly related to the HO_x regeneration, as well as to the differences of NO_x and ORGNTR species that impacts on the distribution of OH in the troposphere. The more detailed representation of ORGNTR in the MOGUNTIA chemistry scheme results in more efficient NO_x release upon the ORGNTR destruction (Table S4), leading overall to O₃ formation in remote locations, and thus to the stimulation of HO_x recycling in higher altitudes.”*

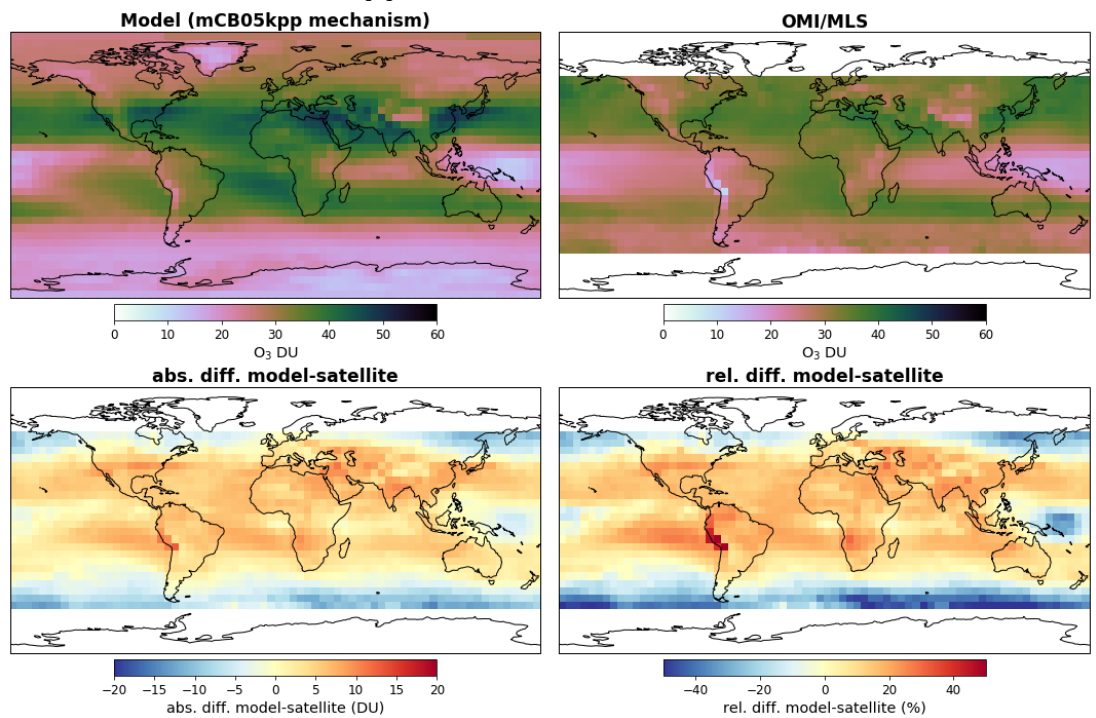
SC30. Page 20, Line 3: What about comparing your model simulations to satellite observations of O₃ (e.g. OMI)?

- For this work we used two extended surface ozone observation databases and one ozonesonde database to evaluate the model and discuss the differences of the different configurations. More extended model evaluation, although always interesting, is not expected to change the conclusions of this work, especially for the simulated tropospheric ozone mixing ratios. As we refer to in the summary (Sect. 6) a more dedicated comparison of the model with the MOGUNTIA configuration with *in-situ* observations and satellite retrievals is planned to be performed in the future. Indeed, we prepare a study with an extended model evaluation with satellite retrievals. As an example of our work in progress, the reviewer can find below an evaluation of tropospheric O₃ columns (for the three configurations of this study) with OMI monthly tropospheric retrievals:

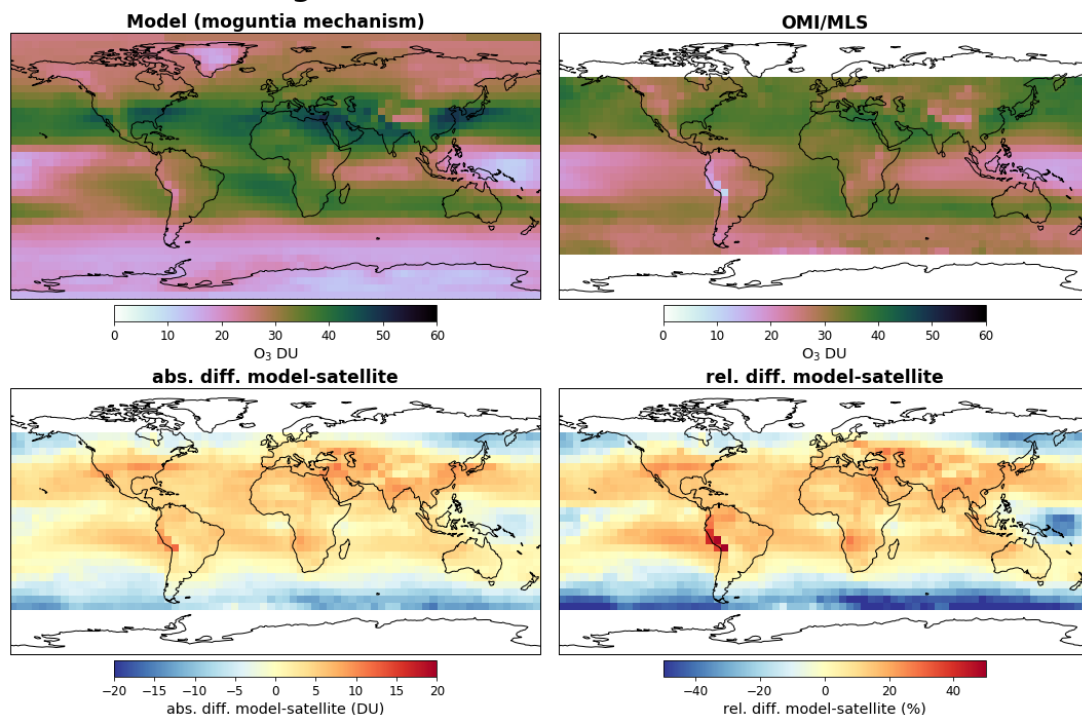
TM5-MP (mCB05ebi mechanism) vs OMI/MLS annual 2006



TM5-MP (mCB05kpp mechanism) vs OMI/MLS annual 2006



TM5-MP (moguntia mechanism) vs OMI/MLS annual 2006



Overall, it is obvious from this evaluation that the MOGUNTIA scheme better simulates the OMI retrievals, thus changing the model in the right direction. Note, again, that we choose not to present this evaluation in this paper, since a separate paper is in progress.

SC31. Line 18-20: The surface ozone bias is lowest for mCB05(KPP) but at the same time the ozone burden is higher than for MOGUNTIA. What causes this difference? Are there significant differences in free tropospheric ozone?

- Indeed, the surface ozone biases are slightly lower for mCB05(KPP). However, this conclusion cannot be straightforwardly applied to the burden differences presented in Table 4, since burdens refer to the whole troposphere, and not only to the surface level. We note also that the ~ 1 ppb difference is relatively small compared to the range of O_3 observations.

SC32. Page 21, Line 10-11: This conclusion is not obvious based on the results you provided. Further analysis is needed here. How well are transport processes modelled in TM5?

- We consider such analysis outside the scope of the current paper. We indicate in the paper that model resolution “*could*” be a reason. Note that the current version of the TM5 model was included in a model intercomparison (Krol et al., 2018), in which vertical resolution were specifically addressed.

SC33. Page 21, Line 15-18: Are these speculations or do you have evidence that this must be the case? If so provide further details.

- As in our answer to SC32, we have no solid proof from the present study, but refer to a previous study that addressed these issues in more detail (Williams et al., 2012). We think this is good practice. However, we agree that the word “can” suggests some form of evidence. Therefore, we changed this to “*could*” in the revised manuscript.

SC34. Page 21, Line 32: This statement is unclear. The current sentence structure implies that the emissions in the SH are lower when using KPP.

- Thanks for pointing this out. This part now reads as: “*Notably, the mCB05(EBI) model configuration tends to produce lower biases in the SH, where the emission strengths*”

are in general low, compared to the other two configurations (i.e., approximately -3 vs. -4 and -5 ppb for mCB05(KPP) and MOGUNTIA, respectively). In contrast, the MOGUNTIA chemistry configuration results in lower biases in the NH where the majority of anthropogenic emissions occur (i.e., approximately -30 vs. -31 and -33 ppb for mCB05(EBI) and mCB05(KPP), respectively)."

SC35. Page 22, Line 21-23: Earlier (i.e. page 21, line 10-11) you state that the convective uplift is too low but now you state that it is too strong. Which is correct? The presented data do not support either. More evidence is needed. I strongly suggest you to perform an elaborated analysis of the performance of TM5 with respect to transport processes, to justify these claims.

- We improved changed this section and added further analyses. Overall, these parts are now read as:
 - *O₃: The model evaluation at pressure levels < 300 hPa indicates there is good agreement of both configuration with the observed mixing ratios. A positive bias in April in the order of ~20 ppb is calculated for the model, but smaller biases are found around the tropics and in the latitudes north of 40°N (Fig. S4a). In October (Fig. 4Sb), a constant positive bias of roughly 20 ppb is calculated for both configurations. This could be caused by the limited vertical resolution of this model version in the UTLS region. Note here that 34 vertical levels were employed for this study with a higher resolution in the upper troposphere–lower stratosphere compared to the low and mid-troposphere region. Part of the model overestimation could also be attributed to systematic errors, as also presented in previous studies (e.g., Huijnen et al., 2010), caused possibly by cumulative effects such as a lack of a diurnal or weekly variation in the NO_x emissions from the road transport sector, an underestimation of surface deposition during summer or even errors in the representation of nocturnal boundary layer dynamics (e.g., Williams et al., 2012), which are common issue in global chemistry transport model.*
 - *CO: Model evaluation at pressure levels < 300 hPa shows a good correlation for both configurations in the SH, with a small positive bias (up to ~20 ppb) for the mCB05(KPP) configuration in April around the equator and a small negative bias (~10 ppb) for the MOGUNTIA configuration for latitudes below 10°N. Both configurations present a strong negative bias (~30 ppb) for latitudes above 20°N (Fig. S4c). In October (Fig. S4d), both the mCB05(KPP) and MOGUNTIA configurations tend to underestimate the observations with a negative bias of ~20 ppb, except for a small positive bias between 0-20°N. This positive model bias in the UTLS could point to a stronger convective uplift in tropical Africa in April or to a possible misrepresentation of biomass burning emissions that are generally uncertain (Nechita-Banda et al., 2018). Indeed, MOZAIC data presents an increase in CO mixing ratios from the NH (April) to the SH (October), owing mainly to the impact of biomass burning processes. Overall, the model configurations of this work present both positive and negative biases compared to the MOZAIC observations, with the observations to exhibit in general larger latitudinal CO variability.*

SC36. Page 22, Line 24-25: Have you analysed biomass burning hotspots to support this claim?

- Analyzing biomass burning hotspots separately would be out of the scope of this work. However, previous studies with the TM5 model show large uncertainties in bottom-up estimates of biomass burning emissions, likely caused by uncertainties in emissions factors (Nechita-Banda et al., 2018). In addition to the biomass burning emission strength and geographic distribution, Daskalakis et al. (2015) have shown the sensitivity

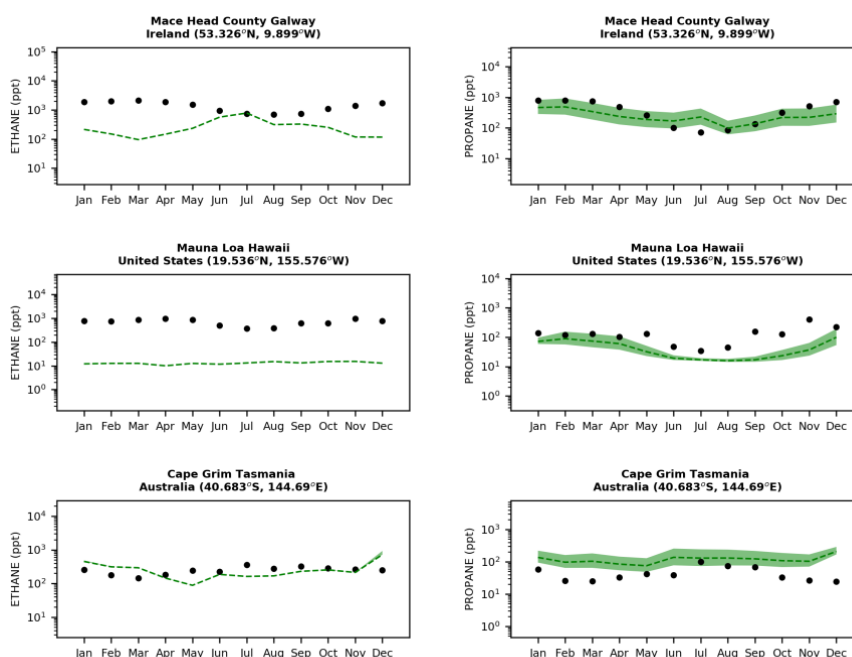
of the model results to the biomass burning emissions injection heights. We added these references to better highlight this uncertainty.

SC37. Page 23, Line 2: What causes the opposite annual cycle? i.e. indicate that C₂H₆ surface mixing ratios are strongly underestimated by all configurations at Mace Head (Fig. 9a) by ~80%, mainly during the winter, indicating also an opposite annual cycle.

- C₂H₆ surface mixing ratios and their seasonal cycle in the model depend on the emission strength and the oxidation by OH radicals. Underestimation of emissions or a faster oxidation could explain the differences between model and observations. We propose to add the following sentence “*This can be attributed to the misinterpretation of seasonal variation of anthropogenic C₂H₆ emission and/or to a winter overestimate of C₂H₆ oxidation by OH radicals in the model.*”

SC38. Page 23, Line 9: Your model underestimates propane but you use a lower emission than other studies. How does your model compare when you use higher emissions?

- The emissions used for this study come from the CMIP6 databases. Indeed, an increase (or decrease) of emissions may help to investigate the response of the model to identify possible biases in the emission databases. To show here how the model responds to an increase of emissions for both ethane and propane, we present bellow a model comparison with flask measurements using 1) the base case emission scenario, 2) doubling (2x) of the anthropogenic fossil fuel emissions of C₂H₆ and C₃H₈, resulting in ~17.1 Tg yr⁻¹ and ~14.9 Tg yr⁻¹, respectively, and 3) quadrupling (4x) of the anthropogenic fossil fuel emissions of C₂H₆ and C₃H₈, resulting in ~29.5 Tg yr⁻¹ and ~27.9 Tg yr⁻¹ respectively. For this sensitivity study, we run the model in 3° x 2° horizontal resolution in longitude by latitude, and 34 hybrid levels in the vertical, which is much cheaper compared to 1x1 horizontal resolution used in the paper. Note that our approach is based on the recent study by Dalsøren et al. (2018) (see also our reply in GC6), showing that an increase of natural (geologic) and anthropogenic fossil fuel emissions by two to three times may improve the simulated C₂H₆ and C₃H₈ mixing ratios compared to observations.



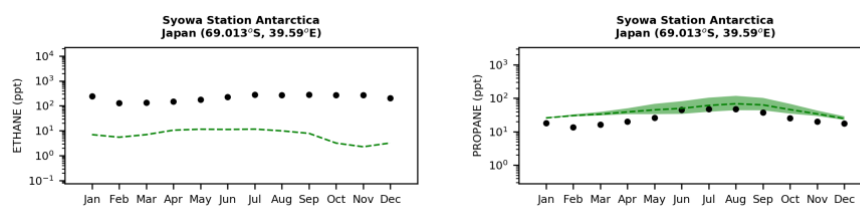


Figure: comparison between TM5 (MOGUNTIA scheme) simulations and observations of ethane (left) and propane (right) for 4 stations.

From the figures above, it is obvious that the increase of C_2H_6 anthropogenic emissions by two or four times does not significantly increase the simulated mixing ratios (please mind here the log scale in the y-axis). This means that (1) even more aggressive increase of emissions (at least over specific regions) is required, (2) other missing sources are needed, or (3) that the oxidation of C_2H_6 is too fast in the model. In contrast, the increase of C_3H_8 emissions by two times tends to improve the model simulations in most of the cases, where an increase by a factor 4 tends to overestimate the observed mixing ratios. Overall, our results suggest that changes in emissions should not be based on fixing the model to a specific value. Instead, scientifically accepted methods, such as data assimilation, should be used to minimize the difference between observations and the model by emissions optimization. Nevertheless, these sensitivity studies give interesting insights!

We suggest adding the following parts in

i) Sect. 5.5.1:

“Dalsøren et al. (2018) showed recently that an increase of natural and anthropogenic fossil fuel emissions by a factor of two to three may significantly improves the simulated C_2H_6 and C_3H_8 mixing ratios compared to observations. This would result in source estimates close to the 16 Tg yr⁻¹ and 23 Tg yr⁻¹ for C_2H_6 and C_3H_8 respectively, as have been calculated by the first global 2-d modeling study of these two hydrocarbons by Kanakidou et al. (1991). To investigate here how the model responses to an increase of ethane emissions, sensitivity simulations with the MOGUNTIA configuration are here performed by i) doubling and ii) quadrupling the anthropogenic C_2H_6 fossil fuel emissions, resulting overall in total C_2H_6 emissions of ~17.1 Tg yr⁻¹ and ~29.5 Tg yr⁻¹, respectively. The comparison with the with flask data (Fig. S7) indicates that the increase of C_2H_6 anthropogenic emissions does not significantly affect the simulated mixing ratios in the model. Overall, this means that i) even a more aggressive increase of emissions (at least over specific regions) or a different geographic distribution of emission is required, ii) other missing sources are needed to be considered in the model, or iii) the oxidation of C_2H_6 is too fast in the model.”

ii) Sect. 5.5.1:

” Additional simulations for C_3H_8 are performed by i) doubling and ii) quadrupling the anthropogenic fossil fuel emissions, resulting overall in total C_3H_8 emissions of ~14.9 Tg yr⁻¹ and ~27.9 Tg yr⁻¹ respectively. Figure S7 indicates that an increase of C_3H_8 emissions by two times tends to improve the model simulations in most of the cases, whereas an increase by a factor 4 tends to overestimate the observed mixing ratios.”

iii) Sect. 6:

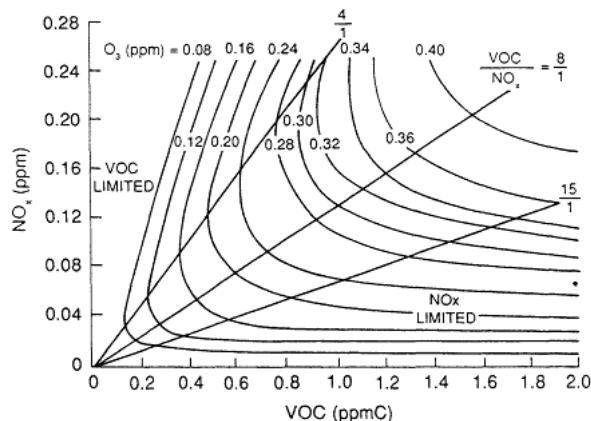
“Sensitivity simulations of this work indicate that increases in emissions may have a significant impact on some light VOC atmospheric concentrations, such as the C_3H_8 . However, our results suggest that changes in emissions should not be based on fixing the model to a specific (constant) value. Instead, scientifically accepted methods should be used.”

- SC39.** Page 24, Line 1-2: Could this underestimation be related to underestimated transport processes (see Page 21 & 22)?
- Some discrepancies in transport could explain part of the model underestimation. However, propane emissions strength or misrepresentation of their horizontal or/and vertical distribution along with a fast propane oxidation by OH radicals seem to be the main reasons for the differences between model and observations.
- SC40.** Page 24, Line 20: What needs to be done to account for the “secondary production from VOC oxidations”?
- We should investigate possible unknown chemical pathways via heavier VOCs oxidation (e.g. in smog chamber studies).
- SC41.** Page 25, Line 30-33: Can you provide some suggestions on how to improve these uncertainties?
- We suggest to add: *“Future studies should aim at improving source estimates and a better understanding of the processes that govern the budgets of the light VOCs. From a chemistry point of view, it would be interesting to study the chemical formation pathways from higher VOCs. Inverse modelling or data-assimilation studies might be used to “optimize” the emissions in order to minimize the differences between observations and model simulations.”*
- SC42.** Page 53, Table 4: What about O₃ scavenging?
- TM5-MP, following a common practice in global chemistry transport models, does not include wet scavenging processes for O₃. Since the washout effects depend on the species’ solubility and considering the low solubility of O₃ (see Sander, 2015), scavenging is not a significant removal process from the atmosphere. This is also supported by observations based on analysis from long-term hourly data (Yoo et al., 2014), where the impact of washout on O₃ was negligible.

Technical corrections:

TC1. Page 2, lines 4-20: A graphical illustration of the NO_x-VOC-O₃ relation would be helpful here.

- A graphical illustration of the NO_x-VOC-O₃ relation is well documented, e.g., see Rethinking the Ozone Problem in Urban and Regional Air Pollution (National Research Council, 1991):



Although such a graphical illustration could be helpful for the reader, this is would be out of the scope of the current work which is focused on model development.

TC2. Page 4, line 22: Check grammar and wording.

- This part now reads as: 'In this new MP version, the two-way zoom capability of TM5 is no longer available.'

TC3. Page 14, line 1-2: Check grammar and wording.

- This part now reads as: 'The MOGUNTIA model configuration yields direct gas-phase OH formation (via O₃ photolysis in the presence of water molecules, Reactions 3 and 4) of 1878 Tg yr⁻¹. Radical recycling terms (Reactions 1 and 5) contribute 1987 Tg yr⁻¹. Finally, the H₂O₂ photodissociation, i.e., $\text{H}_2\text{O}_2 + h\nu \rightarrow 2 \text{OH}$ (7) produces 303 Tg yr⁻¹, and all other reactions add another 120 Tg yr⁻¹ to the global tropospheric OH production in the model.'

TC4. Page 18, line 11-13: Check grammar and wording.

- This part now reads as: "Some discrepancies are nevertheless expected in such a comparison since no seasonal cycle in anthropogenic emissions is considered. Anthropogenic emissions are the major source of NO_x in the Northern Hemisphere (NH)."

TC5. Page 5, line 3: The statement that this study focuses on the troposphere is stated multiple times. Do not use double statements, to improve the reading flow.

- Statement removed.

TC6. Page 6, line 1: This should be Section 2.2.

- Done

TC7. Page 9, line 10-14: Listing all species greatly disturbs the reading flow. I would remove this listing and just refer to Table 3 instead.

- These species refer to the database and not to the model as clearly stated in the beginning of Sect. 2.4. Thus, we cannot just refer to Table 3 since the provided emissions are not the same with the model's species because the required

lumpings/sums have to be performed. This is also stated in the 3rd paragraph of Sect. 2.4, i.e., Overall, the MOGUNTIA chemical scheme considers direct emissions...

- TC8.** Page 10, line 12-28: A table summarizing all simulations performed could be useful.
- We think that such a table is of little added value, as we present only the results of three simulations. that are already presented multiple times in each budget table and each plot. Moreover, a complete description of each simulation (although simple) is provided in each caption.
- TC9.** Page 12, line 22-26: This is a rather complicated sentence. Consider using simpler language (i.e. multiple short sentences).
- This part now reads as:” The calculated net influx from the stratosphere for the MOGUNTIA configuration ($\sim 424 \text{ Tg yr}^{-1}$) remains within one standard deviation of a multi-model mean estimate ($552 \pm 168 \text{ Tg yr}^{-1}$), as reported by Stevenson et al. (2006) and Young et al. (2013). MOGUNTIA calculations are also in line with estimates based on observations (Hsu, 2005; Olsen, 2004) ($\sim 400 \text{ Tg yr}^{-1}$). Our estimates are higher compared to the 306 Tg yr^{-1} calculated in an earlier version of the TM5 model driven by the same meteorological fields (van Noije et al., 2014).”
- TC10.** Page 14, line 26: The word “arrive” should not be used here.
- This part now reads as: “*an atmospheric lifetime of about 7.18 yr is derived*”
- TC11.** Page 17, line 2-19: Presenting the different observations and possible comparisons in a table would be more efficient.
- We prefer to keep the text as is.
- TC12.** Page 17, line 25: In order to improve the reading flow, it would be best to first compare each tracer discussed in Section 4 (in the same order).
- We thank the reviewer for this comment. This is what we intended to do in the presentation of the results. In more detail, in Sect. 4 the budget follows the way the reactions are described (i.e., O_3 , OH and CO). However, for a useful model evaluation of O_3 , CO, and VOCs, we need first a discussion of the modelled NO_x and OH atmospheric mixing ratios.
- TC13.** Page 20, line 25: Is the reference to the introduction correct?
- We thank the referee for pointing out this typo. Sect. 1. changed to *Sect. 3*.
- TC14.** Page 20, line 27: Please be more specific and refer to Section 2.1.
- Done
- TC15.** Page 41-51: Most of the information presented in Tables 1, 2 and even 3 are well documented elsewhere. Thus, I strongly recommend you to move these tables to the supplemental material.
- The information in Tables 1-3 is of course documented elsewhere in the literature since all reactions are based on state-of-the-art databases such as the IUPAC, MCM, but their combination and the assumptions applied for this work are not. Moreover, compared to the previous version of the MOGUNTIA chemistry scheme, numerous updates have been performed. Overall, since the aim of this paper is to present the new coupling of the MOGUNTIA chemistry scheme to the TM5MP CTM, these tables should remain the main text. All other model development papers which are focused to chemistry follow the same procedure.
- TC16.** Supplement, page 3: Table S3 (including caption) cannot be read completely.
- Corrected.

References:

- Dalsøren, S. B., Myhre, G., Hodnebrog, Ø., Myhre, C. L., Stohl, A., Pissò, I., Schwietzke, S., Höglund-Isaksson, L., Helmig, D., Reimann, S., Sauvage, S., Schmidbauer, N., Read, K. A., Carpenter, L. J., Lewis, A. C., Punjabi, S., Wallasch, M., Hodnebrog, O., Myhre, C. L., Stohl, A., Pissò, I., Schwietzke, S., Höglund-Isaksson, L., Helmig, D., Reimann, S., Sauvage, S., Schmidbauer, N., Read, K. A., Carpenter, L. J., Lewis, A. C., Punjabi, S. and Wallasch, M.: Discrepancy between simulated and observed ethane and propane levels explained by underestimated fossil emissions, *Nat. Geosci.*, 11(3), 178–184, doi:10.1038/s41561-018-0073-0, 2018.
- Daskalakis, N., Myriokefalitakis, S. and Kanakidou, M.: Sensitivity of tropospheric loads and lifetimes of short lived pollutants to fire emissions, *Atmos. Chem. Phys.*, 15(6), 3543–3563, doi:10.5194/acp-15-3543-2015, 2015.
- Flemming, J., Huijnen, V., Arteta, J., Bechtold, P., Beljaars, A., Blechschmidt, A.-M., Diamantakis, M., Engelen, R. J., Gaudel, A., Inness, A., Jones, L., Josse, B., Katragkou, E., Marecal, V., Peuch, V.-H., Richter, A., Schultz, M. G., Stein, O. and Tsikerdekis, A.: Tropospheric chemistry in the Integrated Forecasting System of ECMWF, *Geosci. Model Dev.*, 8(4), 975–1003, doi:10.5194/gmd-8-975-2015, 2015.
- Houweling, S., Dentener, F. and Lelieveld, J.: The impact of nonmethane hydrocarbon compounds on tropospheric photochemistry, *J. Geophys. Res. Atmos.*, 103(D9), 10673–10696, doi:10.1029/97JD03582, 1998.
- Hsu, J.: Diagnosing the stratosphere-to-troposphere flux of ozone in a chemistry transport model, *J. Geophys. Res.*, 110(D19), D19305, doi:10.1029/2005JD006045, 2005.
- Huijnen, V., Williams, J., van Weele, M., van Noije, T., Krol, M., Dentener, F., Segers, A., Houweling, S., Peters, W., de Laat, J., Boersma, F., Bergamaschi, P., van Velthoven, P., Le Sager, P., Eskes, H., Alkemade, F., Scheele, R., Nédélec, P. and Pätz, H.-W.: The global chemistry transport model TM5: description and evaluation of the tropospheric chemistry version 3.0, *Geosci. Model Dev.*, 3(2), 445–473, doi:10.5194/gmd-3-445-2010, 2010.
- Kanakidou, M., Singh, H. B., Valentin, K. M. and Crutzen, P. J.: A two-dimensional study of ethane and propane oxidation in the troposphere, *J. Geophys. Res.*, 96(D8), 15395–15413, doi:10.1029/91jd01345, 1991.
- Koffi, E. N., Bergamaschi, P., Karstens, U., Krol, M., Segers, A., Schmidt, M., Levin, I., Vermeulen, A. T., Fisher, R. E., Kazan, V., Klein Baltink, H., Lowry, D., Manca, G., Meijer, H. A. J., Moncrieff, J., Pal, S., Ramonet, M., Scheeren, H. A. and Williams, A. G.: Evaluation of the boundary layer dynamics of the TM5 model over Europe, *Geosci. Model Dev.*, 9(9), 3137–3160, doi:10.5194/gmd-9-3137-2016, 2016.
- Krol, M., Houweling, S., Bregman, B., van den Broek, M., Segers, A., van Velthoven, P., Peters, W., Dentener, F. and Bergamaschi, P.: The two-way nested global chemistry-transport zoom model TM5: algorithm and applications, *Atmos. Chem. Phys.*, 5(2), 417–432, doi:10.5194/acp-5-417-2005, 2005.
- Krol, M., de Bruine, M., Killaars, L., Ouwersloot, H., Pozzer, A., Yin, Y., Chevallier, F., Bousquet, P., Patra, P., Belikov, D., Maksyutov, S., Dhomse, S., Feng, W. and Chipperfield, M. P.: Age of air as a diagnostic for transport timescales in global models, *Geosci. Model Dev.*, 11(8), 3109–3130, doi:10.5194/gmd-11-3109-2018, 2018.
- Liang, J. and Jacob, D. J.: Effect of aqueous phase cloud chemistry on tropospheric ozone, *J. Geophys. Res. Atmos.*, 102(5), 5993–6001, doi:10.1029/96jd02957, 1997.
- Lim, H.-J., Carlton, A. G. and Turpin, B. J.: Isoprene Forms Secondary Organic Aerosol through Cloud Processing: Model Simulations, *Environ. Sci. Technol.*, 39(12), 4441–4446, doi:10.1021/es048039h, 2005.
- Luecken, D. J., Phillips, S., Sarwar, G. and Jang, C.: Effects of using the CB05 vs. SAPRC99 vs. CB4 chemical mechanism on model predictions: Ozone and gas-phase photochemical precursor concentrations, *Atmos. Environ.*, 42(23), 5805–5820, doi:10.1016/j.atmosenv.2007.08.056, 2008.

National Research Council, N. R.: Rethinking the Ozone Problem in Urban and Regional Air Pollution, National Academies Press, Washington, D.C., 1991.

Nechita-Banda, N., Krol, M., van der Werf, G. R., Kaiser, J. W., Pandey, S., Huijnen, V., Clerbaux, C., Coheur, P., Deeter, M. N. and Röckmann, T.: Monitoring emissions from the 2015 Indonesian fires using CO satellite data, *Philos. Trans. R. Soc. B Biol. Sci.*, 373(1760), 20170307, doi:10.1098/rstb.2017.0307, 2018.

van Noije, T. P. C., Le Sager, P., Segers, A. J., van Velthoven, P. F. J., Krol, M. C., Hazeleger, W., Williams, A. G. and Chambers, S. D.: Simulation of tropospheric chemistry and aerosols with the climate model EC-Earth, *Geosci. Model Dev.*, 7(5), 2435–2475, doi:10.5194/gmd-7-2435-2014, 2014.

Olsen, M. A.: Stratosphere-troposphere exchange of mass and ozone, *J. Geophys. Res.*, 109(D24), D24114, doi:10.1029/2004JD005186, 2004.

Peters, W., Krol, M. C., Dlugokencky, E. J., Dentener, F. J., Bergamaschi, P., Dutton, G., Velthoven, P. v., Miller, J. B., Bruhwiler, L. and Tans, P. P.: Toward regional-scale modeling using the two-way nested global model TM5: Characterization of transport using SF 6, *J. Geophys. Res.*, 109(D19), D19314, doi:10.1029/2004JD005020, 2004.

Russell, G. L. and Lerner, J. A.: A New Finite-Differencing Scheme for the Tracer Transport Equation, *J. Appl. Meteorol.*, 20(12), 1483–1498, doi:10.1175/1520-0450(1981)020<1483:ANFDSF>2.0.CO;2, 1981.

Sander, R.: Compilation of Henry's law constants (version 4.0) for water as solvent, *Atmos. Chem. Phys.*, 15(8), 4399–4981, doi:10.5194/acp-15-4399-2015, 2015.

Sommariva, R., Cox, S., Martin, C., Borońska, K., Young, J., Jimack, P. K., Pilling, M. J., Matthaïos, V. N., Nelson, B. S., Newland, M. J., Panagi, M., Bloss, W. J., Monks, P. S. and Rickard, A. R.: AtChem (version 1), an open-source box model for the Master Chemical Mechanism, *Geosci. Model Dev.*, 13(1), 169–183, doi:10.5194/gmd-13-169-2020, 2020.

Stevenson, D. S., Dentener, F. J., Schultz, M. G., Ellingsen, K., van Noije, T. P. C., Wild, O., Zeng, G., Amann, M., Atherton, C. S., Bell, N., Bergmann, D. J., Bey, I., Butler, T., Cofala, J., Collins, W. J., Derwent, R. G., Doherty, R. M., Drevet, J., Eskes, H. J., Fiore, A. M., Gauss, M., Hauglustaine, D. A., Horowitz, L. W., Isaksen, I. S. A., Krol, M. C., Lamarque, J.-F., Lawrence, M. G., Montanaro, V., Müller, J.-F., Pitari, G., Prather, M. J., Pyle, J. A., Rast, S., Rodriguez, J. M., Sanderson, M. G., Savage, N. H., Shindell, D. T., Strahan, S. E., Sudo, K. and Szopa, S.: Multimodel ensemble simulations of present-day and near-future tropospheric ozone, *J. Geophys. Res.*, 111(D8), D08301, doi:10.1029/2005JD006338, 2006.

Tiedtke, M.: A Comprehensive Mass Flux Scheme for Cumulus Parameterization in Large-Scale Models, *Mon. Weather Rev.*, 117(8), 1779–1800, doi:10.1175/1520-0493(1989)117<1779:ACMFSF>2.0.CO;2, 1989.

Williams, J. E., van Velthoven, P. F. J. and Brenninkmeijer, C. A. M.: Quantifying the uncertainty in simulating global tropospheric composition due to the variability in global emission estimates of Biogenic Volatile Organic Compounds, *Atmos. Chem. Phys.*, 13(5), 2857–2891, doi:10.5194/acp-13-2857-2013, 2013.

Williams, J. E., Boersma, K. F., Le Sager, P. and Verstraeten, W. W.: The high-resolution version of TM5-MP for optimized satellite retrievals: description and validation, *Geosci. Model Dev.*, 10(2), 721–750, doi:10.5194/gmd-10-721-2017, 2017.

Yarwood, G., Rao, S. and Yocke, M.: Updates to the carbon bond chemical mechanism: CB05 - Prepared for Deborah Luecken U.S. Environmental Protection Agency Research Triangle Park, NC 27703. [online] Available from: http://www.camx.com/files/cb05_final_report_120805.aspx (Accessed 16 March 2017), 2005.

Yoo, J.-M., Lee, Y.-R., Kim, D., Jeong, M.-J., Stockwell, W. R., Kundu, P. K., Oh, S.-M., Shin, D.-B. and Lee, S.-J.: New indices for wet scavenging of air pollutants (O₃, CO, NO₂, SO₂, and PM₁₀) by summertime rain, *Atmos. Environ.*, 82, 226–237, doi:10.1016/j.atmosenv.2013.10.022, 2014.

Young, A. H., Keene, W. C., Pszenny, A. A. P., Sander, R., Thornton, J. A., Riedel, T. P. and Maben, J. R.: Phase partitioning of soluble trace gases with size-resolved aerosols in near-surface continental air over northern Colorado, USA, during winter, *J. Geophys. Res. Atmos.*, 118(16), 9414–9427, doi:10.1002/jgrd.50655, 2013.

Zaveri, R. A. and Peters, L. K.: A new lumped structure photochemical mechanism for large-scale applications, *J. Geophys. Res. Atmos.*, 104(D23), 30387–30415, doi:10.1029/1999JD900876, 1999.

We thank the reviewer for the careful reading of the manuscript and the insightful comments. Please find below our point-by-point replies:

General comments:

GC1. Additional analyses can be performed with regards to the transport of tracers as it is frequently used in the manuscript to explain differences. How good is the model with respect to transport, especially vertical transport?

- The transport of TM5 has been successfully evaluated many times in the past, e.g., see (Koffi et al., 2016; Krol et al., 2005; Peters et al., 2004; Williams et al., 2017). For this, we consider such analysis outside the scope of the current paper that is focused on presenting the new chemistry developments. Note that the current version of the TM5 model was recently included in a model intercomparison (Krol et al., 2018), in which vertical resolution was specifically addressed. For this, we provide references for each major release of the model that can guide the reader for further reading.

Following, however, the reviewer's comment, brief description and references of the transport processes parameterizations in TM5 are added in Model Description (Sect. 2.1): *"The advection scheme used in TM5 is based on the slopes scheme (Russell and Lerner, 1981) and the deep and shallow cumulus convection scheme is parameterized according to Tiedtke (1989). The performance of the transport in the model has been evaluated by (Peters et al., 2004) using sulphur hexafluoride simulations and by analyzing the vertical and horizontal distribution of radon (^{222}Rn) to simulate the boundary layer dynamics (Koffi et al., 2016; Williams et al., 2017). More recently, global transport features, such as the transport times associated with inter-hemispheric transport, vertical mixing in the troposphere, transport to and in the stratosphere, and transport of air masses between land and ocean, were evaluated via an inter-comparison of six global transport models (Krol et al., 2018)."*

Specific Comments:

SC1. Page 4, lines 4-5: Use of 150 ppb, or any concentration level has caveats, e.g. model bias. Why not use the meteorological tropopause instead? The implications should be addressed. this?

- For this work, as we stated in the manuscript, we use the chemical tropopause level defined by a 150 ppb O₃ mixing ratio following the well-documented model intercomparison study by Stevenson et al. (2006). The use of the 150 ppb O₃ level has been used so far in numerous studies, as also with previous versions of the TM5 model, providing thus an opportunity of a direct comparison of model results with other estimates. On the other hand, the tropopause levels in a model may have various definitions, such as the temperature and the potential vorticity gradients, the altitude or the standard World Meteorological Organization definition that the lowest level above 500 hPa where the vertical temperature gradient decreases to less than or equal 2 °C km⁻¹.

We agree with the reviewer that the definition of the tropopause may lead to great differences, and for this, we stated in the manuscript that the tropopause definition should always be reported when comparing modelling estimates.

For this work, however, we prefer to keep the tropopause based on the 150 ppb O₃ mixing ratio since we here mostly focused on the differences between the different configurations of the model. However, to show the impact of the use of different tropopause levels on the calculated tropospheric budgets, we now provide the relative differences of using the 100 ppb O₃ level, i.e.:

Table 1. Tropospheric budgets of O₃ for the year 2006 in Tg(O₃) yr⁻¹ and burden in Tg(O₃), using the 150 ppb O₃ mixing ratio to define tropopause level. In parenthesis the relative differences using the 100 ppb O₃ mixing ratios are also presented, calculated by reference to the 150 ppb O₃ definition of tropopause level.

Production terms	mCB05 (EBI)		mCB05 (KPP)		MOGUNTIA		Loss terms	mCB05 (EBI)		mCB05 (KPP)		MOGUNTIA	
Stratospheric inflow*	632	(10%)	429	(32%)	424	(30%)	Deposition	955	(0%)	932	(0%)	913	(0%)
Trop. chem. production	5589	(-3%)	5719	(-3%)	5709	(-3%)	Trop. chem. loss	5192	(-1%)	5216	(-1%)	5219	(-1%)
Trop. burden	385	(-8%)	384	(-8%)	375	(-8%)	Trop. lifetime (days)	22.8	(-8%)	22.8	(-8%)	22.3	(-6%)

**sum of the deposition and the tropospheric chemical loss minus the production*

Table 2. Tropospheric chemical budget of OH for the year 2006 in Tg(OH) yr⁻¹, using the 150 ppb O₃ mixing ratio to define tropopause level. In parenthesis the relative differences using the 100 ppb O₃ mixing ratios are also presented, calculated by reference to the 150 ppb O₃ definition of tropopause level.

Production terms	mCB05 (EBI)		mCB05 (KPP)		MOGUNTIA		Loss terms	mCB05 (EBI)		mCB05 (KPP)		MOGUNTIA	
O(iD) + H ₂ O	1960	(0%)	1953	(0%)	1878	(0%)	OH + CO	1665	(-2%)	1671	(-2%)	1775	(-2%)
NO + HO ₂	1268	(-4%)	1312	(-4%)	1426	(-4%)	OH + CH ₄	613	(0%)	626	(0%)	644	(-1%)
O ₃ + HO ₂	560	(-1%)	566	(-1%)	561	(-1%)	OH + O ₃	254	(-2%)	260	(-2%)	262	(-3%)
H ₂ O ₂ + <i>hν</i>	262	(-1%)	265	(-1%)	303	(-1%)	OH + ISOP	114	(-1%)	115	(-1%)	120	(0%)
Other	203	(-2%)	201	(-2%)	120	(-1%)	Other	1606	(-1%)	1626	(-1%)	1487	(-1%)

Table 3. Global budgets of CO for the year 2006 in Tg(CO) yr⁻¹ and burden in Tg(CO), using the 150 ppb O₃ mixing ratio to define tropopause level. In parenthesis the relative differences using the 100 ppb O₃ mixing ratios are also presented, calculated by reference to the 150 ppb O₃ definition of tropopause level.

Production terms	mCB05 (EBI)		mCB05 (KPP)		MOGUNTIA		Loss terms	mCB05 (EBI)		mCB05 (KPP)		MOGUNTIA	
Emissions	1097	(0%)	1097	(0%)	1097	(0%)	Deposition	98	(0%)	97	(0%)	99	(0%)
Trop. chem. production	1809	(-1%)	1818	(-1%)	1992	(-1%)	Trop. chem. loss	2840	(-6%)	2849	(-6%)	2924	(-2%)
Strat. chem. production	26	(69%)	26	(73%)	26	(65%)	Strat. chem. loss	87	(68%)	89	(69%)	90	(68%)
Atmos. burden	370	(0%)	360	(0%)	361	(0%)	Lifetime (days)	47.5	(2%)	46.2	(2%)	43.6	(3%)

SC2. Page 13, line 13. Use of different emissions are not clearly mentioned in section 2.4. Authors should justify the use of different emissions and how this impacts the changes they see in the different scenarios.

- As explained in our replies to the other reviewer (RC1), we use the same emissions (and boundary conditions) for the different chemistry configurations of the model. This choice is made in order to specifically focus only on their differences between the two mechanisms in the model as explicitly presented in Sect. 3. In the manuscript we refer to the different “speciation” of the emitted volatile organic compounds (VOC) i.e. how the VOC emissions are distributed among the VOC species considered in the different chemical mechanisms: the more lumped mCB05 does not resolve all of the NMVOCs provided by the emission datasets, whereas MOGUNTIA explicitly simulates the NMVOCs (C1-4) and isoprene. To make this point clearer, however, we changed the word “speciation” with “*representation*” when we refer here to the differences between the two chemical schemes (see also our reply to SC17) and we clearly state in the manuscript that both mechanisms use the same emission datasets.

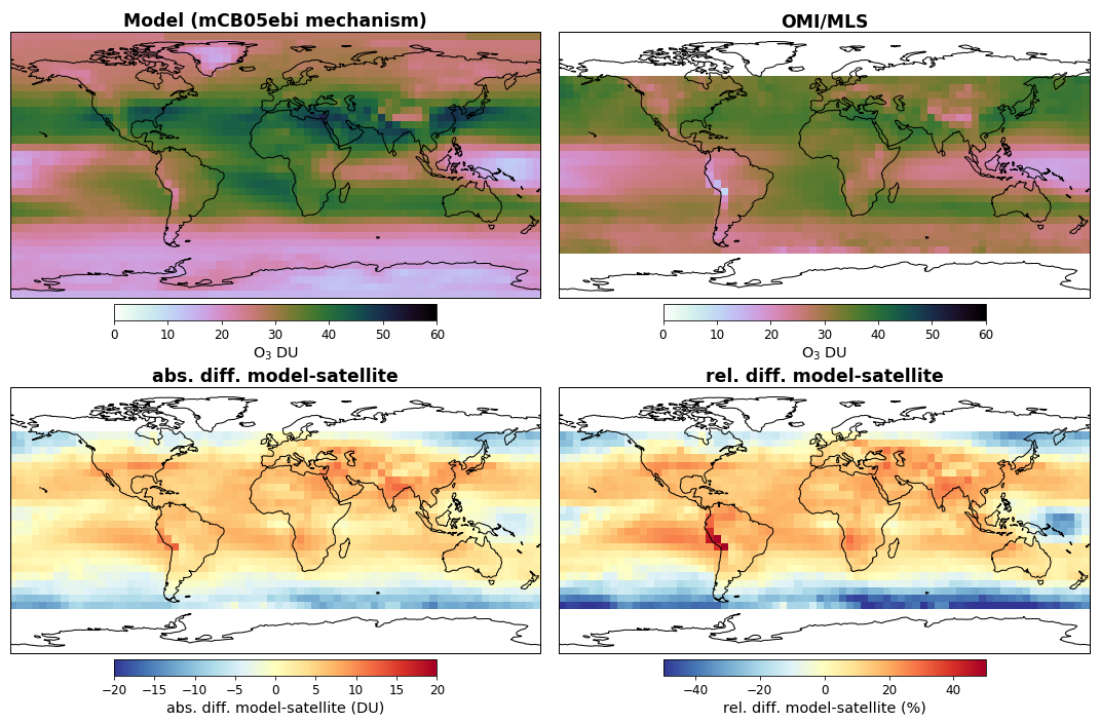
•

SC3.

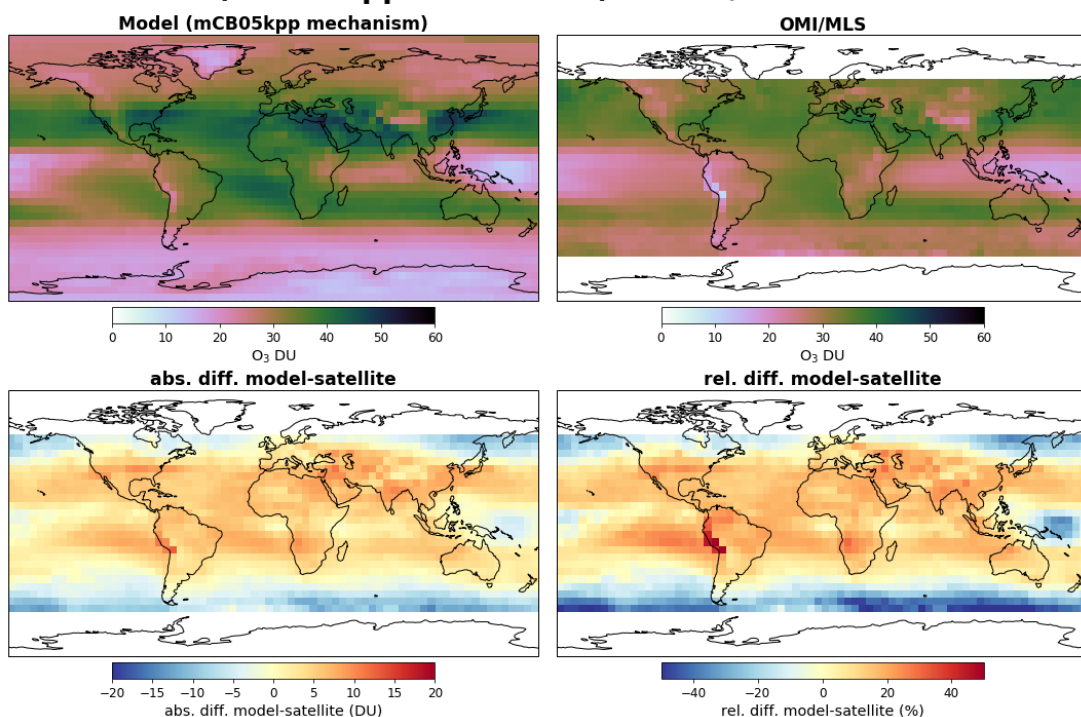
Page 20, Line 3: It would be great if the results are compared with satellites

- For this work we used two extended surface ozone observation databases and one ozonesonde database to evaluate the model and discuss the differences of the different configurations. More extended model evaluation, although always interesting, is not however expected to change the conclusions of this work, especially for the simulated tropospheric ozone mixing ratios. On the other hand, as also we refer in the summary (Sect. 6) a more dedicated comparison of the model with the MOGUNTIA configuration with *in-situ* observations and satellite retrievals is planned to be performed in the future. As an example of our work in progress, the reviewer can find below an evaluation of tropospheric O₃ columns (for the three configurations of this study) with the respective OMI monthly tropospheric retrievals:

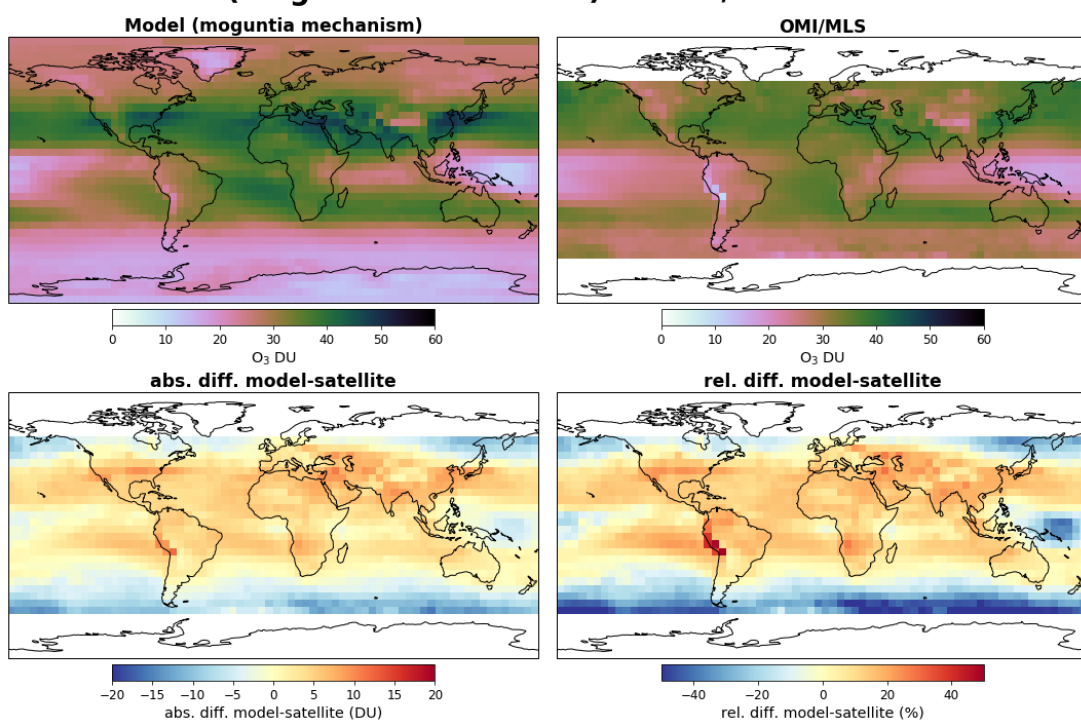
TM5-MP (mCB05ebi mechanism) vs OMI/MLS annual 2006



TM5-MP (mCB05kpp mechanism) vs OMI/MLS annual 2006



TM5-MP (moguntia mechanism) vs OMI/MLS annual 2006



Overall, it is obvious from this evaluation, that the MOGUNTIA scheme simulates better the OMI retrievals, thus leading the model in the right direction. Note, again, that we choose not to present this evaluation in this paper, since a separate paper is in progress.

References:

- Koffi, E. N., Bergamaschi, P., Karstens, U., Krol, M., Segers, A., Schmidt, M., Levin, I., Vermeulen, A. T., Fisher, R. E., Kazan, V., Klein Baltink, H., Lowry, D., Manca, G., Meijer, H. A. J., Moncrieff, J., Pal, S., Ramonet, M., Scheeren, H. A. and Williams, A. G.: Evaluation of the boundary layer dynamics of the TM5 model over Europe, *Geosci. Model Dev.*, 9(9), 3137–3160, doi:10.5194/gmd-9-3137-2016, 2016.
- Krol, M., Houweling, S., Bregman, B., van den Broek, M., Segers, A., van Velthoven, P., Peters, W., Dentener, F. and Bergamaschi, P.: The two-way nested global chemistry-transport zoom model TM5: algorithm and applications, *Atmos. Chem. Phys.*, 5(2), 417–432, doi:10.5194/acp-5-417-2005, 2005.
- Krol, M., de Bruine, M., Killaars, L., Ouwersloot, H., Pozzer, A., Yin, Y., Chevallier, F., Bousquet, P., Patra, P., Belikov, D., Maksyutov, S., Dhomse, S., Feng, W. and Chipperfield, M. P.: Age of air as a diagnostic for transport timescales in global models, *Geosci. Model Dev.*, 11(8), 3109–3130, doi:10.5194/gmd-11-3109-2018, 2018.
- Peters, W., Krol, M. C., Dlugokencky, E. J., Dentener, F. J., Bergamaschi, P., Dutton, G., Velthoven, P. v., Miller, J. B., Bruhwiler, L. and Tans, P. P.: Toward regional-scale modeling using the two-way nested global model TM5: Characterization of transport using SF 6, *J. Geophys. Res.*, 109(D19), D19314, doi:10.1029/2004JD005020, 2004.
- Russell, G. L. and Lerner, J. A.: A New Finite-Differencing Scheme for the Tracer Transport Equation, *J. Appl. Meteorol.*, 20(12), 1483–1498, doi:10.1175/1520-0450(1981)020<1483:ANFDSF>2.0.CO;2, 1981.
- Stevenson, D. S., Dentener, F. J., Schultz, M. G., Ellingsen, K., van Noije, T. P. C., Wild, O., Zeng, G., Amann, M., Atherton, C. S., Bell, N., Bergmann, D. J., Bey, I., Butler, T., Cofala, J., Collins, W. J., Derwent, R. G., Doherty, R. M., Drevet, J., Eskes, H. J., Fiore, A. M., Gauss, M., Hauglustaine, D. A., Horowitz, L. W., Isaksen, I. S. A., Krol, M. C., Lamarque, J.-F., Lawrence, M. G., Montanaro, V., Müller, J.-F., Pitari, G., Prather, M. J., Pyle, J. A., Rast, S., Rodriguez, J. M., Sanderson, M. G., Savage, N. H., Shindell, D. T., Strahan, S. E., Sudo, K. and Szopa, S.: Multimodel ensemble simulations of present-day and near-future tropospheric ozone, *J. Geophys. Res.*, 111(D8), D08301, doi:10.1029/2005JD006338, 2006.
- Tiedtke, M.: A Comprehensive Mass Flux Scheme for Cumulus Parameterization in Large-Scale Models, *Mon. Weather Rev.*, 117(8), 1779–1800, doi:10.1175/1520-0493(1989)117<1779:ACMFSF>2.0.CO;2, 1989.
- Williams, J. E., van Velthoven, P. F. J. and Brenninkmeijer, C. A. M.: Quantifying the uncertainty in simulating global tropospheric composition due to the variability in global emission estimates of Biogenic Volatile Organic Compounds, *Atmos. Chem. Phys.*, 13(5), 2857–2891, doi:10.5194/acp-13-2857-2013, 2013.
- Williams, J. E., Boersma, K. F., Le Sager, P. and Verstraeten, W. W.: The high-resolution version of TM5-MP for optimized satellite retrievals: description and validation, *Geosci. Model Dev.*, 10(2), 721–750, doi:10.5194/gmd-10-721-2017, 2017.

Description and evaluation of a detailed gas-phase chemistry scheme in the TM5-MP global chemistry transport model (r112)

Stelios Myriokefalitakis¹, Nikos Daskalakis², Angelos Gkouvousis^{3,1}, Andreas Hilboll^{†2}, Twan van Noije⁴, Jason E. Williams⁴, Philippe Le Sager⁴, Vincent Huijnen⁴, Sander Houweling^{5,6}, Tommi Bergman⁷, Johann Rasmus Nüß², Mihalis Vrekoussis^{2,8,9}, Maria Kanakidou^{2,3} and Maarten C. Krol^{10,11}

¹ Institute for Environmental Research and Sustainable Development (IERSD), National Observatory of Athens, Penteli, Greece

² Institute of Environmental Physics, University of Bremen, Bremen, Germany

³ Environmental Chemical Processes Laboratory (ECPL), Department of Chemistry, University of Crete, Heraklion, Greece

⁴ Royal Netherlands Meteorological Institute (KNMI), De Bilt, The Netherlands

⁵ Department of Earth Sciences, Vrije Universiteit Amsterdam, The Netherlands

⁶ SRON Netherlands Institute for Space Research, Utrecht, The Netherlands

⁷ Finnish Meteorological Institute, Climate System Research, Helsinki, Finland

⁸ Center for Marine Environmental Sciences, University of Bremen, Bremen, Germany

⁹ Energy, Environment and Water Research Center (EEWRC), The Cyprus Institute, Cyprus

¹⁰ Wageningen University, Wageningen, The Netherlands

¹¹ Institute for Marine and Atmospheric Research (IMAU), Utrecht University, Utrecht, The Netherlands

Correspondence to: Stelios Myriokefalitakis (steliosm@noa.gr) and Maarten C. Krol (maarten.krol@wur.nl)

Abstract. This work documents and evaluates the tropospheric gas-phase chemical mechanism MOGUNTIA in the three-dimensional chemistry transport model TM5-MP. Compared to the modified CB05 (**mCB05**) chemical mechanism previously used in the model, the MOGUNTIA includes a detailed representation of the light hydrocarbons (C1-C4) and isoprene, along with a simplified chemistry representation of terpenes and aromatics. Another feature implemented in TM5-MP for this work is the use of the Rosenbrock solver in the chemistry code, which can replace the classical Euler Backward Integration method of the model. Global budgets of ozone (O₃), carbon monoxide (CO), hydroxyl radicals (OH), nitrogen oxides (NO_x) and volatile organic compounds (VOCs) are analyzed and their mixing ratios are compared with a series of surface, aircraft and satellite observations for the year 2006. Both mechanisms appear to be able to satisfactorily represent observed mixing ratios of important trace gases, with the MOGUNTIA chemistry configuration yielding lower biases than **mCB05** compared to measurements in most of the cases. However, the two chemical mechanisms fail to reproduce the observed mixing ratios of light VOCs, indicating insufficient primary emission source strengths, too fast oxidation, and/or a low bias in the secondary contribution to C2-C3 organics via VOC atmospheric oxidation. Relative computational memory and time requirements of the different model configurations are also compared and discussed. Overall, the MOGUNTIA scheme simulates a large suite of oxygenated VOCs that are observed in the atmosphere at significant levels. This significantly expands the possible applications of TM5-MP.

[†] Deceased 25 March 2020

Deleted: here

Deleted: represent

Deleted: weak vertical mixing in the boundary layer

Deleted: of

Deleted: Overall, compared to other chemistry schemes in use in global CTMs

Deleted: and are involved in aerosol formation, expanding, thus, the...

1 Introduction

Chemistry transport models (CTMs) are tools to effectively study the temporal and spatial evolution of atmospheric species at regional and global scales, as well as to understand how the main physical and chemical processes in the troposphere (e.g., emissions, chemistry, transport, and deposition) influence air quality. Model investigations and analyses of the changes of important tropospheric pollutants, such as ozone (O_3) and carbon monoxide (CO), can further provide essential information about the oxidative capacity of the atmosphere and thus the lifetime of important climate gases like methane (CH_4). The oxidative capacity also controls the rate of formation and growth of aerosols by conversion of sulfur oxides into particulate sulfate (SO_4^{2-}) and volatile organic compounds (VOCs) into condensable organic matter that forms organic particles. Under certain tropospheric conditions (e.g., intense sunlight and high temperatures) the oxidation of VOCs in the presence of nitrogen oxides ($NO_x \equiv NO + NO_2$) enhances the formation of secondary pollutants, such as O_3 (Crutzen, 1974; Derwent et al., 1996; Monks et al., 2009). VOCs and NO_x arise from both natural and anthropogenic emission sources. NO_x can be further converted into other chemical species such as HNO_3 and particulate nitrate (NO_3^-), that together with SO_4^{2-} are key contributors to atmospheric acidity. The photochemical production of tropospheric O_3 , a known toxic air pollutant that is transported over long distances, depends on the NO_x and VOC availability in a nonlinear manner (e.g., Seinfeld and Pandis, 2006). Under very high NO_x conditions, common in densely populated areas (i.e., VOC-limited regimes), the O_3 production is inhibited and reductions in NO_x emissions can locally increase O_3 . In contrast, in rural areas, the O_3 production is more efficient, and NO_x emission reductions will decrease O_3 (i.e., NO_x -limited regimes). Thus, changes in emissions of NO_x and VOC may lead to nonlinear responses in ozone and the oxidation capacity of the troposphere. Overall, understanding the photochemical processes in the troposphere via robust model simulations is key to the development of effective abatement strategies on pollutants that affect both air quality and climate, as well as to the prediction of the future atmospheric composition.

The gas-phase photochemistry in the troposphere consists of numerous and complex reactions between odd oxygen ($O_x \equiv O + O_3$) and NO_x , coupled to the oxidation of various VOCs (e.g., Atkinson, 2000; Atkinson et al., 2004, 2006). Several chemical mechanisms of varying complexity in the representation of VOC oxidation are currently included in state-of-the-art CTMs. One of the most explicit mechanisms ever built for the simulation of the tropospheric VOC oxidation cycles, the Master Chemical Mechanism (MCM v3), comprises more than 12690 reactions, involving more than 4350 organic species, and about 46 associated inorganic reactions (Jenkin et al., 1997a; 2003). Note that recent updates further include detailed aromatic hydrocarbon (Bloss et al., 2005) and isoprene oxidation (Jenkin et al., 2015) mechanisms. Since this level of chemical complexity is far beyond the computational resources potentially available for three-dimensional (3-D) global tropospheric CTMs, simplifications are required that retain the essential features of the chemistry. To this end, various chemical mechanisms of tropospheric chemistry have been developed with different levels of complexity, involving mainly reductions of the number of VOCs considered by lumping organic species into representative surrogates. For example, the Statewide Air Pollution Research Center mechanism (SAPRC-99) is a well-documented gas-phase chemical mechanism used in many CTMs, including a rather detailed representation of tropospheric VOC oxidation based on an evaluation against over 1700 experiments

Deleted: (SAPRC)

performed in different smog chambers (e.g., Carter, 1995, 2010). SAPRC-99 does not model the oxidation of each VOC individually as the MCM, but it uses a molecular lumping approach to assign VOCs to a smaller number of reactive species.

Other well-documented mechanisms often used in CTMs are the Regional Atmospheric Chemistry Mechanism (RACM; e.g., Geiger et al., 2003; Goliff et al., 2013; Stockwell et al., 1997) and the Model of Ozone and Related Chemical Tracers mechanism (MOZART; Emmons et al., 2010; Horowitz et al., 2003). A molecular lumping mechanism has been also developed and initially used in the Model of the Global Universal Tracer transport In the Atmosphere (MOGUNTIA) 3-D climatological CTM (e.g., Kanakidou and Crutzen, 1999; Poisson et al., 2000; Baboukas et al., 2000), as well as in box model applications for field data interpretation (e.g., Poisson et al., 2001; Vrekoussis et al., 2006); that latter chemical mechanism has been the starting point for the model development presented here.

A mechanism that has been extensively used in numerous chemistry and climate modeling studies is the Carbon Bond Mechanism (CBM). CBM has several different versions with different levels of complexity (e.g., reaction rate constants updates, additions of inorganic reactions, as well as additions of organic species to better represent the respective species and radicals in the atmosphere), such as the CB4 (e.g., Gery et al., 1988; Houweling et al., 1998; Luecken et al., 2008), the CBM 2005 (CB05; e.g., Yarwood et al., 2005; Williams et al., 2013, 2017; Flemming et al., 2015) and the CBM-Z (Zaveri and Peters, 1999). The lumped-structure approach of the CBM has been extensively evaluated against chamber studies (e.g., Yarwood et al., 2005).

Several studies focused on the impact of the chemical complexity of the gas-phase mechanism on tropospheric simulations. These studies indicate an inevitable compromise between model accuracy and computational efficiency (e.g., Cai et al., 2011; Gross and Stockwell, 2003; Luecken et al., 2008; Sander et al., 2019). Indeed, for a given atmospheric condition, even different versions of the same mechanism (e.g., the CBM family) may give significantly different results. For instance, the more explicit representation of VOCs in CB05 leads to a higher production of O₃ compared to the more lumped CB4 mainly due to a higher production of peroxy radicals, aldehydes and organic peroxides (Saylor and Stein, 2012). A comparison of CB05 with RACM (Kim et al., 2009) revealed that the most considerable differences appeared in areas with significant biogenic emissions, due to the more complex chemistry of aldehydes in the presence of anthropogenic alkenes and alkanes. Box-model comparisons between the MCM and various state-of-the-art simplified tropospheric chemistry schemes also indicated that the differences between the chemistry schemes can be rather significant under high VOC loadings (Emmerson and Evans, 2009). Thus, the choice of a gas-phase mechanism for a model may introduce uncertainties in predictions of regulated gas-phase pollutants (e.g., Knote et al., 2015). Computational restrictions, such as memory and computing time savings, are always a critical point to consider for large-scale 3-D simulations, especially when higher spatial resolutions are applied. On the other hand, the ability to validate the results of a particular chemical scheme in a global model can be significantly higher for the more extensive schemes that provide an explicit treatment of gases, such as in comparisons with satellite retrievals and *in situ* observations of a series of individual species.

In this work, a detailed and complete chemistry scheme is implemented in the global CTM TM5-MP, the massively parallel (MP) version of the Tracer Model version 5 (TM5), with the aim to investigate whether the consistent biases in important

Deleted: Acid Deposition Model chemical mechanism (RADM; e.g.,...

Deleted: Gross and Stockwell, 2003; Stockwell et al., 1997), the Regional Atmospheric Chemistry Mechanism (RACM; e.g., Geiger et al., 2003; Goliff et al., 2013; Stockwell et al., 1997),

Deleted: (e.g., Poisson et al., 2001a; Vrekoussis et al., 2006)

Deleted: Another

Deleted: CBM-IV

Deleted: ,

Deleted: can

Deleted: CBM-IV

Deleted: respective

Deleted: could

Deleted: The

Deleted: , thus,

Deleted: used in

Deleted: however

Deleted: a rather

Deleted: rather

Deleted: TM5 (

tropospheric tracers, such as O₃, CO, OH, NO_x and light VOCs, found in previous work (e.g., Huijnen et al., 2010; van Noije et al., 2014; Williams et al., 2013, 2017) are sensitive to the chemistry scheme that is used. For this, we use the well-documented tropospheric gas-phase chemistry scheme MOGUNTIA (e.g., Myriokefalitakis et al., 2008 and refs. therein; along with recent updates), and benchmark its performance in TM5-MP. Section 2 provides a short description of the current model version, focusing in particular on the new features implemented in the gas-phase chemistry and the chemistry integration method. In particular, we describe here the implementation of the Kinetic PreProcessor (KPP) software (Damian et al., 2002; Sandu and Sander, 2006) in TM5-MP, which offers higher flexibility for testing, updating, and further developing the chemistry code in the model. Note that we are mostly focusing here on the performance of the new chemical scheme in comparison to the scheme previously included in the model, i.e., the modified CB05 (mCB05). This model was introduced by Huijnen et al. (2010) and Williams et al. (2013), and further updated by Williams et al. (2017). In Sect. 3, the model's performance is analyzed for the different chemical configurations used for this study and in Sect. 4 a detailed budget analysis of important gas-phase species is presented. Section 5 presents the evaluation of the different configurations of this work. The model's ability to reproduce the variability of important tropospheric species in both space and time is discussed, along with the associated uncertainties in atmospheric burdens and lifetimes. Finally, in Sect. 6 the main conclusions are presented, and some of the benefits and drawbacks of both chemical mechanisms are discussed, together with proposed directions for future model development.

2 Model description

2.1 General

The well-documented offline 3-D global CTM TM5 (Krol et al., 2005) is used for this study. Historically, the model has evolved from the original TM2 model (Heimann et al., 1988), via the TM3 model (Dentener et al., 2003; Houweling et al., 1998; Tsigaridis and Kanakidou, 2003), to TM4 (van Noije, 2004; Myriokefalitakis et al., 2008; Daskalakis et al., 2015) and TM5 (Krol et al., 2005; Huijnen et al., 2010; van Noije et al., 2014; Williams et al., 2017). In TM5-MP the parallelization of the TM5 model has been redesigned, allowing for affordable global simulations at high resolution, i.e., 1°x1° globally (Williams et al., 2017). Moreover, in this new MP version, the two-way zoom capability of TM5 is no longer available. All applications of TM5 share the same methods for model discretization and operator splitting (Krol et al., 2005), the treatment of the meteorological fields, and the mass conserving tracer transport (Bregman et al., 2003). TM5-MP is driven by meteorological fields from the ECMWF ERA-Interim reanalysis (Dee et al., 2011) with an update frequency of 3 hours. The advection scheme used is based on the slopes scheme (Russell and Lerner, 1981) and deep and shallow cumulus convection is parameterized according to Tiedtke (1989). The performance of the transport in the model has been evaluated by Peters et al. (2004) using sulfur hexafluoride simulations and by analyzing the vertical and horizontal distribution of radon (²²²Rn) (Koffi et al., 2016; Williams et al., 2017). More recently, global transport features, such as the transport times associated with inter-

Deleted: Note that here we are mostly focusing

Deleted: (

Deleted: ,

Deleted: ;

Deleted: Williams et al., 2017), rather than the full description of the model itself which has been already described in detail in previous publications (e.g., Huijnen et al., 2010; Williams et al., 2013, 2017).

Deleted: In

Deleted: in the MP version

Moved (insertion) [1]

Deleted: For the photolysis reactions, the model utilizes a rather sophisticated online scheme, as described in Williams et al. (2012)

hemispheric transport, vertical mixing in the troposphere, transport to and in the stratosphere, as well as, transport of air masses between land and ocean, were evaluated via an inter-comparison of six global transport models (Krol et al., 2018).

TM5-MP is primarily designed for simulation of the troposphere (i.e., no explicit stratospheric chemistry is considered in the model). To capture stratospheric ozone effects on actinic fluxes and to ensure realistic ozone stratosphere-troposphere exchange (STE), the overhead stratospheric profile is nudged to the ozone data set provided for the Coupled Model Intercomparison Project phase 6 (CMIP6; van Noije et al., manuscript in preparation). The boundary conditions for CH₄, both in the lower troposphere and the stratosphere, are also based on the respective global mean value from CMIP6 data set (see also Sect 2.4) to scale the monthly 2-D climatological fields as derived from HALOE measurements (Groß and Russell, 2005), with the same nudging heights and relaxation times as for the case of stratospheric O₃. This approach is justified due to the relatively long lifetime of CH₄. Additionally, for HNO₃ and CO in the stratosphere monthly mean latitudinal climatologies derived from ODIN space-based observations are applied by prescribing the ratio of HNO₃/O₃ (Jégou et al., 2008; Urban et al., 2009) and CO/O₃ (Dupuy et al., 2004), respectively. Note, however, that when we present the chemical budgets in the troposphere, a tropopause definition using the O₃ mixing ratio threshold of 150 ppb (e.g., see van Noije et al., 2014; Stevenson et al., 2006) is applied. For clarity, we note that, based on this threshold value, the different model configurations presented in this work (see Sect. 2.5) lead to identical tropopause heights.

The gas-phase chemistry of the TM5-MP model is supplemented with the in-cloud oxidation of SO₂ through aqueous-phase reactions with H₂O₂ and O₃, that depend on the acidity of the solution (Dentener and Crutzen, 1993). The heterogeneous conversion of N₂O₅ into HNO₃ on the available surface area of cloud droplets, cirrus particles, and hydrated sulfate aerosols is also accounted for. For cloud droplets, the number of droplets per unit volume is calculated using the liquid water content provided in the ECMWF meteorological data used by TM5-MP, assuming an effective droplet radius of 8 µm. For the heterogeneous conversion of N₂O₅ on hydrated sulfate particles, the approach of Dentener and Crutzen (1993) is employed, using a global mean reaction probability (γ value) of 0.02 and 0.01 on water and ice surfaces, respectively. Heterogeneous conversions also consider the total reactive surface area density of aerosols, with contributions to accumulation mode aerosol from sulfate, nitrate, and ammonium being calculated by the EQuilibrium Simplified Aerosol Model (EQSAM) approach (Metzger et al., 2002). The distribution of these aerosol species is calculated online and coupled to the gas-phase precursors NH₃, H₂SO₄, and HNO₃. Note that the aerosol microphysics module M7 (Vignati et al., 2004) is used in the model, as described in Aan de Brugh et al. (2011) and van Noije et al. (2014), along with recent updates on the inclusion of secondary organic aerosols (van Noije et al., manuscript in preparation). For N₂O₅, the uptake coefficient (γ) is considered as a function of temperature and relative humidity (Evans and Jacob, 2005), whilst for HO₂ and NO₃ radicals fixed γ values of 0.06 and 10⁻³, respectively, are adopted across all aerosol types (Jacob, 2000).

The model considers the wet removal of atmospheric species by liquid and ice precipitation, by both in-cloud and below-cloud scavenging. The fraction of gases removed by precipitation depends on Henry's law (see Table S1 in the supplement), together with the dissociation constants, temperature, and liquid or ice water content. In-cloud scavenging in stratiform precipitation considers an altitude dependent precipitation formation rate (also describing the conversion of cloud water into rainwater). For

Deleted: Thus, since TM5-MP does not consider a full stratospheric chemistry scheme, this study is mostly focused on the troposphere. For this, when presenting the tropospheric chemical budgets...

Deleted: (SAD) from

convective precipitation, highly soluble gases are assumed to be scavenged entirely in the vigorous convective updrafts producing rainfall rates of >1 mm/hour. Removal is exponentially scaled down for lower rainfall rates. For the dry deposition, the removal is calculated online in the model, based on a series of surface and atmospheric resistances on a 1°×1° spatial resolution (Wesely, 1989; Ganzeveld and Lelieveld, 1995; Ganzeveld et al., 1998). Overall, the calculated deposition velocities show both seasonal and diurnal cycles since they are calculated using 3-hourly meteorological and surface parameters, based on the uptake resistances for vegetation (in-canopy aerodynamic, soil, and leaf resistance), soil, water, snow, and ice (see Table S2). A more detailed description of dry and wet deposition schemes for the removal of gases can be found in de Bruine et al. (2017).

2.2 Gas-phase chemistry

2.2.1. The original MOGUNTIA chemical scheme

The new chemical mechanism that has been implemented in TM5-MP for this study was originally developed for box (Poisson et al., 2001) and global (Kanakidou and Crutzen, 1999; Poisson et al., 2000) modelling studies, and initially coupled to the global 3-D CTM MOGUNTIA (Zimmermann, 1988). Since then, the scheme has been continuously updated for box modelling, coupled to the global TM4 model, and applied in numerous studies (e.g., Tsigaridis and Kanakidou, 2002; Gros et al., 2002; Myriokefalitakis et al., 2008; Daskalakis et al., 2015).

The MOGUNTIA chemical scheme employs a rather detailed oxidation scheme of light alkanes (CH₄, C₂H₆, and C₃H₈), light alkenes (C₂H₄ and C₃H₆), acetylene (C₂H₂), and isoprene (C₅H₈). Acetaldehyde (CH₃CHO), glyoxal (GLY; CHOCHO), glycolaldehyde (GLYAL; HOCHCHO), methylglyoxal (MGLY; CH₃COCHO) and acetone (CH₃COCH₃) are also explicitly treated in the mechanism. The oxidation pathways of methacrolein (MACR; CH₃(CH₂)CH=O) and methylvinyl ketone (MVK; CH₃C(O)CH=CH₂) are also considered, together with the formation of formic (HCOOH) and acetic acid (CH₃COOH). Higher VOCs (i.e., C_n>4), besides isoprene, are represented in the mechanism by the surrogate species n-butane (n-C₄H₁₀), motivated by the similar O_x and hydrogen oxides (HO_x) yields per oxidized carbon atom (e.g., see Poisson et al., 2000; Stavrakou et al., 2009a). The second-generation oxidation products of higher hydrocarbons of biogenic origin (such as terpenes) and aromatics are also considered to follow the gas-phase oxidation pathways of the respective isoprene and surrogate n-C₄H₁₀ oxidation species.

The reactions of peroxy radicals (RO₂) with hydrogen peroxide (HO₂), methyl peroxide (CH₃O₂), and NO lead to organic hydroperoxides (ROOH), carbonyls and organic nitrates, respectively. ROOH is removed by photolysis and reaction with OH. The addition of NO to the formed RO₂ radicals leads to alkyl nitrates (RONO₂), which are much longer lived than NO_x. RONO₂ can thus be transported over longer distances than NO_x and serve as a sink for NO_x in high-NO_x regimes and as a source for NO_x in low-NO_x regimes. The RONO₂ compounds explicitly considered in this study are identified by R=CH₃, C₂H₅, C₃H₇, C₄H₉, HOC₂H₄O, and C₃H₈(OH), i.e., the first-generation product of isoprene oxidation. Additionally, the reactions of the acyl peroxy radicals (RC(O)O₂) with NO₂ produce peroxyacyl nitrates (RC(O)O₂NO₂), in particular PAN (R=CH₃), which is the

Deleted: and

Deleted: 1

Deleted: 1

Deleted: employed

Deleted: (Poisson et al., 2001b)

Deleted:) in the mechanism.

Deleted: mainly

Deleted:) and

Deleted: as well as with

Deleted: subsequent

Deleted: areas

Deleted: regions

most abundant organic nitrate observed in the troposphere and the only species of this group that is considered here. Thermal decomposition is dominant for peroxyacyl nitrates, while it is negligible for alkyl nitrates. NO₃ radical reactions with aldehydes, alcohols, n-C₄H₁₀, dimethylsulfide (DMS) and unsaturated hydrocarbons are also considered. A more detailed description of the chemical scheme used for this study can be found in Poisson et al. (2000) and Myriokefalitakis et al. (2008).

5 2.2.2 Updates of the MOGUNTIA chemical mechanism

Several updates have been applied to the original MOGUNTIA chemical scheme with respect to the previous implementations (e.g., Poisson et al., 2000; Myriokefalitakis et al., 2008). These updates include reactions of major hydrocarbons, their rate constants and oxidation pathways. Concerning the terpene chemistry, we here consider one lumped monoterpene species (C₁₀H₁₆) for all terpenes (assuming a 50:50 α -: β -pinene distribution), in contrast to the consideration of the explicit oxidation of α - and β -pinene as performed in the previous implementations of the MOGUNTIA scheme (e.g., Myriokefalitakis et al., 2008, 2010). Thus, monoterpenes represent here all terpenes and terpenoids species. Likewise, toluene is used to represent all aromatics replacing benzene, xylene, and toluene used previously (Myriokefalitakis et al., 2008, 2010). Besides these compounds, toluene is also used to represent trimethyl-benzenes and higher aromatics. Moreover, for this work the coupling of the gas-phase chemistry with the aqueous-phase oxidation scheme of SO₂, as well as the gas-phase oxidation of dimethyl sulfide (DMS), methyl sulfonic acid (MSA) and ammonia (NH₃), follows the oxidation scheme outlined by Williams et al. (2013), which is slightly simpler compared to the MOGUNTIA scheme used in previous studies (e.g., Myriokefalitakis et al., 2010). Note that the lumping mentioned above, and the simplifications implemented here, aim at limiting the number of species without degrading the general performance of the chemical scheme for global-scale tropospheric chemistry.

Isoprene (2-methyl-1,3-butadiene; ISOP) oxidation has been extended with the production of isoprene epoxydiols (IEPOX) and hydroperoxyaldehydes (HPALD), and the HO_x-recycling mechanism under low-NO_x conditions (Paulot et al., 2009; Peeters and Müller, 2010a; Crounse et al., 2011; Browne et al., 2014). The latter species replaces the lumped second-generation oxidation product considered in previous implementations of the MOGUNTIA mechanism (Poisson et al., 2000; Myriokefalitakis et al., 2008). The oxidation of isoprene by the OH radical leads to the formation of several isomers of an unsaturated hydroxy hydroperoxide. In the presence of NO_x, this leads to the formation of carbonyl compounds. However, under low-NO_x conditions, the major product from unsaturated hydroxy hydroperoxides oxidation is IEPOX (i.e., cis- and trans-isomers). The organic peroxy radicals formed from OH oxidation of isoprene, can react with either 1) HO₂ to form hydroperoxides, or 2) NO to form hydroxynitrates, formaldehyde (HCHO), MVK, MACR and HO₂ (e.g., Paulot et al., 2009), or hydroperoxyenals (HPALDs). The latter are produced by the isomerisation of the initial isoprene organic hydroperoxy radicals followed by reaction with O₂ and other oxidized products (Peeters et al., 2009; Peeters and Müller, 2010). Under HO₂-dominated conditions, the main products are unsaturated hydroperoxides (all possible isomers referred to as ISOPOOH; see Table 2). The fate of isoprene peroxy radicals is highly dependent on the mixing ratios of HO₂, NO, organic peroxy radicals, and the local meteorological conditions that affect thermal and photochemical reaction rates and wet and dry removal. Subsequent reactions of ISOPOOH with OH produce epoxydiols (cis- and trans- isomers referred to as IEPOX) and regenerate

Deleted: 1

Deleted: Several updates have been applied here to the original MOGUNTIA chemical scheme compared to the previous implementations (e.g., Poisson et al., 2000; Myriokefalitakis et al., 2008, 2011), regarding the reactions and their rate constants, as well as some oxidation paths of major hydrocarbons. Concerning the terpene chemistry, we here consider one lumped monoterpene species (C₁₀H₁₆) for all terpenes (assuming a 50:50 α -: β -pinene distribution), in contrast to the consideration of the explicit oxidation of α - and β -pinene as performed in the previous implementations of the MOGUNTIA scheme (e.g., Myriokefalitakis et al., 2008, 2010, 2016). Thus, monoterpenes represent here all terpenes and terpenoids species. Likewise, toluene is used to represent all aromatics replacing benzene, xylene, and toluene used previously (Myriokefalitakis et al., 2008, 2016). Besides these compounds, toluene is also used to represent trimethyl-benzenes and higher aromatics. Moreover, for this work the coupling of the gas-phase chemistry with the aqueous-phase oxidation scheme of SO₂, as well as the gas-phase oxidation of dimethyl sulfide (DMS), methyl sulfonic acid (MSA) and ammonia (NH₃), follows the oxidation scheme outlined by

Deleted: , which is slightly simpler compared to that used in previous studies using MOGUNTIA (see Myriokefalitakis et al., 2010). Note that the lumping mentioned above, and the simplifications implemented here, aim at limiting the number of species without however degrading the general performance of the chemical scheme for global-scale tropospheric chemistry.

Deleted: here

Deleted: as well as

Deleted: the

Deleted: the

Deleted: the

Deleted: as well as dry

Deleted: of intermediates

OH radicals (Paulot et al., 2009). Moreover, the isoprene peroxy radical 1,6-H-shift isomerizations (Peeters et al., 2014; Peeters and Müller, 2010) lead to the formation of photolabile C5-hydroperoxyaldehydes (i.e., all possible isomers referred to as HPALDs; see Table 1). Overall, these additions to the chemistry scheme is expected to provide a better representation of OH regeneration during isoprene oxidation (e.g., Browne et al., 2014), compared to the previous implementation of the

Deleted: leads

Deleted: (

MOGUNTIA mechanism. The MOGUNTIA chemistry scheme is in line with the VOCs oxidation pathways as proposed by the Master Chemistry Mechanism (MCM v3.3.1) (e.g., Bloss et al., 2005; Saunders et al., 2003). The thermal and pressure-dependent reaction rate coefficients of the MOGUNTIA chemical mechanism are taken (when available) from the IUPAC kinetic data evaluation (Atkinson et al., 2004; Wallington et al., 2018) and supplemented with reaction rates based on recommendations given by JPL (Burkholder et al., 2015). Photolysis frequencies needed to drive MOGUNTIA are taken from the IUPAC database (Atkinson, 1997; Atkinson et al., 2004) along with the updates from MCM v3.3.1 (Bloss et al., 2005; Jenkin et al., 1997, 2003, 2015; Saunders et al., 2003). Note that the model calculates online the photolysis frequencies as described in Williams et al. (2012). The comprehensive lists of all photochemical and thermal kinetic reactions included in the current MOGUNTIA chemical scheme are presented in Tables 1 and 2, respectively.

Deleted: where

Deleted: in

Deleted: rates

Deleted: The comprehensive lists of all photochemical and thermal kinetic reactions included in the current MOGUNTIA chemical scheme are presented in Tables 1 and 2, respectively.

2.3 The chemical solver

The KPP version 2.2.3 (Damian et al., 2002; Sandu and Sander, 2006) is here employed to generate Fortran 90 code for the numerical integration of the gas-phase chemical mechanisms. An important advantage of this approach is that the implementation of a KPP generated code in the model is less prone to errors than coding the mechanism manually. Upon the translation of the chemistry mechanisms (e.g., species, reactions, rate coefficients) from the KPP language into a Fortran 90 code, a model driver was developed to arrange the respective couplings to TM5-MP. Minor changes, however, were needed in the KPP code to deal with TM5-MP I/O requirements. The photolysis and the thermal reactions are not calculated in KPP, but explicitly calculated by the respective modules of TM5-MP and then directly provided to the aforementioned chemistry driver. To this end, only the integration method has been updated in the model, replacing the default hand-coded chemical solver set-up. Moreover, the NO emission rates (as well as the dry deposition terms of all deposited species) are imported to KPP through the application of appropriate production (and loss) rates, as previously done for the EBI solver, owing mainly to the numerical stiffness of the NO-NO₂-O₃ photo-stationary state and their fast interactions (e.g., see Huijnen et al., 2010). In this study, the Rosenbrock solver is used as the numerical integrator (Sander et al., 2019). Rosenbrock solver has been shown to be robust and capable of integrating very stiff sets of equations (Sander et al., 2011). For all previous versions of the model, the Euler Backward Iterative (EBI) solver (Hertel et al., 1993) was used. This holds for the modified CB4 (Houweling et al., 1998), the mCB05 (Williams et al., 2013) and the MOGUNTIA (Myriokefalitakis et al., 2008) mechanisms. Note, however, that EBI was originally designed for the CB4 mechanism (Gery et al., 1989) and it is a rather fast and robust solver suitable for the use in large-scale atmospheric models that incorporate operator splitting (Huang and Chang, 2001).

Deleted: Kinetic PreProcessor (

Deleted:)

Deleted: mechanism

Deleted: that arranges

Deleted: coupling

Deleted:

Deleted: ¶

Deleted: has been

Deleted: CBM4

Deleted: (Myriokefalitakis et al., 2008, 2011) mechanisms. EBI was originally designed for the CBM4

Deleted: . However, the implementation of KPP generated code in the model is less prone to errors that may occur when relatively detailed chemistry schemes such as the MOGUNTIA need to be manually coded. An automatic code generator, thus, offers higher flexibility for testing, updating, and further developing the chemistry code....

The favorable comparison of the Rosenbrock solver against other widely used methods, such as Facsimile (Curtis and Sweetenham, 1987), has already been described in the literature (e.g., Sander et al., 2005). Focusing specifically on the comparison of a series of Rosenbrock solvers to EBI, Sandu et al. (1997) concluded that, although EBI appears robust, especially when it is used with a relatively large timestep, the Rosenbrock methods with variable timesteps are significantly more accurate and clearly superior for accuracies in the range of 1% compared to EBI, for a range of species examined. **The main aim of this study is not to compare the two chemistry solvers (i.e., the Rosenbrock vs. the EBI). Instead, we present model simulations using the Rosenbrock solver as produced by KPP for the mCB05 scheme (see Sect. 2.5) to isolate the impact of the solver on various species mixing ratios of this work.**

2.4 Emission set-up

For the present study, emissions from anthropogenic activities including aircraft emissions (Hoesly et al., 2018) and biomass burning (**speciated for agricultural waste burning, deforestation fires, boreal forest fires, peat fires, savanna fires and temperate forest fires; van Marle et al. (2017).**), are adopted from the sectoral and gridded historical inventories as developed for the CMIP6 (Eyring et al., 2016). In more details, anthropogenic and biomass burning emissions of CO, NO_x, black carbon aerosol (BC), particulate organic carbon (OC), sulfur dioxide and sulfates (SO_x), as well as speciated non-methane volatile organic compounds (NMVOCs) are considered, such as emissions of ethane (C₂H₆), methanol (CH₃OH), ethanol (C₂H₅OH), propane (C₃H₈), acetylene (C₂H₂), ethane (C₂H₄), propene (C₃H₆), isoprene (C₅H₈), monoterpenes (C₁₀H₁₆), benzene (C₆H₆), toluene (C₇H₈), xylene (C₈H₁₀) and other aromatics, higher alkenes, higher alkanes, HCHO, acetaldehyde (CH₃CHO), acetone (CH₃COCH₃), dimethylsulfide (DMS; C₂H₆S), formic acid (HCOOH), acetic acid (CH₃COOH), methyl ethyl ketone (MEK; CH₃CH₂COCH₃), methylglyoxal (MGLY; CH₃COCHO), and hydroxyacetaldehyde (HOCH₂CHO). Note that all biomass burning emissions (open forest and grassland fires) are vertically distributed in the model over latitude-dependent injection heights, i.e., for tropical (30° S–30° N), temperate (30–60° S/N) and high-latitude (60–90° S/N) forest fires (see Appendix in van Noije et al., 2014).

Biogenic emissions from vegetation include isoprene, terpenes and other volatile organic compounds, and CO. **Emissions** are based on the Model of Emissions of Gases and Aerosols from Nature (MEGAN) version 2.1 (Sindelarova et al., 2014). Isoprene and terpenes emissions are distributed over the first ~50 m **from the surface** and a diurnal cycle is imposed. The biogenic emissions from soils include NO_x (Yienger and Levy, 1995), NH₃ and terrestrial DMS emissions from soils and vegetation (Spiro et al., 1992). Oceanic emissions of CO and NMVOCs come from the POET database (Granier et al., 2005), oceanic emissions of NH₃ from Bouwman et al. (1997), while the DMS oceanic emissions are calculated online (van Noije et al., manuscript in preparation) using the sea water concentration climatology from **Lana et al. (2011)**. The NO_x production by lightning is parameterized based on convective precipitation fields (Meijer et al., 2001) and the SO_x fluxes from continuously emitting volcanoes are taken from Andres and Kasgnoc (1998). Note that **we focus below on the more detailed representation of emissions as used for the MOGUNTIA chemical scheme. Emissions of other tropospheric species in the gas and the particulate phase are described in detail in previous studies (e.g., van Noije et al., 2014).**

Deleted: In

Deleted: , we do

Deleted: aim however

Deleted:); on the contrary

Deleted: , and as an intermediate step between the earlier model version (i.e., using the EBI solver and the mCB05 chemistry scheme) and the new version (i.e., using the Rosenbrock solver and MOGUNTIA chemistry scheme).

Deleted: , including

Deleted: (van Marle et al., 2017),

Deleted: They

Deleted: Lana et al., (2011)

Deleted: here our

Deleted: is mostly

Deleted: NMVOCs speciation

Deleted: since

Deleted: emissions of

Deleted: in the model

The MOGUNTIA chemical scheme considers direct emissions of CO, CH₄, HCHO, HCOOH, CH₃OH, C₂H₆, C₂H₄, C₂H₂, CH₃CHO, CH₃COOH, C₂H₅OH, HOCH₂CHO, CHOCHO, C₃H₈, C₃H₆, *n*-C₄H₁₀, MEK, C₅H₈, C₁₀H₁₆, C₇H₈ as well as NO_x, NH₃, DMS, and SO_x. Butanes, pentanes, hexanes, and higher alkanes emissions are summed up into the lumped *n*-C₄H₁₀ species, which represents the alkanes containing four or more carbon atoms. For reactivity purposes, higher alkenes emissions containing four or more carbon atoms (butenes and higher alkenes) are accounted for as equivalent C₃H₆ emissions. Higher ketones (i.e., except for acetone) from open biomass burning emissions are represented as MEK. Emissions of benzene (C₆H₆), toluene (C₇H₈), xylene (C₈H₁₀), trimethyl-benzenes, and other higher aromatics and VOCs are represented by toluene as in the MOZART mechanism (Emmons et al., 2010a). Note that when VOC emissions are assigned to a lumped species, adjustments are made to preserve their atmospheric reactivity (see also notes in Tables 1 and 2).

The explicit parameterization of VOC species in the MOGUNTIA chemical scheme requires emissions that are not routinely included in available emission databases. Direct biofuel and biomass burning emissions of light carbonyls have been reported in several studies (e.g., Christian et al., 2003; Fu et al., 2008; Hays et al., 2002), and these represent a significant contribution to the VOC budget (e.g., Fu et al., 2008; Myriokefalitakis et al., 2008; Stavrakou et al., 2009b, 2009a; Vrekoussis et al., 2009). For this reason, emissions from biofuel use of 1.4 Tg yr⁻¹, 2.4 Tg yr⁻¹, and 1.6 Tg yr⁻¹ are considered for GLYAL, GLY, and MGLY, respectively. For the biomass burning sector, we use global emissions of GLYAL and GLY of 4.3 Tg yr⁻¹ and 5.2 Tg yr⁻¹, respectively. We base these emission rates on the HCHO emissions distribution, because mass emission rates of low molecular weight carbonyls, such as HCHO and GLY (e.g., Hays et al., 2002), are highly correlated. Global emissions of roughly 1.4 Tg yr⁻¹ (Emmons et al., 2010) are also considered for MEK, accounting for anthropogenic emissions (Rodigast et al., 2016), such as domestic burning and solvent use (e.g., Ware, 1988). For all other carbonyls, primary anthropogenic emissions are considered negligible (e.g., Fu et al., 2008). A list of the global annual emission strengths considered for the MOGUNTIA chemical configuration is presented in Table 3. For completeness, we note that primary aerosol emissions of OC, BC, sea salt, and dust are also considered in the model with sea-salt and dust emissions calculated online. A more detailed description of the gas and aerosol emissions used in the model will be presented in van Noije et al. (manuscript in preparation).

2.5 Simulations

We will present the analysis of TM5-MP simulations with the mCB05 and MOGUNTIA chemical mechanisms for the year 2006, which has been the chosen year of previous benchmarking studies (Huijnen et al., 2010; Williams et al., 2013, 2017). All simulations have been performed at 1°x1° horizontal resolution (e.g., Williams et al., 2017) and 34 vertical layers, and use a 1-year spin-up (i.e., for the year 2005). The same emission datasets have been used in all simulations, albeit with higher speciation for the MOGUNTIA chemical scheme. Overall, two simulations have been performed for the mCB05 configuration: one employing the EBI solver (mCB05(EBI)) and one employing the KPP-generated Rosenbrock solver (mCB05(KPP)). This approach isolates differences that are caused solely by the applied chemistry solver. By comparing MOGUNTIA, generated by KPP, with mCB05(KPP), the differences due to the chemistry set-up in the model are isolated.

Deleted: Overall, the

Deleted: for the MOGUNTIA,

Deleted: corrections

Deleted: mass conservations and

Deleted: , however,

Deleted: representing overall

Deleted: their global budgets

Deleted: To take

Deleted: into account

Deleted: amount in the model to about

Deleted: For this work, the aforementioned

Deleted: are based

Deleted: distributions used in the model, owing to the highly correlated...

Deleted: .

Deleted: here

Deleted: pointing to a contribution from

Deleted: , while for

Deleted: emissions

Deleted: in the model

Deleted: of this work

Deleted: (

Deleted:)

Deleted: For this work, we

Deleted: For all simulations, a 1-year spin-up (i.e., for the year 2005) is applied. Two simulations have been performed for the mCB05 configuration: one with the EBI solver, i.e., the mCB05(EBI) and one with the Rosenbrock solver as generated by the KPP, i.e., the mCB05(KPP).

Deleted: as both generated by the KPP,

Deleted: further

3 Model performance

Concerning the TM5-MP performance, simulations performed on the ECMWF CRAY XC40 high-performance computer facility using 360 cores, indicate that the coupling of KPP software alone, increases the time spent in chemistry by ~59% and overall slows down the code by ~18% compared to the (hand coded) EBI version for the mCB05 mechanism. As expected, the coupling of the MOGUNTIA atmospheric chemistry scheme further increases the model runtime. MOGUNTIA uses 100 transported and 28 non-transported tracers, numbers that are significantly larger than the mCB05 configuration (i.e., 69 transported and 21 non-transported tracers). As a result, time spent to transport the tracers increases by ~43% and the chemistry calculations slow down by ~55%. Altogether, the newly coupled MOGUNTIA chemistry scheme in TM5-MP is computationally ~27% more expensive than the mCB05(EBI) configuration. Overall, the mCB05(EBI), mCB05(KPP) and MOGUNTIA configurations simulate 0.73, 0.60 and 0.44 year per day simulation time, respectively (Table S3a). Note that an additional series of simulations with 450 cores leads only to marginal changes (Table S3b). Finally, the runtime values for the different model configurations presented here are highly hardware dependent, owing mainly to the large I/O component associated with reading the meteorological fields.

4 Comparison of budgets and tropospheric mixing ratios

4.1 Ozone (O₃)

Table 4 presents a detailed description of the chemical budget of tropospheric ozone as calculated by the TM5-MP model, for the three chemical configurations. Following Stevenson et al. (2006), chemical production of ozone is derived from all reactions that convert NO to NO₂, since NO₂ is rapidly photo-dissociated and forms O₃, i.e.,



where, RO₂ represents all the major organic peroxy radicals of the corresponding chemistry mechanism used in the model. For the MOGUNTIA scheme RO₂ includes, CH₃O₂, C₂H₅O₂, H₂YEO₂, n-C₃H₇O₂, i-C₃H₇O₂, ACO₂, HYPO₂, n-C₄H₉O₂, MEKO₂, ISOP₂, IEPOXO₂, MVKO₂, MACRO₂, TERO₂, and AROO₂ radicals. For mCB05, RO₂ includes the CH₃O₂ radical and XO₂ (i.e., the operator for the NO to NO₂ conversion which represents all lumped alkyl-peroxy radicals in mCB05; see Williams et al., 2017 and Yarwood et al., 2005).

The chemical O₃ loss is derived as the sum of the 1) O₃ photolysis to O(¹D), i.e.,



followed by reaction with H₂O to form OH, i.e.,



2) O₃ destruction by HO₂ and OH catalytic cycles, i.e.,



Moved (insertion) [2]

Deleted: All simulations that are presented have been performed at 1°x1° horizontal resolution (e.g., Williams et al., 2017) and 34 vertical layers,

Moved up [1]: driven by meteorological fields from the ECMWF ERA-Interim reanalysis (Dee et al., 2011) with an update frequency of 3 hours.

Moved up [2]: Concerning the TM5-MP performance, simulations performed on the ECMWF CRAY XC40 high-performance computer facility using 360 cores, indicate that the coupling of KPP software alone, increases the time spent in chemistry by ~59% and overall slows down the code by ~18% compared to the (hand coded) EBI version for the mCB05 mechanism.

Deleted: As expected, the coupling of the MOGUNTIA atmospheric chemistry scheme further increases the model runtime; with 100 transported and 28 non-transported tracers for a full simulation, which are significantly more than in the mCB05 configuration (i.e., 69 transported and 21 non-transported tracers), the MOGUNTIA mechanism increases the transport by ~43% and the chemistry by ~55% in the model. Altogether, the newly coupled MOGUNTIA chemistry scheme in TM5-MP is computationally ~27% more expensive than the mCB05 configuration. Overall, the simulated years per day for the mCB05(EBI), mCB05(KPP) and MOGUNTIA configurations of the model correspond to 0.73, 0.60 and 0.44, respectively (Table S3a). Note that an additional series of simulations with 450 cores presents only marginal changes of the above results (Table S3b). Finally, our results indicate that the runtime values for the different model configurations presented here are highly hardware dependent, owing mainly to the large I/O component due to the meteorological fields reading.

Deleted: ; for

Deleted: the

Deleted: , and for the

Deleted: scheme

Deleted: the

and 3) reactions of O₃ with unsaturated VOCs. Chemical loss calculations exclude contribution from HNO₃, NO₃ and N₂O₅ and other fast cycles between ozone-related species, as proposed by Stevenson et al. (2006).

For the MOGUNTIA scheme, the tropospheric chemical production is calculated to be 5709 Tg yr⁻¹, which is only ~10 Tg yr⁻¹ smaller compared to the mCB05(KPP) configuration. Chemical destruction in the troposphere is similar in the MOGUNTIA and mCB05(KPP) chemistry configurations (Table 4). The use of EBI compared to the Rosenbrock solver decreases the O₃ chemical production (5719 vs. 5589 Tg yr⁻¹) and destruction (5216 vs. 5192 Tg yr⁻¹) terms in the troposphere (Table 4). Besides some expected differences due to the behavior of the two solvers, the calculated differences may also be partly attributed to the mass fixer for NO_y (i.e., the sum of NO, NO₂, NO₃, HNO₃, HNO₄, 2×N₂O₅, PAN and the organic nitrate compounds) that is applied in the mCB05(EBI) configuration to ensure no artificial loss of nitrogen. NO_y fixing occurs mainly over highly polluted regions with active NO_x photochemistry to improve the accuracy of the EBI solver.

Focusing on the impact of the stratosphere on the tropospheric O₃ budget, the net STE flux of O₃ for the MOGUNTIA configuration is somewhat lower (~1%) than for mCB05(KPP). Considering that all configurations use the same stratospheric ozone relaxation parameterization, this difference can only be attributed to the chemical schemes. Note that the global STE of O₃ is defined by simply considering the chemical production and loss budget terms, as proposed by Stevenson et al. (2006).

Thus, differences in the O₃ stratospheric inflow budgets for the three chemistry configurations (Table 4) do not imply that the tropospheric chemistry impacts on O₃ transport from the stratosphere, but rather that the global budget is closed by an inferred stratospheric input term. Thus, the higher net chemical production of O₃ in the troposphere implies a lower contribution from the stratosphere to the troposphere for roughly the same deposition losses. The calculated net influx from the stratosphere for the MOGUNTIA configuration (~424 Tg yr⁻¹) remains within one standard deviation of a multi-model mean (552 ± 168 Tg yr⁻¹), as reported by both Stevenson et al. (2006) and Young et al. (2013). MOGUNTIA calculations are also in line with estimates (~400 Tg yr⁻¹) based on observations (Hsu, 2005; Olsen, 2004), although higher compared to the 306 Tg yr⁻¹ calculated by an earlier version of the TM5 model driven by the same meteorological fields (van Noije et al., 2014). Overall, compared to the mCB05(EBI) simulation, the lower net stratosphere-troposphere exchange flux simulated in the MOGUNTIA configuration brings the model results closer to the current best estimates of the net STE.

The MOGUNTIA configuration also results in a reduction of roughly 2% in the tropospheric O₃ burden compared to both mCB05 configurations. No significant change in the O₃ lifetime in the troposphere (i.e., 22.3 - 22.8 days) is found and the calculated lifetimes remain close to other model estimates of ~22 days (Stevenson et al., 2006; Young et al., 2013). Compared to previous studies, the tropospheric O₃ burden calculated using the MOGUNTIA chemical configuration (~375 Tg) is ~12% higher compared to the multi-model mean estimate of Stevenson et al. (2006) (336 ± 27 Tg), the 335±10 Tg burden derived from O₃ climatology from pre-2000 data (Wild, 2007), and ~20% higher compared to the tropospheric burden of 309 Tg reported by van Noije et al. (2014). The calculated burden for the MOGUNTIA chemistry configuration is also ~11% higher compared to the burden derived from the ACCMIP models (337 ± 23 Tg; Young et al. 2013), roughly 17% higher than the burden reported by Schultz et al. (2018) and 8-15% higher than the Lamarque et al. (2012) estimations who used a tropopause level at 100 ppb of O₃ mixing ratios. Table 4 also presents the relative differences of the budget calculations when a tropopause

Deleted: as well as the

Deleted: Note that for the chemical

Deleted: of this work, the

Deleted: contributions, together with the

Deleted: are ignored

Deleted: in the model

Deleted: higher for

Deleted: compared to the

Deleted: configuration

Deleted:), which can be attributed to the respective changes in the mixing ratios of the O₃ precursor gases. Moreover, the

Deleted: in the model

Deleted: is

Deleted: applied

Deleted: fixing

Deleted: This

Deleted: in the model

Deleted: .

Deleted: here

Deleted: and routinely used in many global models.

Deleted: the

Deleted: among

Deleted: TM5-MP

Deleted: 3

Deleted: the

Deleted: In short

Deleted: tropospheric

Deleted: chemistry O₃

Deleted: stratosphere influx

Deleted: ,

Deleted: as

Deleted: for

level of 100 ppb O₃ is adopted. Note that tropospheric burden estimates remain susceptible to the tropopause definition, leading potentially to significant differences between modelling studies. For this reason, the tropopause level(s) should always be reported when comparing modelling estimates. Overall, the use of the MOGUNTIA mechanism tends to bring the model closer to other published estimates, by lowering the O₃ burden compared to the mCB05 scheme in TM5-MP.

Deleted: and for

Deleted: seems

Ozone surface and zonal mean mixing ratios simulated by the MOGUNTIA configuration for the year 2006 are presented in Figs. 1a,b, respectively. Figures 1c,d show small differences in surface and zonal mean mixing ratios between MOGUNTIA and mCB05(KPP). Differences in surface simulated O₃ mixing ratios between the two mechanisms are evident mainly downwind of regions with biogenic and tropical fire emissions. The mCB05(KPP) simulation shows higher mixing ratios (~2-4 ppb) over the ITCZ, India and East Asia (up to ~10 ppb). This is mainly attributed to the different representation of VOCs, with MOGUNTIA being significantly more explicit than mCB05. This behavior can also be observed in the zonal mean O₃ distribution presented in Fig. 1d, where the impact of the different representation of VOCs, originating mainly from the tropics, is reaching the mid- and upper troposphere lifted by convection following the upward branch of the tropical Hadley cell. The use of different solvers alone does not result in any critical difference in the O₃ mixing ratios for mCB05 (Fig. 1e,f), presenting only some small negative differences of ~1 ppb downwind of regions with high anthropogenic emissions (e.g., India) for mCB05(EBI).

Deleted: compared to the MOGUNTIA configuration, as well as over...

Deleted: due

Deleted: speciation of VOC emissions used in the two model configurations, since the VOC speciation of the emissions has to follow the VOC speciation used in the chemical schemes,

Deleted: the

Deleted: seen

Deleted: speciation

Deleted: where the majority of emissions occur

Deleted: although

Deleted: for the mCB05(EBI),

4.2 Hydroxyl radical (OH)

The hydroxyl radical (OH) is the primary oxidant in the atmosphere under sunlit conditions, initiating the oxidation of various VOCs, and thus the production of hydroperoxy (HO₂) and organic peroxy (RO₂) radicals. However, due to the high complexity of OH recycling pathways in atmospheric VOC degradation, the different representations of VOC oxidation pathways in chemical mechanisms may lead to significant discrepancies between models. CH₄ is routinely used as a diagnostic for the calculated OH abundance in the troposphere since its background concentration is highly sensitive to the OH abundance in the tropics, where the water vapor and the biogenic emissions are high. Uncertainties in CH₄ global sources (e.g., a rapid rise in the CH₄ growth rates since 2007; Nisbet et al., 2019) together with uncertainties in anthropogenic emissions of the NO_x, CO, and NMVOC (e.g., Hoesly et al., 2018), may cause considerable divergence in model simulated CH₄ mixing ratios, for different simulation years. For the present study, however, the surface mixing ratios of CH₄ are prescribed according to the CMIP6 recommendations for each simulation year (van Noije et al., manuscript in preparation).

Deleted: (

Deleted: is high), where

Deleted: also

Deleted: This approach is justified by the relatively long lifetime of CH₄, which allows fast global mixing of the emitted amounts.

Deleted: For this work,

Deleted: are presented in Table 5. TM5-MP simulations with the

Deleted: model

Deleted: yield

Deleted: primary

Deleted: due to

Deleted: (Reaction 3)

Deleted: in the gas-phase (Reaction

Deleted: The

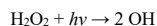
Deleted: another

Deleted: of the mechanism

Deleted: . The total OH production in the troposphere

Deleted: respective

Table 5 presents the global tropospheric OH production budgets for the various chemical configurations. The MOGUNTIA configuration yields a gas-phase OH formation via O₃ photolysis in the presence of water molecules (Reactions 3 and 4) of about 1878 Tg yr⁻¹. Additionally, the radical recycling terms (Reactions 1 and 5) contribute 1987 Tg yr⁻¹, the H₂O₂ photodissociation, i.e.,



(7)

produces 303 Tg yr⁻¹, and all other reactions add another 120 Tg yr⁻¹ to the global tropospheric OH production in the model. Overall, the total tropospheric OH production amounts to 4288 Tg yr⁻¹, which is in close agreement with the budget estimations

by Lelieveld et al. (2016), i.e., $\sim 4270 \text{ Tg yr}^{-1}$. Some difference is however expected due to the definition of the troposphere in Lelieveld et al. (2016), where they define the tropopause in the tropics using temperature, and in the extratropics using potential vorticity gradients. We remind the reader that for the present study the chemical troposphere is defined using a threshold of 150 ppb O_3 . It is striking that the OH chemical production calculated for the MOGUNTIA model set-up is much higher (28 - 35%) than for previous TM5 model configurations (i.e., 3355 ± 30 and $3184 \pm 20 \text{ Tg yr}^{-1}$) as presented by van Noije et al. (2014), using a similar 150 ppb O_3 tropopause. This difference is mainly attributed to the various updates of the model, compared to the version used in Noije et al. (2014), such as the emission database and the applied VOC representation (i.e., CMIP5; Lamarque et al. (2010) vs. CMIP6 for this study), the chemistry scheme (i.e., CB4 vs. MOGUNTIA), and the photolysis scheme (i.e., the previous implemented Landgraf et al. (1998) photolysis scheme vs. the Modified Band Approach scheme implemented by Williams et al. (2012)).

Focusing on the differences between the MOGUNTIA and the CB05(KPP) mechanism, the MOGUNTIA OH production is very close to CB05(KPP) on a global scale (Table 5). Note that for mCB05, the comparison of the two solvers indicates that EBI calculates a $\sim 1\%$ lower chemical destruction of OH in the troposphere than Rosenbrock. The contribution of the CO and CH_4 oxidation terms to the global tropospheric OH losses are calculated as 41% and 15%, respectively, for the MOGUNTIA scheme. This is slightly higher (by $\sim 6\%$ and $\sim 3\%$, respectively) compared to mCB05(KPP).

Focusing further on the MOGUNTIA scheme, the calculated tropospheric CH_4 chemical lifetime is $\sim 8.0 \text{ yr}$, as obtained through dividing the CH_4 global atmospheric mean burden ($\sim 4871 \text{ Tg}$) by the loss due to oxidation by OH radicals in the troposphere ($\sim 607 \text{ Tg yr}^{-1}$). Accounting, however, for additional CH_4 sinks due to oxidation in soils and the stratosphere with assumed lifetimes of 160 yr and 120 yr (Ehhalt et al., 2001), respectively, an atmospheric lifetime of about 7.18 yr is derived, which is roughly 15% shorter than the ensemble model mean atmospheric lifetime reported by Stevenson et al. (2006) of $8.45 \pm 0.38 \text{ yr}$.

The multi-model chemistry-climate simulations performed during the Atmospheric Chemistry and Climate Model Intercomparison Project (ACCMIP) (Naik et al., 2013; Voulgarakis et al., 2013), revealed vast diversities among models with a wide range of CH_4 chemical lifetime values (i.e., $\sim 7\text{--}14 \text{ yr}$) and a mean value of $9.7 \pm 1.5 \text{ yr}$ (i.e., 5–10% higher than observation-derived estimates). Lelieveld et al. (2016) derived a CH_4 chemical lifetime of 8.5 yr for the year 2010, and Schultz et al. (2018) estimated a tropospheric CH_4 chemical lifetime of about 9.9 yr using also an O_3 threshold of 150 ppb to define the tropopause. Finally, Lamarque et al. (2012) reported a chemical lifetime of $\sim 8.7 \text{ yr}$ by taking a tropopause level at 100 ppb O_3 .

4.3 Carbon monoxide (CO)

Table 6 presents the chemical CO budget calculated by TM5-MP for the three chemical configurations. The different model configurations show that approximately $62 \pm 1\%$ of the CO global production in the troposphere is due to the oxidation of CH_4 and NMVOC, with the remaining owing to direct emissions. Overall, the global CO budget is significantly affected by the interactions between OH and CO. Thus, changes in OH tropospheric chemical production (i.e., $\sim -0.2\%$ from mCB05(KPP) to MOGUNTIA) modulate the tropospheric secondary formation of CO from the oxidation of CH_4 and NMVOC ($\sim -10\%$ change)

Deleted: For clarity, we also note that no differences are calculated in the tropopause levels between the model configurations of this work. ...

Deleted: notable, however,

Deleted: here

Deleted: .

Deleted: ,

Deleted: speciation

Deleted: mCBM-IV

Deleted: the more detailed

Deleted: as well as

Deleted: as coupled in the model

Deleted: mCB05

Deleted: in the TM5-MP set up using the Rosenbrock solver, the

Deleted: calculated by the MOGUNTIA chemistry scheme

Deleted: also

Deleted: alone

Deleted: the

Deleted: On the other hand, the

Deleted: , which

Deleted: than using

Deleted: we arrive at

Deleted: somewhat

Deleted: demonstrated

Deleted: to

Deleted: ,

Deleted: , and

Deleted: but

Deleted: into account

and the CO chemical loss (~ -3% change) in the model. The global chemical production (i.e., the sum of chemical production terms in troposphere and stratosphere; Table 6) of CO for both the MOGUNTIA and the mCB05(KPP) chemical configurations, i.e., 2018 and 1844 Tg yr⁻¹, respectively, is however higher than the multi-model mean estimate (1505 ± 236 Tg yr⁻¹) reported by Shindell et al. (2006), which can be partially attributed to the different year of NMVOC emissions used (i.e., 2000 vs. 2006 for this work).

The dominant chemical reaction responsible for the increase in the tropospheric CO chemical production for the MOGUNTIA compared to mCB05(KPP) chemical configuration is the HCHO oxidation by OH radicals (i.e., ~1.5% increase compared to mCB05(KPP)). Indeed, although the lumped nature of the mCB05(KPP) mechanism leads to a higher tropospheric HCHO chemical production (~1896 Tg yr⁻¹) compared to MOGUNTIA configuration (~1843 Tg yr⁻¹), the HCHO tropospheric chemical destruction is calculated roughly 2% higher for the MOGUNTIA scheme. HCHO is mainly formed via the oxidation of CH₄, isoprene, and other NMVOC in the model. However, for both mCB05 configurations, the HCHO production via CH₃O₂H photolysis is calculated to be ~1.65 times higher compared to MOGUNTIA. The latter scheme seems to recycle the methyl-peroxy radical (CH₃O₂) more efficiently via the CH₃O₂ gas-phase reactions with organic peroxy radicals (RO₂) produced by higher-order NMVOC oxidation. In contrast, other higher aldehydes that represent the second most important producer of CO contribute more significantly in MOGUNTIA than in mCB05. This could be due to the more detailed representation of the higher aldehydes in the MOGUNTIA mechanism (e.g., considering the production and destruction reaction of GLY, GLYAL, and C₂H₃CHO) compared to the single lumped species (i.e., the ALD2) that represents all higher aldehydes in mCB05.

The global annual mean burden of CO for the MOGUNTIA chemical scheme is 361 Tg, almost the same as in the mCB05(KPP) configuration, but ~2 % lower compared to mCB05(EBI). Higher CO losses by OH oxidation and deposition in MOGUNTIA lead to a CO atmospheric lifetime of ~44 days, i.e., about 6% shorter compared to the mCB05(KPP) chemical mechanism. Note that the reduction in the atmospheric lifetime of CO is in line with the reduction in the atmospheric lifetime of CH₄ (~3%), reflecting overall an increase in tropospheric OH mixing ratios for the MOGUNTIA configuration compared to mCB05(KPP); i.e., higher OH levels in the atmosphere lead to a proportionally larger CO and CH₄ sinks.

Focusing further on the impact of the solver alone, we calculate roughly a 3% reduction in the CO atmospheric burden when the EBI solver is applied on the mCB05 mechanism in the model. This is directly connected to the ~1% increase in OH mixing ratios that is calculated when the Rosenbrock solver is used in the model. Furthermore, the CO tropospheric production is increased by ~0.5% in mCB05(KPP) compared to mCB05(EBI). Overall, the presented differences between the EBI and Rosenbrock solvers confirm that the choice of solver may impact on the simulated mixing ratios, owing mainly to the use of a constant versus a variable timestep in the chemistry integration (e.g., see Sandu et al., 1997).

Zonal mean CO mixing ratios at the surface for the year 2006 using the MOGUNTIA scheme are presented in Fig. 2 (a,b). Compared to mCB05(KPP), the results from MOGUNTIA show slightly higher surface CO mixing ratios (up to ~2 ppb) over highly populated regions, such as India. This regional increase is due to the differences in surface OH mixing ratios, owing mainly to the differences in NO_x chemistry between the two simulations (see also Sect. 5.2). In contrast, in South America

Deleted: total

Deleted: are

Deleted: reactions

Deleted: reduction

Deleted: chemistry are

Deleted: photolysis and OH

Deleted: 2

Deleted:).

Deleted: which

Deleted: , here,

Deleted: respective

Deleted:). Higher

Deleted: respective

Deleted: respective

Deleted: On the contrary, at

negative differences of ~5-15 ppb are calculated at the surface (Fig. 2c). The effective HO_x regeneration together with the detailed VOC representation and oxidation pathways considered in MOGUNTIA result in an increase of the surface OH mixing ratios in locations with high biogenic VOC emissions. This subsequently leads to a regional decrease in the tropospheric CO mixing ratios compared to the mCB05(KPP) configuration. Similar results are found for the zonal mean CO distribution. Free tropospheric CO mixing ratios in the tropics are also affected due to effective tropical convection. Finally, the use of different solvers for the mCB05 mechanism does not lead to any notable differences in the annual mean CO mixing ratios (Fig. 2e,f).

- Deleted: rather
- Deleted: speciation
- Deleted: the
- Deleted: scheme
- Deleted: where
- Deleted: occur, leading thus

5 Model evaluation

Model simulations are evaluated with a series of surface, flask, aircraft, and sonde measurements, as well as with satellite retrievals and climatological data. The simulated NO₂ tropospheric columns are compared with satellite retrievals from the European project Quality Assurance for Essential Climate Variables (QA4ECV) project (Boersma et al., 2017), provided by the Ozone Monitoring Instrument (OMI) and the SCanning Imaging Absorption SpectroMeter for Atmospheric CHartographY (SCIAMACHY) instruments. The simulated OH mixing ratios are evaluated against calculations of global mean tropospheric values from other modelling studies, as well as against climatological data compiled by Spivakovsky et al. (2000). Modeled O₃ mixing ratios are evaluated against surface observations and ozonesonde data for the year 2006, as compiled by the World Ozone and Ultraviolet Radiation Data Centre (WOUDC; <http://www.woudc.org>; last access 20/08/2019); surface observations from the European Monitoring Evaluation Program network (EMEP; <http://www.emep.int>; last access 20/08/2019) have been also used. For the CO model evaluation, flask observations for the year 2006 are used, as compiled by National Oceanic and Atmospheric Administration Earth System Research Laboratory, Global Monitoring Division (NOAA, <https://www.esrl.noaa.gov/gmd>; last access 20/08/2019). O₃ and CO mixing ratios in the upper troposphere/lower stratosphere (UTLS) are compared to *in-situ* measurements from the MOZAIC (Measurement of Ozone and Water Vapour by Airbus In-Service Aircraft) data record (Thouret et al., 1998). The modelled CO total columns are compared with satellite retrievals from Measurement of Pollution in the Troposphere (MOPITT) instrument, version MOP02J_V008 (Deeter et al., 2013, 2019; Ziskin, 2019), i.e., the combined thermal/near-infrared data product. Finally, light VOCs (i.e., C₂H₄, C₂H₆, C₃H₆, C₃H₈) as simulated for the year 2006 are evaluated against flask measurements from the NOAA database, and against climatological data from aircraft campaigns, as produced by Emmons et al. (2000). Overall, to quantify and discuss the model performance, commonly used statistical parameters are calculated, such as the correlation coefficient (R_p), which reflects the strength of the linear relationship between model results and observations (the ability of the model to simulate the observed variability), the absolute bias (BIAS), the normalized mean bias (NMB), and the root mean square error (RMSE) as a measure of the mean deviation of the model from the measurement due to random and systematic errors. All equations used for the statistical analysis of model results are provided in the supplementary material (Eq. S1–S5).

5.1 Nitrogen dioxide (NO₂)

NO_x is a rate-limiting precursor of O₃ formation and thus an essential species for other tropospheric oxidants, such as OH. NO_x is emitted by both natural (lightning, soils, and fires) and anthropogenic combustion sources, with lightning mainly impacting NO_x mixing ratios at the top of convective up-drafts and anthropogenic fuel emissions being the principal source of NO at the surface. Tropospheric NO₂ vertical column densities retrieved from OMI (Boersma et al., 2017) are compared against the MOGUNTIA and mCB05(KPP) simulations (Fig. 3). Note that since the differences between mCB05(EBI) and mCB05(KPP) are small for tropospheric NO₂ columns, mCB05(EBI) is not shown. NO₂ column densities are retrieved using a consistent set of retrieval parameters and validated against ground-based MAX-DOAS measurements (Boersma et al., 2018).

Deleted: here

Deleted: also

Deleted: by the model

Deleted: as well as

Deleted: model's

Deleted:)

Deleted:) and

Deleted: as well as

To consider the vertical sensitivity of the satellite measurements to NO₂ molecules at different altitudes, the tropospheric column averaging kernels, provided in the QA4ECV data product, are applied separately to both sets of modelled NO₂ vertical profiles, extracted from the hourly 3-D model output by linear and nearest-neighbor interpolation in space and time. The resulting NO₂ tropospheric column density is what would have been retrieved by the satellite if the actual vertical profile of NO₂ mixing ratios were identical to the modeled profile. The tropospheric NO₂ columns retrieved from the satellite are averaged per model grid cell and day, resulting in a comparison dataset consisting of one NO₂ vertical column density per model grid cell and day.

For the MOGUNTIA configuration, the model shows a mean overestimation of 1.78×10^{14} (R=0.71) and 1.96×10^{14} molecules cm⁻² (R=0.95) against OMI measurements for daily and annual values, respectively, performing slightly better than the correlation of mCB05(KPP) configuration (R=0.71 and R=0.94 for daily and annual values). An overview of the statistical comparison of the three model simulations against OMI measurements is given in Fig. S1a. Some discrepancies, especially in the Northern Hemisphere (NH) may be attributed to the absence of a significant seasonal cycle in monthly anthropogenic emissions. Over the biomass burning source regions in Africa, the model overestimates the satellite retrievals. When the model is compared against NO₂ tropospheric columns from the SCIAMACHY instrument using the QA4ECV retrieval (not shown), the MOGUNTIA configuration shows a similar improvement over mCB05(KPP), as with the OMI data.

Williams et al. (2017) showed that the TM5-MP model significantly underestimates the NO and NO₂ mixing ratios, both at the surface and in vertical profiles. The model satisfactorily reproduces the NO₂ mixing ratios in the boundary layer but overestimates mixing ratios at higher altitudes and in pristine environments. The MOGUNTIA scheme shows generally a better agreement with satellite retrievals compared to the mCB05(KPP) configuration, as expressed by a higher correlation coefficient and a generally lower bias (Fig. S1a). The differences between the two chemistry schemes can be mainly attributed to the representation of organic NO_x reservoir species (i.e., the organic nitrates; ORGNTRs) in the two mechanisms (Fig. S2). Overall, since deep convection may efficiently transport ORGNTRs to the upper troposphere, the more explicit representation of VOC chemistry in the MOGUNTIA chemistry scheme alters the distribution of ORGNTR compared to the more lumped chemistry of the mCB05. Although production of ORGNTR is about 10% larger in the MOGUNTIA scheme, the ORGNTR burden is dominated by the loss term (Table S4). Due to the more detailed ORGNTR representation in the MOGUNTIA scheme, the destruction becomes significantly more efficient compared to the mCB05 configuration. As a result, the global ORGNTR burden calculated using the MOGUNTIA scheme in the model is about 60% smaller.

Several modelling studies have compared the simulated NO₂ columns with *in situ* and satellite observations (e.g., Travis et al., 2016; Williams et al., 2017). These studies demonstrated an overestimate of the observed NO/NO₂ ratios compared to observations in higher altitudes, possibly due to a respective underestimate of peroxy radicals in the upper troposphere that contribute to the NO to NO₂ conversion. A deviation in the NO/NO₂ ratio has also been reported for the GEOS-Chem model (Silvern et al., 2018; Travis et al., 2016). This model significantly underestimated the observed upper tropospheric NO₂ observations from the SEAC⁴RS aircraft campaign over the southeast United States. Silvern et al. (2018) calculated that the reaction with ozone accounts for roughly 75% of the NO to NO₂ conversion in the upper troposphere; thus, this deviation from

Deleted: are nevertheless expected in such a comparison. since not

Deleted: annual

Deleted: is usually applied to

Deleted: which are the principal source of NO_x, especially in the Northern Hemisphere (NH).

Deleted: Note also that when

Deleted: again

Deleted: a significant underestimation in

Deleted: as calculated by the TM5-MP model

Deleted: , with the

Deleted: reproducing

Deleted: overestimating

Deleted: speciation

Deleted: .

Deleted: transports organic NO_x reservoir species

Formatted: Font: Times New Roman

Formatted: Font: Times New Roman

Formatted: Font: Times New Roman

Deleted: efficiently

Formatted: Font: Times New Roman

Deleted: NO_x reservoir species

Formatted: Font: Times New Roman

Deleted: , resulting in

Deleted: , with the

Deleted: to

Formatted: Font: +Body (Times New Roman)

Deleted: underestimate

the photochemical equilibrium could be due to an error in kinetic data. Overall, the authors indicated that reducing the NO₂ photolysis by 20% and increasing the low-temperature NO + O₃ reaction rate constant by 40%, improves the model simulation of the NO/NO₂ ratio in the upper tropospheric data significantly compared to the aircraft data. Another source of uncertainty could be the strength of the direct soil emissions that, according to Miyazaki et al. (2017), are lower in our model (i.e., ~5 Tg-N yr⁻¹; Yienger and Levy, 1995) compared to the emissions of 7.9 Tg-N yr⁻¹ derived using a multi-constituent satellite data assimilation.

5.2 Hydroxyl radical (OH)

Figures 4a and 4b illustrate the zonal mean tropospheric distributions of OH for two seasons (i.e., boreal winter and boreal summer) for 2006, as simulated with the MOGUNTIA chemistry scheme. The highest atmospheric mixing ratios of OH in the model are calculated in the tropics from close to surface up to roughly the tropopause, as a result of intense solar radiation and high humidity in the region, with the main OH maximum being roughly below 400 hPa (and a secondary maximum at ~300 hPa). The differences in OH zonal mean mixing ratios compared to the mCB05(KPP) configuration are presented in Figs. 4c,d. During the boreal winter, the mCB05(KPP) configuration results on average in lower OH mixing ratios in the northern subtropical lower troposphere (~3-6%) than the MOGUNTIA simulation (Fig. 4c), with the largest differences (~20-30%) around 20°-40° N. In the subtropical Southern Hemisphere (SH) during boreal summer, OH mixing ratios are on average lower (~2-3%) in the MOGUNTIA configuration than in mCB05(KPP) (Fig. 4d) almost everywhere, except for a small increase (up to 10%) at around 30° S. These small differences in OH mixing ratios are mainly related to the HO_x regeneration and differences of NO_x and ORGNTR species that influence the distribution of OH in the troposphere. The more detailed representation of ORGNTR in the MOGUNTIA chemistry scheme results in more efficient NO_x release upon the ORGNTR destruction (Table S4), leading overall to O₃ formation in remote locations, and thus to the stimulation of HO_x recycling at higher altitudes. Note that globally the NO + HO₂ reaction is roughly 9% higher in the MOGUNTIA configuration on an annual basis compared to mCB05(KPP) (see Table 5).

Focusing on global means, a global mean tropospheric OH concentration of 10.1×10^5 molecules cm⁻³ is obtained from the MOGUNTIA chemistry configuration for the year 2006, which is roughly 4% higher than in the mCB05(KPP) configuration, but closer to the low end of the multi-model mean of $11 \pm 1.6 \times 10^5$ molecules cm⁻³ as derived by Naik et al. (2013) for the year 2000, and the mean tropospheric mixing ratios of 11.3×10^5 molecules cm⁻³ as calculated by Lelieveld et al. (2016) for the year 2013. In the tropical troposphere (30°S - 30°N), the mean OH level in the MOGUNTIA configuration of 16.74×10^5 molecules cm⁻³ is ~6% higher than in mCB05(KPP). In all model configurations, higher OH mixing ratios are calculated in the NH compared to the SH, directly related to the asymmetry in the hemispheric O₃ and NO_x burdens. Figures 4e,f show the climatological mean OH mixing ratios from the surface up to ~200hPa from Spivakovsky et al. (2000), reduced by 8% based on the observed decay of methyl-chloroform mixing ratios (see Huijnen et al., 2010; van Noije et al., 2014). The mean tropospheric OH concentration for the MOGUNTIA configuration is calculated to be roughly 25% and 30% higher compared to the optimized climatology from Spivakovsky et al. (2000) for boreal winter and summer, respectively. Moreover, a ~28%

Deleted: the
Deleted: used in the model
Deleted: ,
Deleted: also

Deleted: and
Deleted: by the model for
Deleted: OH
Deleted: one
Deleted: for the two seasons are also

Deleted: higher decreases
Deleted: to be calculated at

Formatted: Font: Times New Roman
Deleted: relatively
Formatted: Font: Times New Roman
Deleted: , as well as the
Formatted: Font: Times New Roman
Deleted: the organic NO_x reservoir
Formatted: Font: Times New Roman
Deleted: production and thus the
Formatted: Font: Times New Roman
Deleted: organic NO_x reservoir species
Formatted: Font: Times New Roman
Deleted: transport of these species
Formatted: Font: Times New Roman
Deleted: higher altitudes by deep convection increasing the OH mixing ratios
Formatted: Font: Times New Roman
Deleted: Globally,
Deleted: mixing ratios, a mean
Deleted: but
Deleted: here

higher NH/SH ratio of annual mean hemispheric OH mixing ratios in the troposphere is derived for the MOGUNTIA configuration compared to Spivakovsky et al. (2000). The NH/SH ratios are calculated ~ 1.37 and ~ 1.35 for the MOGUNTIA and the mCB05(KPP) configuration, respectively, being on the high end of other modeling estimates, such as the multi-model estimate of an NH/SH ratio of 1.28 ± 0.10 by Naik et al. (2013) and the 1.20 ratio as reported by Lelieveld et al. (2016).

Deleted: Note that in this work, the

Deleted: a

Deleted: roughly 12-15% lower

Deleted: for the year 2013.

5.3 Ozone (O₃)

The evaluation of modeled O₃ mixing ratios against surface observations for the three simulations for the year 2006 is presented in Fig. 5. The seasonal cycle across surface stations is generally well captured by all model configurations for most of the cases. TM5-MP, however, generally overestimates O₃ mixing ratios at most NH sites and for all model configurations, as, for example, can be seen at the Barrow (Fig. 5a) and Mace Head (Fig. 5b) stations, especially during the summer (June-July-August, JJA) season, when O₃ is overestimated by about 8 and 3 ppb, respectively. However, at Viznar (Spain) and Mauna Loa (USA) (Figs. 5c and 5d, respectively), model results are closer to the observed O₃ mixing ratios, showing overall lower biases (i.e., ~ 1 -3 ppb). In the SH (except for the polar circle), the model simulates the seasonal cycle of the O₃ surface mixing ratios well, however, with average positive biases of ~ 6 -10 ppb in Cape Point (South Africa) and Baring Head (New Zealand) (Figs. 5e,f). At the South Pole (USA) and Sayowa (Japan) stations in Antarctica (Figs. 5g,h), the model also captures the observed seasonality well ($R = \sim 0.9$), except for a negative bias of ~ 3 ppb during the local winter season. Focusing further on the chemistry mechanisms applied in the model, a slightly better consistency is achieved for the MOGUNTIA chemistry scheme in most of the cases. For the mCB05 chemistry scheme, the choice of the solver does not result in any notable difference in simulated surface O₃ mixing ratios. Considering all surface O₃ observations available for the year 2006 (Fig. S3), the MOGUNTIA chemistry configuration tends to overestimate the available observations with a mean bias of ~ 6.5 ppb. Note that although the differences between the different chemistry configurations for surface O₃ are small, the mCB05(KPP) configuration shows the lowest bias (~ 5.2 ppb) whereas the mCB05(EBI) bias is closer to that of the MOGUNTIA configuration (~ 6.1 ppb).

Deleted: performed for this work

Deleted: in this work

Deleted: S2

Deleted: by

Ozonesonde observations are used to evaluate the models' ability to reproduce the O₃ vertical profiles. Indicatively, Fig. 6 presents the comparison of model results with ozonesonde observations in 2006 at the Hohenpeissenberg in Germany and at the Macquarie Island in the Southwestern Pacific Ocean, at five pressure levels (900 hPa, 800 hPa, 500 hPa, 400 hPa, and 200 hPa) covering the boundary layer and the low and high free troposphere. For this evaluation, all ozonesonde data have been binned to the 34 model pressure levels (see Sect. 3). The seasonal cycle at the two stations is well captured by each model configuration. For the highest model levels, above 200 hPa, all simulations are very close to the measurements, since O₃ mixing ratios are mainly determined by the upper boundary condition that is used (see Sect. 2.1). Comparisons for other WOUDC stations around the globe for the year 2006 are presented in the supplementary material (Fig. S4). Overall, all model simulations capture the O₃ distribution quite well at almost all sites in the lower troposphere. The MOGUNTIA scheme shows a slightly better agreement with observations than the mCB05 configurations with smaller biases in most of the cases, especially at lower levels (i.e. from ~ 900 hPa and up to ~ 500 hPa). Concerning the impact of the chemistry solver, the vertical O₃ concentration

Deleted: 1

Deleted: available by WOUDC

Deleted: S3

Deleted: Some differences in the model performance at the various stations are nevertheless expected due to their different characteristics such as precursor source regions and transport patterns.

simulated using the mCB05 mechanism shows no notable differences between the use of KPP and EBI in most of the cases. Overall, considering all available ozonesonde data for the year 2006 (Fig. S4), the MOGUNTIA chemistry in TM5-MP results in an overestimation of the ozonesondes observations by roughly 16% ($R = 0.96$, $BIAS = 4.7$ ppb, $NME=15.6\%$), which is slightly smaller compared to the mCB05 chemistry configurations.

Figure S5 presents a comparison of O_3 mixing ratios in the upper troposphere/lower stratosphere (UTLS) simulated by TM5-MP for the two chemistry configurations (i.e., mCB05(KPP) and MOGUNTIA) with in-situ observations from the MOZAIC airborne program (see Sect. 3.1), as a function of latitude. The accuracy of the MOZAIC O_3 measurements is ± 2 ppb (Marenco et al., 1998). For this comparison, the MOZAIC measurements are binned on the vertical grid of TM5-MP. The model evaluation at pressure levels < 300 hPa indicates there is good agreement of both configurations with the observed mixing ratios. A positive bias in April in the order of ~ 20 ppb is calculated for the model, but smaller biases are found around the tropics and in the latitudes north of $40^\circ N$ (Fig. S5a). In October (Fig. S5b), a constant positive bias of roughly 20 ppb is calculated for both configurations. This could be caused by the limited vertical resolution of this model version in the UTLS region. Note that 34 vertical levels were employed for this study with a higher resolution in the upper troposphere–lower stratosphere region. Part of the model overestimation could also be attributed to systematic errors, as also reported in previous studies (e.g., Huijnen et al., 2010). Possible causes include cumulative effects such as a lack of a diurnal or weekly variation in the NO_x emissions from the road transport sector, an underestimation of surface deposition during summer, or errors in the representation of nocturnal boundary layer dynamics (e.g., see Williams et al., 2012).

5.4 Carbon monoxide (CO)

Figure 7 presents the model performance concerning surface CO mixing ratios, by comparing a series of flask observations for the year 2006. CO is underestimated at most sites in the NH for all TM5-MP configurations, e.g., at the Barrow Observatory and Mace Head station (Figs. 7a,b), especially during boreal spring (March–April–May, MAM), by about 30 ppb on average. In the tropics, negative biases (~ 16 –20 ppb) are observed at Mauna Loa and Mahe Island (Figs. 7c,d). At other stations in the SH, the model simulates the CO surface mixing ratios well with both positive and negative biases depending on the season (Figs. 7e,f). In Antarctica, at the South Pole and Sayowa stations (Figs. 7g,h), the model also shows a small positive bias up to ~ 3 ppb during the local winter season. The seasonal cycle across stations is generally well captured by all model's chemistry configurations (i.e., $R = 0.7$ – 0.9). The full set of CO comparisons with flask data is further presented in the supplement (Fig. S6). Overall, the MOGUNTIA and the mCB05(KPP) configurations underestimate the flask observations for the year 2006 with a negative bias of around 30 ppb, and with a correlation coefficient for both configurations of $R=0.45$. Notably, the mCB05(EBI) model configuration tends to produce lower biases in the SH, where the emission strengths are in general low, compared to the other two configurations (i.e., approximately -3 vs. -4 and -5 ppb for mCB05(KPP) and MOGUNTIA, respectively). In contrast, the MOGUNTIA chemistry configuration results in lower biases in the NH where the majority of anthropogenic emissions occur (i.e., approximately -30 vs. -31 and -33 ppb for mCB05(EBI) and mCB05(KPP), respectively).

Deleted: S4 further...5 presents a comparison of O_3 mixing ratios [1]
Formatted ... [2]
Deleted: a
Formatted ... [3]
Deleted: of
Formatted ... [4]
Deleted: clearly seen at
Formatted ... [5]
Deleted: S4a). The negative model bias in the tropical UTLS po [6]
Formatted ... [7]
Deleted: ~
Formatted ... [8]
Deleted: in October (Fig. 4Sb), although the variability is ... [9]
Formatted ... [10]
Deleted: ; note
Formatted ... [11]
Deleted: can
Formatted ... [12]
Deleted: a
Formatted ... [13]
Deleted: error,
Formatted ... [14]
Deleted: presented
Formatted ... [15]
Deleted: , caused possibly by
Formatted ... [16]
Deleted: ,
Formatted ... [17]
Deleted: missing
Formatted ... [18]
Deleted: , or a weak convective mixing out of the boundary layer
Formatted ... [19]
Deleted:
Deleted: three ...odel's chemistry configurations (i.e., $R = 0.7$ - [20]
Formatted ... [21]
Deleted: (
Formatted ... [22]
Deleted:) compared to the other two configurations that use the [23]
Formatted ... [24]
Deleted: (
Formatted ... [25]
Deleted:), where the majority of emissions occur.

Total CO columns from the MOGUNTIA and the mCB05(KPP) model configurations are compared to the total column densities retrieved from the MOPITT satellite instrument (Deeter et al., 2013, 2019; Ziskin, 2019) for the year 2006 (Fig. 8). Co-sampling with averaging kernel has been applied to the modelled CO concentration profiles (i.e., in the same manner as for NO₂; see Sect. 5.1). Note that when the absolute difference in surface pressure between the MOPITT retrieval and the TM5-MP simulation is larger than 5 hPa, the measurements were excluded from the comparison. For the MOGUNTIA configuration, the model shows a mean underestimation of -8.54×10^{16} (R=0.82) and -1.18×10^{17} molecules cm⁻² (R=0.91) compared to daily and annual averages of MOPITT data, respectively. However, the correlation is slightly improved compared to the mCB05(KPP) configuration (R=0.78 and R=0.88 for daily and annual values, respectively). As in the comparison with surface data, the biases in total column CO in the MOGUNTIA and mCB05(KPP) configurations deteriorated compared to the mCB05(EBI) configuration, albeit biases are still small (~5% and ~7% for daily and annual values, respectively). As this pattern can be seen in both KPP configurations, this difference seems to be caused by the implementation of the more accurate Rosenbrock solver. An overview of the statistical comparison of the three model configurations against MOPITT CO measurements is given in Fig. S1b.

Figure S5 further presents the comparison of CO mixing ratios in the upper troposphere/lower stratosphere (UTLS) simulated by TM5-MP with *in-situ* measurements from the MOZAIC airborne program (see Sect. 3.1). Model evaluation at pressure levels < 300 hPa shows a good correlation for both configurations in the SH, with a small positive bias (up to ~20 ppb) for the mCB05(KPP) configuration in April around the equator and a small negative bias (~10 ppb) for the MOGUNTIA configuration for latitudes below 10°N. Both configurations present a strong negative bias (~30 ppb) for latitudes above 20°N (Fig. S5c). In October (Fig. S5d), both the mCB05(KPP) and MOGUNTIA configurations tend to underestimate the observations with a negative bias of ~20 ppb, except for a small positive bias between 0-20°N. This positive model bias in the UTLS could point to a stronger convective uplift (e.g., Krol et al., 2018) in tropical Africa in April, or to possible misrepresentations of biomass burning emission strengths and horizontal and vertical distributions (e.g., Daskalakis et al., 2015; Nechita-Banda et al., 2018). Indeed, MOZAIC data show an increase in CO mixing ratios from the NH (April) to the SH (October), mainly due to the impact of biomass burning processes. Overall, the model configurations of this work present both positive and negative biases compared to the MOZAIC observations, with observations indicating larger latitudinal CO variability than simulated.

5.5 Volatile organic compounds (VOCs)

5.5.1 Ethane and propane

Ethane (C₂H₆) is the lightest alkane with emissions primarily of anthropogenic origin, associated mainly with fossil fuel extraction and use. In the model, the global ethane emission is 11 Tg yr⁻¹ (Table 3) with an atmospheric lifetime of about 56 days for all chemistry configurations, in close agreement with other studies (e.g., Hodnebrog et al., 2018). Flask measurements indicate that C₂H₆ surface mixing ratios are strongly underestimated by all configurations at Mace Head (Fig. 9a) by ~80%, mainly during the winter, indicating also an opposite annual cycle. The latter can be attributed to the misinterpretation of

Deleted: Figure S4 further presents the comparison of CO mixing ratios in the upper troposphere/lower stratosphere (UTLS) simulated by TM5-MP with the *in-situ* measurements from the MOZAIC data (see Sect. 3.1). Model evaluation at pressure levels < 300 hPa shows a positive bias for mCB05(KPP) configuration in April of the order of ~20 ppb and a small negative bias (~10 ppb) for the MOGUNTIA for latitudes below 10°N, but a negative bias for both simulations for latitudes above 20°N (Fig. S4c). For October, both configurations show a good correlation for the SH, with a negative bias (~20 ppb) for latitudes above 20°N (Fig. S4d). However, a strong positive bias of roughly 30 ppb is simulated in the tropics, for latitudes up to 20°N. The positive model bias in the UTLS in the tropics could point to an excessively strong convective uplift in tropical Africa in April, and/or during the summer monsoon over Southern Asia in October. The model shows both positive and negative biases compared to the MOZAIC observations, with the observations exhibiting larger latitudinal CO variability. This might also point to a possible misrepresentation of biomass burning emissions that are generally uncertain. Overall, and also considering the respective O₃ evaluation, this suggests that the MOGUNTIA chemistry scheme tends to slightly better simulate the chemical composition of the troposphere at remote locations away from direct emission sources and improves upon the mCB05 scheme.

Deleted: configuration

seasonal variation of anthropogenic emission and/or to the C₂H₆ oxidation by OH radicals in the model. Significant underestimations are also observed in the tropics at Mauna Loa, Hawaii (Fig. 9c), of roughly 98% ($R \approx -0.5$). In contrast, at Cape Grim, Australia (Fig. 9e), the model is better reproducing the measured C₂H₆ mixing ratios for all configurations, with a higher correlation coefficient ($R = 0.5$) and an NME of around 63%.

The underestimation of the C₂H₆ mixing ratio likely indicates that the model lacks primary emissions of C₂H₆ and can thus better reproduce atmospheric observations in the SH where the anthropogenic emissions are not as strong as in the NH. Dalsøren et al. (2018) showed recently that an increase of natural and anthropogenic fossil fuel emissions by a factor of two to three may significantly improve the simulated C₂H₆ and C₃H₈ mixing ratios compared to observations. Note that this increase in emissions would result in source estimates close to those calculated by the first global 2-D modeling study of these two hydrocarbons by Kanakidou et al. (1991). To investigate, here, how the model responds to an increase of ethane emissions, sensitivity simulations with the MOGUNTIA configuration are performed by 1) doubling and 2) quadrupling the anthropogenic C₂H₆ fossil fuel emissions, resulting in total C₂H₆ emissions of ~17.1 Tg yr⁻¹ and ~29.5 Tg yr⁻¹, respectively. The global tropospheric burdens have been also increased by a factor of ~1.4 and 2.2, respectively. The comparison, however, with the with flask data (Fig. S7) indicates that the increase of C₂H₆ anthropogenic emissions does not significantly affect the simulated mixing ratios in the model at these specific stations. Overall, this means that even a more aggressive increase of emissions (at least over specific regions) is required, other missing sources are needed to be considered in the model, or that the oxidation of C₂H₆ is too fast in the model. The full set of C₂H₆ comparisons with flask data is presented in the supplement (Fig. S8).

Propane (C₃H₈) is also emitted mainly from anthropogenic sources, and in the current simulations the total emission is 8.5 Tg yr⁻¹ (Table 3), lower compared to other reported emission estimates of ~15 Tg yr⁻¹ (Jacob et al., 2002). Model comparison with flask observations (Fig. 9) shows that the model tends to underestimate the measured mixing ratios for all simulations, however, with higher correlation coefficients compared to C₂H₆ in most of the cases. C₃H₈ is underestimated in the NH at Mace Head (Fig. 9b) during the winter and autumn seasons by 72-74%. In the tropics, strong negative biases of ~100 ppt are observed at Mauna Loa (Fig. 9d). However, the model simulates the C₃H₈ surface mixing ratios better in the SH at Cape Grim compared to stations in the NH (Figs. 9b,d,f) due to the weaker impact of anthropogenic emissions. In contrast to the C₂H₆ evaluation however, the model satisfactorily simulates the observed C₃H₈ mixing ratios at the South Pole (Fig. 9h), with a small overestimation during the local summer season. The full set of C₃H₈ comparisons with flask data is presented in Fig. S9. As for the case of C₂H₆, to further investigate the impact of emissions on the simulated C₃H₈ mixing ratios, additional simulations are performed by 1) doubling and 2) quadrupling the anthropogenic fossil fuel emissions, resulting overall in total C₃H₈ emissions of ~14.9 Tg yr⁻¹ and ~27.9 Tg yr⁻¹, respectively. The global C₃H₈ tropospheric burdens have been increased by a factor of ~1.7 and 3.2, respectively. Figure S7 indicates that an increase of C₃H₈ emissions by two times tends to significantly improve the model simulations, whereas a respective increase by four times tends to overestimate the observed mixing ratios. Comparison with C₂H₆ and C₃H₈ aircraft climatological data (Fig. 10) further indicates that all chemistry configurations tend to underestimate the observed mixing ratios (~20-60%) in most of the cases, especially in the upper troposphere. In more

Deleted: capable of

Deleted: This

Deleted: , it can

Deleted: The full set of C₂H₆ comparisons with flask data is presented in the supplement (Fig. S6)

Formatted: Font: Times New Roman

Deleted: appearing here however

Deleted: also

Deleted: , as for C₂H₆.

Deleted: satisfactory

Deleted: however of the measured mixing ratios during the local summer season. The full set of C₂H₆ comparisons with flask data is also presented in Fig. S7.

detail, at Boulder and East Brazil, the model significantly underestimates the observed mixing ratios for both compounds, while at Hawaii, C₂H₆ is underestimated, but C₃H₈ is well simulated by all three configurations. In contrast, at Easter Island, all schemes overestimate the observed mixing ratios for both compounds, although the MOGUNTIA overestimate is larger for C₂H₆ and lower for C₃H₈ compared to the two mCB05 configurations. The full sets of C₂H₆ and C₃H₈ comparisons with aircraft climatological data are presented in the supplement (Fig. S10 and Fig. S11, respectively). Overall, considering that the model reasonably simulates the oxidative capacity of the atmosphere, direct emissions are the likely reason for these differences, since both alkanes are oxidized in the troposphere by OH radicals and no secondary production terms of these alkanes are known. Note, however, that alkane emission fluxes are on the low side, as also reported by other studies (e.g., Aydin et al., 2011; Huijnen et al., 2019; Monks et al., 2018).

5.5.2 Ethene and propene

Ethene is mainly emitted from biogenic sources, as well as by the incomplete combustion from biomass burning, power plants, and combustion engines. C₂H₄ emissions in the model are roughly 30 Tg yr⁻¹ (Table 3), close to the estimate of Huijnen et al. (2019), but on the high side compared to the 21 Tg yr⁻¹ reported by Toon et al. (2018). The three chemistry configurations produce similar mixing ratios of C₂H₄ in most of the cases. Nevertheless, the comparison with aircraft observations (Fig. 11) indicates underestimated mixing ratios in the upper troposphere. In more detail, the model reproduces well (R=0.97) the vertical distribution of C₂H₄ at Boulder (USA). However, observed mixing ratios close to the surface (up to ~ 2 km) are overestimated by the model, while observations at the higher levels (up to ~ 6 km) are underestimated. In the tropics, the observed mixing ratios in the lower and upper troposphere (e.g., at Hawaii) are slightly overestimated by the model for all configurations, although for the MOGUNTIA configuration this overestimate is the lowest. In remote regions, where the impact of direct emissions is negligible (e.g., at the Easter Island), the model overestimates C₂H₄ close to the surface (~1 km), but some negative biases appear aloft. At higher altitudes, however, all configurations overestimate the observed C₂H₄ mixing ratios (Fig. 11g), but again the MOGUNTIA model configuration better reproduces the observations. Overall, these deviations from the observations could be attributed to 1) the not well-resolved background concentrations by the model, 2) the severe uncertainties in emission fluxes, and 3) a not well-understood chemistry (e.g., Huijnen et al., 2019; Pozzer et al., 2007), such as the C₂H₄ production during the VOC decomposition in the atmosphere.

Propene (C₃H₆) emissions in the model are ~32 Tg yr⁻¹ (Table 3). The two mCB05 configurations produce similar C₃H₆ mixing ratios, but the MOGUNTIA tends to simulate higher values, especially in the tropics, at Hawaii (Fig. 11d) and at East Brazil (Fig. 11f). Close to the surface, where the impact of the emissions is stronger, the model severely overestimates observations (Figs. d,f), except for Japan (Fig 11b). For the MOGUNTIA configuration, this overestimation is more substantial in the tropics compared to the mCB05 chemistry scheme. An overestimation of the observed mixing ratio close to the surface is also found in other regions, especially in the SH, such as in Eastern Brazil (Fig. 11f) or in remote regions, where the direct impact of emissions is negligible, such as in the Easter Island (Fig. 11h). However, at Easter Island (Fig. 11h), the model fails to reproduce the observed C₃H₆ vertical profile, resulting in a significant underestimation of the observed mixing ratios. Overall,

Deleted: the
Deleted: the
Deleted: On the contrary
Deleted: overestimates higher the
Deleted: but
Deleted: the
Deleted: further
Deleted: S8
Deleted: S9
Deleted: should be
Deleted: not any
Deleted: alkanes
Deleted: in the model should be considered
Deleted: suggested
Deleted: in the literature
Deleted: For this work,
Deleted: account for
Deleted: however
Deleted: TM5-MP.
Deleted: significantly
Deleted: for all model configurations, especially
Deleted: (~10 km) at almost all locations.
Deleted:) (R=0.97), however, it overestimates the
Deleted: and underestimates
Deleted: for all configurations, with an average positive bias of around 5 ppt.
Deleted: model underestimates the
Deleted: by roughly 25 ppt
Deleted: underestimations can
Deleted: also
Deleted: underestimated
Deleted: , because of
Deleted: or even due to
Deleted: For propene
Deleted:),
Deleted: in TM5-MP
Deleted: mixing ratios
Deleted: However, close
Deleted: This can be attributed to the more involved chemistry [26]
Deleted: shown

even though the evaluation of vertical profiles should be considered [here](#) only as a climatological comparison, the reason for the model underestimation of C_3H_6 mixing ratios at higher altitudes, is likely a combination of the emission strengths, the simulated vertical distribution, and the potential but still unaccounted secondary production from higher VOC oxidation. All comparisons for C_2H_4 and C_3H_6 with aircraft climatological data are presented in [Figs. S12](#) and [S13](#), respectively.

Deleted: calculated

Deleted: Fig. S10

Deleted: Fig. S11

6. Summary and conclusions

This study documents and evaluates the implementation of the tropospheric chemistry scheme MOGUNTIA in the global chemistry and transport model TM5-MP. The MOGUNTIA scheme is a comprehensive gas-phase chemistry mechanism that explicitly accounts for the oxidation of light hydrocarbons, coupled with an updated representation of isoprene oxidation, along with a simplified representation of terpenes and aromatics chemistry. The newly coupled chemistry scheme in TM5-MP is compared to the existing chemistry scheme of the model, the mCB05. Another feature implemented in the TM5-MP chemistry code is the Rosenbrock solver, that replaces the classical EBI method. For this, a simple preprocessor directive has been implemented in the model to choose between the two solvers during model compilation. In the case of the Rosenbrock solver, the KPP software has been used to generate the chemistry code coupled with the TM5-MP. To further examine the impact of the solver on the TM5-MP atmospheric simulations and performance, the mCB05 scheme is also tested using the Rosenbrock solver.

Global budgets of O₃, CO, and OH, for all simulations performed for this work, are calculated and compared with estimates published in the literature. In more detail, the O₃ budget calculated with the MOGUNTIA chemistry scheme falls within one standard-deviation of mean estimates from other modelling studies. However, the new MOGUNTIA scheme reduces the tropospheric O₃ burden by ~3% compared to the mCB05 configurations. For tropospheric CO, a respective reduction in the atmospheric lifetime (~6%) provides evidence that the implementation of the MOGUNTIA chemistry leads to an increase in the oxidative capacity of the troposphere in TM5-MP. This also holds for the atmospheric CH₄ chemical lifetime that is calculated here to be about 8.0 yr for the MOGUNTIA chemistry scheme, which is roughly 3-5% shorter compared to mCB05(KPP) and mCB05(EBI) configurations.

The large-scale variability in space and time of modeled tropospheric NO₂, OH, O₃, CO, and light VOCs (i.e., C₂H₆, C₂H₄, C₃H₈, C₃H₆) has been evaluated for the year 2006 and compared to several sets of in-situ observations, satellite retrievals, and climatological data. Overall, both the lumped-structure (i.e., the mCB05) and the lumped-molecule (i.e., the MOGUNTIA) mechanisms appear to be able to satisfactorily represent the tropospheric chemistry. In most of the cases, lower biases compared to measurements are calculated when the MOGUNTIA chemistry configuration is used. The model simulates well the major observed features of the spatial and temporal variability in surface observations for O₃ and CO. The observed background surface O₃ mixing ratios are captured with a bias of ~6.5 ppb for the MOGUNTIA configuration, very close to the mCB05 configurations. Ozone in the vertical matches on average within ~5 ppb for all configurations, and the model is able to capture well the variability observed by ozone sondes. In contrast, the model underestimates the available CO flask observations by roughly 30% for all configurations, most likely linked to uncertainties in the seasonal cycle of anthropogenic emissions and the representation of biomass burning CO emissions. For the model comparison with observed light VOC mixing ratios, all chemistry configurations clearly show that significant uncertainties still exist regarding their emission strength or poorly understood chemistry, such as the secondary chemical production during the decomposition of higher VOC in the atmosphere. Sensitivity simulations performed indicate that increases of emissions may improve the simulation of the

Deleted: detailed

Deleted: scheme

Deleted: replacing

Deleted: , as well as an intermediate step between the existing and new chemistry version of the model

Deleted: with

Deleted: however,

Deleted: model uses the

Deleted: generally produces lower biases compared to measurements...

Deleted: well. On the other hand, for all configurations,

Deleted: %,

Deleted: in the model

Deleted: not well-

atmospheric mixing ratios of some light VOCs, such as the C₃H₈. However, our results suggest that changes in emissions should not just be based on fixing the model's emissions using a specific (constant) value, but that scientifically accepted methods should be used. Future studies should therefore aim at improving source estimates and a better understanding of the processes that govern the budgets of light VOCs. From a chemistry point of view, it would be interesting to study the chemical formation pathways from higher VOCs. Inverse modelling or data-assimilation studies might be also used to "optimize" the emissions in order to minimize the differences between observations and model simulations.

The presented model configurations result in a benchmark of the TM5-MP tropospheric chemistry version upon which future model improvements may take place. Inherent uncertainties need to be reduced and further work is required, focusing mainly on the most poorly understood chemistry-related processes. For example, further attention concerns the uncertainties in NO₂-O₃ cycling along with the atmospheric fate of ORGNTRs and their impacts on the oxidative capacity of the troposphere. Attention is also needed for the treatment of aerosols and clouds, in particular ice clouds and their impact on photolysis frequencies. Other issues that need to be resolved are related to the significant uncertainties in light hydrocarbons mixing ratios – as clearly noticed by the model comparison to surface and aircraft observations – and their potential impact on the oxidative capacity of the troposphere. Considering that both chemistry schemes underestimate light VOCs mixing ratios in most of the cases, the use of a more detailed scheme such as the MOGUNTIA will allow us to better understand the causes of this deviation compared to the lumped representation of VOC chemistry in the mCB05 mechanism. This is especially relevant over tropical regions with high biogenic VOC emissions under low-NO_x conditions. For this, a more dedicated comparison of the model with *in-situ* observations and satellite retrievals is needed. MOGUNTIA contains also an ample number of oxygenated VOCs that are observed in the atmosphere at significant levels and further involved in aerosol formation, making the scheme appropriate for detailed studies. On top of this, the implementation of the KPP software in the model makes the code a lot more flexible for chemistry updates compared to the previous EBI-based chemistry versions. The use of the KPP in TM5-MP reduces the uncertainties in solving stiff chemistry equations and opens up new possibilities on model development, such as the construction of an adjoint of the chemistry mechanism that can be used in 4D-VAR data assimilation systems (e.g., Henze et al., 2007). Another possible application is to more accurately explore atmospheric chemistry-climate interactions, since TM5-MP is also coupled to the Earth System Model EC-Earth (e.g., Van Noije et al., 2014; Van Noije et al., manuscript in preparation). Note, however, that despite the clear benefits regarding code development and management, the use of a more sophisticated solver such as the Rosenbrock, and the implementation of a detailed chemistry scheme such as the MOGUNTIA, make the code computationally more expensive. Overall, this work shows that the newly coupled chemistry version of TM5-MP works as good – or better in some of the cases – as the previous chemistry versions of the model, opening opportunities for further chemistry developments and more detailed tropospheric investigations by the TM and EC-Earth communities.

Formatted: Justified, Line spacing: 1.5 lines

Deleted: resulted organic NO_x reservoirs formation

Deleted: , as well as

Deleted: rates

Deleted: needed

Deleted: ,

Deleted: , thus,

Deleted: , however,

Deleted: a

Deleted: as

Deleted: CB05

Deleted: , e.g.,

Deleted: planned to be performed in the future.

Deleted: thus

Deleted: use of this

Deleted: such

Deleted: to construct

Deleted: the

Deleted: system of the model

Deleted: , or even

Deleted: On the other hand, and

Deleted: solver

Deleted: unavoidably

Deleted: , as indicated here by increases of the model's performance (i.e., ~18% and ~27%, respectively).

Deleted: ,

Deleted: ,

Deleted: giving confidence to

Deleted: ¶

Deleted: from

Code availability. The TM5-MP code used for this study can be downloaded from Zenodo (doi: 10.5281/zenodo.3759200); a request to generate a new user account for access the SVN server hosted at KNMI, the Netherlands, can be made by e-mailing to P. Le Sager (sager@knmi.nl). Any new user groups need to agree to the protocol set out for use, where it is expected that any developments are accessible to all users after the publication of results. Attendance at 9-monthly TM5 international meetings is encouraged to avoid duplicity and conflict of interests.

Deleted: 3759201

Supplement. The Supplement related to this article is available online.

Competing interests. The authors declare that they have no conflict of interest.

Author contributions. This paper resulted from the deliberations of 27th International TM5 Meeting, 28-29 June 2018, Utrecht, the Netherlands (SM, MCK, TvN, PLS, SH, ND, MK). SM and MCK developed the chemistry code coupled to the model. SM and MK provided the original chemistry scheme equations. JEW developed both the photolysis code and mCB05 chemical mechanism, including the implementation of updated photolysis frequencies for the additional organics included in the MOGUNTIA chemistry scheme. AG contributed to reaction data updates and coupling. AH developed and provided model evaluation tools with satellite retrievals. VH provided model evaluation tools and a collection of observation data. SM, ND, AH, and PLS performed the model evaluation. SM wrote the manuscript and all authors contributed to the preparation of this paper.

Acknowledgements. Stelios Myriokefalitakis acknowledges financial support for this research from the European Union's Horizon 2020 research and innovation programme under the Marie Skłodowska-Curie grant agreement no. 705652 – ODEON. Maarten C. Kroll is supported by the European Research Council (ERC) under the European Union's Horizon 2020 research and innovation programme under grant agreement no. 742798 – COS-OCS. Stelios Myriokefalitakis and Angelos Gouvousis acknowledge financial support from the National Observatory of Athens research grant (no. 5065 - Atmospheric Deposition Impacts on the Ocean System). Maria Kanakidou and Nikos Daskalakis acknowledge funding by the Deutsche Forschungsgemeinschaft (DFG, German Research Foundation) under Germany's Excellence Strategy (University Allowance, EXC 2077, University of Bremen). Model development was carried out on the Greek Research & Technology Network (GRNET) in the National HPC facility ARIS, the Dutch national e-infrastructure with the support of the SURF Cooperative and the ECMWF CRAY XC40 high-performance computer facility. Model simulations were performed at the GRNET HPC ARIS and the AETHER HPC cluster at the University of Bremen, funded by DFG within the scope of the Excellence Initiative. MOPITT CO data were obtained from the NASA Langley Research Center Atmospheric Science Data Center. NO₂ and HCHO satellite data from OMI and SCIAMACHY were produced in the scope of the European FP7 project QA4ECV (grant no. 6007405). This paper is dedicated to the memory of Dr. Andreas Hilboll.

Deleted: Kroll

References

- Aan de Brugh, J. M. J., Schaap, M., Vignati, E., Dentener, F., Kahnert, M., Sofiev, M., Huijnen, V. and Krol, M. C.: The European aerosol budget in 2006, *Atmos. Chem. Phys.*, 11(3), 1117–1139, doi:10.5194/acp-11-1117-2011, 2011.
- Andres, R. J. and Kasgnoc, A. D.: A time-averaged inventory of subaerial volcanic sulfur emissions, *J. Geophys. Res.*, 103(D19), 25251, doi:10.1029/98JD02091, 1998.
- Atkinson, R.: Gas-Phase Tropospheric Chemistry of Volatile Organic Compounds: 1. Alkanes and Alkenes, *J. Phys. Chem. Ref. Data*, 26(2), 215–290, doi:10.1063/1.556012, 1997.
- Atkinson, R.: Atmospheric chemistry of VOCs and NO_x, *Atmos. Environ.*, 34(12–14), 2063–2101, doi:10.1016/S1352-2310(99)00460-4, 2000.
- Atkinson, R., Baulch, D. L., Cox, R. A., Crowley, J. N., Hampson, R. F., Hynes, R. G., Jenkin, M. E., Rossi, M. J. and Troe, J.: Evaluated kinetic and photochemical data for atmospheric chemistry: Volume II - gas phase reactions of organic species, *Atmos. Chem. Phys.*, 4(11), 1461–1738, doi:10.5194/acp-4-1461-2004, 2004.
- Aydin, M., Verhulst, K. R., Saltzman, E. S., Battle, M. O., Montzka, S. A., Blake, D. R., Tang, Q. and Prather, M. J.: Recent decreases in fossil-fuel emissions of ethane and methane derived from firm air, *Nature*, 476(7359), 198–201, doi:10.1038/nature10352, 2011.
- Baboukas, E. D., Kanakidou, M. and Mihalopoulos, N.: Carboxylic acids in gas and particulate phase above the Atlantic Ocean, *J. Geophys. Res. Atmos.*, 105(D11), 14459–14471, doi:10.1029/1999JD900977, 2000.
- Bloss, C., Wagner, V., Bonzanini, A., Jenkin, M. E., Wirtz, K., Martin-Reviejo, M. and Pilling, M. J.: Evaluation of detailed aromatic mechanisms (MCMv3 and MCMv3.1) against environmental chamber data, *Atmos. Chem. Phys.*, 5(3), 623–639, doi:10.5194/acp-5-623-2005, 2005.
- Boersma, K. F., Eskes, H., Richter, A., De Smedt, I., Lorente, A., Beirle, S., Van Geffen, J., Peters, E., Van Roozendaal, M. and Wagner, T.: QA4ECV NO₂ tropospheric and stratospheric vertical column data from SCIAMACHY (Version 1.1) [Data set], *R. Netherlands Meteorol. Inst.*, doi:10.21944/qa4ecv-no2-omi-v1.1, 2017.
- Boersma, K. F., Eskes, H. J., Richter, A., De Smedt, I., Lorente, A., Beirle, S., van Geffen, J. H. G. M., Zara, M., Peters, E., Van Roozendaal, M., Wagner, T., Maasakkers, J. D., van der A, R. J., Nightingale, J., De Rudder, A., Irie, H., Pinardi, G., Lambert, J.-C. and Compernelle, S. C.: Improving algorithms and uncertainty estimates for satellite NO₂ retrievals: results from the quality assurance for the essential climate variables (QA4ECV) project, *Atmos. Meas. Tech.*, 11(12), 6651–6678, doi:10.5194/amt-11-6651-2018, 2018.
- Bouwman, A. F., Lee, D. S., Asman, W. A. H., Dentener, F. J., Van Der Hoek, K. W. and Olivier, J. G. J.: A global high-resolution emission inventory for ammonia, *Global Biogeochem. Cycles*, 11(4), 561–587, doi:10.1029/97GB02266, 1997.
- Bregman, B., Segers, A., Krol, M., Meijer, E. and Van Velthoven, P.: On the use of mass-conserving wind fields in chemistry-transport models, *Atmos. Chem. Phys.*, 3(2), 447–457, doi:10.5194/acp-3-447-2003, 2003.
- Browne, E. C., Wooldridge, P. J., Min, K.-E. and Cohen, R. C.: On the role of monoterpene chemistry in the remote continental

- p>boundary layer,
- Atmos. Chem. Phys.*
- , 14(3), 1225–1238, doi:10.5194/acp-14-1225-2014, 2014.
p>de Bruine, M., Krol, M., van Noije, T., Le Sager, P. and Röckmann, T.: The impact of precipitation evaporation on the atmospheric aerosol distribution in EC-Earth v3.2.0,
- Geosci. Model Dev. Discuss.*
- , 1–34, doi:10.5194/gmd-2017-259, 2017.
p>Cai, C., Kelly, J. T., Avise, J. C., Kaduwela, A. P. and Stockwell, W. R.: Photochemical Modeling in California with Two Chemical Mechanisms: Model Intercomparison and Response to Emission Reductions,
- J. Air Waste Manage. Assoc.*
- , 61(5), 559–572, doi:10.3155/1047-3289.61.5.559, 2011.
p>Carter, W. P. L.: Computer modeling of environmental chamber measurements of maximum incremental reactivities of volatile organic compounds,
- Atmos. Environ.*
- , 29(18), 2513–2527, doi:10.1016/1352-2310(95)00150-W, 1995.
p>Carter, W. P. L.: Development of a condensed SAPRC-07 chemical mechanism,
- Atmos. Environ.*
- , 44(40), 5336–5345, doi:10.1016/j.atmosenv.2010.01.024, 2010.
p>Christian, T. J., Kleiss, B., Yokelson, R. J., Holzinger, R., Crutzen, P. J., Hao, W. M., Saharjo, B. H. and Ward, D. E.: Comprehensive laboratory measurements of biomass-burning emissions: 1. Emissions from Indonesian, African, and other fuels,
- J. Geophys. Res.*
- , 108(D23), 4719, doi:10.1029/2003JD003704, 2003.
p>Crounse, J. D., Paulot, F., Kjaergaard, H. G. and Wennberg, P. O.: Peroxy radical isomerization in the oxidation of isoprene,
- Phys. Chem. Chem. Phys.*
- , 13(30), 13607, doi:10.1039/c1cp21330j, 2011.
p>Crutzen, P. J.: Photochemical reactions initiated by and influencing ozone in unpolluted tropospheric air,
- Tellus*
- , 26(1–2), 47–57, doi:10.1111/j.2153-3490.1974.tb01951.x, 1974.
p>Curtis, A. R. and Sweetenham, W. P.: Facsimile/Chekmat User's Manual, Tech. rep., Oxfordshire, Great Britain., 1987.
p>Dalsøren, S. B., Myhre, G., Hodnebrog, Ø., Myhre, C. L., Stohl, A., Pissò, I., Schwietzke, S., Höglund-Isaksson, L., Helmig, D., Reimann, S., Sauvage, S., Schmidbauer, N., Read, K. A., Carpenter, L. J., Lewis, A. C., Punjabi, S., Wallasch, M., Hodnebrog, Ø., Myhre, C. L., Stohl, A., Pissò, I., Schwietzke, S., Höglund-Isaksson, L., Helmig, D., Reimann, S., Sauvage, S., Schmidbauer, N., Read, K. A., Carpenter, L. J., Lewis, A. C., Punjabi, S. and Wallasch, M.: Discrepancy between simulated and observed ethane and propane levels explained by underestimated fossil emissions,
- Nat. Geosci.*
- , 11(3), 178–184, doi:10.1038/s41561-018-0073-0, 2018.
p>Damian, V., Sandu, A., Damian, M., Potra, F. and Carmichael, G. R.: The kinetic preprocessor KPP-a software environment for solving chemical kinetics,
- Comput. Chem. Eng.*
- , 26(11), 1567–1579, doi:10.1016/S0098-1354(02)00128-X, 2002.
p>Daskalakis, N., Myriokefalitakis, S. and Kanakidou, M.: Sensitivity of tropospheric loads and lifetimes of short lived pollutants to fire emissions,
- Atmos. Chem. Phys.*
- , 15(6), 3543–3563, doi:10.5194/acp-15-3543-2015, 2015.
p>Dee, D. P., Uppala, S. M., Simmons, A. J., Berrisford, P., Poli, P., Kobayashi, S., Andrae, U., Balmaseda, M. A., Balsamo, G., Bauer, P., Bechtold, P., Beljaars, A. C. M., van de Berg, L., Bidlot, J., Bormann, N., Delsol, C., Dragani, R., Fuentes, M., Geer, A. J., Haimberger, L., Healy, S. B., Hersbach, H., Hólm, E. V., Isaksen, I., Kållberg, P., Köhler, M., Matricardi, M., McNally, A. P., Monge-Sanz, B. M., Morcrette, J.-J., Park, B.-K., Peubey, C., de Rosnay, P., Tavolato, C., Thépaut, J.-N., Vitart, F., Berg, L., Van De, Bidlot, J., Bormann, N., Delsol, C., Dragani, R., Fuentes, M., Geer, A. J. and Dee, D. P.: The ERA-Interim reanalysis: configuration and performance of the data assimilation system,
- Q. J. R. Meteorol. Soc.*
- , 137(656),

- 553–597, doi:10.1002/qj.828, 2011.
- Deeter, M. N., Martínez-Alonso, S., Edwards, D. P., Emmons, L. K., Gille, J. C., Worden, H. M., Pittman, J. V., Daube, B. C. and Wofsy, S. C.: Validation of MOPITT Version 5 thermal-infrared, near-infrared, and multispectral carbon monoxide profile retrievals for 2000–2011, *J. Geophys. Res. Atmos.*, 118(12), 6710–6725, doi:10.1002/jgrd.50272, 2013.
- 5 Deeter, M. N., Edwards, D. P., Francis, G. L., Gille, J. C., Mao, D., Martínez-Alonso, S., Worden, H. M., Ziskin, D. and Andreae, M. O.: Radiance-based retrieval bias mitigation for the MOPITT instrument: the version 8 product, *Atmos. Meas. Tech.*, 12(8), 4561–4580, doi:10.5194/amt-12-4561-2019, 2019.
- Dentener, F., Van Weele, M., Krol, M., Houweling, S. and Van Velthoven, P.: Trends and inter-annual variability of methane emissions derived from 1979–1993 global CTM simulations, *Atmos. Chem. Phys.*, 3(1), 73–88, doi:10.5194/acp-3-73-2003, 10 2003.
- Dentener, F. J. and Crutzen, P. J.: Reaction of N₂O₅ on tropospheric aerosols: Impact on the global distributions of NO_x, O₃, and OH, *J. Geophys. Res. Atmos.*, 98(D4), 7149–7163, doi:10.1029/92JD02979, 1993.
- Derwent, R. G., Jenkin, M. E. and Saunders, S. M.: Photochemical ozone creation potentials for a large number of reactive hydrocarbons under European conditions, *Atmos. Environ.*, 30(2), 181–199, doi:10.1016/1352-2310(95)00303-G, 1996.
- 15 Dupuy, É., Urban, J., Ricaud, P., Le Flochmoën, É., Lautié, N., Murtagh, D., De La Noë, J., El Amraoui, L., Eriksson, P., Forkman, P., Frisk, U., Jégou, F., Jiménez, C. and Olberg, M.: Strato-mesospheric measurements of carbon monoxide with the Odin sub-millimetre radiometer: Retrieval and first results, *Geophys. Res. Lett.*, doi:10.1029/2004GL020558, 2004.
- Ehhalt, D., Prather, M., Dentener, F., Derwent, R., Dlugokencky, E., Holland, E., Isaksen, I., Katima, J., Kirchhoff, V., Matson, P., Midgley, P. and Wang, M.: Chapter 4: Atmospheric and Greenhouse Gases, in *Climate change 2001: The scientific basis*.
- 20 Contribution of Working Group I to the Third Assessment Report of the Intergovernmental Panel on Climate Change, edited by J. T. Houghton, pp. 239–287, Cambridge University Press., 2001.
- Emmerson, K. M. and Evans, M. J.: Comparison of tropospheric gas-phase chemistry schemes for use within global models, *Atmos. Chem. Phys. Atmos. Chem. Phys.*, 9, 1831–1845 [online] Available from: www.atmos-chem-phys.net/9/1831/2009/ (Accessed 7 May 2017), 2009.
- 25 Emmons, L. K., Hauglustaine, D. A., Mfiller, J.-F., Carroll, M. A., Brasseur, G. P., Brunner, D., Stachelin, J., Thouret, V. and Marenco, A.: Data composites of airborne observations of tropospheric ozone and its precursors., 2000.
- Emmons, L. K., Walters, S., Hess, P. G., Lamarque, J.-F., Pfister, G. G., Fillmore, D., Granier, C., Guenther, A., Kinnison, D., Laepple, T., Orlando, J., Tie, X., Tyndall, G., Wiedinmyer, C., Baughcum, S. L. and Kloster, S.: Description and evaluation of the Model for Ozone and Related chemical Tracers, version 4 (MOZART-4), *Geosci. Model Dev.*, 3(1), 43–67, 30 doi:10.5194/gmd-3-43-2010, 2010.
- Evans, M. J. and Jacob, D. J.: Impact of new laboratory studies of N₂O₅ hydrolysis on global model budgets of tropospheric nitrogen oxides, ozone, and OH, *Geophys. Res. Lett.*, 32(9), L09813, doi:10.1029/2005GL022469, 2005.
- Eyring, V., Bony, S., Meehl, G. A., Senior, C. A., Stevens, B., Stouffer, R. J. and Taylor, K. E.: Overview of the Coupled Model Intercomparison Project Phase 6 (CMIP6) experimental design and organization, *Geosci. Model Dev.*, 9(5), 1937–

- 1958, doi:10.5194/gmd-9-1937-2016, 2016.
- Flemming, J., Huijnen, V., Arteta, J., Bechtold, P., Beljaars, A., Blechschmidt, A.-M., Diamantakis, M., Engelen, R. J., Gaudel, A., Inness, A., Jones, L., Josse, B., Katragkou, E., Marecal, V., Peuch, V.-H., Richter, A., Schultz, M. G., Stein, O. and Tsikerdekis, A.: Tropospheric chemistry in the Integrated Forecasting System of ECMWF, *Geosci. Model Dev.*, 8(4), 975–1003, doi:10.5194/gmd-8-975-2015, 2015.
- 5 Fu, T., Jacob, D. J., Wittrock, F., Burrows, J. P., Vrekoussis, M. and Henze, D. K.: Global budgets of atmospheric glyoxal and methylglyoxal, and implications for formation of secondary organic aerosols, *J. Geophys. Res.*, 113(D15), D15303, doi:10.1029/2007JD009505, 2008.
- Ganzeveld, L. and Lelieveld, J.: Dry deposition parameterization in a chemistry general circulation model and its influence on the distribution of reactive trace gases, *J. Geophys. Res. Atmos.*, 100(D10), 20999–21012, doi:10.1029/95jd02266, 1995.
- 10 Ganzeveld, L., Lelieveld, J. and Roelofs, G. J.: A dry deposition parameterization for sulfur oxides in a chemistry and general circulation model, *J. Geophys. Res. Atmos.*, doi:10.1029/97JD03077, 1998.
- Geiger, H., Barnes, I., Bejan, I., Benter, T. and Spittler, M.: The tropospheric degradation of isoprene: an updated module for the regional atmospheric chemistry mechanism, *Atmos. Environ.*, 37(11), 1503–1519, doi:10.1016/S1352-2310(02)01047-6, 2003.
- 15 Gery, M. W., Whitten, G. Z., Killus, J. P. and Dodge, M. C.: A photochemical kinetics mechanism for urban and regional scale computer modeling, *J. Geophys. Res.*, 94(D10), 12925, doi:10.1029/JD094iD10p12925, 1989.
- Goliff, W. S., Stockwell, W. R. and Lawson, C. V: The regional atmospheric chemistry mechanism, version 2, *Atmos. Environ.*, 68, 174–185, doi:10.1016/j.atmosenv.2012.11.038, 2013.
- 20 Granier, C. J., Lamarque, F., Mieville, A., Muller, J. F., Olivier, J., Orlando, J., Peters, J., Petron, G., Tyndall, S. and Wallens, S.: POET, a database of surface emissions of ozone precursors, GEIA-ACCENT Emiss. data portal [online] Available from: <http://www.aero.jussieu.fr/projet/ACCENT/POET.php> (Accessed 10 March 2016), 2005.
- Groß, J.-U. and Russell, J. M.: Technical note: A stratospheric climatology for O_3 , O_2 , CH_4 , NO_x , HCl and HF derived from HALOE measurements, *Atmos. Chem. Phys.*, 5(10), 2797–2807, doi:10.5194/acp-5-2797-2005, 2005.
- 25 Gros, V., Tsigaridis, K., Bonsang, B., Kanakidou, M. and Pio, C.: Factors controlling the diurnal variation of CO above a forested area in southeast Europe, *Atmos. Environ.*, doi:10.1016/S1352-2310(02)00237-6, 2002.
- Gross, A. and Stockwell, W. R.: Comparison of the EMEP, RADM2 and RACM mechanisms, *J. Atmos. Chem.*, 44(3), 151, doi:10.1023/A:102248341, 2003.
- 30 Hays, M. D., Geron, C. D., Linna, K. J., Smith, N. D. and Schauer, J. J.: Speciation of Gas-Phase and Fine Particle Emissions from Burning of Foliar Fuels, *Environ. Sci. Technol.*, 36(11), 2281–2295, doi:10.1021/es0111683, 2002.
- Heimann, M., Monfray, P. and Polian, G.: Long-range transport of ^{222}Rn – a test for 3D tracer models, *Chem. Geol.*, 70(98), 98, 1988.
- Henze, D. K., Hakami, A. and Seinfeld, J. H.: Development of the adjoint of GEOS-Chem, *Atmos. Chem. Phys.*, 7(9), 2413–

- 2433, doi:10.5194/acp-7-2413-2007, 2007.
- Hertel, O., Berkowicz, R., Christensen, J. and Hov, Ø.: Test of two numerical schemes for use in atmospheric transport-chemistry models, *Atmos. Environ. Part A. Gen. Top.*, 27(16), 2591–2611, doi:10.1016/0960-1686(93)90032-T, 1993.
- Hodnebrog, Ø., Dalsøren, S. B. and Myhre, G.: Lifetimes, direct and indirect radiative forcing, and global warming potentials of ethane (C₂H₆), propane (C₃H₈), and butane (C₄H₁₀), *Atmos. Sci. Lett.*, 19(2), e804, doi:10.1002/asl.804, 2018.
- Hoesly, R. M., Smith, S. J., Feng, L., Klimont, Z., Janssens-Maenhout, G., Pitkanen, T., Seibert, J. J., Vu, L., Andres, R. J., Bolt, R. M., Bond, T. C., Dawidowski, L., Kholod, N., Kurokawa, J., Li, M., Liu, L., Lu, Z., Moura, M. C. P., O'Rourke, P. R. and Zhang, Q.: Historical (1750–2014) anthropogenic emissions of reactive gases and aerosols from the Community Emissions Data System (CEDS), *Geosci. Model Dev.*, 11(1), 369–408, doi:10.5194/gmd-11-369-2018, 2018.
- Horowitz, L. W., Walters, S., Mauzerall, D. L., Emmons, L. K., Rasch, P. J., Granier, C., Tie, X., Lamarque, J.-F., Schultz, M. G., Tyndall, G. S., Orlando, J. J. and Brasseur, G. P.: A global simulation of tropospheric ozone and related tracers: Description and evaluation of MOZART, version 2, *J. Geophys. Res. Atmos.*, 108(D24), 4784, doi:10.1029/2002JD002853, 2003.
- Houweling, S., Dentener, F. and Lelieveld, J.: The impact of nonmethane hydrocarbon compounds on tropospheric photochemistry, *J. Geophys. Res. Atmos.*, 103(D9), 10673–10696, doi:10.1029/97JD03582, 1998.
- Hsu, J.: Diagnosing the stratosphere-to-troposphere flux of ozone in a chemistry transport model, *J. Geophys. Res.*, 110(D19), D19305, doi:10.1029/2005JD006045, 2005.
- Huang, H.-C. and Chang, J. S.: On the performance of numerical solvers for a chemistry submodel in three-dimensional air quality models: 1. Box model simulations, *J. Geophys. Res. Atmos.*, 106(D17), 20175–20188, doi:10.1029/2000JD000121, 2001.
- Huijnen, V., Williams, J., van Weele, M., van Noije, T., Krol, M., Dentener, F., Segers, A., Houweling, S., Peters, W., de Laat, J., Boersma, F., Bergamaschi, P., van Velthoven, P., Le Sager, P., Eskes, H., Alkemade, F., Scheele, R., Nédélec, P. and Pätz, H.-W.: The global chemistry transport model TM5: description and evaluation of the tropospheric chemistry version 3.0, *Geosci. Model Dev.*, 3(2), 445–473, doi:10.5194/gmd-3-445-2010, 2010.
- Huijnen, V., Pozzer, A., Arteta, J., Brasseur, G., Bouarar, I., Chabrilat, S., Christophe, Y., Doumbia, T., Flemming, J., Guth, J., Josse, B., Karydis, V. A., Marécal, V. and Pelletier, S.: Quantifying uncertainties due to chemistry modelling – evaluation of tropospheric composition simulations in the CAMS model (cycle 43R1), *Geosci. Model Dev.*, 12(4), 1725–1752, doi:10.5194/gmd-12-1725-2019, 2019.
- Jacob, D.: Heterogeneous chemistry and tropospheric ozone, *Atmos. Environ.*, 34(12–14), 2131–2159, doi:10.1016/S1352-2310(99)00462-8, 2000.
- Jacob, D. J., Field, B. D., Jin, E. M., Bey, I., Li, Q., Logan, J. A., Yantosca, R. M. and Singh, H. B.: Atmospheric budget of acetone, *J. Geophys. Res. Atmos.*, 107(D10), 4100, doi:10.1029/2001JD000694, 2002.
- Jégou, F., Urban, J., de La Noë, J., Ricaud, P., Le Flochmoën, E., Murtagh, D. P., Eriksson, P., Jones, A., Petelina, S., Llewellyn, E. J., Lloyd, N. D., Haley, C., Lumpe, J., Randall, C., Bevilacqua, R. M., Catoire, V., Huret, N., Berthet, G., Renard,

- J. B., Strong, K., Davies, J., Mc Elroy, C. T., Goutail, F. and Pommereau, J. P.: Technical Note: Validation of Odin/SMR limb observations of ozone, comparisons with OSIRIS, POAM III, ground-based and balloon-borne instruments, *Atmos. Chem. Phys.*, 8(13), 3385–3409, doi:10.5194/acp-8-3385-2008, 2008.
- Jenkin, M. E., Saunders, S. M. and Pilling, M. J.: The tropospheric degradation of volatile organic compounds: a protocol for mechanism development, *Atmos. Environ.*, 31(1), 81–104, doi:10.1016/S1352-2310(96)00105-7, 1997.
- Jenkin, M. E., Saunders, S. M., Wagner, V. and Pilling, M. J.: Protocol for the development of the Master Chemical Mechanism, MCM v3 (Part B): tropospheric degradation of aromatic volatile organic compounds, *Atmos. Chem. Phys.*, 3(1), 181–193, doi:10.5194/acp-3-181-2003, 2003.
- Jenkin, M. E., Young, J. C. and Rickard, A. R.: The MCM v3.3.1 degradation scheme for isoprene, *Atmos. Chem. Phys.*, 15, 11433–11459, doi:10.5194/acp-15-11433-2015, 2015.
- Kanakidou, M. and Crutzen, P. J.: The photochemical source of carbon monoxide: Importance, uncertainties and feedbacks, *Chemosph. - Glob. Chang. Sci.*, 1(1–3), 91–109, doi:http://dx.doi.org/10.1016/S1465-9972(99)00022-7, 1999.
- [Kanakidou, M., Singh, H. B., Valentin, K. M. and Crutzen, P. J.: A two-dimensional study of ethane and propane oxidation in the troposphere, *J. Geophys. Res.*, 96\(D8\), 15395–15413, doi:10.1029/91jd01345, 1991.](#)
- Kim, Y., Sartelet, K. and Seigneur, C.: Comparison of two gas-phase chemical kinetic mechanisms of ozone formation over Europe, *J. Atmos. Chem.*, 62(2), 89–119, doi:10.1007/s10874-009-9142-5, 2009.
- Knote, C., Tuccella, P., Curci, G., Emmons, L., Orlando, J. J., Madronich, S., Bar, R., Jim Enez-Guerrero, P., Luecken, D., Hogrefe, C., Forkel, R., Werhahn, J., Hirtl, M., Erez, J. L. P., San Jos, R., Giordano, L., Brunner, D., Yahya, K. and Zhang, Y.: Influence of the choice of gas-phase mechanism on predictions of key gaseous pollutants during the AQMEII phase-2 intercomparison, *Atmos. Environ.*, 115, 553–568, doi:10.1016/j.atmosenv.2014.11.066, 2015.
- [Koffi, E. N., Bergamaschi, P., Karstens, U., Krol, M., Segers, A., Schmidt, M., Levin, I., Vermeulen, A. T., Fisher, R. E., Kazan, V., Klein Baltink, H., Lowry, D., Manca, G., Meijer, H. A. J., Moncrieff, J., Pal, S., Ramonet, M., Scheeren, H. A. and Williams, A. G.: Evaluation of the boundary layer dynamics of the TM5 model over Europe, *Geosci. Model Dev.*, 9\(9\), 3137–3160, doi:10.5194/gmd-9-3137-2016, 2016.](#)
- Krol, M., Houweling, S., Bregman, B., van den Broek, M., Segers, A., van Velthoven, P., Peters, W., Dentener, F. and Bergamaschi, P.: The two-way nested global chemistry-transport zoom model TM5: algorithm and applications, *Atmos. Chem. Phys.*, 5(2), 417–432, doi:10.5194/acp-5-417-2005, 2005.
- [Krol, M., de Bruine, M., Killaars, L., Ouwersloot, H., Pozzer, A., Yin, Y., Chevallier, F., Bousquet, P., Patra, P., Belikov, D., Maksyutov, S., Dhomse, S., Feng, W. and Chipperfield, M. P.: Age of air as a diagnostic for transport timescales in global models, *Geosci. Model Dev.*, 11\(8\), 3109–3130, doi:10.5194/gmd-11-3109-2018, 2018.](#)
- Lamarque, J.-F., Bond, T. C., Eyring, V., Granier, C., Heil, A., Klimont, Z., Lee, D., Lioussé, C., Mieville, A., Owen, B., Schultz, M. G., Shindell, D., Smith, S. J., Stehfest, E., Van Aardenne, J., Cooper, O. R., Kainuma, M., Mahowald, N., McConnell, J. R., Naik, V., Riahi, K. and van Vuuren, D. P.: Historical (1850–2000) gridded anthropogenic and biomass burning emissions of reactive gases and aerosols: methodology and application, *Atmos. Chem. Phys.*, 10(15), 7017–7039,

doi:10.5194/acp-10-7017-2010, 2010.

- Lamarque, J.-F., Emmons, L. K., Hess, P. G., Kinnison, D. E., Tilmes, S., Vitt, F., Heald, C. L., Holland, E. A., Lauritzen, P. H., Neu, J., Orlando, J. J., Rasch, P. J. and Tyndall, G. K.: CAM-chem: description and evaluation of interactive atmospheric chemistry in the Community Earth System Model, *Geosci. Model Dev.*, 5(2), 369–411, doi:10.5194/gmd-5-369-2012, 2012.
- 5 Lana, A., Bell, T. G., Simó, R., Vallina, S. M., Ballabrera-Poy, J., Kettle, A. J., Dachs, J., Bopp, L., Saltzman, E. S., Stefels, J., Johnson, J. E. and Liss, P. S.: An updated climatology of surface dimethylsulfide concentrations and emission fluxes in the global ocean, *Global Biogeochem. Cycles*, 25(1), GB1004, doi:10.1029/2010GB003850, 2011.
- Landgraf, J., Crutzen, P. J., Landgraf, J. and Crutzen, P. J.: An Efficient Method for Online Calculations of Photolysis and Heating Rates, *J. Atmos. Sci.*, 55(5), 863–878, doi:10.1175/1520-0469(1998)055<0863:AEMFOC>2.0.CO;2, 1998.
- 10 Lelieveld, J., Gromov, S., Pozzer, A. and Taraborrelli, D.: Global tropospheric hydroxyl distribution, budget and reactivity, *Atmos. Chem. Phys.*, 16(19), 12477–12493, doi:10.5194/acp-16-12477-2016, 2016.
- Luecken, D. J., Phillips, S., Sarwar, G. and Jang, C.: Effects of using the CB05 vs. SAPRC99 vs. CB4 chemical mechanism on model predictions: Ozone and gas-phase photochemical precursor concentrations, *Atmos. Environ.*, 42(23), 5805–5820, doi:10.1016/j.atmosenv.2007.08.056, 2008.
- 15 Marengo, A., Thouret, V., Nédélec, P., Smit, H., Helten, M., Kley, D., Karcher, F., Simon, P., Law, K., Pyle, J., Poschmann, G., Von Wrede, R., Hume, C. and Cook, T.: Measurement of ozone and water vapor by Airbus in-service aircraft: The MOZAIC airborne program, an overview, *J. Geophys. Res. Atmos.*, 103(D19), 25631–25642, doi:10.1029/98JD00977, 1998.
- van Marle, M. J. E., Kloster, S., Magi, B. I., Marlon, J. R., Daniau, A.-L., Field, R. D., Arneeth, A., Forrest, M., Hantson, S., Kehrwald, N. M., Knorr, W., Lasslop, G., Li, F., Mangeon, S., Yue, C., Kaiser, J. W. and van der Werf, G. R.: Historic global biomass burning emissions for CMIP6 (BB4CMIP) based on merging satellite observations with proxies and fire models (1750–2015), *Geosci. Model Dev.*, 10(9), 3329–3357, doi:10.5194/gmd-10-3329-2017, 2017.
- 20 Meijer, E. W. W., Van Velthoven, P. F. J. F. J., Brunner, D. W. W., Huntrieser, H. and Kelder, H.: Improvement and evaluation of the parameterisation of nitrogen oxide production by lightning, *Phys. Chem. Earth, Part C Solar, Terr. Planet. Sci.*, 26(8), 577–583, doi:10.1016/S1464-1917(01)00050-2, 2001.
- 25 Metzger, S., Dentener, F., Pandis, S. and Lelieveld, J.: Gas/aerosol partitioning: 1. A computationally efficient model, *J. Geophys. Res.*, 107(D16), 4312, doi:10.1029/2001JD001102, 2002.
- Miyazaki, K., Eskes, H., Sudo, K., Boersma, K. F., Bowman, K. and Kanaya, Y.: Decadal changes in global surface NO_x emissions from multi-constituent satellite data assimilation, *Atmos. Chem. Phys.*, 17(2), 807–837, doi:10.5194/acp-17-807-2017, 2017.
- 30 Monks, P. S., Granier, C., Fuzzi, S., Stohl, A., Williams, M. L., Akimoto, H., Amann, M., Baklanov, A., Baltensperger, U., Bey, I., Blake, N., Blake, R. S., Carslaw, K., Cooper, O. R., Dentener, F., Fowler, D., Fragkou, E., Frost, G. J., Generoso, S., Ginoux, P., Grewe, V., Guenther, A., Hansson, H. C., Henne, S., Hjorth, J., Hofzumahaus, A., Huntrieser, H., Isaksen, I. S. A., Jenkin, M. E., Kaiser, J., Kanakidou, M., Klimont, Z., Kulmala, M., Laj, P., Lawrence, M. G., Lee, J. D., Liousse, C., Maione, M., McFiggans, G., Metzger, A., Mieville, A., Moussiopoulos, N., Orlando, J. J., O'Dowd, C. D., Palmer, P. I.,

- Parrish, D. D., Petzold, A., Platt, U., Pöschl, U., Prévôt, A. S. H., Reeves, C. E., Reimann, S., Rudich, Y., Sellegri, K., Steinbrecher, R., Simpson, D., ten Brink, H., Theloke, J., van der Werf, G. R., Vautard, R., Vestreng, V., Vlachokostas, C. and von Glasow, R.: Atmospheric composition change – global and regional air quality, *Atmos. Environ.*, 43(33), 5268–5350, doi:10.1016/j.atmosenv.2009.08.021, 2009.
- 5 Monks, S. A., Wilson, C., Emmons, L. K., Hannigan, J. W., Helmig, D., Blake, N. J. and Blake, D. R.: Using an Inverse Model to Reconcile Differences in Simulated and Observed Global Ethane Concentrations and Trends Between 2008 and 2014, *J. Geophys. Res. Atmos.*, 123(19), 11,262–11,282, doi:10.1029/2017JD028112, 2018.
- Myriokefalitakis, S., Vrekoussis, M., Tsigaridis, K., Wittrock, F., Richter, A., Brühl, C., Volkamer, R., Burrows, J. P. and Kanakidou, M.: The influence of natural and anthropogenic secondary sources on the glyoxal global distribution, *Atmos. Chem. Phys.*, 8(16), 4965–4981, doi:10.5194/acp-8-4965-2008, 2008.
- Myriokefalitakis, S., Vignati, E., Tsigaridis, K., Papadimas, C., Sciare, J., Mihalopoulos, N., Facchini, M. C., Rinaldi, M., Dentener, F. J., Ceburnis, D., Hatzianastasiou, N., O'Dowd, C. D., van Weele, M. and Kanakidou, M.: Global Modeling of the Oceanic Source of Organic Aerosols, *Adv. Meteorol.*, 2010, 1–16, doi:10.1155/2010/939171, 2010.
- Myriokefalitakis, S., Tsigaridis, K., Mihalopoulos, N., Sciare, J., Nenes, A., Kawamura, K., Segers, A. and Kanakidou, M.: In-cloud oxalate formation in the global troposphere: a 3-D modeling study, *Atmos. Chem. Phys.*, 11(12), 5761–5782, doi:10.5194/acp-11-5761-2011, 2011.
- Myriokefalitakis, S., Daskalakis, N., Fanourgakis, G. S., Voulgarakis, A., Krol, M. C., Aan de Brugh, J. M. J. and Kanakidou, M.: Ozone and carbon monoxide budgets over the Eastern Mediterranean, *Sci. Total Environ.*, 563–564, 40–52, doi:10.1016/j.scitotenv.2016.04.061, 2016.
- 20 Naik, V., Voulgarakis, A., Fiore, A. M., Horowitz, L. W., Lamarque, J.-F., Lin, M., Prather, M. J., Young, P. J., Bergmann, D., Cameron-Smith, P. J., Cionni, I., Collins, W. J., Dalsøren, S. B., Doherty, R., Eyring, V., Faluvegi, G., Folberth, G. A., Josse, B., Lee, Y. H., MacKenzie, I. A., Nagashima, T., van Noije, T. P. C., Plummer, D. A., Righi, M., Rumbold, S. T., Skeie, R., Shindell, D. T., Stevenson, D. S., Strode, S., Sudo, K., Szopa, S. and Zeng, G.: Preindustrial to present-day changes in tropospheric hydroxyl radical and methane lifetime from the Atmospheric Chemistry and Climate Model Intercomparison Project (ACCMIP), *Atmos. Chem. Phys.*, 13(10), 5277–5298, doi:10.5194/acp-13-5277-2013, 2013.
- 25 [Nechita-Banda, N., Krol, M., van der Werf, G. R., Kaiser, J. W., Pandey, S., Huijnen, V., Clerbaux, C., Coheur, P., Deeter, M. N. and Röckmann, T.: Monitoring emissions from the 2015 Indonesian fires using CO satellite data, *Philos. Trans. R. Soc. B Biol. Sci.*, 373\(1760\), 20170307, doi:10.1098/rstb.2017.0307, 2018.](#)
- Nisbet, E. G., Manning, M. R., Dlugokencky, E. J., Fisher, R. E., Lowry, D., Michel, S. E., Myhre, C. L., Platt, S. M., Allen, G., Bousquet, P., Brownlow, R., Cain, M., France, J. L., Hermansen, O., Hossaini, R., Jones, A. E., Levin, I., Manning, A. C., Myhre, G., Pyle, J. A., Vaughn, B. H., Warwick, N. J. and White, J. W. C.: Very Strong Atmospheric Methane Growth in the 4 Years 2014–2017: Implications for the Paris Agreement, *Global Biogeochem. Cycles*, 33(3), 318–342, doi:10.1029/2018GB006009, 2019.
- van Noije et al., manuscript in preparation, T.: EC-Earth3-AerChem, A global climate model with interactive aerosols and

- atmospheric chemistry for use in CMIP6, n.d.
- van Noije, T. P. C.: Implications of the enhanced Brewer-Dobson circulation in European Centre for Medium-Range Weather Forecasts reanalysis ERA-40 for the stratosphere-troposphere exchange of ozone in global chemistry transport models, *J. Geophys. Res.*, 109(D19), D19308, doi:10.1029/2004JD004586, 2004.
- 5 van Noije, T. P. C., Le Sager, P., Segers, A. J., van Velthoven, P. F. J., Krol, M. C., Hazeleger, W., Williams, A. G. and Chambers, S. D.: Simulation of tropospheric chemistry and aerosols with the climate model EC-Earth, *Geosci. Model Dev.*, 7(5), 2435–2475, doi:10.5194/gmd-7-2435-2014, 2014.
- Olsen, M. A.: Stratosphere-troposphere exchange of mass and ozone, *J. Geophys. Res.*, 109(D24), D24114, doi:10.1029/2004JD005186, 2004.
- 10 Orlando, J. J., Tyndall, G. S. and Calvert, J. G.: Thermal decomposition pathways for peroxyacetyl nitrate (PAN): Implications for atmospheric methyl nitrate levels, *Atmos. Environ. Part A. Gen. Top.*, 26(17), 3111–3118, doi:10.1016/0960-1686(92)90468-Z, 1992.
- Paulot, F., Crounse, J. D., Kjaergaard, H. G., Kurten, A., St. Clair, J. M., Seinfeld, J. H. and Wennberg, P. O.: Unexpected Epoxide Formation in the Gas-Phase Photooxidation of Isoprene, *Science*, 325(5941), 730–733, doi:10.1126/science.1172910, 2009.
- 15 Peeters, J. and Müller, J.-F.: HOx radical regeneration in isoprene oxidation via peroxy radical isomerisations. II: experimental evidence and global impact, *Phys. Chem. Chem. Phys.*, 12(42), 14227, doi:10.1039/c0cp00811g, 2010.
- Peeters, J., Nguyen, T. L., Vereecken, L., Peeters, J., Bayes, K. D., Ganzeveld, L., Harder, H., Lawrence, M. G., Martinez, M., Taraborrelli, D., Williams, J., Scholes, B., Steinbrecker, R., Tallamraju, R., Taylor, J. and Zimmerman, P.: HOx radical regeneration in the oxidation of isoprene, *Phys. Chem. Chem. Phys.*, 11(28), 5935, doi:10.1039/b908511d, 2009.
- 20 Peeters, J., Müller, J.-F., Stavrou, T. and Nguyen, V. S.: Hydroxyl Radical Recycling in Isoprene Oxidation Driven by Hydrogen Bonding and Hydrogen Tunneling: The Upgraded LIM1 Mechanism, *J. Phys. Chem. A*, 118(38), 8625–8643, doi:10.1021/jp5033146, 2014.
- [Peters, W., Krol, M. C., Dlugokencky, E. J., Dentener, F. J., Bergamaschi, P., Dutton, G., Velthoven, P. v., Miller, J. B., Bruhwiler, L. and Tans, P. P.: Toward regional-scale modeling using the two-way nested global model TM5: Characterization of transport using SF 6, *J. Geophys. Res.*, 109\(D19\), D19314, doi:10.1029/2004JD005020, 2004.](#)
- Poisson, N., Kanakidou, M. and Crutzen, P. J.: Impact of Non-Methane Hydrocarbons on Tropospheric Chemistry and the Oxidizing Power of the Global Troposphere: 3-Dimensional Modelling Results, *J. Atmos. Chem.*, 36(2), 157–230, doi:10.1023/A:1006300616544, 2000.
- 30 Poisson, N., Kanakidou, M., Bonsang, B., Behmann, T., Burrows, J. P., Fischer, H., Gölz, C., Harder, H., Lewis, A., Moortgat, G. K., Nunes, T., Pio, C. A., Platt, U., Sauer, F., Schuster, G., Seakins, P., Senzig, J., Seuwen, R., Trapp, D., Volz-Thomas, A., Zenker, T. and Zitzelberger, R.: The impact of natural non-methane hydrocarbon oxidation on the free radical and ozone budgets above a eucalyptus forest, *Chemosph. - Glob. Chang. Sci.*, 3(3), 353–366, doi:10.1016/S1465-9972(01)00016-2, 2001.
- Pozzer, A., Jöckel, P., Tost, H., Sander, R., Ganzeveld, L., Kerkweg, A. and Lelieveld, J.: Simulating organic species with the

Deleted: 2001a

Deleted: Poisson, N., Kanakidou, M., Bonsang, B., Behmann, T., Burrows, J. P., Fischer, H., Gölz, C., Harder, H., Lewis, A., Moortgat, G. K., Nunes, T., Pio, C. A., Platt, U., Sauer, F., Schuster, G., Seakins, P., Senzig, J., Seuwen, R., Trapp, D., Volz-Thomas, A., Zenker, T. and Zitzelberger, R.: The impact of natural non-methane hydrocarbon oxidation on the free radical and ozone budgets above a eucalyptus forest, *Chemosph. - Glob. Chang. Sci.*, 3(3), 353–366, doi:10.1016/S1465-9972(01)00016-2, 2001b.

- global atmospheric chemistry general circulation model ECHAM5/MESSy1: a comparison of model results with observations, *Atmos. Chem. Phys.*, 7(10), 2527–2550, doi:10.5194/acp-7-2527-2007, 2007.
- Rodigast, M., Mutzel, A., Schindelka, J. and Herrmann, H.: A new source of methylglyoxal in the aqueous phase, *Atmos. Chem. Phys.*, 16(4), 2689–2702, doi:10.5194/acp-16-2689-2016, 2016.
- 5 [Russell, G. L. and Lerner, J. A.: A New Finite-Differencing Scheme for the Tracer Transport Equation, *J. Appl. Meteorol.*, 20\(12\), 1483–1498, doi:10.1175/1520-0450\(1981\)020<1483:ANFDSF>2.0.CO;2, 1981.](#)
- Sander, R., Kerkweg, A., Jöckel, P. and Lelieveld, J.: Technical note: The new comprehensive atmospheric chemistry module MECCA, *Atmos. Chem. Phys.*, 5(2), 445–450, doi:10.5194/acp-5-445-2005, 2005.
- Sander, R., Baumgaertner, A., Gromov, S., Harder, H., Jöckel, P., Kerkweg, A., Kubistin, D., Regelin, E., Riede, H., Sandu, A., Taraborrelli, D., Tost, H. and Xie, Z. Q.: The atmospheric chemistry box model CAABA/MECCA-3.0, *Geosci. Model Dev.*, 4(2), 373–380, doi:10.5194/gmd-4-373-2011, 2011.
- 10 Sander, R., Baumgaertner, A., Cabrera-Perez, D., Frank, F., Gromov, S., Groöb, J.-U., Harder, H., Huijnen, V., Jöckel, P., Karydis, V. A., Niemeyer, K. E., Pozzer, A., Riede, H., Schultz, M. G., Taraborrelli, D. and Tauer, S.: The community atmospheric chemistry box model CAABA/MECCA-4.0, *Geosci. Model Dev.*, 12(4), 1365–1385, doi:10.5194/gmd-12-1365-
- 15 2019, 2019.
- Sandu, A. and Sander, R.: Technical note: Simulating chemical systems in Fortran90 and Matlab with the Kinetic PreProcessor KPP-2.1, *Atmos. Chem. Phys.*, 6(1), 187–195, doi:10.5194/acp-6-187-2006, 2006.
- Sandu, A., Verwer, J. G., Blom, J. G., Spee, E. J., Carmichael, G. R. and Potra, F. A.: Benchmarking Stii ODE Solvers for Atmospheric Chemistry Problems II: Rosenbrock Solvers. [online] Available from:
- 20 <https://pdfs.semanticscholar.org/98cb/d122e1b1054074a1a330cfc8cff36db751d9.pdf> (Accessed 21 August 2019), 1997.
- Saunders, S. M., Jenkin, M. E., Derwent, R. G., Pilling, M. J., Saunders, S. M., Wagner, V., Pilling, M. J., Jenkin, M. E., Derwent, R. G., Pilling, M. J., Saunders, S. M., Wagner, V. and Pilling, M. J.: Protocol for the development of the Master Chemical Mechanism, MCM v3 (Part A): tropospheric degradation of non-aromatic volatile organic compounds, *Atmos. Chem. Phys.*, 3(1), 161–180, doi:10.5194/acp-3-161-2003, 2003.
- 25 Saylor, R. D. and Stein, A. F.: Identifying the causes of differences in ozone production from the CB05 and CBMIV chemical mechanisms, *Geosci. Model Dev.*, 5(1), 257–268, doi:10.5194/gmd-5-257-2012, 2012.
- Schultz, M. G., Stadtler, S., Schröder, S., Taraborrelli, D., Franco, B., Krefting, J., Henrot, A., Ferrachat, S., Lohmann, U., Neubauer, D., Siegenthaler-Le Drian, C., Wahl, S., Kokkola, H., Kühn, T., Rast, S., Schmidt, H., Stier, P., Kinnison, D., Tyndall, G. S., Orlando, J. J. and Wespes, C.: The chemistry–climate model ECHAM6.3-HAM2.3-MOZ1.0, *Geosci. Model Dev.*, 11(5), 1695–1723, doi:10.5194/gmd-11-1695-2018, 2018.
- 30 Seinfeld, J. H. and Pandis, S. N.: *Atmospheric Chemistry and Physics: From Air Pollution to Climate Change.*, 2006.
- Shindell, D. T., Faluvegi, G., Stevenson, D. S., Krol, M. C., Emmons, L. K., Lamarque, J.-F., Pétron, G., Dentener, F. J., Ellingsen, K., Schultz, M. G., Wild, O., Amann, M., Atherton, C. S., Bergmann, D. J., Bey, I., Butler, T., Cofala, J., Collins, W. J., Derwent, R. G., Doherty, R. M., Drevet, J., Eskes, H. J., Fiore, A. M., Gauss, M., Hauglustaine, D. A., Horowitz, L. W.,

- Isaksen, I. S. A., Lawrence, M. G., Montanaro, V., Müller, J.-F., Pitari, G., Prather, M. J., Pyle, J. A., Rast, S., Rodriguez, J. M., Sanderson, M. G., Savage, N. H., Strahan, S. E., Sudo, K., Szopa, S., Unger, N., van Noije, T. P. C. and Zeng, G.: Multimodel simulations of carbon monoxide: Comparison with observations and projected near-future changes, *J. Geophys. Res.*, 111(D19), D19306, doi:10.1029/2006JD007100, 2006.
- 5 Silvern, R. F., Jacob, D. J., Travis, K. R., Sherwen, T., Evans, M. J., Cohen, R. C., Laughner, J. L., Hall, S. R., Ullmann, K., Crounse, J. D., Wennberg, P. O., Peischl, J. and Pollack, I. B.: Observed NO/NO₂ Ratios in the Upper Troposphere Imply Errors in NO-NO₂-O₃ Cycling Kinetics or an Unaccounted NO_x Reservoir, *Geophys. Res. Lett.*, 45(9), 4466–4474, doi:10.1029/2018GL077728, 2018.
- Sindelarova, K., Granier, C., Bouarar, I., Guenther, A., Tilmes, S., Stavrakou, T., Müller, J.-F., Kuhn, U., Stefani, P. and Knorr, W.: Global data set of biogenic VOC emissions calculated by the MEGAN model over the last 30 years, *Atmos. Chem. Phys.*, 14(17), 9317–9341, doi:10.5194/acp-14-9317-2014, 2014.
- 10 Spiro, P. A., Jacob, D. J. and Logan, J. A.: Global inventory of sulfur emissions with 1°×1° resolution, *J. Geophys. Res.*, 97(D5), 6023, doi:10.1029/91JD03139, 1992.
- Spivakovsky, C. M., Logan, J. A., Montzka, S. A., Balkanski, Y. J., Foreman-Fowler, M., Jones, D. B. A., Horowitz, L. W., Fusco, A. C., Brenninkmeijer, C. A. M., Prather, M. J., Wofsy, S. C. and McElroy, M. B.: Three-dimensional climatological distribution of tropospheric OH: Update and evaluation, *J. Geophys. Res. Atmos.*, 105(D7), 8931–8980, doi:10.1029/1999JD901006, 2000.
- Stavrakou, T., Müller, J.-F., De Smedt, I., Van Roozendaal, M., van der Werf, G. R., Giglio, L. and Guenther, A.: Evaluating the performance of pyrogenic and biogenic emission inventories against one decade of space-based formaldehyde columns, *Atmos. Chem. Phys.*, 9(3), 1037–1060, doi:10.5194/acp-9-1037-2009, 2009a.
- 20 Stavrakou, T., Müller, J.-F., De Smedt, I., Van Roozendaal, M., Kanakidou, M., Vrekoussis, M., Wittrock, F., Richter, A. and Burrows, J. P.: The continental source of glyoxal estimated by the synergistic use of spaceborne measurements and inverse modelling, *Atmos. Chem. Phys. Discuss.*, 9(3), 13593–13628, doi:10.5194/acpd-9-13593-2009, 2009b.
- Stevenson, D. S., Dentener, F. J., Schultz, M. G., Ellingsen, K., van Noije, T. P. C., Wild, O., Zeng, G., Amann, M., Atherton, C. S., Bell, N., Bergmann, D. J., Bey, I., Butler, T., Cofala, J., Collins, W. J., Derwent, R. G., Doherty, R. M., Drevet, J., Eskes, H. J., Fiore, A. M., Gauss, M., Hauglustaine, D. A., Horowitz, L. W., Isaksen, I. S. A., Krol, M. C., Lamarque, J.-F., Lawrence, M. G., Montanaro, V., Müller, J.-F., Pitari, G., Prather, M. J., Pyle, J. A., Rast, S., Rodriguez, J. M., Sanderson, M. G., Savage, N. H., Shindell, D. T., Strahan, S. E., Sudo, K. and Szopa, S.: Multimodel ensemble simulations of present-day and near-future tropospheric ozone, *J. Geophys. Res.*, 111(D8), D08301, doi:10.1029/2005JD006338, 2006.
- 25 Stockwell, W. R., Kirchner, F., Kuhn, M. and Seefeld, S.: A new mechanism for regional atmospheric chemistry modeling, *J. Geophys. Res. Atmos.*, 102(D22), 25847–25879, doi:10.1029/97JD00849, 1997.
- Thouret, V., Marengo, A., Logan, J. A., Nédélec, P. and Grouhel, C.: Comparisons of ozone measurements from the MOZAIC airborne program and the ozone sounding network at eight locations, *J. Geophys. Res. Atmos.*, 103(D19), 25695–25720, doi:10.1029/98JD02243, 1998.
- 30

Tiedtke, M.: A Comprehensive Mass Flux Scheme for Cumulus Parameterization in Large-Scale Models, Mon. Weather Rev., 117(8), 1779–1800, doi:10.1175/1520-0493(1989)117<1779:ACMFSF>2.0.CO;2, 1989.

Toon, G. C., Blavier, J.-F. L. and Sung, K.: Measurements of atmospheric ethene by solar absorption FTIR spectrometry, *Atmos. Chem. Phys.*, 18(7), 5075–5088, doi:10.5194/acp-18-5075-2018, 2018.

- 5 Travis, K. R., Jacob, D. J., Fisher, J. A., Kim, P. S., Marais, E. A., Zhu, L., Yu, K., Miller, C. C., Yantosca, R. M., Sulprizio, M. P., Thompson, A. M., Wennberg, P. O., Crounse, J. D., St. Clair, J. M., Cohen, R. C., Laughner, J. L., Dibb, J. E., Hall, S. R., Ullmann, K., Wolfe, G. M., Pollack, I. B., Peischl, J., Neuman, J. A. and Zhou, X.: Why do models overestimate surface ozone in the Southeast United States?, *Atmos. Chem. Phys.*, 16(21), 13561–13577, doi:10.5194/acp-16-13561-2016, 2016.

- Tsigaridis, K. and Kanakidou, M.: Importance of volatile organic compounds photochemistry over a forested area in central Greece, *Atmos. Environ.*, 36(19), 3137–3146, doi:10.1016/S1352-2310(02)00234-0, 2002.

Tsigaridis, K. and Kanakidou, M.: Global modelling of secondary organic aerosol in the troposphere: a sensitivity analysis, *Atmos. Chem. Phys.*, 3(5), 1849–1869, doi:10.5194/acp-3-1849-2003, 2003.

- Urban, J., Pommier, M., Murtagh, D. P., Santee, M. L. and Orsolini, Y. J.: Nitric acid in the stratosphere based on Odin observations from 2001 to 2009 – Part 1: A global climatology, *Atmos. Chem. Phys.*, 9(18), 7031–7044, doi:10.5194/acp-9-7031-2009, 2009.

Vignati, E., Wilson, J. and Stier, P.: M7: An efficient size-resolved aerosol microphysics module for large-scale aerosol transport models, *J. Geophys. Res. Atmos.*, 109(D22), D22202, doi:10.1029/2003JD004485, 2004.

Voulgarakis, A., Naik, V., Lamarque, J.-F., Shindell, D. T., Young, P. J., Prather, M. J., Wild, O., Field, R. D., Bergmann, D., Cameron-Smith, P., Cionni, I., Collins, W. J., Dalsøren, S. B., Doherty, R. M., Eyring, V., Faluvegi, G., Folberth, G. A.,

- 20 Horowitz, L. W., Josse, B., MacKenzie, I. A., Nagashima, T., Plummer, D. A., Righi, M., Rumbold, S. T., Stevenson, D. S., Strode, S. A., Sudo, K., Szopa, S. and Zeng, G.: Analysis of present day and future OH and methane lifetime in the ACCMIP simulations, *Atmos. Chem. Phys.*, 13(5), 2563–2587, doi:10.5194/acp-13-2563-2013, 2013.

Vrekoussis, M., Liakakou, E., Mihalopoulos, N., Kanakidou, M., Crutzen, P. J. and Lelieveld, J.: Formation of HNO₃ and NO₃ – in the anthropogenically-influenced eastern Mediterranean marine boundary layer, *Geophys. Res. Lett.*, 33(5), L05811, doi:10.1029/2005GL025069, 2006.

- 25 Vrekoussis, M., Wittrock, F., Richter, A. and Burrows, J. P.: Temporal and spatial variability of glyoxal as observed from space, *Atmos. Chem. Phys.*, 9(13), 4485–4504, doi:10.5194/acp-9-4485-2009, 2009.

Wallington, T. J., Ammann, M., Cox, R. A., Crowley, J. N., Herrmann, H., Jenkin, M. E., McNeill, V., Mellouki, A., Rossi, M. J., Troe, J., H., H., Jenkin, M. E., McNeill, V., Mellouki, A., J., R. M. and Troe, J.: IUPAC Task group on atmospheric chemical kinetic data evaluation: Evaluated kinetic data, [online] Available from: <http://iupac.pole-ether.fr> (Accessed 10 April 2019), 2018.

Ware, G. W.: Methyl ethyl ketone, in *Reviews of Environmental Contamination and Toxicology*, pp. 165–174., 1988.

Wesely, M. L.: Parameterization of surface resistances to gaseous dry deposition in regional-scale numerical models, *Atmos. Environ.*, 41(SUPPL.), 52–63, doi:10.1016/j.atmosenv.2007.10.058, 1989.

- Wild, O.: Modelling the global tropospheric ozone budget: exploring the variability in current models, *Atmos. Chem. Phys.*, 7(10), 2643–2660, doi:10.5194/acp-7-2643-2007, 2007.
- Williams, J. E., Strunk, A., Huijnen, V. and van Weele, M.: The application of the Modified Band Approach for the calculation of on-line photodissociation rate constants in TM5: implications for oxidative capacity, *Geosci. Model Dev.*, 5(1), 15–35, doi:10.5194/gmd-5-15-2012, 2012.
- Williams, J. E., van Velthoven, P. F. J. and Brenninkmeijer, C. A. M.: Quantifying the uncertainty in simulating global tropospheric composition due to the variability in global emission estimates of Biogenic Volatile Organic Compounds, *Atmos. Chem. Phys.*, 13(5), 2857–2891, doi:10.5194/acp-13-2857-2013, 2013.
- Williams, J. E., Boersma, K. F., Le Sager, P. and Verstraeten, W. W.: The high-resolution version of TM5-MP for optimized satellite retrievals: description and validation, *Geosci. Model Dev.*, 10(2), 721–750, doi:10.5194/gmd-10-721-2017, 2017.
- Yarwood, G., Rao, S. and Yocke, M.: Updates to the carbon bond chemical mechanism: CB05 - Prepared for Deborah Luecken U.S. Environmental Protection Agency Research Triangle Park, NC 27703. [online] Available from: http://www.camx.com/files/cb05_final_report_120805.aspx (Accessed 16 March 2017), 2005.
- Yienger, J. J. and Levy, H.: Empirical model of global soil-biogenic NO_x emissions, *J. Geophys. Res.*, 100(D6), 11447, doi:10.1029/95JD00370, 1995.
- Young, A. H., Keene, W. C., Pszenny, A. A. P., Sander, R., Thornton, J. A., Riedel, T. P. and Maben, J. R.: Phase partitioning of soluble trace gases with size-resolved aerosols in near-surface continental air over northern Colorado, USA, during winter, *J. Geophys. Res. Atmos.*, 118(16), 9414–9427, doi:10.1002/jgrd.50655, 2013.
- Zaveri, R. A. and Peters, L. K.: A new lumped structure photochemical mechanism for large-scale applications, *J. Geophys. Res. Atmos.*, 104(D23), 30387–30415, doi:10.1029/1999JD900876, 1999.
- Zimmermann, P. H.: A handy global tracer model, in *Air Pollution Modeling and its Applications VI*, in Plenum, edited by H. van Dop, pp. 593–608, NATO/CCMS, New York., 1988.
- Ziskin, D.: Measurements Of Pollution In The Troposphere (MOPITT) Level 2 Derived CO (Near and Thermal Infrared Radiances) (MOP02J) V008 Beta [Data set], Atmospheric Sci. Data Center, NASA, doi:10.5067/TERRA/MOPITT/MOP02J_L2.008, 2019.

Tables

Table 1. Photolysis reactions (J) in the MOGUNTIA chemistry scheme.

#	Reactants	Products ^a	References
J1	$O_3 + h\nu$	$\rightarrow O(^1D)$	1
J2	$H_2O_2 + h\nu$	$\rightarrow 2\ OH$	1
J3	$NO_2 + h\nu$	$\rightarrow NO + O$	1
J4	$NO_3 + h\nu$	$\rightarrow NO_2 + O$	1
J5	$NO_3 + h\nu$	$\rightarrow NO$	1
J6	$N_2O_5 + h\nu$	$\rightarrow NO_2 + NO_3$	1
J7	$N_2O_5 + h\nu$	$\rightarrow NO + NO_3$	1
J8	$HONO + h\nu$	$\rightarrow OH + NO$	1
J9	$HNO_3 + h\nu$	$\rightarrow NO_2 + OH$	1
J10	$HNO_4 + h\nu$	$\rightarrow NO_2 + HO_2$	1
J11	$HCHO + h\nu$	$\rightarrow CO$	1
J12	$HCHO + h\nu$	$\rightarrow CO + 2\ HO_2$	1
J13	$CH_3OOH + h\nu$	$\rightarrow HCHO + HO_2 + OH$	1
J14	$CH_3ONO_2 + h\nu$	$\rightarrow HCHO + HO_2 + NO_2$	1
J15	$CH_3OONO_2 + h\nu$	$\rightarrow CH_3OO + NO_2$	1
J16	$CH_3OONO_2 + h\nu$	$\rightarrow HCHO + HO_2 + NO_3$	1
J17	$CH_3C(O)OONO_2 + h\nu$	$\rightarrow CH_3C(O)OO + NO_2$	J10
J18	$CH_3C(O)OONO_2 + h\nu$	$\rightarrow CH_3OO + NO_3 + CO_2$	J10
J19	$CH_3C(O)OOH + h\nu$	$\rightarrow CH_3C(O)OO + OH$	J13
J20	$C_2H_5OOH + h\nu$	$\rightarrow CH_3CHO + HO_2 + OH$	J13
J21	$C_2H_5ONO_2 + h\nu$	$\rightarrow HCHO + CO + HO_2 + NO_2$	1
J22	$HOCH_2CH_2OOH + h\nu$	$\rightarrow 2\ HCHO + HO_2 + OH$	f 0.5 * J13
J23	$HOCH_2CH_2OOH + h\nu$	$\rightarrow HOCH_2CHO + HO_2 + OH$	(1 - f) 0.5 * J13
J24	$HOCH_2CH_2ONO_2 + h\nu$	$\rightarrow 2\ HCHO + HO_2 + NO_2$	f 0.5 * JORGN
J25	$HOCH_2CH_2ONO_2 + h\nu$	$\rightarrow HOCH_2CHO + HO_2 + NO_2$	(1 - f) 0.5 * JORGN
J26	$CH_3CHO + h\nu$	$\rightarrow CH_3OO + CO + HO_2$	1
J27	$HOCH_2CHO + h\nu$	$\rightarrow CH_3OH + CO$	1
J28	$CHOCHO + h\nu$	$\rightarrow 2\ CO + 2\ HO_2$	1
J29	$CHOCHO + h\nu$	$\rightarrow HCHO + CO$	1
J30	$CHOCHO + h\nu$	$\rightarrow 2\ CO$	1
J31	$CH_3C(O)CH_3 + h\nu$	$\rightarrow 2\ CH_3OO + CO$	1
J32	$CH_3C(O)CH_3 + h\nu$	$\rightarrow CH_3C(O)OO + CH_3OO$	1
J33	$HOCH_2C(O)CH_3 + h\nu$	$\rightarrow CH_3C(O)OO + HCHO + HO_2$	1
J34	$CH_3C(O)CH_2OOH + h\nu$	$\rightarrow 0.3\ CH_3C(O)CHO\ 0.7(CH_3C(O)OO + HCHO) + OH$	J13
J35	$n\text{-}C_3H_7OOH + h\nu$	$\rightarrow C_2H_5CHO + HO_2 + OH$	0.5 * J13
J36	$n\text{-}C_3H_7ONO_2 + h\nu$	$\rightarrow C_2H_5CHO + HO_2 + NO_2$	1
J37	$i\text{-}C_3H_7OOH + h\nu$	$\rightarrow CH_3C(O)CH_3 + HO_2 + OH$	0.5 * J13
J38	$i\text{-}C_3H_7ONO_2 + h\nu$	$\rightarrow CH_3C(O)CH_3 + HO_2 + NO_2$	1
J39	$C_2H_5CHO + h\nu$	$\rightarrow C_2H_5OO + CO + HO_2$	1

J40	$\text{HOC}_3\text{H}_6\text{OOH} + h\nu$	$\rightarrow \text{CH}_3\text{CHO} + \text{HCHO} + \text{HO}_2$	J13
J41	$\text{CH}_3\text{COCHO} + h\nu$	$\rightarrow \text{CH}_3\text{C(O)OO} + \text{CO} + \text{HO}_2$	1
J42	$\text{C}_4\text{H}_9\text{OOH} + h\nu$	$\rightarrow 0.67(\text{CH}_3\text{CH}_2\text{COCH}_3 + \text{HO}_2) + 0.33(\text{C}_2\text{H}_5\text{OO} + \text{CH}_3\text{CHO}) + \text{OH}$	J13
J43	$\text{C}_4\text{H}_9\text{ONO}_2 + h\nu$	$\rightarrow 0.67(\text{CH}_3\text{CH}_2\text{COCH}_3 + \text{HO}_2) + 0.33(\text{C}_2\text{H}_5\text{OO} + \text{CH}_3\text{CHO}) + \text{NO}_2$	J _{ORGN}
J44	$\text{CH}_3\text{CH}_2\text{C(O)CH}_3 + h\nu$	$\rightarrow \text{CH}_3\text{C(O)OO} + \text{C}_2\text{H}_5\text{OO}$	1
J45	$\text{CH}_3\text{CH(OOH)COCH}_3 + h\nu$	$\rightarrow \text{CH}_3\text{CHO} + \text{CH}_3\text{C(O)OO} + \text{OH}$	J13
J46	$\text{CH}_3\text{CH(ONO}_2\text{)COCH}_3 + h\nu$	$\rightarrow \text{CH}_3\text{CHO} + \text{CH}_3\text{C(O)OO} + \text{NO}_2$	J _{ORGN}
J47	$\text{ISOPOOH} + h\nu$	$\rightarrow \text{HCHO} + 0.64 \text{ MVK} + 0.36 \text{ MACR} + \text{HO}_2 + \text{OH}$	13
J48	$\text{ISOPONO}_2 + h\nu$	$\rightarrow \text{HCHO} + 0.64 \text{ MVK} + 0.36 \text{ MACR} + \text{HO}_2 + \text{NO}_2$	J _{ORGN}
J49	$\text{MACR} + h\nu$	$\rightarrow 0.5 \text{ MACROO} + 0.5 \text{ HCHO} + 0.175 \text{ CH}_3\text{C(O)OO} + 0.325 \text{ CH}_3\text{OO} + 0.825 \text{ CO} + \text{HO}_2$	1
J50	$\text{MACROOH} + h\nu$	$\rightarrow \text{CH}_3\text{COCH}_2\text{OH} + \text{CO} + \text{HO}_2 + \text{OH}$	J13
J51	$\text{MACRONO}_2 + h\nu$	$\rightarrow \text{CH}_3\text{COCH}_2\text{OH} + \text{CO} + \text{HO}_2 + \text{NO}_2$	J _{ORGN}
J52	$\text{MVK} + h\nu$	$\rightarrow 0.6 (\text{C}_3\text{H}_6 + \text{CO}) + 0.4 (\text{CH}_3\text{C(O)OO} + \text{CH}_3\text{OO} + \text{HCHO})$	1
J53	$\text{MVKOOH} + h\nu$	$\rightarrow 0.7(\text{CH}_3\text{C(O)OO} + \text{HOCH}_2\text{CHO}) + 0.3(\text{CH}_3\text{COCHO} + \text{HCHO} + \text{HO}_2) + \text{OH}$	J13
J54	$\text{MVKONO}_2 + h\nu$	$\rightarrow 0.7(\text{CH}_3\text{C(O)OO} + \text{HOCH}_2\text{CHO}) + 0.3(\text{CH}_3\text{COCHO} + \text{HCHO} + \text{HO}_2) + \text{NO}_2$	J _{ORGN}
J55	$\text{CH}_3\text{C(O)C(O)CH}_3 + h\nu$	$\rightarrow 2 \text{ CH}_3\text{C(O)OO}$	1
J56	$\text{CH}_3\text{C(O)COOH} + h\nu$	$\rightarrow \text{CH}_3\text{C(O)OO} + \text{HO}_2 + \text{CO}_2$	1
J57	$\text{HPALD} + h\nu$	$\rightarrow 0.5 \text{ HOCH}_2\text{C(O)CH}_3 + 0.5 \text{ CH}_3\text{COCHO} + 0.25 \text{ HOCH}_2\text{CHO} + 0.25 \text{ CHOCHO} + \text{HCHO} + \text{HO}_2 + \text{OH}$	4, 5
J58	$\text{O}_2 + h\nu$	$\rightarrow \text{O}_3$	1

[#] The reaction products O₂, H₂, and H₂O are not shown.

¹ <http://iupac.pole-ether.fr>

²Atkinson, (1997):

$$\begin{aligned}
 5 \quad & R_1 = 2.7 \times 10^{14} \exp(-6350/T) \\
 & R_2 = 6.3 \times 10^{14} \exp(-550/T) \\
 & f = R_1 / (R_1 + R_2 \times [\text{O}_2])
 \end{aligned}$$

³ J_{ORGN} is calculated based on average of σ-values for 1-C₄H₉ONO₂ and 2-C₄H₉ONO₂ as described in Williams et al. (2012)

⁴ Browne et al. (2014)

10 ⁵ Peeters and Müller (2010)

Table 2. Thermal reactions (K) in MOGUNTIA chemistry scheme.

#	Reactants	Products ^a	Rate expression ^b	References
K0a	O(¹ D) (+ M)	O	$3.3 \times 10^{-11} \exp(55/T) [\text{O}_2] + 2.5 \times 10^{-11} \exp(110/T) [\text{N}_2]$	1
K0b	O(¹ D) + H ₂ O	OH + OH	$1.63 \times 10^{-10} \exp(60/T)$	1
K1	O ₃ + OH	→ HO ₂	$1.7 \times 10^{-12} \exp(-940/T)$	1
K2	HO ₂ + O ₃	→ OH	$2.03 \times 10^{-16} (T/300)^{4.57} \exp(693/T)$	1
K3	HO ₂ + OH	→ H ₂ O	$4.8 \times 10^{-11} \exp(250/T)$	1
K4	HO ₂ + HO ₂	→ H ₂ O ₂	$2.2 \times 10^{-13} \exp(600/T)$ $1.9 \times 10^{-31} [\text{N}_2] \exp(980/T)$ $1.4 \times 10^{-21} [\text{H}_2\text{O}] \exp(2200/T)$	1
K5	H ₂ O ₂ + OH	→ HO ₂	$2.9 \times 10^{-12} \exp(-160/T)$	1
K6	HO ₂ + NO	→ NO ₂ + HO	$3.45 \times 10^{-12} \exp(270/T)$	1
K7	NO + O ₃	→ NO ₂	$2.07 \times 10^{-12} \exp(-1400/T)$	1
K8	NO + NO ₃	→ 2NO ₂	$1.8 \times 10^{-11} \exp(110/T)$	1
K9	NO ₂ + O ₃	→ NO ₃	$1.4 \times 10^{-13} \exp(-2470/T)$	1
K10	OH + NO {+ M}	→ HONO	$7.4 \times 10^{-31} \times (T/300)^{2.4} [\text{N}_2]$ $3.3 \times 10^{-11} (T/300)^{0.3}$ $F_c = 0.81$	1
K11	OH + NO ₂ {+ M}	→ HONO ₂	$3.2 \times 10^{-30} (T/300)^{4.5} [\text{N}_2]$ 3.0×10^{-11} $F_c = 0.41$	1
K12	NO ₂ + NO ₃ {+ M}	→ N ₂ O ₅	$3.6 \times 10^{-30} (T/300)^{4.1} [\text{N}_2]$ $1.9 \times 10^{-12} (T/300)^{0.2}$ $F_c = 0.35$	1
K13	NO ₂ + HO ₂	→ HO ₂ NO ₂	$1.4 \times 10^{-31} (T/300)^{3.1} [\text{N}_2]$ 4.0×10^{-12} $F_c = 0.40$	1
K14	HO ₂ + NO ₃	→ OH + NO ₂	4.0×10^{-12}	1
K15	HONO + OH	→ NO ₂	$2.5 \times 10^{-12} \exp(260/T)$	1
K16	HNO ₃ + OH	→ NO ₃	$2.4 \times 10^{-14} \exp(460/T)$ $6.5 \times 10^{-24} \exp(1335/T)$ $2.7 \times 10^{-17} \exp(2199/T)$	1
K17	HO ₂ NO ₂ + OH	→ NO ₂	$1.9 \times 10^{-12} \exp(270/T)$	1
K18	HO ₂ NO ₂	→ HO ₂ + NO ₂	$4.1 \times 10^{-5} \exp(-10650/T) [\text{N}_2]$ $6.0 \times 10^{15} \exp(-11170/T)$ $F_c = 0.40$	1
K19	N ₂ O ₅	→ NO ₂ + NO ₃	$1.3 \times 10^{-3} (T/300)^{3.5} \exp(-11000/T) [\text{N}_2]$ $9.7 \times 10^{14} (T/300)^{0.1} \exp(-11080/T)$ $F_c = 0.35$	1
K20	OH + H ₂	→ HO ₂	$7.7 \times 10^{-12} \exp(-2100/T)$	1
K21	CH ₄ + OH	→ CH ₃ OO	$2.45 \times 10^{-12} \exp(-1775/T)$	2
K22	CH ₃ OO + HO ₂	→ CH ₃ OOH	$3.8 \times 10^{-13} \exp(780/T)^*$ $(1 - 1/(1 + 498.0 \exp(-1160/T)))$	1, 3

K23	$\text{CH}_3\text{OO} + \text{HO}_2$	$\rightarrow \text{HCHO}$	$3.8 \times 10^{-13} \exp(780/T)^*$ $(1/(1+498.0 \exp(-1160/T)))$	1, 3
K24	$\text{CH}_3\text{OO} + \text{NO}$	$\rightarrow 0.999 (\text{HCHO} + \text{HO}_2 + \text{NO}_2) +$ $0.001 \text{CH}_3\text{ONO}_2$	$2.3 \times 10^{-12} \exp(360/T)$	1, 3
K25	$\text{CH}_3\text{OO} + \text{NO}_2$	$\rightarrow \text{CH}_3\text{O}_2\text{NO}_2$	$2.5 \times 10^{-30} (T/300)^{-5.5} [\text{N}_2]$ 1.8×10^{-11} $F_c = 0.36$	1
K26	$\text{CH}_3\text{OO} + \text{NO}_3$	$\rightarrow \text{HCHO} + \text{NO}_2$	1.2×10^{-12}	1
K27	$\text{CH}_3\text{OO} + \text{CH}_3\text{OO}$	$\rightarrow 2\text{HCHO} + 2\text{HO}_2$	$7.48 \exp(-885/T) \times$ $1.03 \times 10^{-13} \exp(365/T)$	2
K28	$\text{CH}_3\text{OO} + \text{CH}_3\text{OO}$	$\rightarrow \text{CH}_3\text{OH} + \text{HCHO}$	$(1 - 7.48 \exp(-885/T) \times$ $1.03 \times 10^{-13} \exp(365/T))$	2
K29	$\text{CH}_3\text{OOH} + \text{OH}$	$\rightarrow \text{HCHO} + \text{OH}$	$0.4 \times 5.3 \times 10^{-12} \exp(190/T)$	1
K30	$\text{CH}_3\text{OOH} + \text{OH}$	$\rightarrow \text{CH}_3\text{OO}$	$0.6 \times 5.3 \times 10^{-12} \exp(190/T)$	1
K31	$\text{CH}_3\text{ONO}_2 + \text{OH}$	$\rightarrow \text{HCHO} + \text{NO}_2$	$4.0 \times 10^{-13} \exp(-845/T)$	1
K32	CH_3OONO_2	$\rightarrow \text{CH}_3\text{O}_2 + \text{NO}_2$	$9.0 \times 10^{-5} \exp(-9690/T) [\text{N}_2]$ $1.1 \times 10^{-16} \exp(-10560/T)$	1
K33	$\text{HCHO} + \text{OH}$	$\rightarrow \text{CO} + \text{HO}_2$	$F_c = 0.26$ $5.4 \times 10^{-12} \exp(135/T)$	1
K34	$\text{HCHO} + \text{NO}_3$	$\rightarrow \text{CO} + \text{HO}_2 + \text{HNO}_3$	$2.0 \times 10^{-12} \exp(-2440/T)$	1
K35	$\text{CH}_3\text{OH} + \text{OH}$	$\rightarrow \text{HCHO} + \text{HO}_2$	$2.85 \times 10^{-12} \exp(-345/T)$	1
K36	$\text{CH}_3\text{OH} + \text{NO}_3$	$\rightarrow \text{HCHO} + \text{HO}_2 + \text{HNO}_3$	$9.4 \times 10^{-13} \exp(-2650/T)$	1
K37	$\text{HCOOH} + \text{OH}$	$\rightarrow \text{CO}_2 + \text{HO}_2$	4.5×10^{-13} $5.9 \times 10^{-33} (300/T)^{1.4}$ $1.1 \times 10^{-12} (300/T)^{-1.3}$ $1.5 \times 10^{-13} (300/T)^{-0.6}$ $2.9 \times 10^6 (300/T)^{-6.1}$	1
K38	$\text{CO} + \text{OH}$	$\rightarrow \text{CO}_2 + \text{HO}_2$	$6.9 \times 10^{-12} \exp(-1000/T)$	2
K39	$\text{C}_2\text{H}_6 + \text{OH}$	$\rightarrow \text{C}_2\text{H}_5\text{OO}$	$6.4 \times 10^{-13} \exp(710/T)$	1
K40	$\text{C}_2\text{H}_5\text{OO} + \text{HO}_2$	$\rightarrow \text{C}_2\text{H}_5\text{OOH}$		1
K41	$\text{C}_2\text{H}_5\text{OO} + \text{NO}$	$\rightarrow \text{CH}_3\text{CHO} + \text{HO}_2 + \text{NO}_2$	$(1 - \text{RTC2P}) \times 2.55 \times 10^{-12} \exp(380/T)$	1, 4
K42	$\text{C}_2\text{H}_5\text{OO} + \text{NO}$	$\rightarrow \text{C}_2\text{H}_5\text{ONO}_2$	$\text{RTC2P} \times 2.55 \times 10^{-12} \exp(380/T)$	1, 4
K43	$\text{C}_2\text{H}_5\text{OO} + \text{CH}_3\text{OO}$	$\rightarrow \text{CH}_3\text{CHO} + \text{HCHO} + 2\text{HO}_2$	$0.8 \times (6.4 \times 10^{-14} \times 1.03 \times 10^{-13} \exp(365/T))^{0.5}$	3
K44	$\text{C}_2\text{H}_5\text{OO} + \text{CH}_3\text{OO}$	$\rightarrow 0.5 \text{CH}_3\text{CHO} + 0.5 \text{CH}_3\text{CH}_2\text{OH} + \text{CH}_3\text{OH}$	$0.2 \times (6.4 \times 10^{-14} \times 1.03 \times 10^{-13} \exp(365/T))^{0.5}$	3
K45	$\text{C}_2\text{H}_5\text{OOH} + \text{OH}$	$\rightarrow \text{C}_2\text{H}_5\text{OO}$	$1.90 \times 10^{-12} \exp(190/T)$	2
K46	$\text{C}_2\text{H}_5\text{OOH} + \text{OH}$	$\rightarrow \text{CH}_3\text{CHO} + \text{OH}$	8.01×10^{-12}	3
K47	$\text{C}_2\text{H}_5\text{ONO}_2 + \text{OH}$	$\rightarrow \text{CH}_3\text{CHO} + \text{NO}_2$	$6.7 \times 10^{-13} \exp(-395/T)$	1
K48	$\text{CH}_3\text{CHO} + \text{OH}$	$\rightarrow \text{CH}_3\text{C(O)OO}$	$4.7 \times 10^{-12} \exp(345/T)$	1
K49	$\text{CH}_3\text{CHO} + \text{NO}_3$	$\rightarrow \text{CH}_3\text{C(O)OO} + \text{HNO}_3$	$1.4 \times 10^{-12} \exp(-1860/T)$	1
K50	$\text{CH}_3\text{C(O)OO} + \text{HO}_2$	$\rightarrow \text{CH}_3\text{C(O)OOH}$	$0.41 * 5.2 \times 10^{-13} \exp(980/T)$	3
K51	$\text{CH}_3\text{C(O)OO} + \text{HO}_2$	$\rightarrow \text{CH}_3\text{COOH} + \text{O}_3$	$0.15 * 5.2 \times 10^{-13} \exp(980/T)$	3
K52	$\text{CH}_3\text{C(O)OO} + \text{HO}_2$	$\rightarrow \text{CH}_3\text{O}_2 + \text{CO}_2 + \text{OH}$	$0.44 * 5.2 \times 10^{-13} \exp(980/T)$	3
K53	$\text{CH}_3\text{C(O)OO} + \text{NO}$	$\rightarrow \text{CH}_3\text{OO} + \text{CO}_2 + \text{NO}_2$	$7.5 \times 10^{-12} \exp(290/T)$	1
K54	$\text{CH}_3\text{C(O)OO} + \text{NO}_2$	$\rightarrow \text{CH}_3\text{C(O)OONO}_2$	$3.28 \times 10^{-28} (T/300)^{-6.87} [\text{N}_2]$	1

Deleted: 4

Deleted: 520

Deleted: 1,

Deleted: 4

Deleted: 520

Deleted: 1,

Deleted: 40

Deleted: 1

Deleted: 6.0

			$1.125 \times 10^{-11} (T/300)^{-1.105}$ $Fc = 0.3$	
K55	$\text{CH}_3\text{C}(\text{O})\text{OO} + \text{NO}_2$	$\rightarrow \text{CH}_3\text{OO} + \text{NO}_2$	4.0×10^{-12}	2
K56	$\text{CH}_3\text{C}(\text{O})\text{OO} + \text{CH}_3\text{OO}$	$\rightarrow \text{CH}_3\text{C}(\text{O})\text{OOH} + \text{HCHO}$	$0.9 * 2.0 \times 10^{-12} \exp(500/T)$	2
K57	$\text{CH}_3\text{C}(\text{O})\text{OO} + \text{CH}_3\text{OO}$	$\rightarrow \text{CH}_3\text{COOH} + \text{HCHO}$	$0.1 * 2.0 \times 10^{-12} \exp(500/T)$	2
K58	$\text{CH}_3\text{C}(\text{O})\text{OO} + \text{CH}_3\text{C}(\text{O})\text{OO}$	$\rightarrow 2 (\text{CH}_3\text{OO} + \text{CO}_2)$	$2.9 \times 10^{-12} \exp(500/T)$	2
K59	$\text{CH}_3\text{C}(\text{O})\text{OO} + \text{CH}_3\text{COCH}_2\text{O}_2$	$\rightarrow \text{CH}_3\text{COOH} + \text{CH}_3\text{COCHO}$	2.5×10^{-12}	2
K60	$\text{CH}_3\text{C}(\text{O})\text{OO} + \text{CH}_3\text{COCH}_2\text{O}_2$	$\rightarrow \text{CH}_3\text{OO} + \text{CH}_3\text{COCH}_2\text{OH} + \text{CO}_2$	2.5×10^{-12}	2
K61	$\text{CH}_3\text{C}(\text{O})\text{OO} + \text{C}_2\text{H}_5\text{OO}$	$\rightarrow \text{CH}_3\text{CHO} + 2 \text{CH}_3\text{OO}$	$0.7 * 4.4 \times 10^{-13} \exp(1070/T)$	1, 3
K62	$\text{CH}_3\text{C}(\text{O})\text{OO} + \text{C}_2\text{H}_5\text{OO}$	$\rightarrow \text{CH}_3\text{CHO} + \text{CH}_3\text{COOH}$	$0.3 * 4.4 \times 10^{-13} \exp(1070/T)$	1, 3
K63	$\text{CH}_3\text{C}(\text{O})\text{OONO}_2 + \text{OH}$	$\rightarrow \text{HCHO} + \text{CO} + \text{NO}_2$	3.0×10^{-14}	1
K64	$\text{CH}_3\text{C}(\text{O})\text{OONO}_2$	$\rightarrow \text{CH}_3\text{C}(\text{O})\text{OO} + \text{NO}_2$	$1.1 \times 10^{-5} \exp(-10100/T) [\text{N}_2]$ $1.9 \times 10^{-17} \exp(-14100/T)$ $Fc = 0.3$	1
K65	$\text{CH}_3\text{C}(\text{O})\text{OONO}_2$	$\rightarrow \text{CH}_3\text{ONO}_2 + \text{CO}_2$	$2.1 \times 10^{-12} \exp(-12525/T)$	5
K66	$\text{CH}_3\text{C}(\text{O})\text{OOH} + \text{OH}$	$\rightarrow \text{CH}_3\text{C}(\text{O})\text{OO}$	1.1×10^{-11}	3
K67	$\text{C}_2\text{H}_4 + \text{OH}$	$\rightarrow \text{HOCH}_2\text{CH}_2\text{OO}$	$8.6 \times 10^{-20} (T/300)^{-3.1} [\text{N}_2]$ $9.0 \times 10^{-12} (T/300)^{-0.85}$ $Fc = 0.48$	1
K68	$\text{C}_2\text{H}_4 + \text{NO}_3$	$\rightarrow \text{HOCH}_2\text{CH}_2\text{ONO}_2$	$3.3 \times 10^{-12} \exp(-2880/T)$	1
K69	$\text{C}_2\text{H}_4 + \text{O}_3$	$\rightarrow 1.37 \text{HCHO} + 0.63 \text{CO} + 0.13 \text{HO}_2 + 0.13 \text{OH}$	$6.82 \times 10^{-15} \exp(-2500/T)$	1
K70	$\text{HOCH}_2\text{CH}_2\text{OO} + \text{HO}_2$	$\rightarrow \text{HOCH}_2\text{CH}_2\text{OOH}$	1.3×10^{-11}	1
K71	$\text{HOCH}_2\text{CH}_2\text{OO} + \text{NO}$	$\rightarrow \text{NO}_2 + 2\text{HCHO} + \text{HO}_2$	$(1 - \text{RTC2P}) \times f \times 2.7 \times 10^{-12} \exp(360/T)$	3
K72	$\text{HOCH}_2\text{CH}_2\text{OO} + \text{NO}$	$\rightarrow \text{NO}_2 + \text{HOCH}_2\text{CHO} + \text{HO}_2$	$(1 - \text{RTC2P}) \times (1 - f) \times 2.7 \times 10^{-12} \exp(360/T)$	3
K73	$\text{HOCH}_2\text{CH}_2\text{OO} + \text{NO}$	$\rightarrow \text{HOCH}_2\text{CH}_2\text{ONO}_2$	$\text{RTC2P} \times 2.7 \times 10^{-12} \exp(360/T)$	1
K74	$\text{HOCH}_2\text{CH}_2\text{OO} + \text{CH}_3\text{OO}$	$\rightarrow \text{HOCH}_2\text{CHO} + \text{HCHO} + 2\text{HO}_2$	$0.8 * (7.8 \times 10^{-14} \exp(1000/T) * 1.03 \times 10^{-13} \exp(365/T))^{0.5}$	3
K75	$\text{HOCH}_2\text{CH}_2\text{OO} + \text{CH}_3\text{OO}$	$\rightarrow \text{HOCH}_2\text{CHO} + \text{CH}_3\text{OH}$	$0.2 * (7.8 \times 10^{-14} \exp(1000/T) * 1.03 \times 10^{-13} \exp(365/T))^{0.5}$	3
K76	$\text{HOCH}_2\text{CH}_2\text{OOH} + \text{OH}$	$\rightarrow \text{HOCH}_2\text{CH}_2\text{OO}$	K45	
K77	$\text{HOCH}_2\text{CH}_2\text{OOH} + \text{OH}$	$\rightarrow \text{HOCH}_2\text{CHO} + \text{OH}$	1.38×10^{-11}	3
K78	$\text{HOCH}_2\text{CH}_2\text{ONO}_2 + \text{OH}$	$\rightarrow \text{HOCH}_2\text{CHO} + \text{NO}_2$	K47	
K79	$\text{C}_2\text{H}_2 + \text{OH}$	$\rightarrow 0.636(\text{CHOCHO} + \text{OH}) + 0.364(\text{HCOOH} + \text{CO} + \text{HO}_2)$	$5.0 \times 10^{-30} (T/300)^{-1.5} [\text{N}_2]$ 1.0×10^{-12} $Fc = 0.37$	1
K80	$\text{C}_2\text{H}_2 + \text{NO}_3$	$\rightarrow 0.635 \text{CHOCHO} + 0.365(\text{HCOOH} + \text{CO}) + \text{HNO}_3$	1.0×10^{-16}	1
K81	$\text{C}_2\text{H}_2 + \text{O}_3$	$\rightarrow 0.635 \text{CHOCHO} + 0.365(\text{HCOOH} + \text{CO})$	1.0×10^{-20}	1

K82	HOCH ₂ CHO + OH	→ HCHO + CO ₂	6.4×10^{-12}	1
K83	HOCH ₂ CHO + OH	→ CHOCHO + HO ₂	1.6×10^{-12}	1
K84	CHOCHO + OH	→ 2CO + HO ₂	$3.1 \times 10^{-12} \exp(340/T)$	1
K85	CHOCHO + NO ₃	→ 2CO + HO ₂ + HNO ₃	4.0×10^{-16}	1
K86	CH ₃ COOH + OH	→ CH ₃ OO + CO ₂	$4.0 \times 10^{-14} \exp(850/T)$	1
K87	CH ₃ CH ₂ OH + OH	→ 0.95 (CH ₃ CHO + HO ₂) + 0.05 HOCH ₂ CH ₂ OO	$3.0 \times 10^{-12} \exp(20/T)$	1
K88	C ₃ H ₈ + OH	→ 0.264 <i>n</i> -C ₃ H ₇ O ₂ + 0.736 <i>i</i> -C ₃ H ₇ O ₂	$7.6 \times 10^{-12} \exp(-585/T)$	1, 3
K89	<i>n</i> -C ₃ H ₇ O ₂ + HO ₂	→ <i>n</i> -C ₃ H ₇ OOH	$0.52 \times 2.91 \times 10^{-13} \exp(1300/T)$	3
K90	<i>n</i> -C ₃ H ₇ O ₂ + NO	→ C ₂ H ₅ CHO + HO ₂ + NO ₂	$(1 - RTC3P) \times 2.9 \times 10^{-12} \exp(350/T)$	1, 4
K91	<i>n</i> -C ₃ H ₇ O ₂ + NO	→ <i>n</i> -C ₃ H ₇ ONO ₂	$RTC3P \times 2.9 \times 10^{-12} \exp(350/T)$	1, 4
K92	<i>n</i> -C ₃ H ₇ O ₂ + CH ₃ OO	→ C ₂ H ₅ CHO + CH ₃ OH	$0.8 \times (3.5 \times 10^{-13} \times 3.0 \times 10^{13})^{0.5}$	3
K93	<i>n</i> -C ₃ H ₇ O ₂ + CH ₃ OO	→ C ₂ H ₅ CHO + HCHO + 2HO ₂	$0.2 \times (3.5 \times 10^{-13} \times 3.0 \times 10^{13})^{0.5}$	3
K94	<i>n</i> -C ₃ H ₇ OOH + OH	→ <i>n</i> -C ₃ H ₇ O ₂	K76	
K95	<i>n</i> -C ₃ H ₇ OOH + OH	→ C ₂ H ₅ CHO + OH	1.66×10^{-11}	3
K96	<i>n</i> -C ₃ H ₇ ONO ₂ + OH	→ C ₂ H ₅ CHO + NO ₂	5.8×10^{-13}	1
K97	<i>i</i> -C ₃ H ₇ O ₂ + HO ₂	→ <i>i</i> -C ₃ H ₇ OOH	K89	
K98	<i>i</i> -C ₃ H ₇ O ₂ + NO	→ CH ₃ COCH ₃ + HO ₂ + NO ₂	$(1 - RTC3S) * 2.7 \times 10^{-12} \exp(360/T)$	1, 4
K99	<i>i</i> -C ₃ H ₇ O ₂ + NO	→ <i>i</i> -C ₃ H ₇ ONO ₂	$RTC3S * 2.7 \times 10^{-12} \exp(360/T)$	1, 4
K100	<i>i</i> -C ₃ H ₇ O ₂ + CH ₃ OO	→ CH ₃ COCH ₃ + HCHO + 2HO ₂	$0.8 * (1.03 \times 10^{-13} \exp(365/T) * 1.6 \times 10^{-12} \exp(-2200/T))^{0.5}$	3
K101	<i>i</i> -C ₃ H ₇ O ₂ + CH ₃ OO	→ CH ₃ COCH ₃ + CH ₃ OH	$0.2 * (1.03 \times 10^{-13} \exp(365/T) * 1.6 \times 10^{-12} \exp(-2200/T))^{0.5}$	3
K102	<i>i</i> -C ₃ H ₇ OOH + OH	→ <i>i</i> -C ₃ H ₇ O ₂	$1.9 \times 10^{-12} \exp(190/T)$	3
K103	<i>i</i> -C ₃ H ₇ OOH + OH	→ CH ₃ COCH ₃ + OH	1.66×10^{-11}	3
K104	<i>i</i> -C ₃ H ₇ ONO ₂ + OH	→ CH ₃ COCH ₃ + NO ₂	$6.2 \times 10^{-13} \exp(-230/T)$	1
K105	C ₂ H ₄ CHO + OH	→ CH ₃ C(O)OO + CO	$4.9 \times 10^{-12} \exp(405/T)$	1
K106	C ₂ H ₅ CHO + NO ₃	→ CH ₃ C(O)OO + CO + HNO ₃	6.3×10^{-15}	1
K107	CH ₃ COCH ₃ + OH	→ CH ₃ COCH ₂ OO	$8.8 \times 10^{-12} \exp(-1320/T) + 1.7 \times 10^{-14} \exp(423/T)$	1
K108	CH ₃ COCH ₂ OO + NO	→ CH ₃ COCHO + NO ₂ + HO ₂	$2.7 \times 10^{-13} \exp(360/T)$	3
K109	CH ₃ COCH ₂ OO + HO ₂	→ CH ₃ COCH ₂ OOH	$1.36 \times 10^{-13} \exp(1250/T)$	3
K110	CH ₃ COCH ₂ OOH + OH	→ 0.7 CH ₃ COCHO + 0.3 CH ₃ COCH ₂ OO + OH	$1.90 \times 10^{-12} \exp(190/T)$	3
K111	C ₃ H ₈ + OH	→ HOC ₃ H ₆ OO	$8 \times 10^{-27} (T/300)^{-3.5} [N_2]$ $3.0 \times 10^{-11} (T/300)^{-1.0}$ $Fc = 0.5$	1
K112	C ₃ H ₈ + NO ₃	→ 0.35 <i>n</i> -C ₃ H ₇ ONO ₂ + 0.65 <i>i</i> -C ₃ H ₇ ONO ₂	$4.6 \times 10^{-13} \exp(-1155/T)$	1, 3
K113	C ₃ H ₈ + O ₃	→ 0.62 HCHO + 0.62 CH ₃ CHO + 0.38 CH ₃ OO + 0.56 CO + 0.36 HO ₂ + 0.36 OH + 0.2 CO ₂	$5.77 \times 10^{-15} \exp(-1880/T)$	1, 3
K114	HOC ₃ H ₆ OOH + OH	→ 0.928 CH ₃ COCH ₂ OH + 0.072 HOC ₃ H ₆ OO + 0.928 OH	$2.44 \times 10^{-11} + 1.9 \times 10^{-12} \exp(190/T)$	3
K115	HOC ₃ H ₆ OO + HO ₂	→ HOC ₃ H ₆ OOH	K89	3
K116	HOC ₃ H ₆ OO + NO	→ CH ₃ CHO + HCHO + HO ₂ + NO ₂	$(1 - 0.35RTC3P - 0.65RTC3S) * 2.55 \times 10^{-12} \exp(380/T)$	1, 3
K117	HOC ₃ H ₆ OO + NO	→ 0.35 <i>n</i> -C ₃ H ₇ ONO ₂ + 0.65 <i>i</i> -C ₃ H ₇ ONO ₂	$(0.35RTC3P + 0.65RTC3S) *$	1, 3

			2.55 x 10 ⁻¹² exp(380/T)		
K118	HOC ₃ H ₆ OO + CH ₃ OO	→ CH ₃ CHO + 2HCHO + 2HO ₂	0.8 * 6.0 x 10 ⁻¹³	3	
K119	HOC ₃ H ₆ OO + CH ₃ OO	→ CH ₃ COCH ₂ OH + CH ₃ OH	0.2 * 6.0 x 10 ⁻¹³	3	
K120	CH ₃ COCH ₂ OH + OH	→ CH ₃ COCHO + HO ₂	1.6 x 10 ⁻¹² exp(305/T)	1	
K121	CH ₃ COCHO + OH	→ CH ₃ C(O)OO + CO	1.9 x 10 ⁻¹² exp(575/T)	1	
K122	CH ₃ COCHO + NO ₃	→ CH ₃ C(O)OO + CO + HNO ₃	5.0 x 10 ⁻¹⁶	1	
K123	CH ₃ C(O)COOH + OH	→ CH ₃ C(O)OO + CO ₂	8.0 x 10 ⁻¹³	3	
K124	C ₄ H ₁₀ + OH	→ C ₄ H ₉ OO	9.8 x 10 ⁻¹² exp(-425/T)	3	
K125	C ₄ H ₁₀ + NO ₃	→ C ₄ H ₉ OO + HNO ₃	2.8 x 10 ⁻¹² exp(-3280/T)	1	
K126	C ₄ H ₉ OO + HO ₂	→ C ₄ H ₉ OOH	0.625 * 2.91 x 10 ⁻¹³ exp(1300/T)	3	
K127	C ₄ H ₉ OO + NO	→ NO ₂ + 0.67(CH ₃ CH ₂ COCH ₃ + HO ₂) + 0.33(C ₃ H ₇ OO + CH ₃ CHO)	(1 -RTC4P) x 8.3 x 10 ⁻¹²	1, 4	
K128	C ₄ H ₉ OO + NO	→ C ₄ H ₉ ONO ₂	RTC4P x 8.3 x 10 ⁻¹²	1, 4	
K129	C ₄ H ₉ OO + CH ₃ OO	→ HCHO + HO ₂ + 0.67(CH ₃ CH ₂ C(O)CH ₃ + HO ₂) + 0.33(CH ₃ CHO + CH ₃ CH ₂ OO)	0.8 * 1.3 x 10 ⁻¹²	3	
K130	C ₄ H ₉ OO + CH ₃ OO	→ CH ₃ CH ₂ COCH ₃ + CH ₃ OH	0.2 * 1.3 x 10 ⁻¹²	3	
K131	C ₄ H ₉ OOH + OH	→ C ₄ H ₉ OO	1.90 x 10 ⁻¹² exp(190/T)	3	
K132	C ₄ H ₉ OOH + OH	→ CH ₃ CH ₂ COCH ₃ + OH	2.15 x 10 ⁻¹¹	3	
K133	C ₄ H ₉ ONO ₂ + OH	→ CH ₃ CH ₂ COCH ₃ + NO ₂	8.6 x 10 ⁻¹³	1	
K134	CH ₃ CH ₂ COCH ₃ + OH	→ CH ₃ CH(OO)COCH ₃	1.5 x 10 ⁻¹² exp(-90/T)	1	
K135	CH ₃ CH(OO)COCH ₃ + HO ₂	→ CH ₃ CH(OOH)COCH ₃	K126		
K136	CH ₃ CH(OO)COCH ₃ + NO	→ CH ₃ CHO + CH ₃ C(O)OO + NO ₂	(1 -RTC4S) x 2.55 x 10 ⁻¹² exp(380/T)	1, 4	
K137	CH ₃ CH(OO)COCH ₃ + NO	→ CH ₃ CH(ONO ₂)COCH ₃	RTC4S x 2.55 x 10 ⁻¹² exp(380/T)	1, 4	
K138	CH ₃ CH(OOH)COCH ₃ + OH	→ CH ₃ CH(OO)COCH ₃	K131		
K139	CH ₃ CH(OOH)COCH ₃ + OH	→ CH ₃ C(O)C(O)CH ₃ + OH	1.88 x 10 ⁻¹¹	3	
K140	CH ₃ CH(ONO ₂)COCH ₃ + OH	→ CH ₃ C(O)C(O)CH ₃ + NO ₂	1.2 x 10 ⁻¹²	1	
K141	ISOP + OH	→ 0.98 ISOPOO + 0.0003 ELVOC + 0.007 SVOC	2.7 x 10 ⁻¹¹ exp(390/T)	1, 3	
K142	ISOP + NO ₃	→ ISOPONO ₂	2.95 x 10 ⁻¹² exp(-450/T)	1, 3	
K143	ISOP + O ₃	→ 0.98 * (0.3 MACR + 0.3 MACROO + 0.2 MVK + 0.2 MVKOO + 0.78 HCHO + 0.22CO + 0.125 HO ₂ + 0.125OH) + 0.0001 ELVOC + 0.009 SVOC	1.05 x 10 ⁻¹⁴ exp(-2000/T)	1, 3	
K144	ISOPOO + HO ₂	→ ISOPOOH	2.06 x 10 ⁻¹³ exp(1300/T)	3, 7	
K145	ISOPOO + NO	→ HCHO + 0.64 MVK + 0.36 MACR + HO ₂ + NO ₂	(1-RTCSS) * 2.7 x 10 ⁻¹² exp(360/T)	3	
K146	ISOPOO + NO	→ ISOPONO ₂	RTCSS * 2.7 x 10 ⁻¹² exp(360/T)	3	
K147	ISOPOO + NO ₃	→ HCHO + 0.64 MVK + 0.36 MACR + HO ₂ + NO ₂	2.3 x 10 ⁻¹²	3	
K148	ISOPOO + CH ₃ OO	→ 0.64 MVK + 0.36 MACR + 2HCHO + 2HO ₂	0.8 * 2.65 x 10 ⁻¹²	3	

K149	ISOPOO + CH ₃ OO	→ 0.64 MVK + 0.36 MACR + HCHO + CH ₃ OH	0.2 * 2.65 x 10 ⁻¹²	3
K150	ISOPOO	→ HPALD + HO ₂	4.12×10 ⁶ exp(-7700/T)	6, 7
K151	ISOPOOH + OH	→ IEPOX + OH	1.9×10 ⁻¹¹ exp(-390/T)	8
K152	ISOPOOH + OH	→ ISOPOO	0.7 * 3.8×10 ⁻¹² exp(-200/T)	8
K153	ISOPOOH + OH	→ 0.64 CH ₃ COCHO + 0.64 HOCH ₂ CHO + 0.36 HOCH ₂ C(O)CH ₃ + 0.36 CHOCHO + OH	0.3 * 3.8×10 ⁻¹² exp(-200/T)	8, 9
K154	ISOPONO ₂ + OH	→ 0.64 CH ₃ COCHO + 0.64 HOCH ₂ CHO + 0.36 HOCH ₂ C(O)CH ₃ + 0.36 CHOCHO + NO ₂	1.77×10 ⁻¹¹ exp(-500/T)	8
K155	HPALD + OH	→ 0.5 HOCH ₂ C(O)CH ₃ + 0.5 CH ₃ C(O)CHO + 0.25 HOCH ₂ CHO + 0.25 CHOCHO + HCHO + HO ₂ + OH	4.6×10 ⁻¹¹	6
K156	IEPOX + OH	→ IEPOXOO	5.78×10 ⁻¹¹ exp(-400/T)	8
K157	IEPOXOO + HO ₂	→ 0.725 HOCH ₂ C(O)CH ₃ + 0.275 HOCH ₂ CHO + 0.275 HOCH ₂ CHO + 0.275 CH ₃ C(O)CHO + 1.125 OH + 0.825 HO ₂ + 0.2 CO ₂ + 0.375 HCHO + 0.074 HCOOH + 0.251 CO	7.4×10 ⁻¹¹ exp(700/T)	8
K158	IEPOXOO + NO	→ 0.725 HOCH ₂ C(O)CH ₃ + 0.275 HOCH ₂ CHO + 0.275 HOCH ₂ CHO + 0.275 CH ₃ C(O)CHO + 1.125 OH + 0.825 HO ₂ + 0.2 CO ₂ + 0.375 HCHO + 0.074 HCOOH + 0.251 CO + NO ₂	2.7×10 ⁻¹² exp(360/T)	3
K159	IEPOXOO + NO ₃	→ 0.725 HOCH ₂ C(O)CH ₃ + 0.275 HOCH ₂ CHO + 0.275 HOCH ₂ CHO + 0.275 CH ₃ C(O)CHO + 1.125 OH + 0.825 HO ₂ + 0.2 CO ₂ + 0.375 HCHO + 0.074 HCOOH + 0.251 CO + NO ₂	1.74 * 2.3×10 ⁻¹²	3
K160	MVK + OH	→ MVKOO	2.6 x 10 ⁻¹² exp(610/T)	1
K161	MVK + NO ₃	→ 0.65 HCOOH + 0.65 CH ₃ COCHO + 0.35 HCHO + 0.35 CH ₃ C(O)OOH + HNO ₃	6.0 x 10 ⁻¹⁶	1
K162	MVK + O ₃	→ 0.38 CH ₃ COCHO + 0.2088 CH ₃ C(O)OO + 0.26 CH ₃ COCO ₂ OH + 0.26 CO + 0.0432 CH ₃ COOH + 0.108 CH ₃ CHO + 0.62 HCHO + 0.48 CO ₂ + 0.54 HO ₂ + 0.1008 OH	8.5 x 10 ⁻¹⁶ exp(-1520/T)	1, 3
K163	MVKOO + HO ₂	→ MVKOOH	K144	
K164	MVKOO + NO	→ 0.295 CH ₃ C(O)CHO + 0.295 HCHO + 0.670 CH ₃ CHO + 0.670 HOCHCHO + 0.295 HO ₂ + 0.965 NO ₂ + 0.0352 MVKONO ₂	2.7 x 10 ⁻¹² exp(260/T)	3
K165	MVKOOH + OH	→ CH ₃ C(O)CHO + CO + 2HO ₂ + OH	2.55 x 10 ⁻¹¹	3
K166	MVKOOH + OH	→ MVKOO	1.9 x 10 ⁻¹² exp(190/T)	3
K167	MVKONO ₂ + OH	→ CH ₃ C(O)CHO + CO + HO ₂ + NO ₂	1.33 x 10 ⁻¹²	3
K168	MACR + OH	→ MACROO	8.0 x 10 ⁻¹² exp(380/T)	1
K169	MACR + NO ₃	→ MACROO + HNO ₃	3.4 x 10 ⁻¹⁵	1
K170	MACR + O ₃	→ 0.90 CH ₃ COCHO + 0.5 HCHO + 0.5 CO + 0.14 HO ₂ + 0.24 OH	1.4 x 10 ⁻¹⁵ exp(-2100/T)	1, 3
K171	MACROO + HO ₂	→ MACROOH	0.625 * 2.91 x 10 ⁻¹³ exp(1300/T)	3
K172	MACROO + NO	→ 0.987 (CH ₃ COCH ₂ OH + CO + NO ₂ + HO ₂) + 0.013 MACRONO ₂	K164	1, 3
K173	MACROOH + OH	→ CH ₃ COCH ₂ OH + CO + OH	3.77 x 10 ⁻¹¹	

Deleted: 6

Deleted: 380

K174	MACROOH + OH	→	MACROO	K166	
K175	MACRONO ₂ + OH	→	CH ₃ COCHO + CO + HO ₂ + NO ₂	4.34 x 10 ⁻¹²	3
K176	TERP + OH	→	0.81 TERPOO + 0.05 ELVOC + 0.14 SVOC	0.5 * 1.34 x 10 ⁻¹¹ exp(410/T) + 0.5 * 1.62 x 10 ⁻¹¹ exp(460/T)	1, 10
K177	TERP + NO ₃	→	TERPOO + HNO ₃	0.5 * 1.2 x 10 ⁻¹² exp(490/T) + 0.5 * 2.5 x 10 ⁻¹²	1, 10
K178	TERP + O ₃	→	0.915 MACR + 0.36 MVK + 0.24 PRV + 1.68 HCHO + 0.16 CO + 0.6 HCOOH + 0.08 C ₃ H ₆ + 0.68 OH + 0.05 ELVOC + 0.14 SVOC	0.5 * 8.22 x 10 ⁻¹⁶ exp(-640/T) + 0.5 * 1.39 x 10 ⁻¹⁵ exp(-1280/T)	1, 10
K179	TERPOO + HO ₂	→	2 ISOPOOH	K144	
K180	TERPOO + NO	→	2 (HCHO + 0.64MVK + 0.36MACR + HO ₂) + NO ₂	K145	
K181	TERPOO + NO	→	2 ISOPONO ₂	K146	
K182	TERPOO + NO ₃	→	2 (HCHO + 0.64MVK + 0.36MACR + HO ₂) + NO ₂	K147	
K183	TERPOO + CH ₃ OO	→	2 (0.64MVK + 0.36MACR + 2HCHO + 2HO ₂)	K148	
K184	TERPOO + CH ₃ OO	→	2 (0.64MVK + 0.36MACR + HCHO + CH ₃ OH)	K149	
K185	AROM + OH	→	AROMOO + HO ₂	A1 * 1.8 x 10 ⁻¹² exp(340/T) + A2 * 1.72 x 10 ⁻¹¹ + A3 * 2.3 x 10 ⁻¹² exp(-190/T)	1, 11
K186	AROM + NO ₃	→	AROMOO + HNO ₃	A1 * 7.8 x 10 ⁻¹⁷ + A2 * 3.54 x 10 ⁻¹⁶	1, 11
K187	AROM + O ₃	→	AROMOO	A1 * 1.0x 10 ⁻²¹ + A2 * (2.4 x 10 ⁻¹³ exp(-5586/T) + 5.37 x 10 ⁻¹³ exp(-6039/T) + 1.91 x 10 ⁻¹³ exp(-5586/T))/3	1, 11, 12
K188	AROMOO + HO ₂	→	C ₆ H ₉ OOH + CHOCHO + HCHO	K126	
K189	AROMOO + NO	→	NO ₂ + 0.67CH ₃ CH ₂ COCH ₃ + 0.67 HO ₂ + 0.33C ₂ H ₅ OO + 0.33CH ₃ CHO + CHOCHO + HCHO	K127	
K190	AROMOO + NO	→	C ₆ H ₉ ONO ₂ + CHOCHO + HCHO	K128	
K191	AROMOO + CH ₃ OO	→	HCHO + HO ₂ + 0.67(CH ₃ CH ₂ C(O)CH ₃ + HO ₂) + 0.33(CH ₃ CHO + CH ₃ CH ₂ OO) + CHOCHO + HCHO	K129	
K192	AROMOO + CH ₃ OO	→	CH ₃ CH ₂ COCH ₃ + CH ₃ OH + CHOCHO + HCHO	K130	
K193	SO ₂ + OH	→	HO ₂ + H ₂ SO ₄	3.3 x 10 ⁻³¹ (T/300) ^{-4.3} [N ₂] 1.6 x 10 ⁻¹² (T/300) ^{0.7} Fc = 0.6	2
K194	DMS + OH	→	CH ₃ OO + HCHO + SO ₂	1.1 x 10 ⁻¹¹ exp(-240/T)	2
K195	DMS + OH	→	0.75 CH ₃ OO + 0.75 HCHO + 0.75 SO ₂ + 0.25 MSA	1.0 x 10 ⁻³⁹ [O ₂] exp(5820/T) / (1 + 5.0 x 10 ⁻³⁹ [O ₂] exp(6280/T))	2
K196	DMS + NO ₃	→	CH ₃ OO + HCHO + SO ₂ + HNO ₃	1.9 x 10 ⁻¹³ exp(520/T)	2
K197	NH ₃ + OH	→	NH ₂ + HO ₂	1.7 x 10 ⁻¹² exp(-710/T)	2
K198	NH ₂ + O ₂	→	NH ₂ O ₂	6.0 x 10 ⁻²¹	2

K199	$\text{NH}_2 + \text{O}_3$	$\rightarrow \text{NH}_2\text{O}_2$	$4.3 \times 10^{-12} \exp(-930/T)$	2
K200	$\text{NH}_2 + \text{OH}$	$\rightarrow \text{NH}_2\text{O}_2$	3.4×10^{-11}	2
K201	$\text{NH}_2 + \text{HO}_2$	$\rightarrow \text{NH}_3$	3.4×10^{-11}	2
K202	$\text{NH}_2 + \text{NO}$	$\rightarrow \text{NH}_2\text{O}_2 + \text{NO}_2$	$4.0 \times 10^{-12} \exp(450/T)$	2
K203	$\text{NH}_2 + \text{NO}_2$	$\rightarrow \text{NH}_2\text{O}_2 + \text{NO}$	$2.1 \times 10^{-12} \exp(650/T)$	2
K204	$\text{NH}_2\text{O}_2 + \text{O}_3$	$\rightarrow \text{NH}_2$	K199	
K205	$\text{NH}_2\text{O}_2 + \text{HO}_2$	$\rightarrow \text{NH}_2$	K201	
K206	$\text{NH}_2\text{O}_2 + \text{NO}$	$\rightarrow \text{NH}_2 + \text{NO}_2$	K202	

⁸ The reaction products O_2 , H_2 , and H_2O are not shown.

¹ The chemical kinetic data and mechanistic information was taken from the website of the IUPAC Task Group on Atmospheric Chemical Kinetic Data Evaluation: www.iupac-kinetic.ch.cam.ac.uk

5 ² The chemical kinetic data and mechanistic information was taken from the website of the NASA Panel for Data Evaluation (Evaluation No. 18, JPL Publication 15-10) <http://jpldataeval.jpl.nasa.gov>

³ The chemistry mechanistic information was taken from the Master Chemical Mechanism (MCM v3.1):

- for non-aromatic schemes: Jenkin et al. (1997); Saunders et al. (2003)
- for the isoprene scheme: Jenkin et al. (2015)
- 10 ▪ for aromatic schemes: Jenkin et al. (2003); Bloss et al. (2005)
- and via the website: <http://mcm.leeds.ac.uk/MCM>

⁴ Atkinson (1997):

$$R_1 = 2.7 \times 10^{14} \exp(-6350/T)$$

$$R_2 = 6.3 \times 10^{14} \exp(-550/T)$$

15 $f = R_1/(R_1 + R_2 \times [\text{O}_2])$

$$R_1 = 1.94 \times 10^{-22} [\text{AIR}] \exp(0.972 \times N_c)$$

$$R_2 = 0.826 \times (T/300)^{8.1}$$

$$A = 1/(1 + \log_{10}(R_1/R_2)^2)$$

$$\text{RTC}(N_c)\text{P} = 0.4 \times R_1/(1 + R_1/R_2) \times 0.411^A$$

20 $\text{RTC}(N_c)\text{S} = R_1/(1 + R_1/R_2) \times 0.411^A$

where, N_c is the number of carbons (i.e., 1-5)

⁵ Orlando et al. (1992); Poisson et al. (2000)

⁶ Peeters and Müller (2010)

⁷ Crounse et al. (2011)

25 ⁸ Paulot et al. (2009)

⁹ Browne et al. (2014)

¹⁰ Average of α - and β -pinene

¹¹ A1, A2, A3 represents the relative contributions of *ortho*-, *meta*-, and *para*-xylene, toluene and benzene (roughly 0.4, 0.6 and 0.4, respectively, for the year 2006)

30 ¹² Average of *ortho*-, *meta*- and *para*-isomers of xylene

Deleted: 2

Table 3. Global annual emissions of trace gases used for the MOGUNTIA chemistry scheme in TM5-MP for the year 2006, in Tg yr⁻¹ unless specified otherwise.

Species	Long name	Emissions					
		Anthropogenic ^{&}	Biomass Burning	Biogenic	Soil	Oceanic	Other
CO	carbon monoxide	600.5	386.4	90.2		19.9	
HCHO	formaldehyde	2.4	5.2	4.7			
HCOOH	formic acid	4.6	1.8	3.5			
CH ₃ OH	methanol	4.7	9.8	131.9			
C ₂ H ₆	ethane	6.2	3.4	0.3		1.0	
C ₂ H ₄	ethene	5.3	4.8	18.3		1.4	
C ₂ H ₂	acetylene	3.3					
CH ₃ CHO	acetaldehyde	1.2	4.4	21.9			
CH ₃ COOH	acetic acid	4.6	18.0	3.5			
CH ₃ CH ₂ OH	ethanol	0.5	0.1	18.6			
HOCH ₂ CHO	glycol-aldehyde	1.4	4.3				
CHOCHO	glyoxal	2.4	5.2				
C ₃ H ₈	propane	6.5	0.7	0.03		1.3	
C ₃ H ₆	propene and higher alkenes	8.3	4.8	17.5		1.5	
CH ₃ COCH ₃	acetone	2.7	1.7	37.7			
CH ₃ COCHO	methylglyoxal	1.6	3.4				
C ₄ H ₁₀	butane and higher alkanes (including butane, pentane, hexane, higher alkanes, and other vocs)	52.8	0.5	0.1			
CH ₃ CH ₂ COCH ₃	methyl-ethyl-ketone (including higher ketones except for acetone)	1.4	1.4	0.9			
C ₅ H ₈	isoprene			579.4			
C ₁₀ H ₁₆	monoterpenes			97.9			
C ₇ H ₈	toluene and aromatics (including toluene, xylene benzene, trimethylbenzene and higher aromatics)	25.3	4.0	1.5			

NO _x [#]	nitrogen oxides	42.3	6.6	5.0	6.0 [*]	59.9
NH ₃	ammonia	56.1	4.4	2.3	8.1	70.9
SO ₂	sulfur dioxide	120.5	2.3		9.3 [§]	132.1
CH ₃ SCH ₃	dimethylsulphide			1.7	95.8	97.5

[#]including aircraft emissions

[#] in Tg-N yr⁻¹

^{*}NO_x production from lightning

[§] SO₂ from volcanoes

Table 4. Tropospheric budgets of O₃ for the year 2006 in Tg(O₃) yr⁻¹ and burden in Tg(O₃), using the 150 ppb O₃ mixing ratio to define tropopause level. In parentheses, the relative differences using the 100 ppb O₃ mixing ratios are also presented, calculated by reference to the 150 ppb O₃ tropopause level definition.

Production terms	mCB05 (EBI)	mCB05 (KPP)	MOGUNTIA	Loss terms	mCB05 (EBI)	mCB05 (KPP)	MOGUNTIA
Stratospheric inflow*	632 (10%)	429 (32%)	424 (30%)	Deposition	955 (0%)	932 (0%)	913 (0%)
Trop. chem. production	5589 (-3%)	5719 (-3%)	5709 (-3%)	Trop. chem. loss	5192 (-1%)	5216 (-1)	5219 (-1%)
Trop. burden	385 (-8%)	384 (-8%)	375 (-8%)	Trop. lifetime (days)	22.8 (-8%)	22.8 (-8%)	22.3 (-6%)

*sum of the deposition and the tropospheric chemical loss minus the production

Table 5. Tropospheric chemical budget of OH for the year 2006 in Tg(OH) yr⁻¹, using the 150 ppb O₃ mixing ratio to define tropopause level. In parentheses, the relative differences using the 100 ppb O₃ mixing ratios are also presented, calculated by reference to the 150 ppb O₃ tropopause level definition.

Production terms	mCB05 (EBI)	mCB05 (KPP)	MOGUNTIA	Loss terms	mCB05 (EBI)	mCB05 (KPP)	MOGUNTIA
O(¹ D) + H ₂ O	1960 (0%)	1953 (0%)	1878 (0%)	OH + CO	1665 (-2%)	1671 (-2%)	1775 (-4%)
NO + HO ₂	1268 (-4%)	1312 (-4%)	1426 (-4%)	OH + CH ₄	613 (0%)	626 (0%)	644 (-4%)
O ₃ + HO ₂	560 (-1%)	566 (-1%)	561 (-1%)	OH + O ₃	254 (-2%)	260 (-2%)	262 (-4%)
H ₂ O ₂ + hν	262 (-1%)	265 (-1%)	303 (-1%)	OH + ISOP	114 (-1%)	115 (-1%)	120 (-4%)
Other	203 (-2%)	201 (-2%)	120 (-1%)	Other	1606 (-1%)	1626 (-1%)	1487 (-4%)

Table 6. Global budgets of CO for the year 2006 in Tg(CO) yr⁻¹ and burden in Tg(CO), using the 150 ppb O₃ mixing ratio to define tropopause level. In parentheses, the relative differences using the 100 ppb O₃ mixing ratios are also presented, calculated by reference to the 150 ppb O₃ tropopause level definition.

Production terms	mCB05 (EBI)	mCB05 (KPP)	MOGUNTIA	Loss terms	mCB05 (EBI)	mCB05 (KPP)	MOGUNTIA
Emissions	1097 (0%)	1097 (0%)	1097 (0%)	Deposition	98 (0%)	97 (0%)	99 (2%)
Trop. chem. production	1809 (-1%)	1818 (-1%)	1992 (-1%)	Trop. chem. loss	2840 (-6%)	2849 (-6%)	2924 (-2%)
Strat. chem. production	26 (69%)	26 (73%)	26 (65%)	Strat. chem. loss	87 (68%)	89 (69%)	90 (67%)
Atmos. burden	370 (0%)	360 (0%)	361 (0%)	Lifetime (days)	47.5 (2%)	46.2 (2%)	43.6 (-2%)

Deleted:).

Formatted ... [27]

Formatted ... [28]

Formatted ... [29]

Formatted ... [30]

Inserted Cells ... [31]

Inserted Cells ... [33]

Inserted Cells ... [35]

Inserted Cells ... [41]

Formatted ... [34]

Inserted Cells ... [37]

Inserted Cells ... [39]

Formatted ... [32]

Formatted ... [36]

Formatted ... [38]

Formatted ... [40]

Formatted ... [42]

Formatted ... [45]

Formatted ... [43]

Formatted ... [44]

Formatted ... [46]

Formatted ... [47]

Formatted ... [51]

Formatted ... [48]

Formatted ... [49]

Formatted ... [50]

Formatted ... [52]

Formatted ... [53]

Deleted: .

Formatted ... [54]

Formatted ... [55]

Formatted ... [56]

Formatted ... [57]

Formatted ... [58]

Inserted Cells ... [59]

Formatted ... [60]

Inserted Cells ... [61]

Formatted ... [62]

Inserted Cells ... [63]

Formatted ... [64]

Inserted Cells ... [65]

Formatted ... [66]

Inserted Cells ... [67]

Formatted ... [68]

Inserted Cells ... [69]

Formatted ... [70]

Formatted ... [71]

Formatted ... [72]

Formatted ... [73]

Formatted ... [74]

Formatted ... [75]

Formatted ... [76]

Formatted ... [77]

Formatted ... [78]

Figures

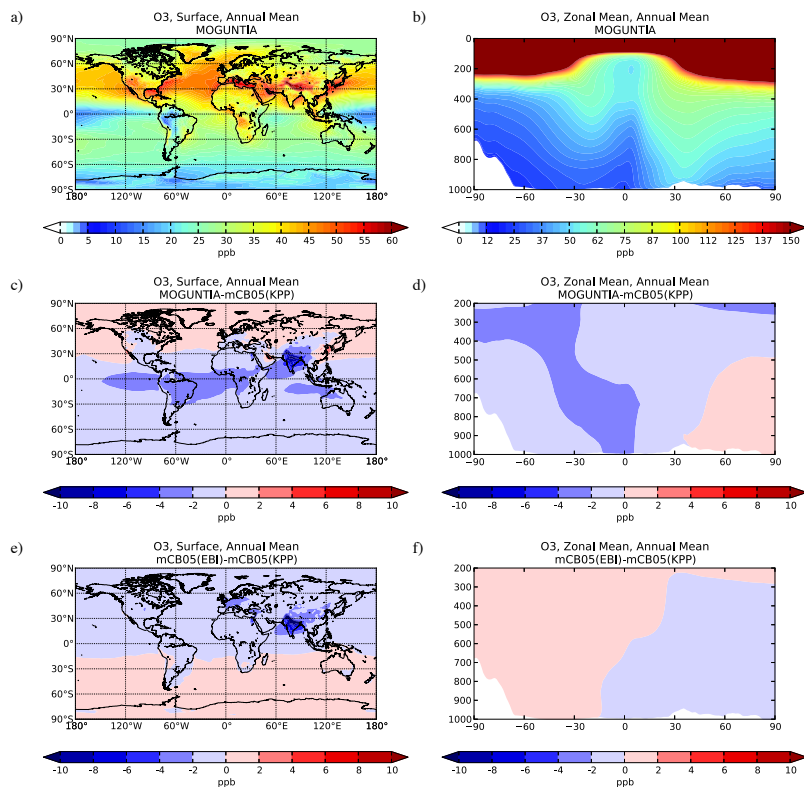


Figure 1: Simulated annual mean surface (left columns) and zonal mean (right columns) O₃ mixing ratios (ppb) for the MOGUNTIA chemistry scheme for the year 2006 (a,b), and the respective differences compared to mCB05(KPP) (c,d); the surface and zonal mean absolute differences between mCB05(KPP) and mCB05(EBI) are also presented (e,f).

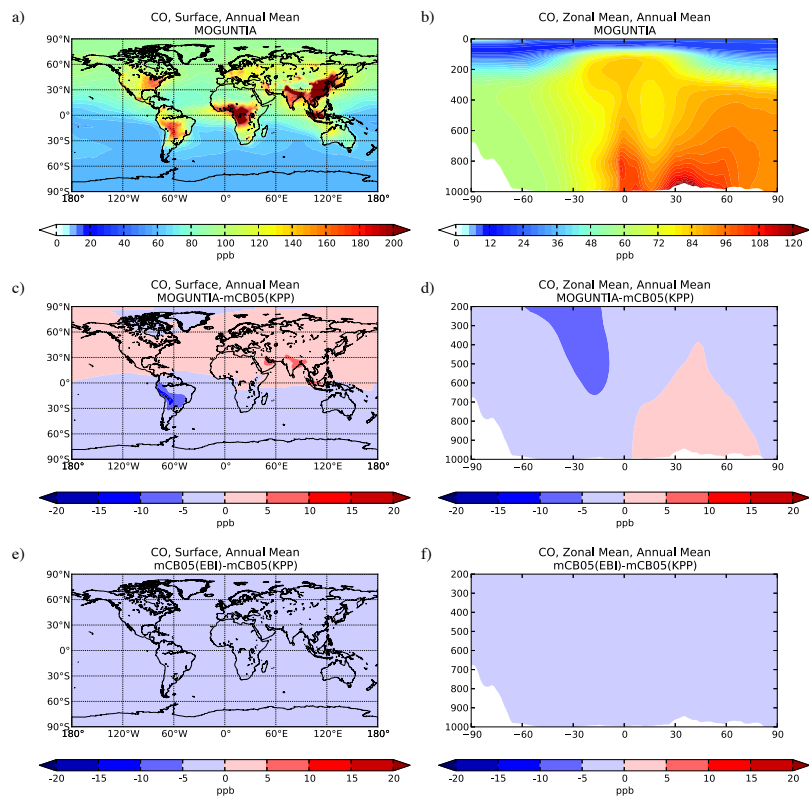


Figure 2: Simulated annual mean surface (left columns) and zonal mean (right columns) CO mixing ratios (ppb) for the MOGUNTIA chemistry scheme for the year 2006 (a,b), and the respective differences compared to mCB05(KPP) (c,d); the surface and zonal mean absolute differences between mCB05(KPP) and mCB05(EBI) are also presented (e,f).

Trop. NO₂ columns / OMI / 2006

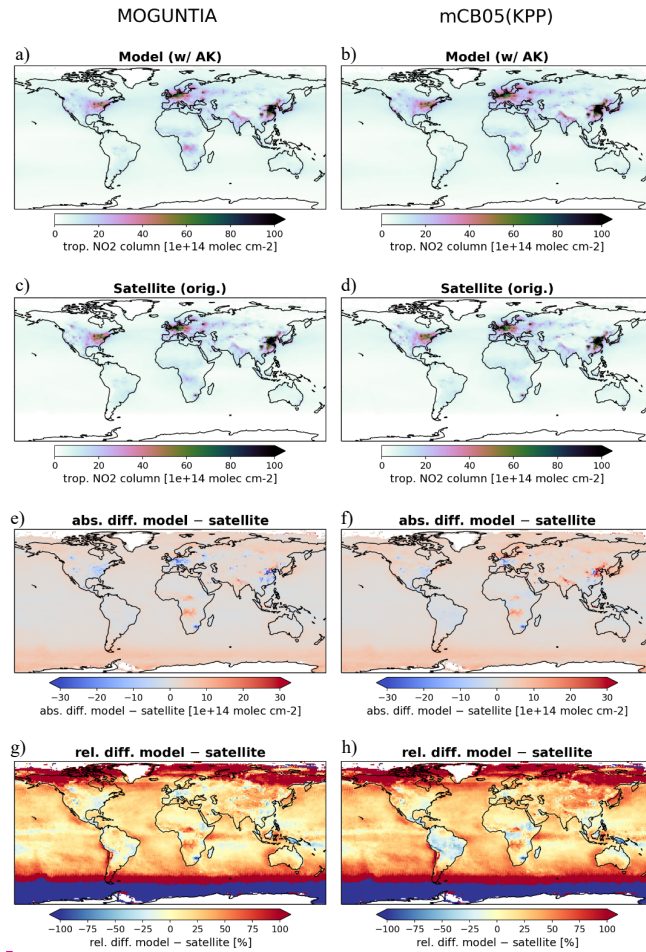
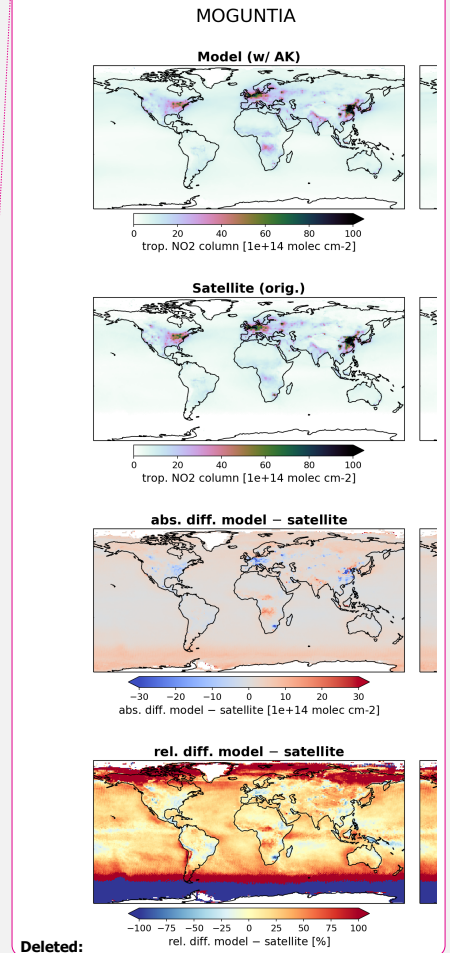


Figure 3: Annual mean comparison of tropospheric NO₂ vertical columns (molecules cm⁻²) for the two chemistry schemes MOGUNTIA and mCB05(KPP) (a,b), against the Ozone Monitoring Instrument (OMI) satellite data (c,d), using the respective averaging kernel information for 2006. The absolute (e,f) and relative (g,h) differences are also presented.

Trop. NO₂ columns



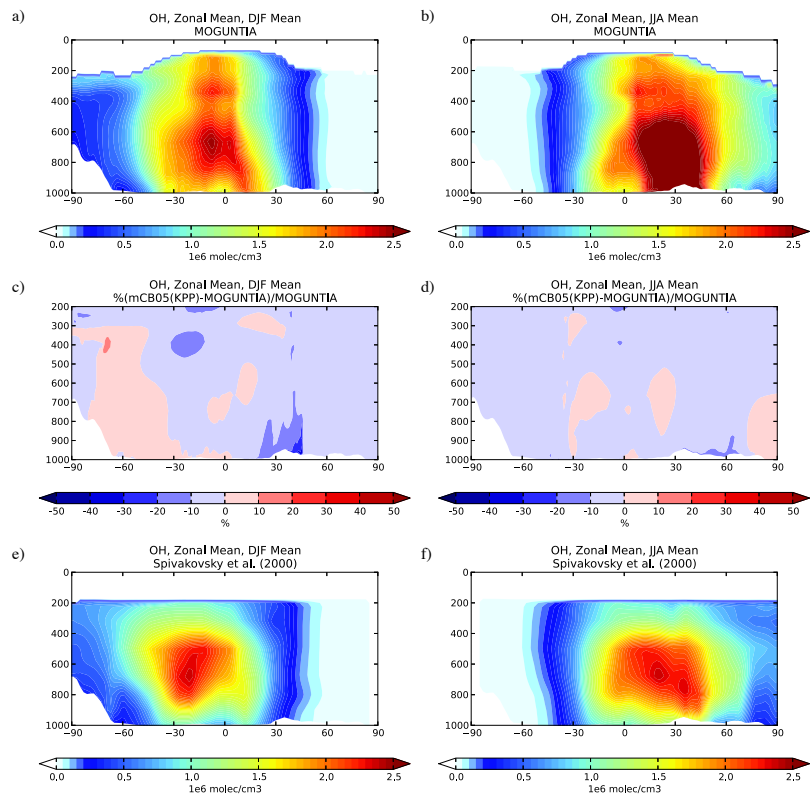


Figure 4: Zonal mean OH mixing ratios for December-January-February (DJF; left) and June-July-August (JJA; right) 2006, as simulated by the TMS-MP model with the MOGUNTIA chemistry scheme (top), the differences (%) between the mCB05(KPP) and the MOGUNTIA chemical configuration (middle), and the optimized climatological average from Spivakovsky et al. (2000), up to 200 hPa (bottom).

Deleted: February

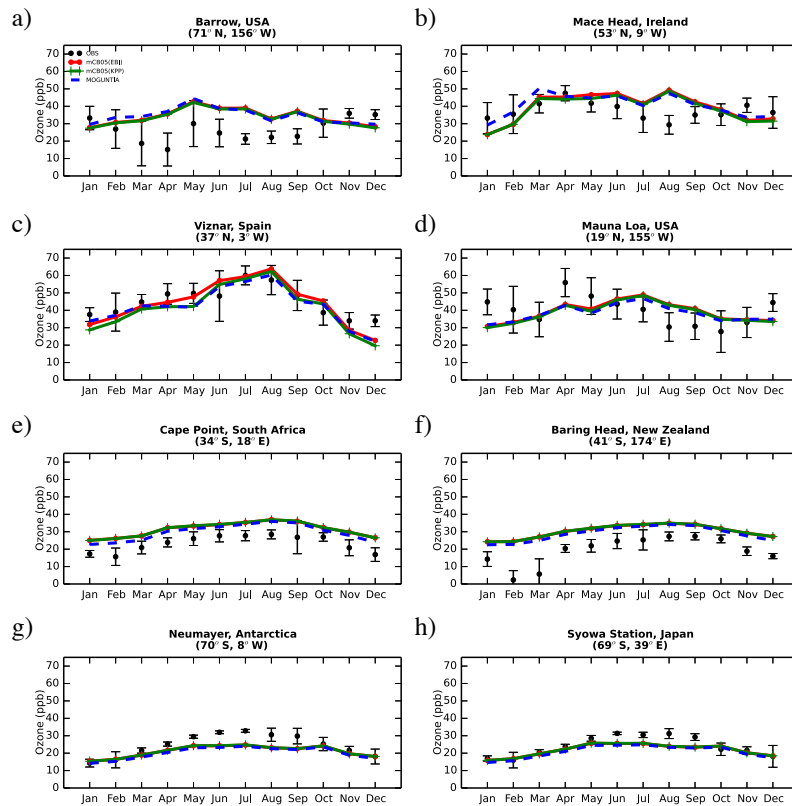
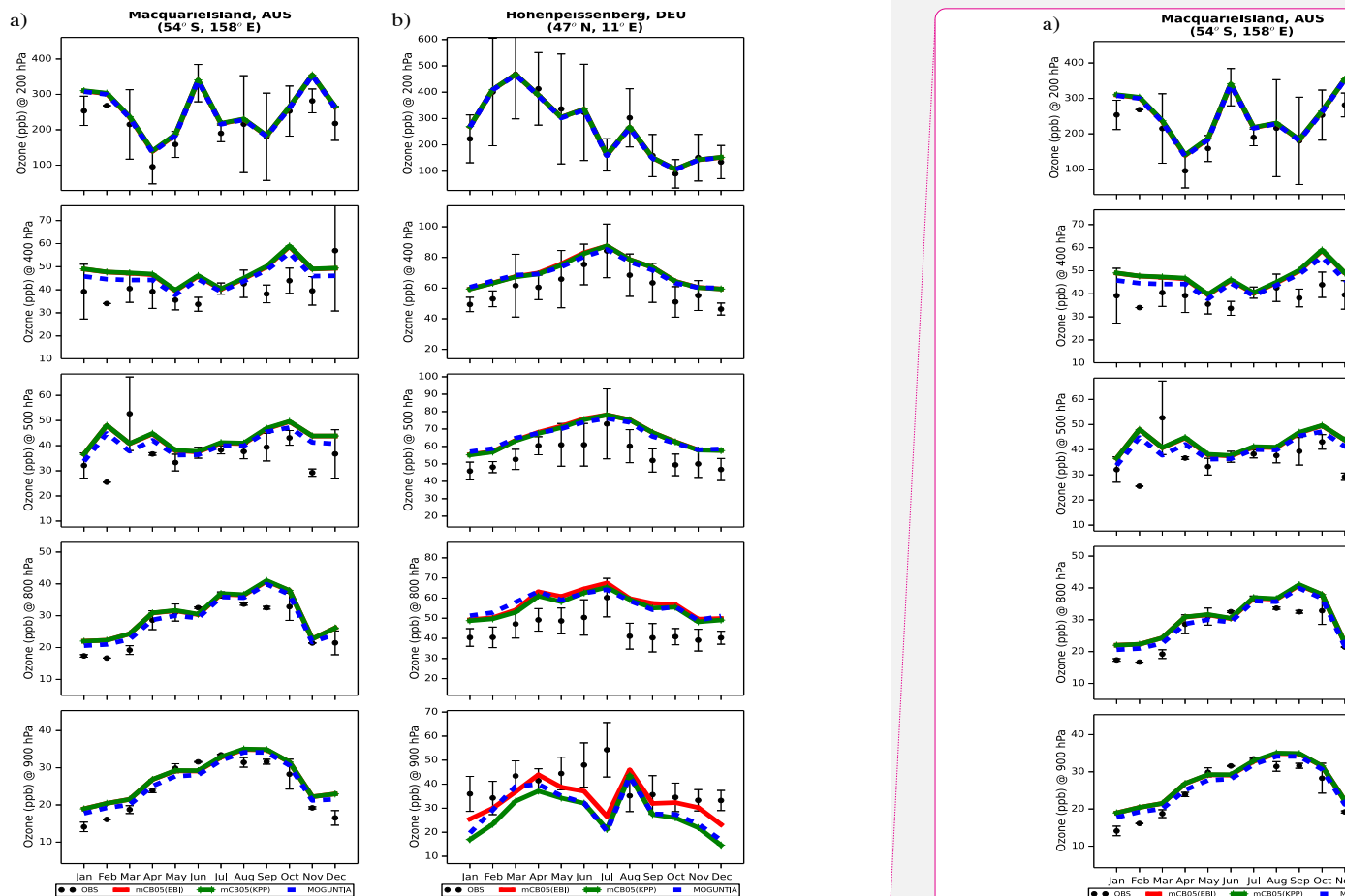


Figure 5: Monthly mean comparison of TMS-MP surface O_3 (ppb) against surface observations (black line) from EMEP and WOUDC databases for the two chemistry schemes, mCB05(KPP) (green line) and MOGUNTIA (blue line), using co-located model output for 2006 sampled at the measurement times; error bars indicate the standard deviation in the monthly means. For comparison, model results of the mCB05 with the EBI solver (red line) are also presented.



Deleted:

Figure 6: Monthly mean comparison of TMS-MP O₃ (ppb) against sonde observations (black dots, mean and standard deviation) at a) Hohenpeissenberg and b) Macquarie Island, for different pressure levels (900; 800; 500; 400; 200 hPa) for the two chemistry schemes, mCB05(KPP) (green line) and MOGUNTIA (blue line), using co-located model output for 2006 sampled at the

measurement times; error bars indicate the standard deviation in the monthly means. For comparison, the results of mCB05 with the EBI solver (red line) are also presented.

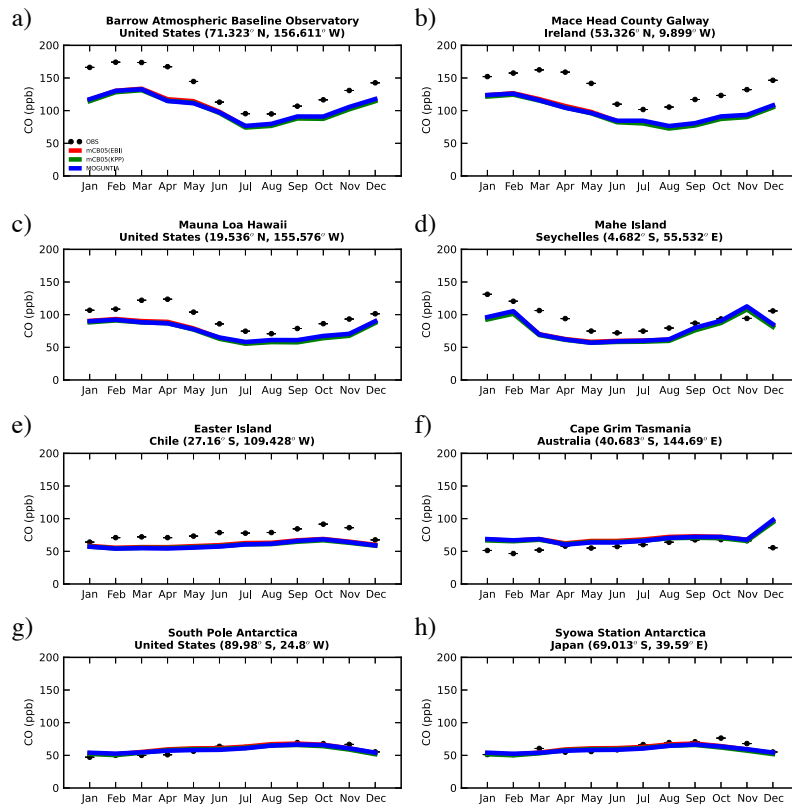


Figure 7: Monthly mean comparison of TM5-MP surface CO (ppb) against flask measurements (black line) for the two chemistry schemes, mCB05(KPP) (green line) and MOGUNTIA (blue line), using co-located model output for 2006 sampled at the measurement times; error bars indicate the standard deviation in the monthly means. For comparison, model results of the mCB05 with the EBI solver (red line) are also presented.

CO columns / MOPITT / 2006

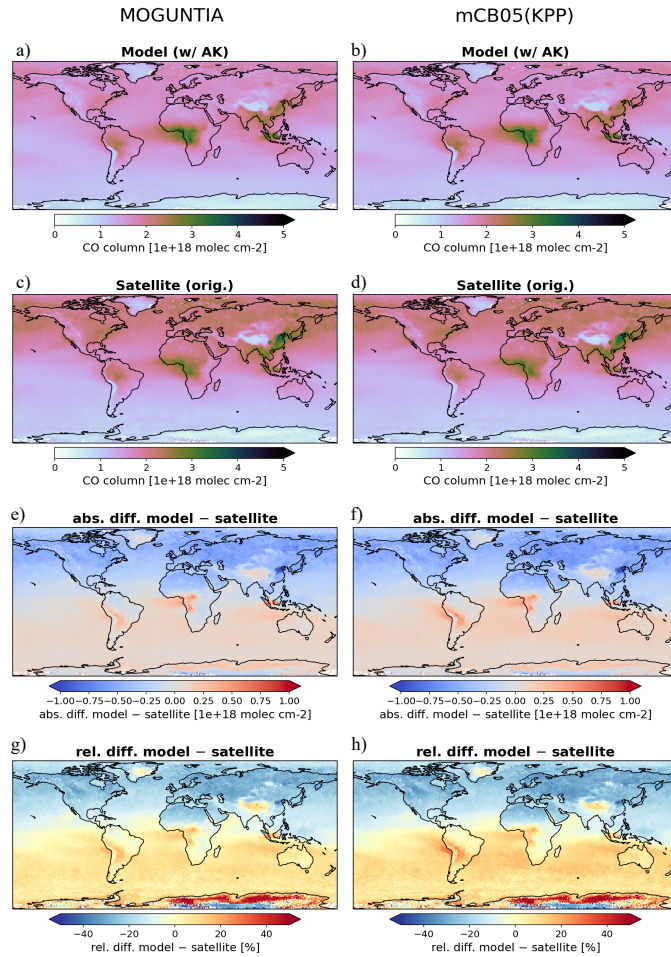


Figure 8: Annual mean comparison of total CO vertical columns (molecules cm^{-2}) for the two chemistry schemes of TM5-MP, MOGUNTIA and mCB05(KPP) (a,b), against MOPITT satellite data (c,d), using the respective averaging kernel information for 2006. The absolute (e,f) and relative (g, h) differences are also presented.

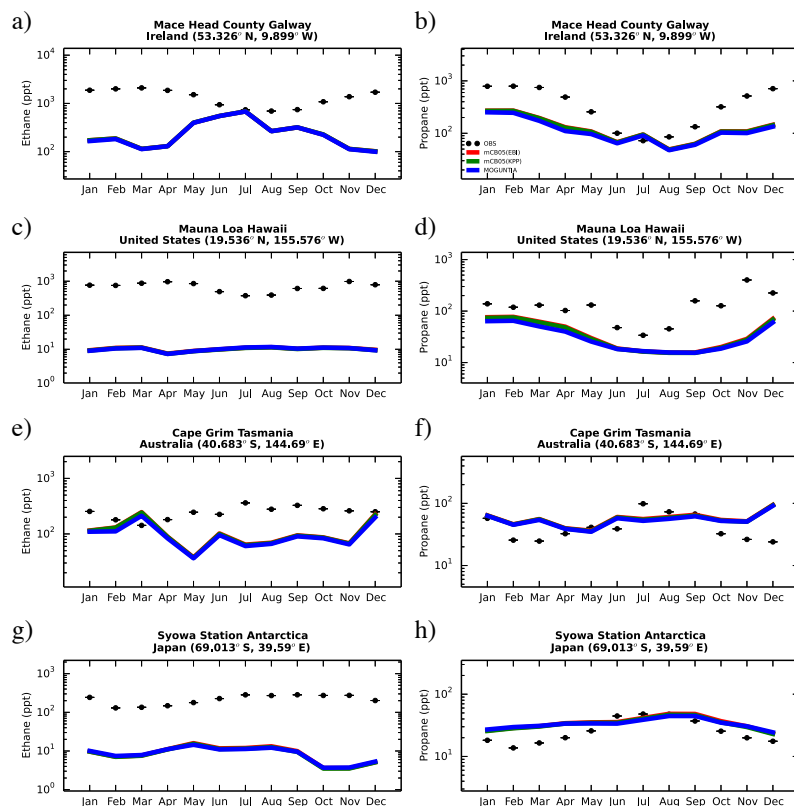


Figure 9: Monthly mean comparison of TM5-MP surface C_2H_6 (left column) and C_3H_8 (right column) against flask measurements (black dots) in ppt for the two chemistry schemes, mCB05(KPP) (green line) and MOGUNTIA (blue line), using co-located model output for 2006 sampled at the measurement times; error bars indicate the standard deviation in the monthly means. For comparison, model results of the mCB05 with the EBI solver (red line) are also presented.

Deleted: column

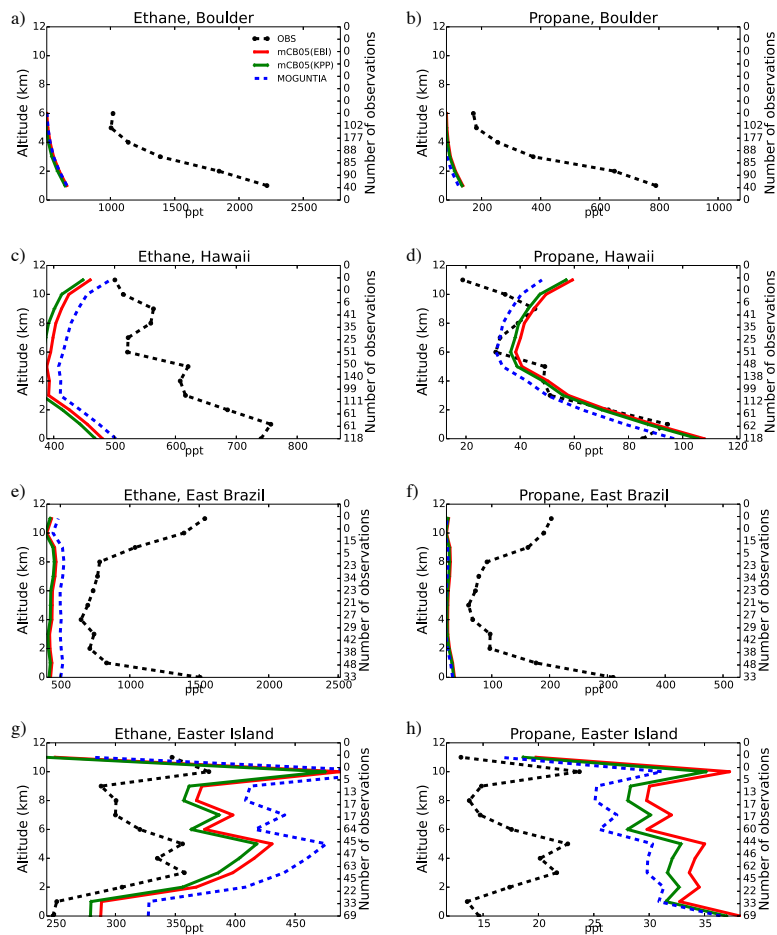


Figure 10: Comparison of TM5-MP vertical profiles (in km) of C_2H_6 (left column) and C_3H_8 (right column) against aircraft observations (black line) in ppt, for the two chemistry schemes, mCB05(KPP) (green line) and MOGUNTIA (blue line), using co-located model output for 2006 sampled at the measurement times; error bars indicate the standard deviation. For comparison, model results of the mCB05 with the EBI solver (red line) are also presented. The numbers on the right vertical axis indicate the number of available measurements.

Deleted:

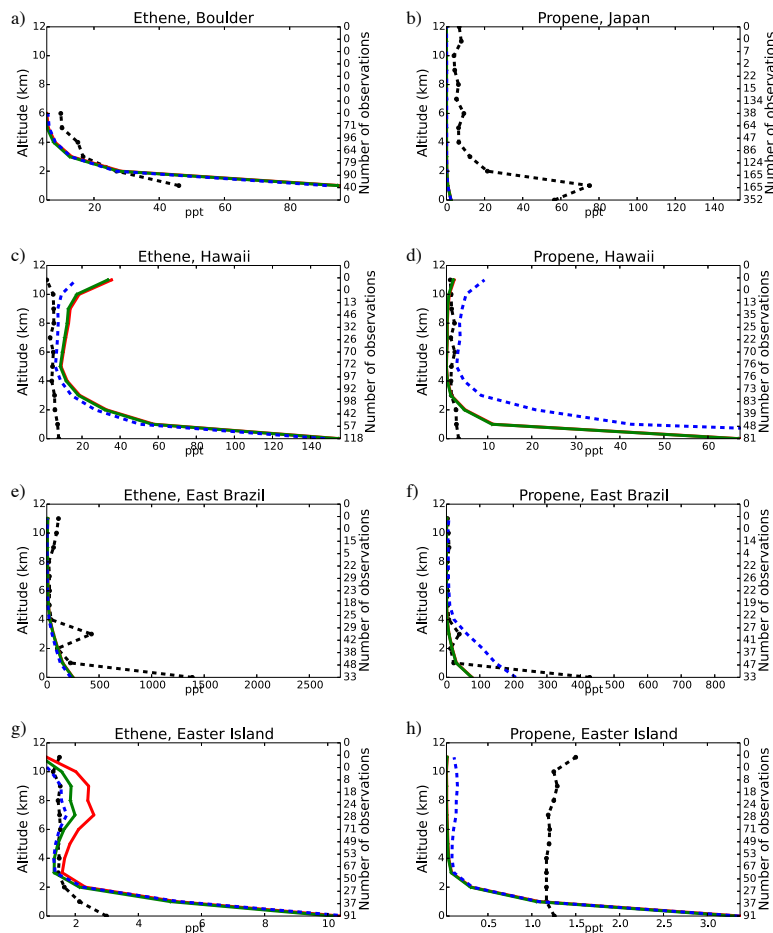


Figure 11: Comparison of TM5-MP vertical profiles (in km) of C_2H_4 (left column) and C_3H_6 (right column) against aircraft observations (black line) in ppt, for the two chemistry schemes, mCB05(KPP) (green line) and MOGUNTIA (blue line), using co-located model output for 2006 sampled at the measurement times; error bars indicate the standard deviation. For comparison, model results of the mCB05 with the EBI solver (red line) are also presented. The numbers on the right vertical axis indicate the number of available measurements.

Deleted:

Supplementary Tables

Table S1: Selection of effective Henry law coefficients (H^*) used in TMS-MP for the MOGUNTIA chemical scheme.

Trace gas	H^* (M atm ⁻¹)	ΔH R ⁻¹ (K)	Reference
CH ₃ OOH, <i>n</i> -C ₃ H ₇ OOH, <i>i</i> -C ₃ H ₇ OOH, CH ₃ COCH ₂ OH, C ₄ H ₉ OOH, MEKOOH, ISOPOOH, MVKOOH, MACROOH	2.9 x 10 ²	5200	1
CH ₃ ONO ₂	2.0	4700	1
CH ₃ OONO ₂	2.0	4700	1
HCHO	3.2 x 10 ³	6800	1
CH ₃ OH	2.0 x 10 ²	5600	1
HCOOH	8.8 x 10 ³	6100	1
CH ₃ CH ₂ OOH	3.3	6000	1
CH ₃ CH ₂ ONO ₂	1.6	5400	1
HOCH ₂ CH ₂ OOH	1.7 x 10 ⁶	9700	1
HOCH ₂ CH ₂ ONO ₂	3.9 x 10 ⁴		1
CH ₃ CHO	13	5900	1
CH ₃ COOH	8.3 x 10 ²	5300	1
HOCH ₂ CHO	4.1 x 10 ⁴	4600	1
CHOCHO	4.19 x 10 ⁵	7500	1
CH ₃ CH ₂ OH	190	6400	1
CH ₃ COOH	4.0 x 10 ³	6200	1
<i>n</i> -C ₃ H ₇ ONO ₂	1.1	5500	1
<i>i</i> -C ₃ H ₇ ONO ₂	0.78	5400	1
HOC ₂ H ₄ OOH	1.7 x 10 ⁶	9700	1
CH ₃ COCH ₃	27	5500	1
CH ₃ CH ₂ CHO	9.9	4300	1
CH ₃ COC ₂ HO	3.2 x 10 ³	7500	1
CH ₃ C(O)COOH	3.1 x 10 ⁵	5100	1
C ₄ H ₉ ONO ₂	1	5800	1
MEK	18	5700	1
MEKONO ₂	0.7	5200	1
CH ₃ COCOC ₂ H ₅	73	5700	1
ISOPONO ₂ , MACRONONO ₂ , MVKONO ₂	1.7 x 10 ⁴	9200	2
IEPOX	9.1 x 10 ⁴	6600	3
HPALD	2.3		1
MVK	26	4800	1
MACR	4.8	4300	1

¹ Sander (2015) and references therein
² Ito et al. (2007) for all biogenic hydroxy nitrates
³ Browne et al. (2014), as for H₂O₂

Style Definition: List Paragraph

Formatted: Right: -0.05 cm

Deleted: 1

Formatted: Right: -0.05 cm, Line spacing: single

Formatted: Right: -0.05 cm, Line spacing: single

Formatted: Right: -0.05 cm, Line spacing: single

Formatted: Right: -0.05 cm, Line spacing: single

Formatted: Right: -0.05 cm, Line spacing: single

Formatted: Right: -0.05 cm, Line spacing: single

Formatted: Right: -0.05 cm, Line spacing: single

Formatted: Right: -0.05 cm, Line spacing: single

Formatted: Right: -0.05 cm, Line spacing: single

Formatted: Right: -0.05 cm, Line spacing: single

Formatted: Right: -0.05 cm, Line spacing: single

Formatted: Right: -0.05 cm, Line spacing: single

Formatted: Right: -0.05 cm, Line spacing: single

Formatted: Right: -0.05 cm, Line spacing: single

Formatted: Right: -0.05 cm, Line spacing: single

Formatted: Right: -0.05 cm, Line spacing: single

Formatted: Right: -0.05 cm, Line spacing: single

Formatted: Right: -0.05 cm, Line spacing: single

Formatted: Right: -0.05 cm, Line spacing: single

Formatted: Right: -0.05 cm, Line spacing: single

Formatted: Right: -0.05 cm, Line spacing: single

Formatted: Right: -0.05 cm, Line spacing: single

Formatted: Right: -0.05 cm, Line spacing: single

Formatted: Right: -0.05 cm, Line spacing: single

Formatted: Right: -0.05 cm, Line spacing: single

Formatted: Right: -0.05 cm, Line spacing: single

Formatted: Right: -0.05 cm, Line spacing: single

Formatted: Right: -0.05 cm, Line spacing: single

Formatted: Right: -0.05 cm, Line spacing: single

Formatted: Right: -0.05 cm, Line spacing: single

Formatted: Right: -0.05 cm, Line spacing: single

Formatted: Right: -0.05 cm, Line spacing: single

Formatted: Right: -0.05 cm, Line spacing: single

Formatted: Right: -0.05 cm, Line spacing: single

Formatted: Right: -0.05 cm, Line spacing: single

Table S2: Soil, water, snow/ice and mesophyl resistances (s m⁻¹) used in TMS-MP for the CB05 and MOGUNTIA chemical schemes.

Trace gas	r _{soil}	r _{wat}	r _{snow/ice}	r _{mes}	r _{ext}
O ₃	400	2000	2000	1	10 ⁵
CO	5000	10 ⁵	10 ⁵	5000	10 ⁵
NO	10 ⁵	10 ⁵	10 ⁵	500	10 ⁵
NO ₂ /NO ₃	600	3000	3000	1	10 ⁵
HNO ₃ /N ₂ O ₅	1	1	1	1	1
H ₂ O ₂ , IEPOX	80	72	80	1	10 ⁵
SO ₂	100	1	1	1	10 ⁵
CH ₃ ONO ₂ , CH ₃ OONO ₂ , CH ₃ C(O)OONO ₂ , <i>n</i> -C ₃ H ₇ ONO ₂ , <i>i</i> -C ₃ H ₇ ONO ₂ , C ₄ H ₉ ONO ₂ , MEKONO ₂ , ISOPONO ₂	3994	295	3394	1	10 ⁵
CH ₃ CHO, C ₂ H ₅ CHO, CH ₃ C(O)CH ₃ , CH ₃ C(O)C(O)CH ₃ , HOCH ₂ C(O)CH ₃ , MEK, MVK, MACR, HPALD	10 ⁵	300	10 ⁵	200	10 ⁵
HCHO, CH ₃ COCHO, CHOCHO, HOCH ₂ CHO,	1666	254	1666	1	10 ⁵
CH ₃ OOH, CH ₃ OH, HCOOH, CH ₃ CH ₂ OOH, CH ₃ CH ₂ OH, CH ₃ COOH, <i>n</i> - C ₃ H ₇ OOH, <i>i</i> -C ₃ H ₇ OOH, CH ₃ C(O)CH ₂ OOH, <i>n</i> -C ₃ H ₇ OOH, <i>i</i> -C ₃ H ₇ OOH, HOC ₂ H ₄ OOH, CH ₃ C(O)COOH, C ₄ H ₉ OOH, MEKOOH, MVKOOH, MACROOH, CH ₃ C(O)OOH, ISOPOOH	3650	293	3650	1	10 ⁵
NH ₃	100	1	10 ⁵	1	10 ⁵

- Formatted: Right: -0.05 cm
- Deleted: 2
- Formatted: Right: -0.05 cm, Line spacing: single
- Formatted: Right: -0.05 cm, Line spacing: single
- Formatted: Right: -0.05 cm, Line spacing: single
- Formatted: Right: -0.05 cm, Line spacing: single
- Formatted: Right: -0.05 cm, Line spacing: single
- Formatted: Right: -0.05 cm, Line spacing: single
- Formatted: Right: -0.05 cm, Line spacing: single
- Formatted: Right: -0.05 cm, Line spacing: single
- Formatted: Right: -0.05 cm, Line spacing: single
- Formatted: Right: -0.05 cm, Line spacing: single
- Formatted: Right: -0.05 cm, Line spacing: single
- Formatted: Right: -0.05 cm, Line spacing: single
- Formatted: Right: -0.05 cm, Line spacing: single
- Deleted: ¶
- Formatted: Right: -0.05 cm

Table S3: TMS-MP performance calculations of the mCB05(EBI), mCB05(KPP) and MOGUNTIA configurations for the different components, i.e., the transport (advection in the x-, y- and z-directions along with the vertical transport), the chemistry as well as all other procedures contribution, the simulated years per day (SYPD), and the core-hours per simulated years (CHPSY) using a) 360 cores, and b) 450 cores. Timings are in seconds and changes are in %. In parentheses, the runtime and the SYPD without the meteorology reading are also presented. All simulations have been performed in the ECMWF CRAY XC40 high-performance computer facility.

10

a)

360 cores										
Configuration	Transport					Chemistry	Other	Runtime	SYDP	CHPSY
	Adv _x	Adv _y	Adv _z	Vertical	Total					
CB05(EBI)	1322	948	165	364	2799	3338	3925	10062 (6723)	0.73 (1.10)	12000
CB05(KPP)	1312	934	165	362	2773	5301	4222	12296 (9105)	0.60 (0.81)	14000
MOGUNTIA	1892	1303	233	527	3955	8230	4680	16865 (13556)	0.44 (0.54)	20000
% solver changes	-1%	-1%	0%	-1%	-1%	-1%	59%	8% (35%)	-18% (-26%)	17%
% chemistry scheme changes	44%	40%	41%	46%	43%	43%	55%	11% (49%)	-27% (-33%)	43%

b)

450 cores										
Configuration	Transport					Chemistry	Other	Runtime	SYDP	CHPSY
	Adv _x	Adv _y	Adv _z	Vertical	Total					
CB05(EBI)	1268	860	138	292	2558	2639	3687	8884 (5696)	0.83 (1.30)	13000
CB05(KPP)	1292	853	133	300	2578	4320	4079	10977 (7733)	0.67 (0.95)	16000
MOGUNTIA	1806	1126	193	423	3548	6526	4376	14450 (11211)	0.51 (0.65)	21000
% solver changes	2%	-1%	-4%	3%	1%	64%	11%	24% (36%)	-19% (-27%)	23%
% chemistry scheme changes	40%	32%	45%	41%	38%	51%	7%	32% (45%)	-24% (-32%)	31%

Table S4: Tropospheric chemical budget of ORGNTR^{*} for the year 2006 in Tg(N) yr⁻¹, using the 150 ppb O₃ mixing ratio to define tropopause level. Tropospheric burdens in Gg(N) yr⁻¹.

Production terms	mCB05 (EBI)	mCB05 (KPP)	MOGUNTIA	Loss terms	mCB05 (EBI)	mCB05 (KPP)	MOGUNTIA
XO ₂ N/RO ₂ + NO	8.6	8.1	7.0	ORGNTR + hv	4.1	4.0	2.6
RH + NO ₃	4.3	4.2	6.7	ORGNTR + OH	1.3	1.4	5.8
Tropospheric Burden	159.6	159.8	63.0	Deposition	7.4	7.6	5.1

^{*}For the MOGUNTIA configuration ORGNTR represents the sum of CH₃ONO₂, C₂H₅ONO₂, OHCH₂CH₂ONO₂, CH₃CH₂CH₂ONO₂, CH₃CH(ONO₂)CH₃, CH₃CH₂CH(ONO₂)CH₃, nitrates from isoprene (ISOPNO₃), nitrates from methyl-ethyl ketone (MEKNO₃), nitrates from methyl vinyl ketone (MVKNO₃) and nitrates from methacrolein (MACRNO₃)

Deleted: 3

Formatted: Right: -0.05 cm

Formatted: Right: -0.05 cm, Line spacing: single

Deleted:

Formatted Table

Formatted: Right: -0.05 cm, Line spacing: single

Formatted Table

Formatted: Right: -0.05 cm, Line spacing: single

Formatted: Right: -0.05 cm, Line spacing: single

Formatted: Right: -0.05 cm, Line spacing: single

Formatted: Right: -0.05 cm, Line spacing: single

Formatted: Right: -0.05 cm, Line spacing: single

Deleted:

Formatted Table

Formatted: Right: -0.05 cm, Line spacing: single

Formatted Table

Formatted: Right: -0.05 cm, Line spacing: single

Formatted: Right: -0.05 cm, Line spacing: single

Formatted: Right: -0.05 cm, Line spacing: single

Formatted: Right: -0.05 cm, Line spacing: single

Deleted: ¶

Page Break:.....

Formatted: English (UK)

Formatted: Font color: Black, English (US), Kern at 16 pt

Supplementary Equations

Statistics Formulas: Correlation coefficient (R; Eq. S1), mean normalized bias (MNB; Eq. S2), root mean square error (RMSE; Eq. S3), mean normalized error (MNE; Eq. S4) and standard error (STD; Eq. S5) values have been calculated to compare the model calculations, where O_i and P_i stand for observations and predictions respectively and N is the number of pairs (observations, predictions) that are compared.

$$R = \left[\frac{\frac{1}{N} \sum_{i=1}^N (O_i - \bar{O})(P_i - \bar{P})}{\sigma_O \sigma_P} \right]$$

(Eq. S1)

$$NMB = \frac{\sum_{i=1}^N (M_i - O_i)}{\sum_{i=1}^N O_i} \times 100$$

(Eq. S2)

$$RMSE = \sqrt{\frac{1}{N} \sum_{i=1}^N (P_i - O_i)^2}$$

(Eq. S3)

$$NME = \frac{\sum_{i=1}^N |M_i - O_i|}{\sum_{i=1}^N O_i} \times 100$$

(Eq. S4)

$$STD = \frac{\sqrt{\frac{1}{N} \sum_{i=1}^N (O_i - \bar{O})^2}}{\sqrt{N}}$$

(Eq. S5)

Formatted: Right: -0.05 cm

Formatted: Right: -0.05 cm, Line spacing: single

Deleted: $R = \left[\frac{\frac{1}{N} \sum_{i=1}^N (O_i - \bar{O})(P_i - \bar{P})}{\sigma_O \sigma_P} \right]$

Field Code Changed

Deleted: $NMB = \frac{\sum_{i=1}^N (M_i - O_i)}{\sum_{i=1}^N O_i} \times 100$

Field Code Changed

Deleted: $NME = \frac{\sum_{i=1}^N |M_i - O_i|}{\sum_{i=1}^N O_i} \times 100$

Field Code Changed

Deleted: $STD = \frac{\sqrt{\frac{1}{N} \sum_{i=1}^N (O_i - \bar{O})^2}}{\sqrt{N}}$

Field Code Changed

Supplementary Figures

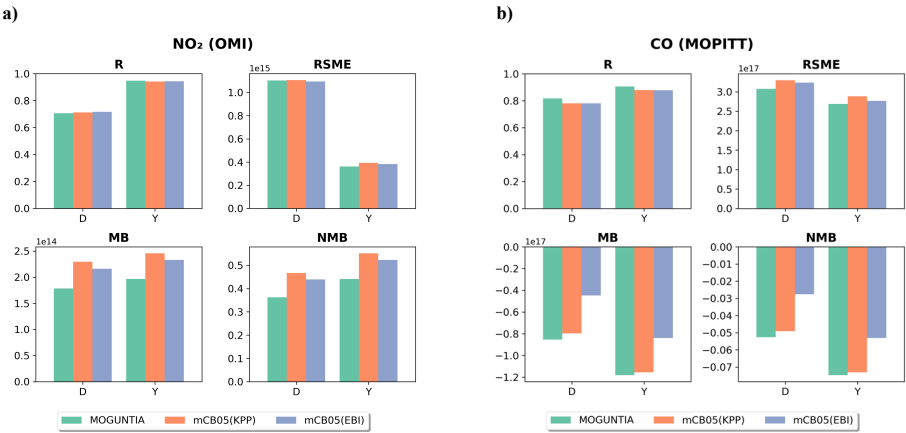


Figure S 1: Comparison of simulated a) tropospheric NO₂ columns with OMI retrievals from the QA4ECV dataset and b) simulated total CO columns with MOPITT retrievals (vers. MOP02J_V008) for the year 2006. Green, orange, and blue bars show the comparison of OMI with the MOGUNTIA, mCB05(KPP), and mCB05(EBI) chemistry mechanisms, respectively: Pearson correlation coefficient (top left), root mean square error (top right), mean bias (measurement minus model, bottom left), and normalized mean bias (measurement minus model, bottom right) are given for both daily (D) and yearly (Y) averages per model grid cell.

10

Formatted: Right: -0.05 cm, Line spacing: single

Formatted: Right: -0.05 cm

Formatted: Font: Bold

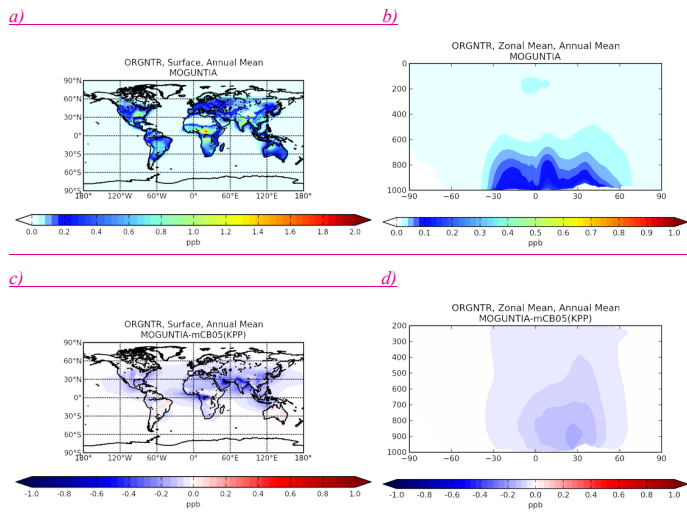
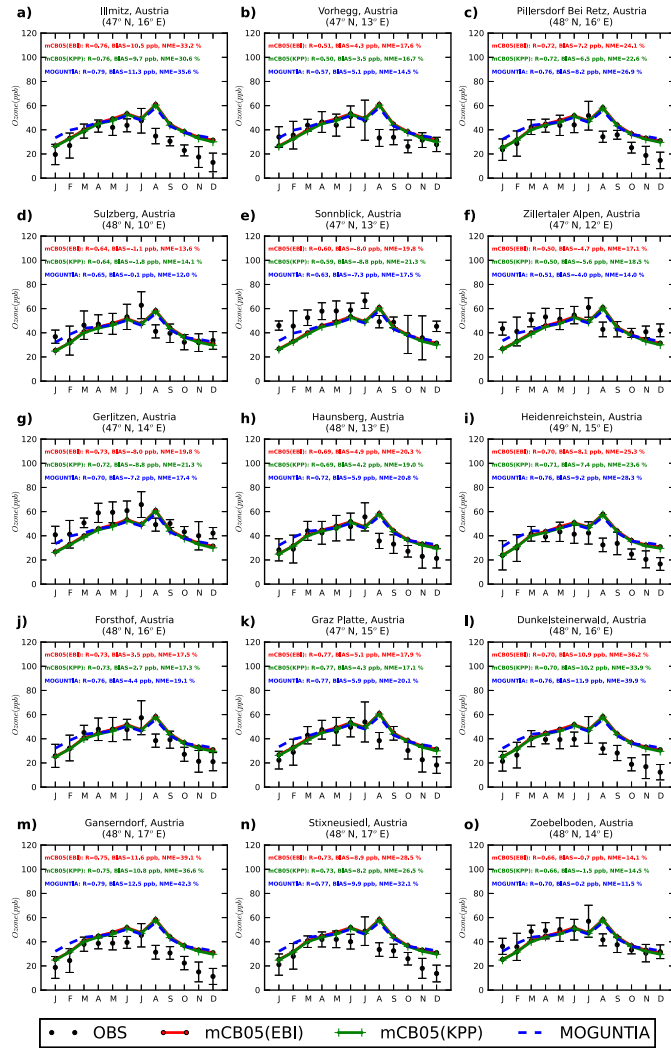
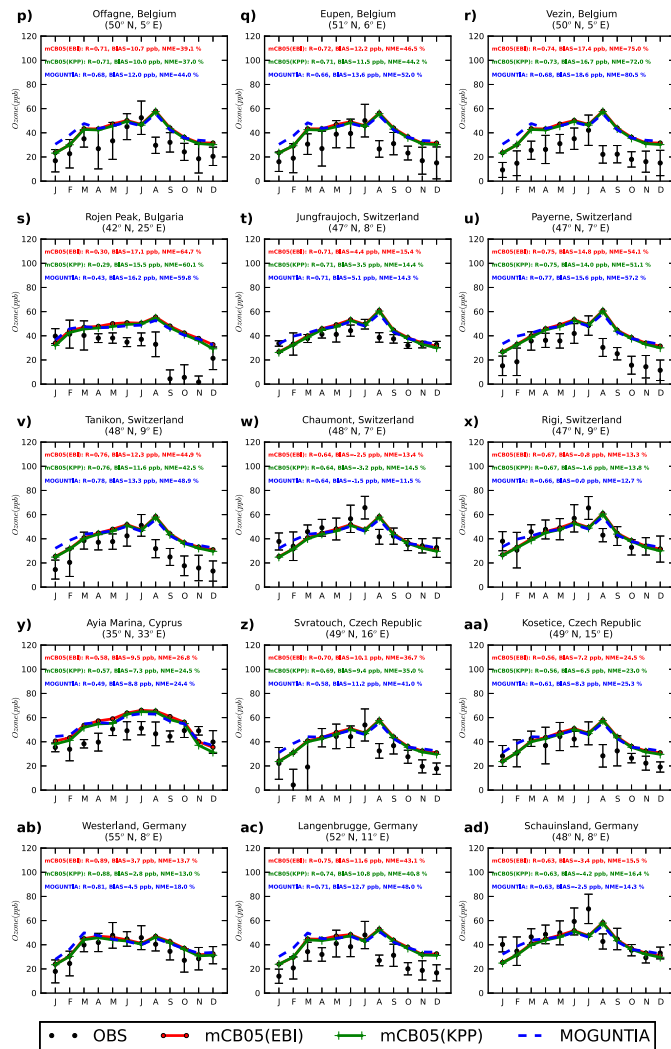


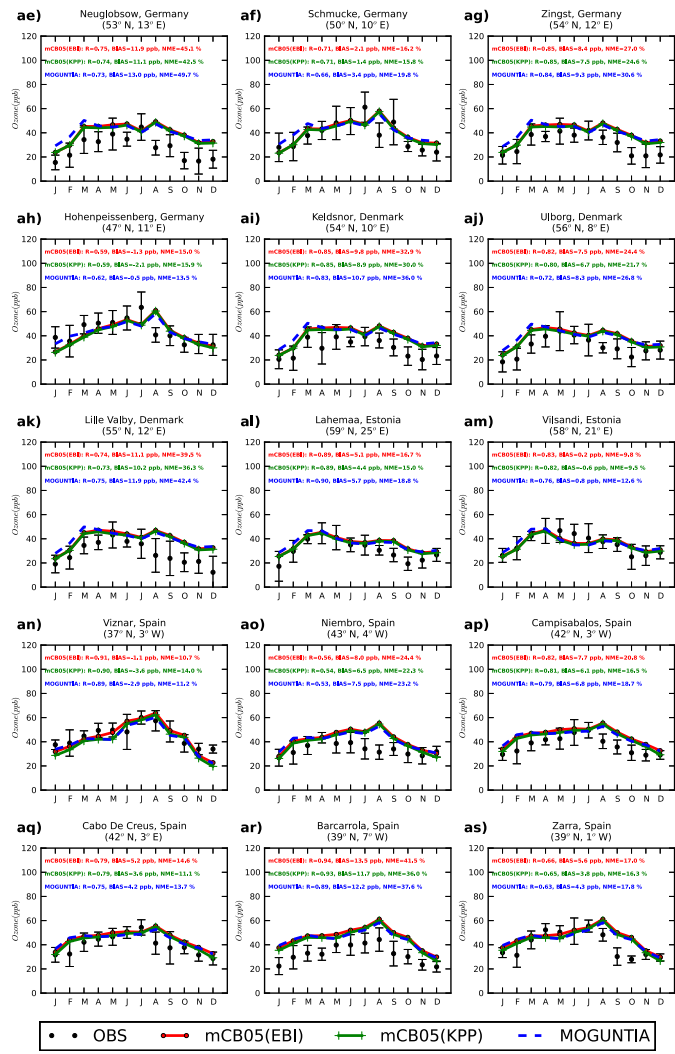
Figure S2: Simulated annual mean surface (left columns) and zonal mean (right columns) mixing ratios (ppb) of organic nitrates (ORGNTR) for the MOGUNTIA chemistry scheme for the year 2006 (a,b), and the respective differences compared to mCB05(KPP) (c,d). For the MOGUNTIA configuration, ORGNTR represents the sum of CH_3ONO_2 , $\text{C}_2\text{H}_5\text{ONO}_2$, $\text{OHCH}_2\text{CH}_2\text{ONO}_2$, $\text{CH}_3\text{CH}_2\text{CH}_2\text{ONO}_2$, $\text{CH}_3\text{CH}(\text{ONO}_2)\text{CH}_3$, $\text{CH}_3\text{CH}_2\text{CH}(\text{ONO}_2)\text{CH}_3$, nitrates from isoprene (ISOPNO_2), nitrates from methyl-ethyl ketone (MEKNO_2), nitrates from methyl vinyl ketone (MVKNO_2) and nitrates from methacrolein (MACRNO_2)."



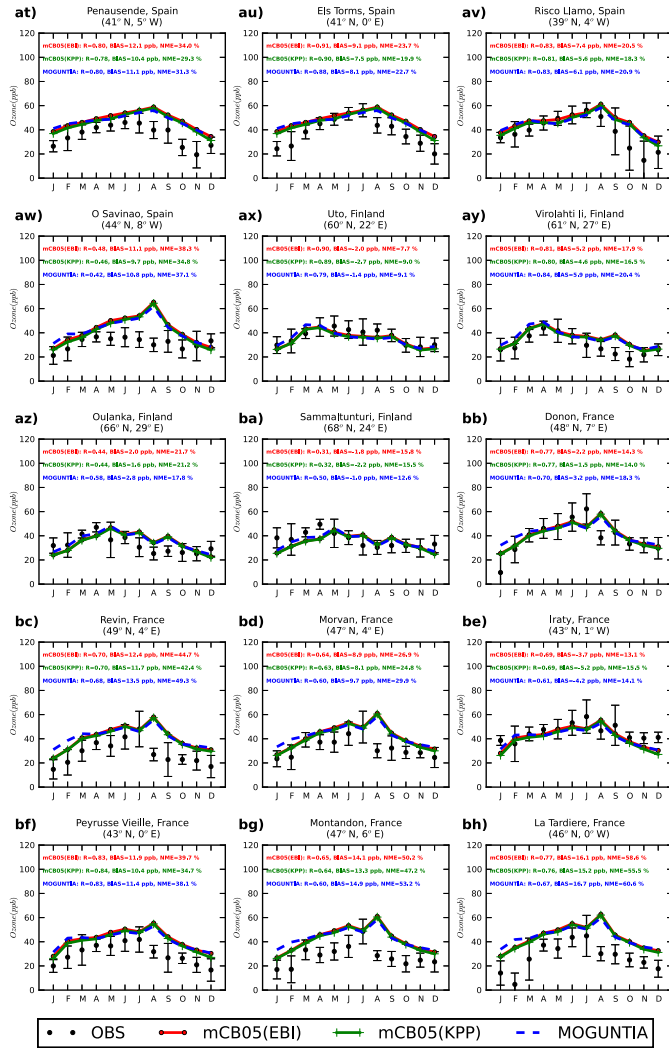
Formatted: Right: -0.05 cm, Line spacing: single

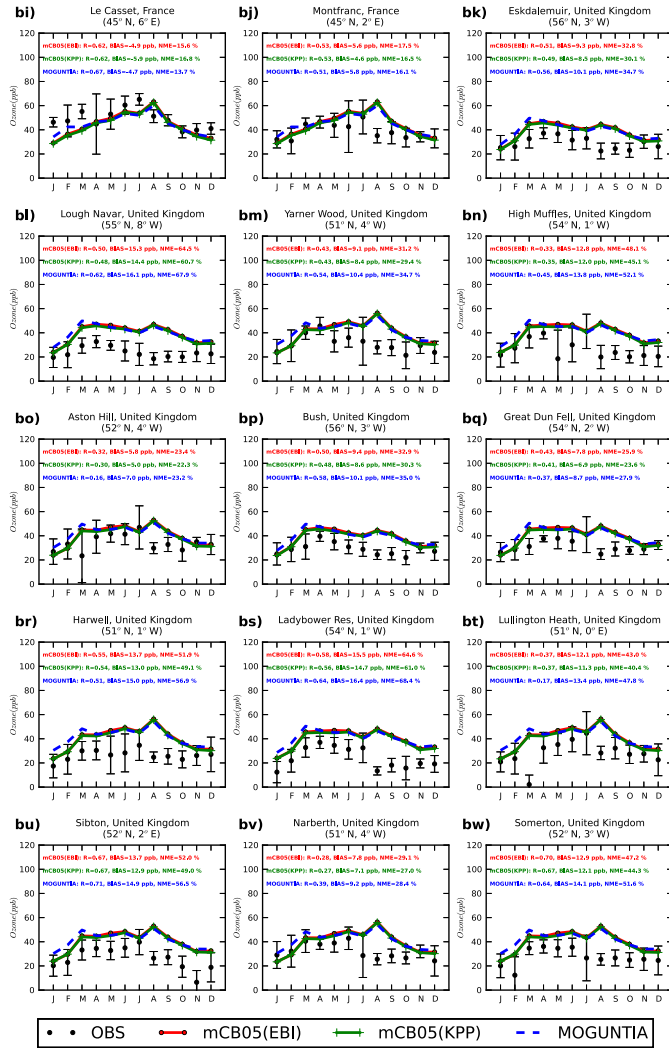


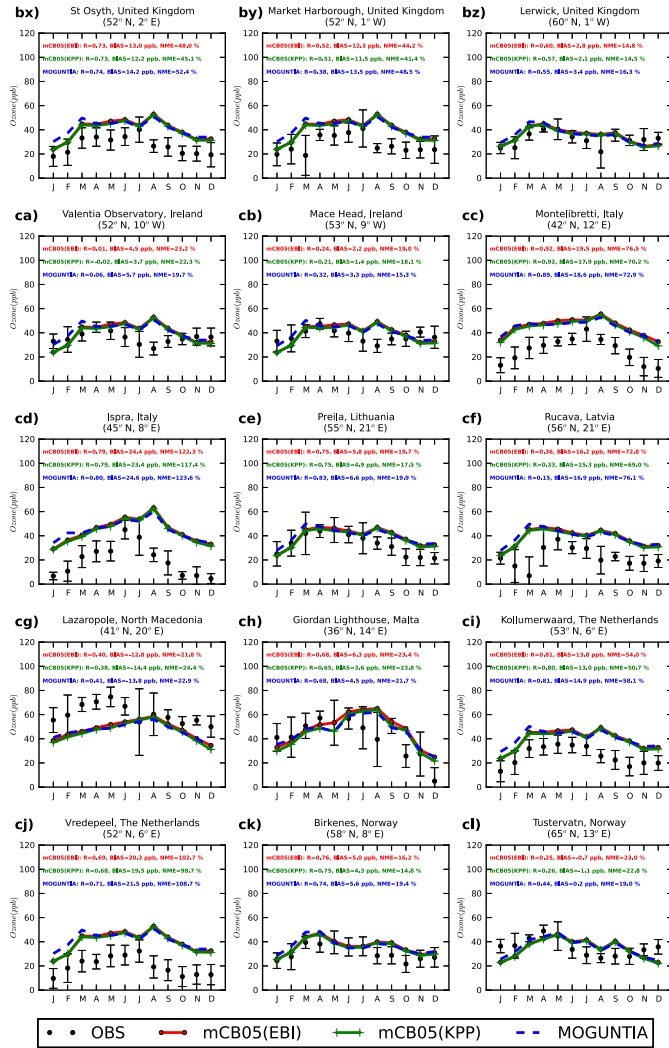
Formatted: Right: -0.05 cm

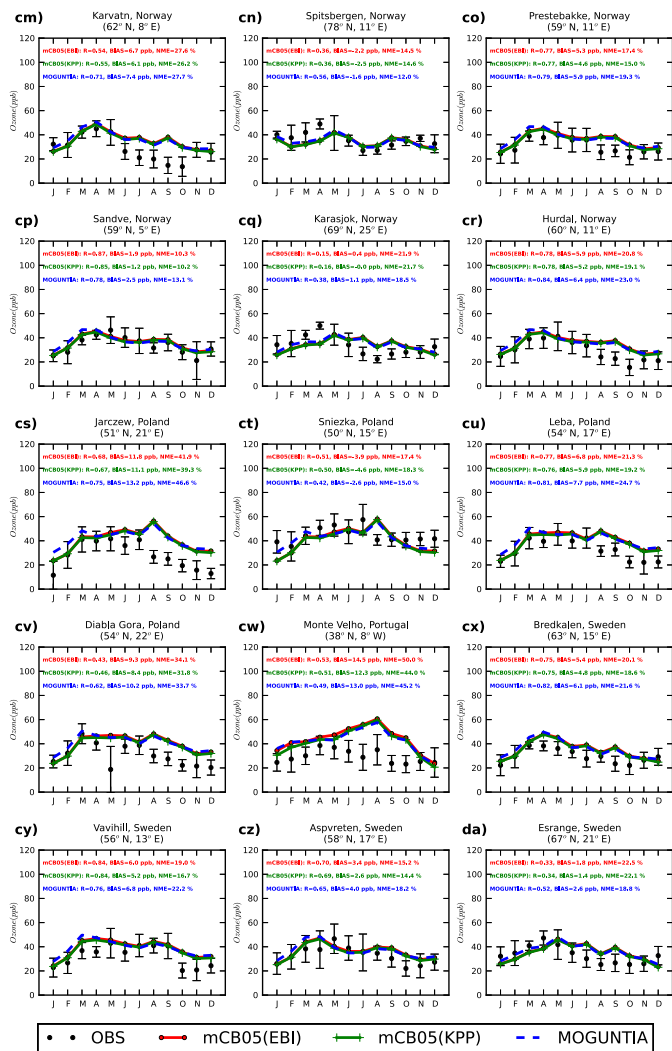


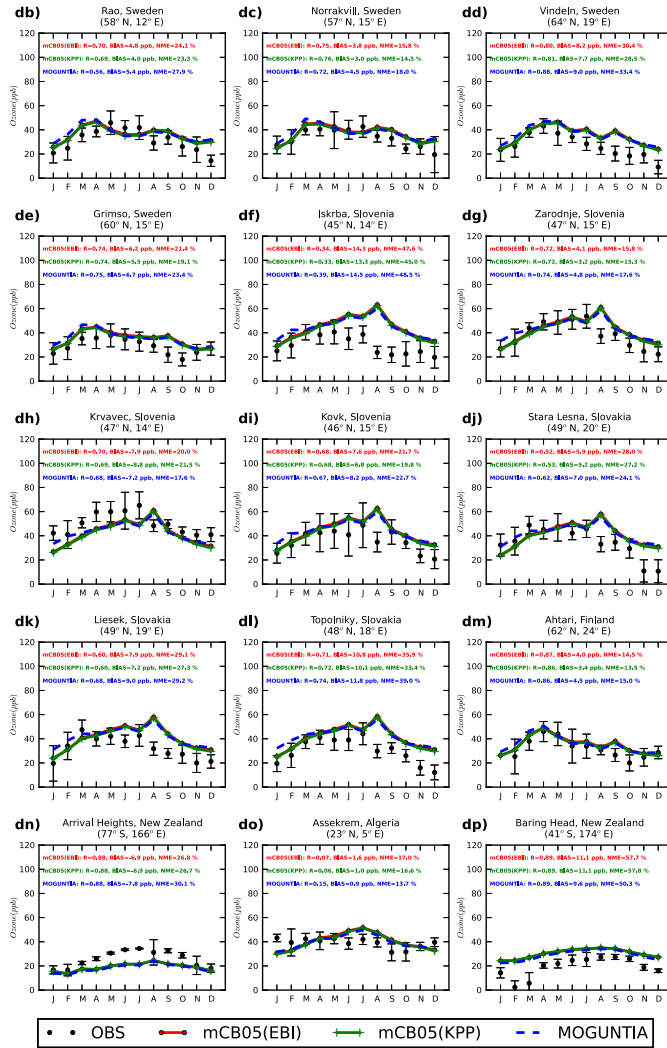
Formatted: Right: -0.05 cm, Line spacing: single

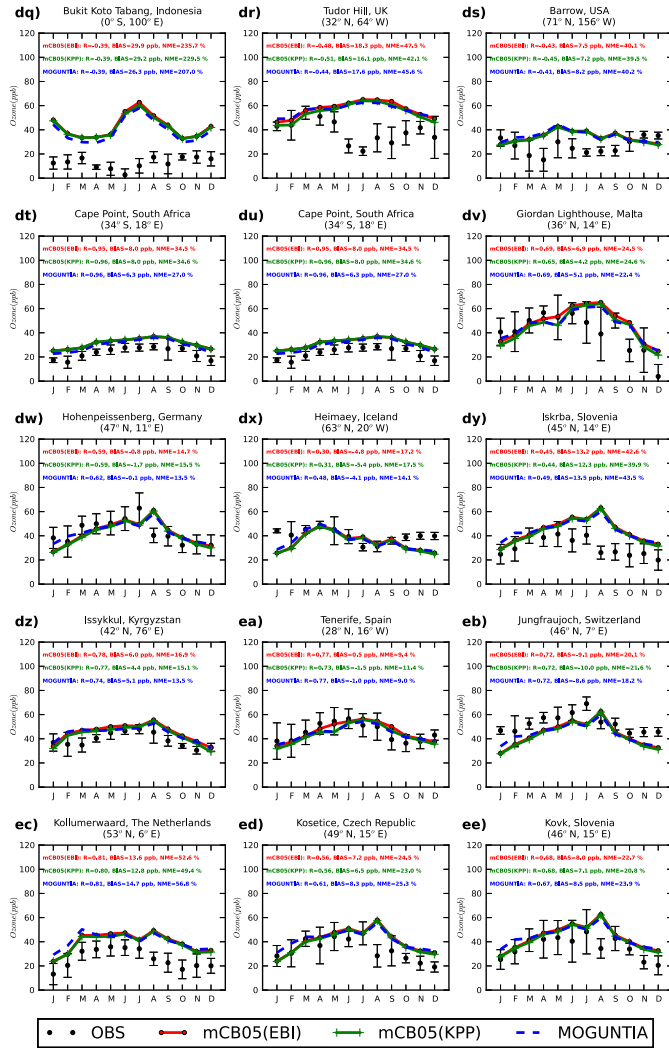


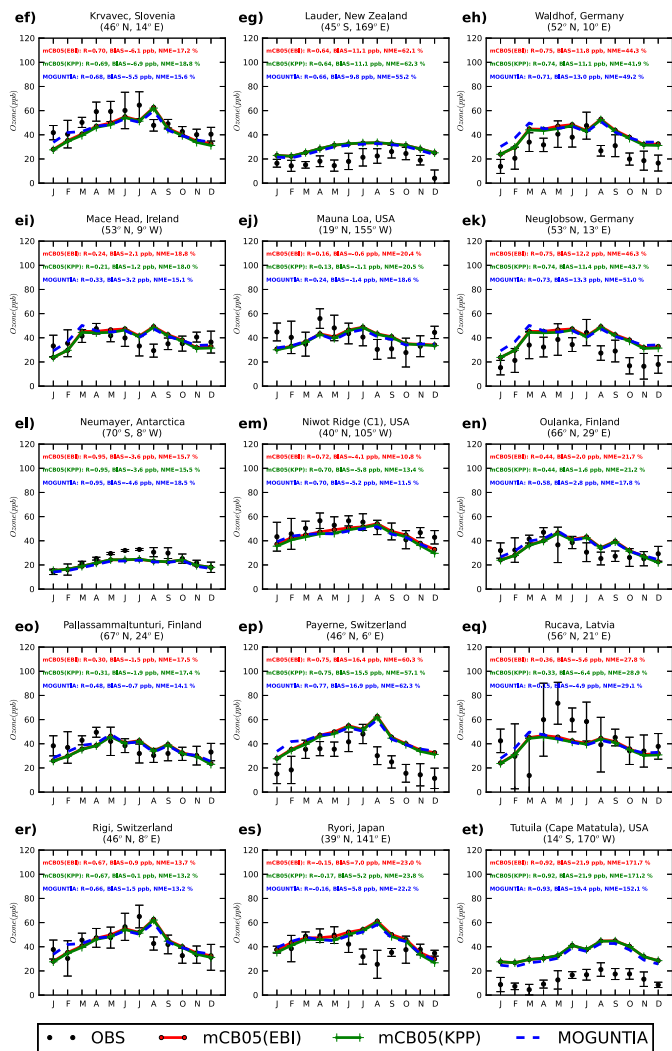


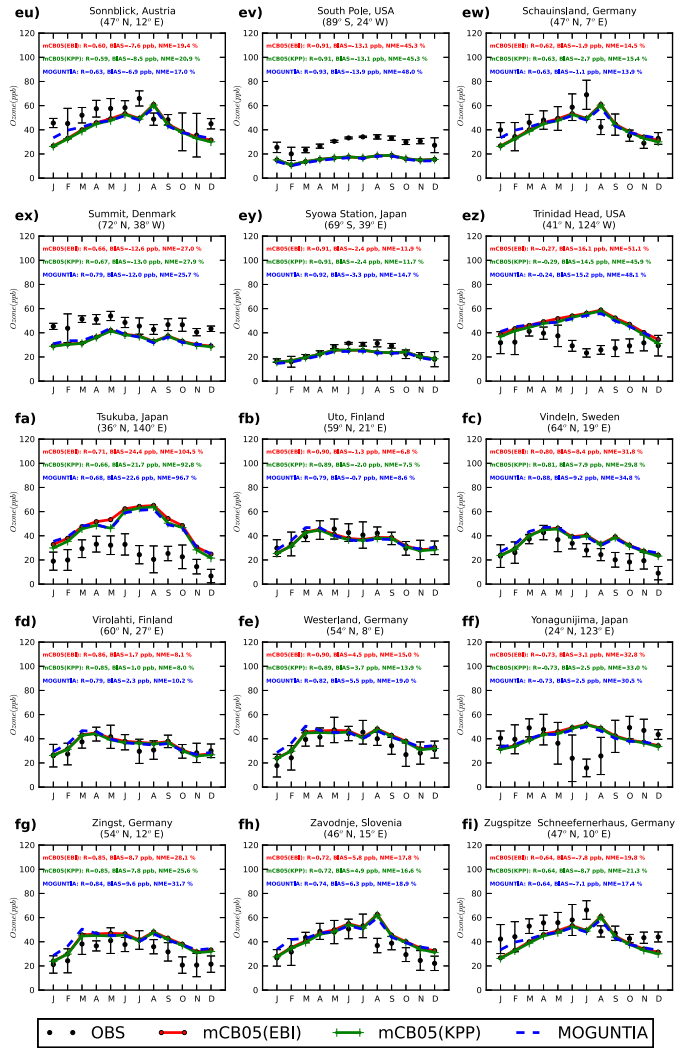












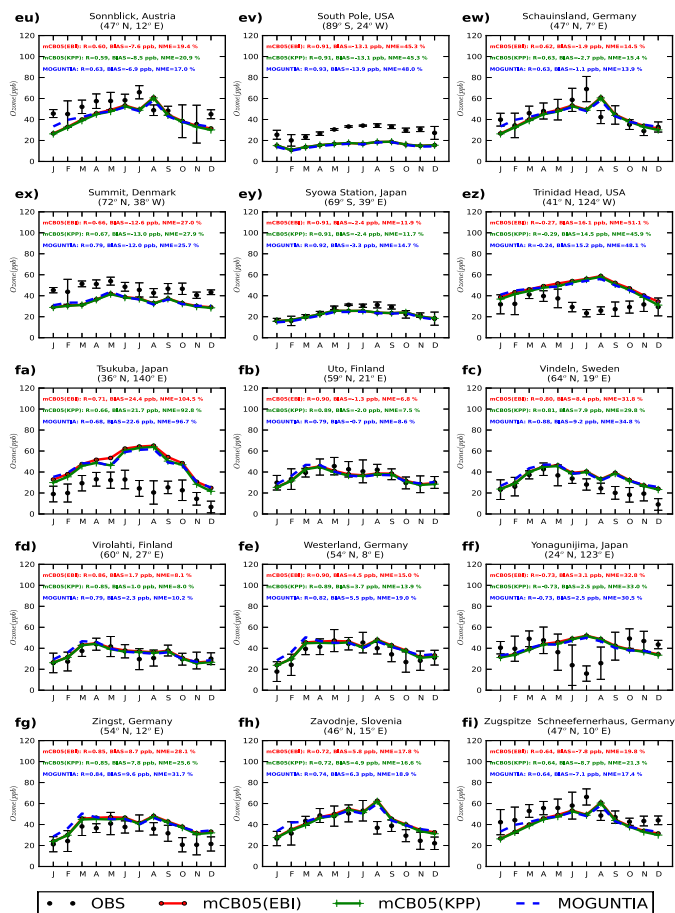
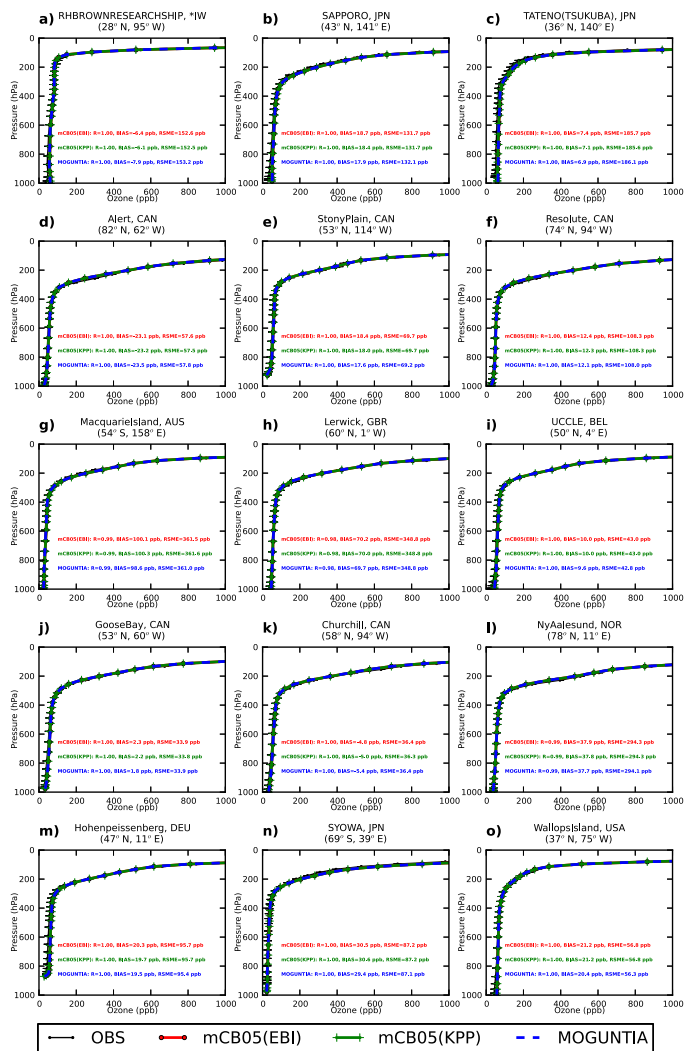


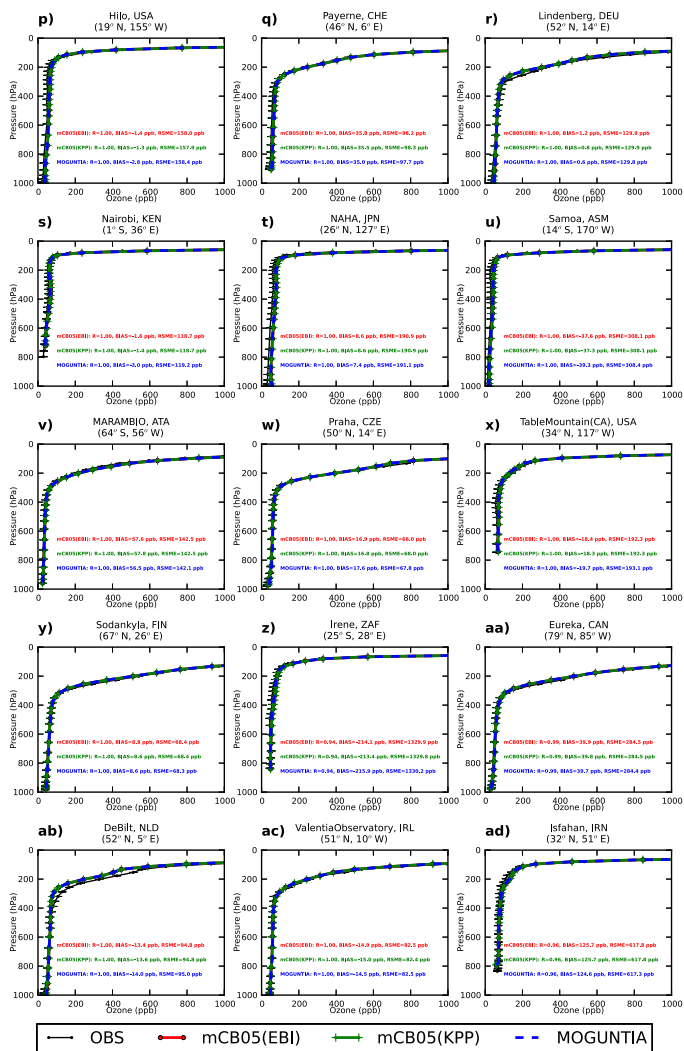
Figure S3: Comparison of monthly mean surface O₃ observations (black dots) in ppb with model results (red-line for mCB05(EBI), green-line for mCB05(KPP) and blue-line for MOGUNTIA) at various stations around the globe, as obtained from the European Monitoring and Evaluation Programme (EMEP; <http://www.emep.int>) and the World Data Centre for Greenhouse Gases (WDCGG; <http://ds.data.ima.go.jp/gmd/wdceg/introduction.html>), for the year 2006.

Formatted: Right: -0.05 cm

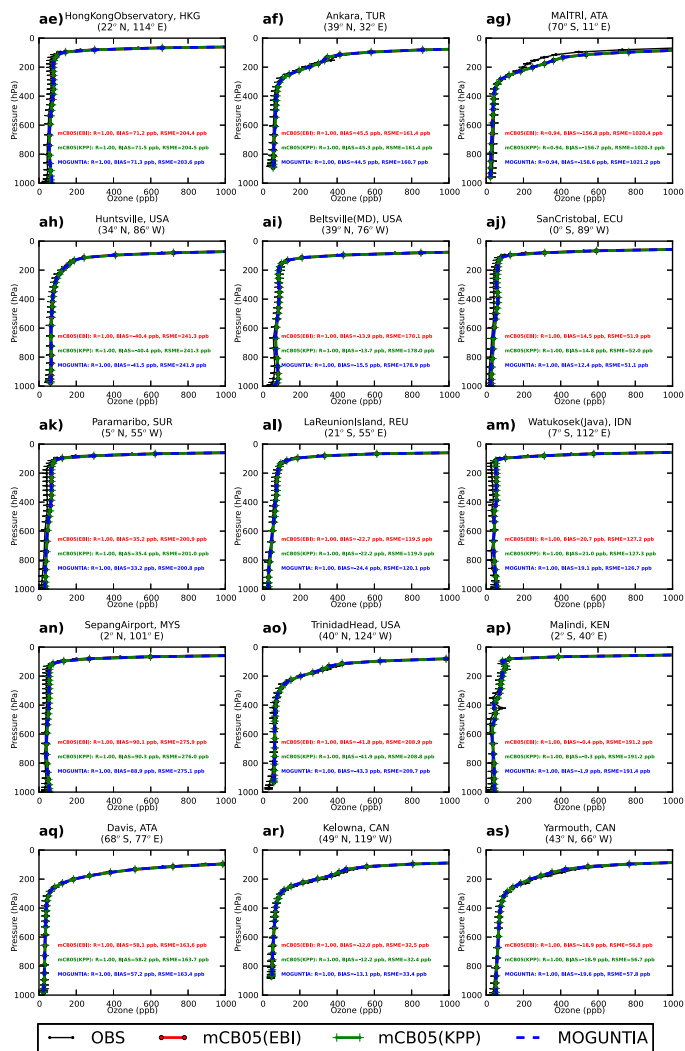
Deleted: 1



Formatted: Right: -0.05 cm, Line spacing: single



Formatted: Right: -0.05 cm



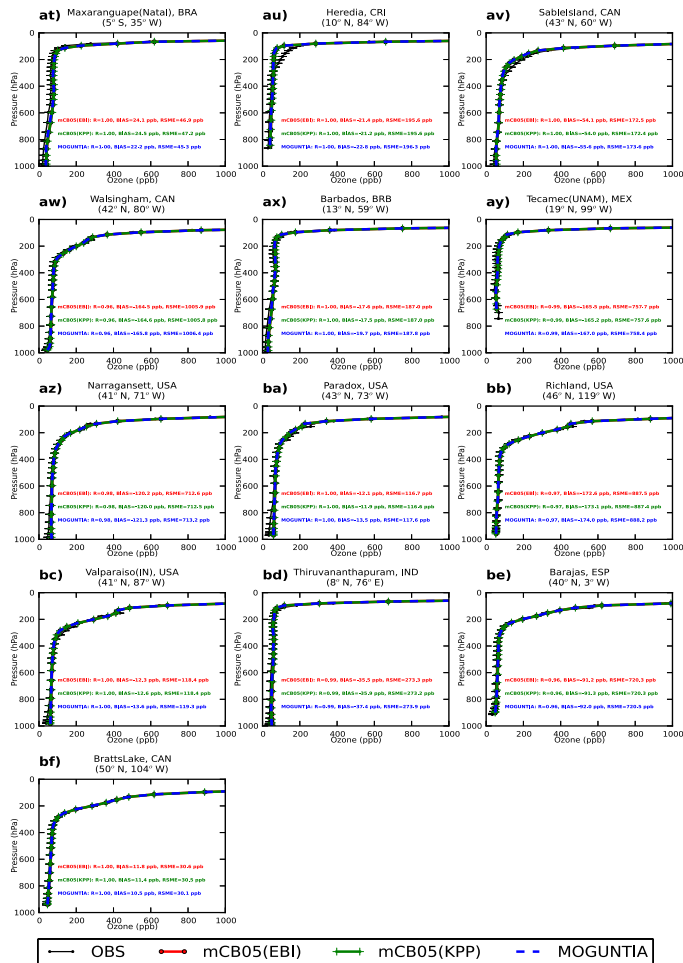
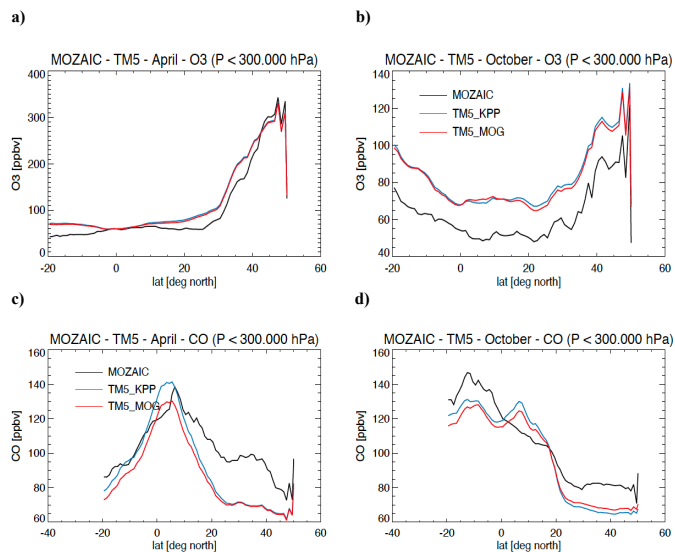


Figure S4: Comparison of monthly mean ozone sonde observations (black line) in ppb with model results (red-line for mCB05 configuration using the EBI solver, green-line for mCB05 configuration using the solver as generated by the KPP software and blue-line for MOGUNTIA configuration) at various stations around the globe, as obtained from the World Data Centre for Greenhouse Gases (WDCGG; <https://gaw.kishou.go.jp>), for the year 2006.

Formatted: Right: -0.05 cm, Line spacing: single

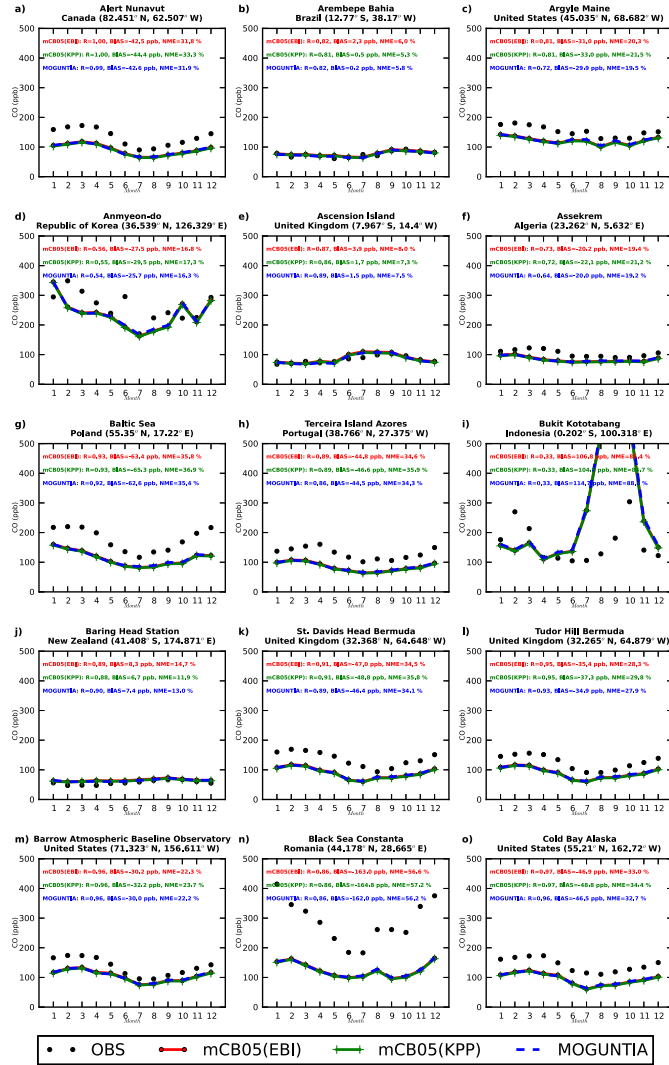
Formatted: Right: -0.05 cm

Deleted: 2

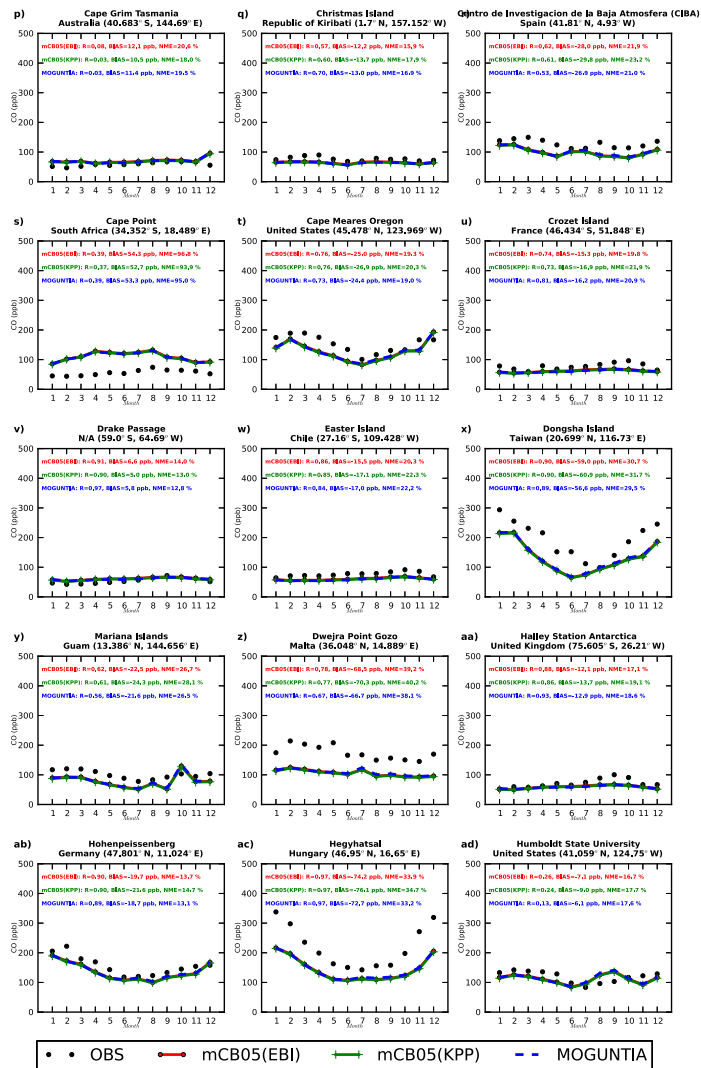


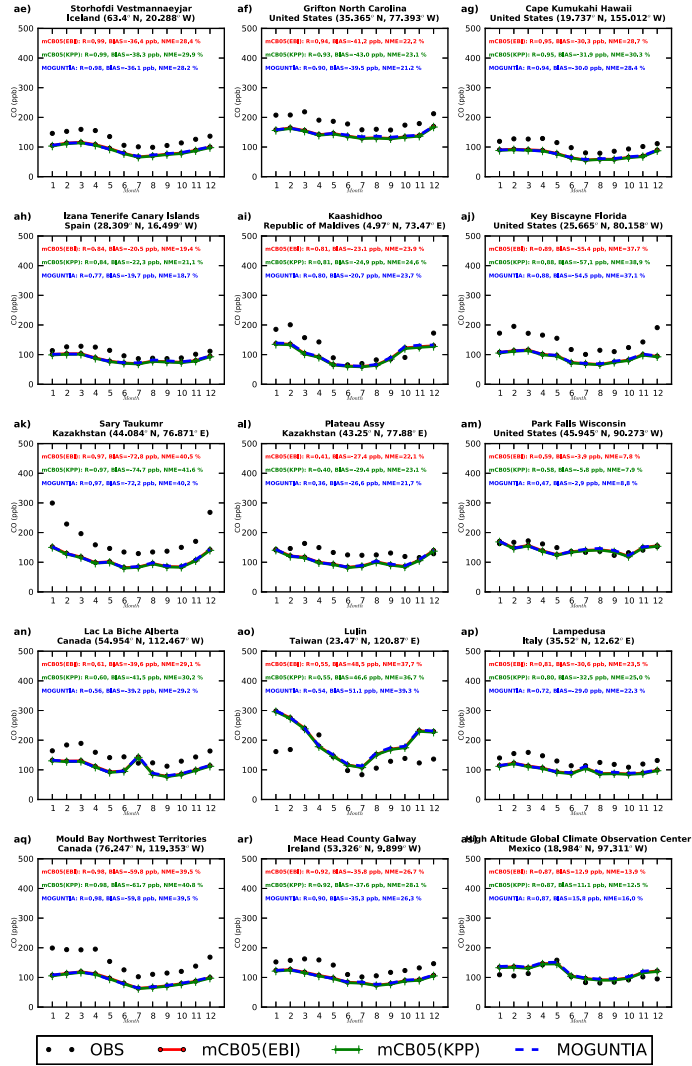
5 **Figure S5: Monthly mean comparisons of TMS-MP UTLS O₃ (top) and CO (bottom) mixing ratios (ppb) for the two chemistry schemes; mCB05(KPP) (blue line) and MOGUNTIA (red line), sampled at the measurement place and time against MOZAIC flight data (black line) between Frankfurt (50.0° N, 8.6° E) and Windhoek (22.5° S, 17.7° E) for April (left column) and October 2006 (right column). Data at pressures (P) lower than 300 hPa has been filtered out.**

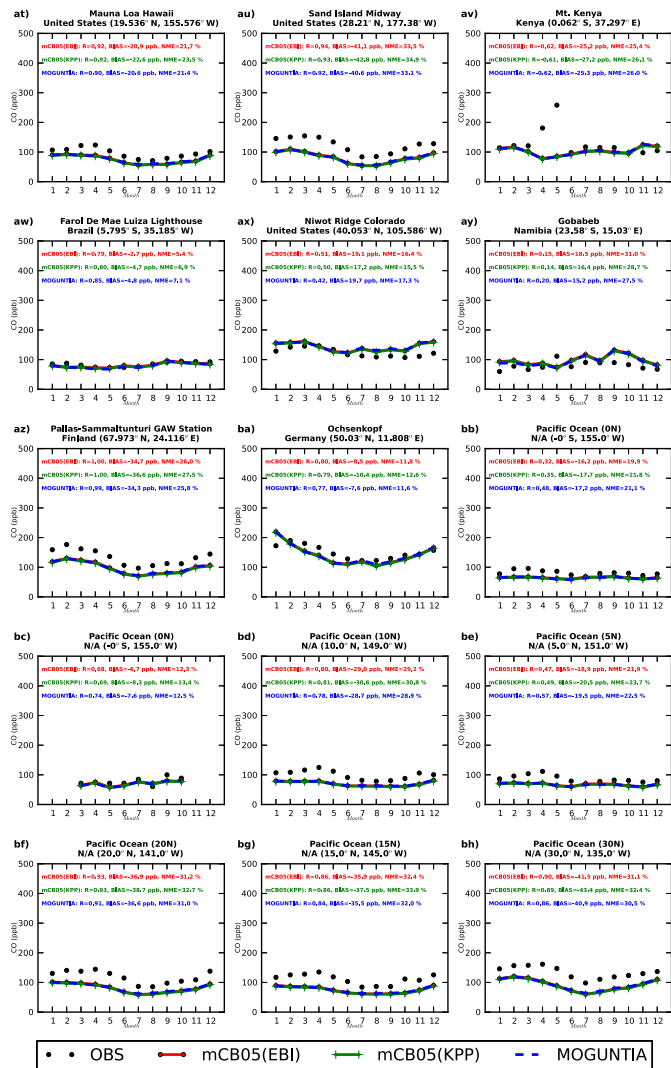
Deleted: 3

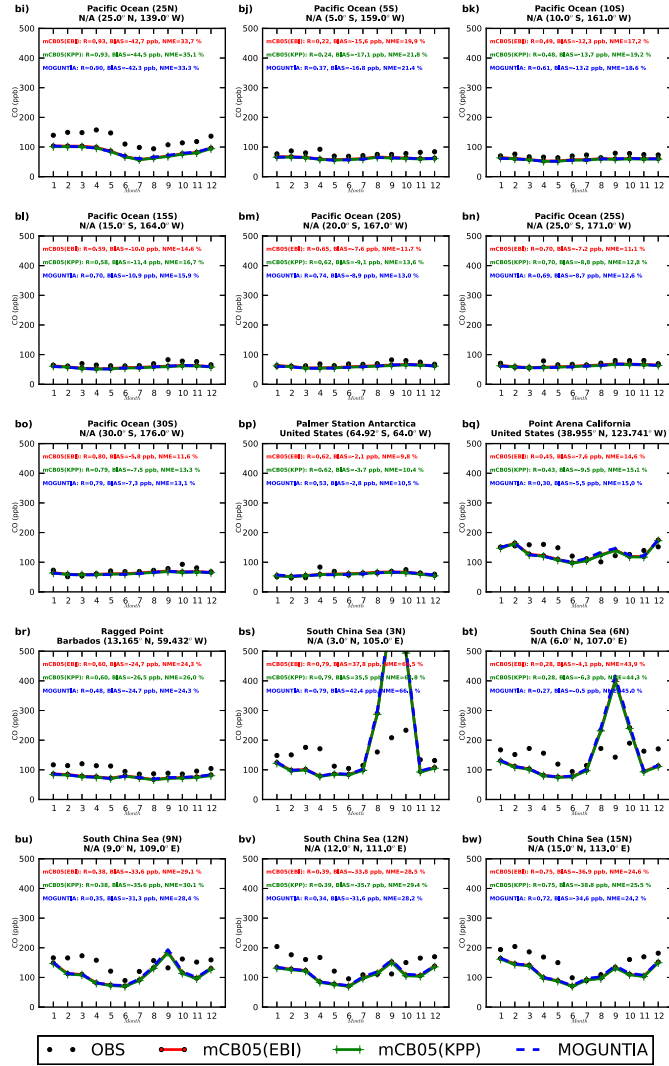


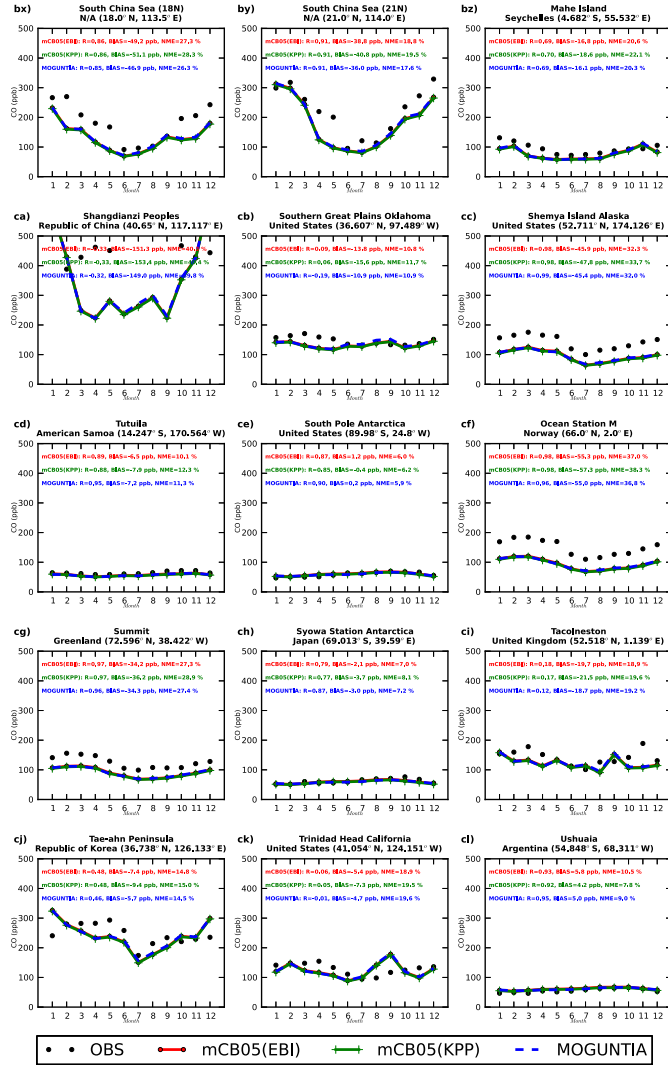
Formatted: Right: -0.05 cm, Line spacing: single











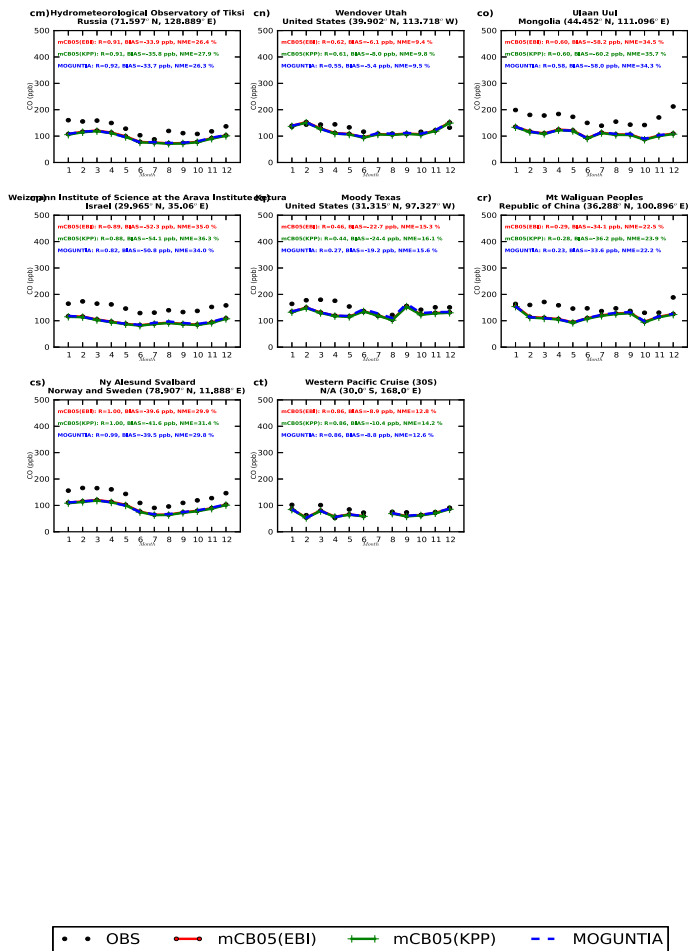


Figure S6: Comparison of monthly mean surface CO flask measurements (black dots) in ppb with model results (red-line for mCB05(EBI), green-line for mCB05(KPP) and blue-line for MOGUNTIA) at various stations around the globe, as obtained from NOAA database, for the year 2006.

Formatted: Right: -0.05 cm

Deleted: 4

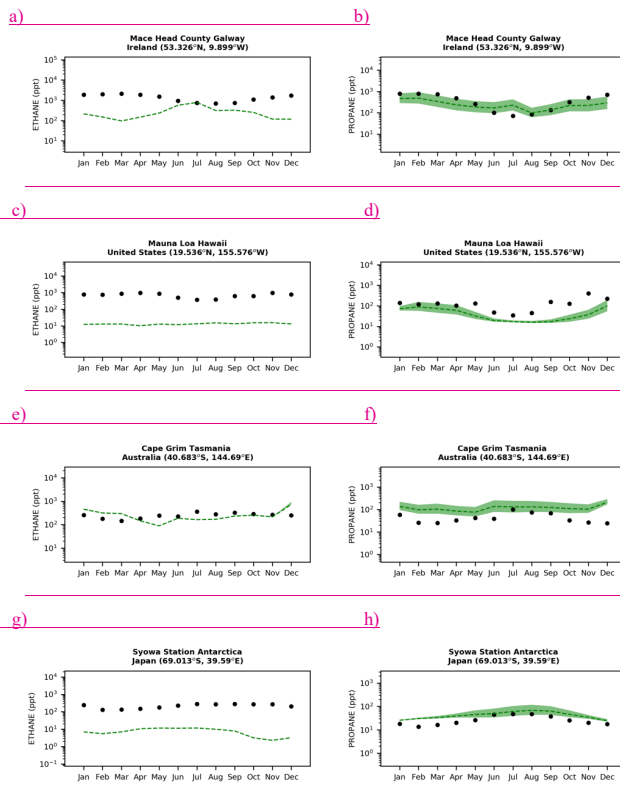
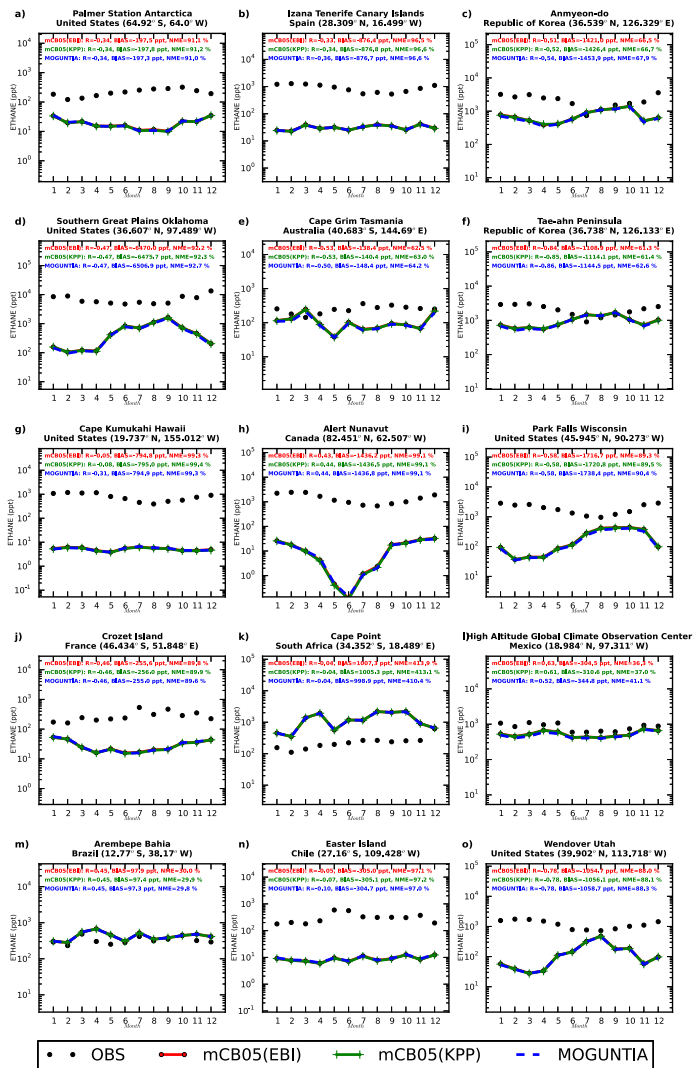
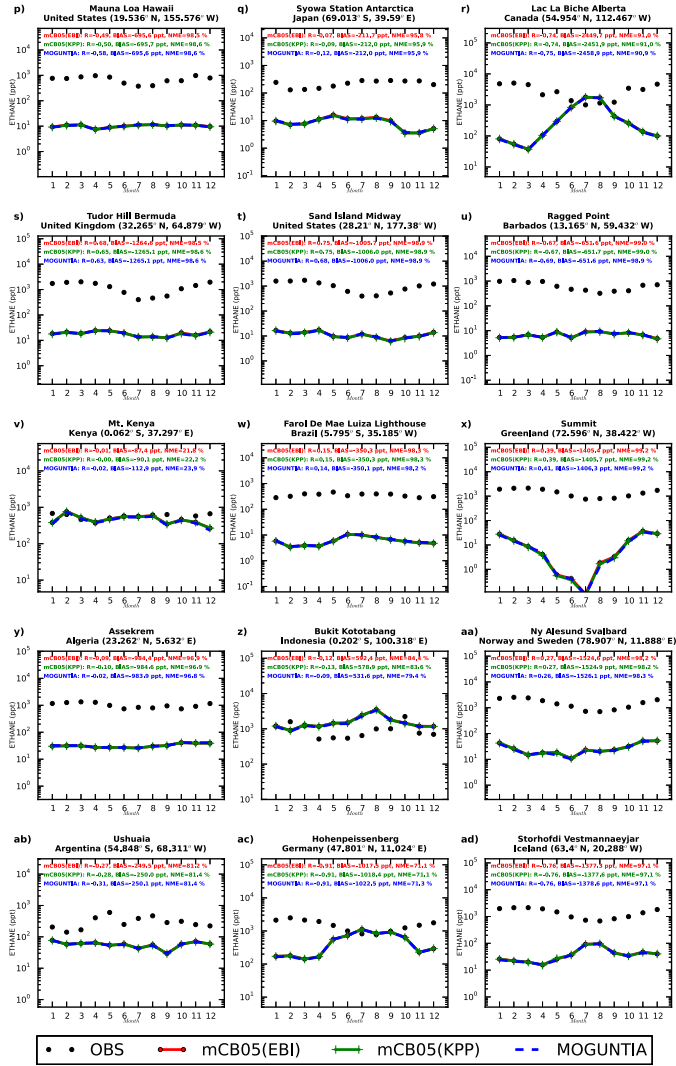
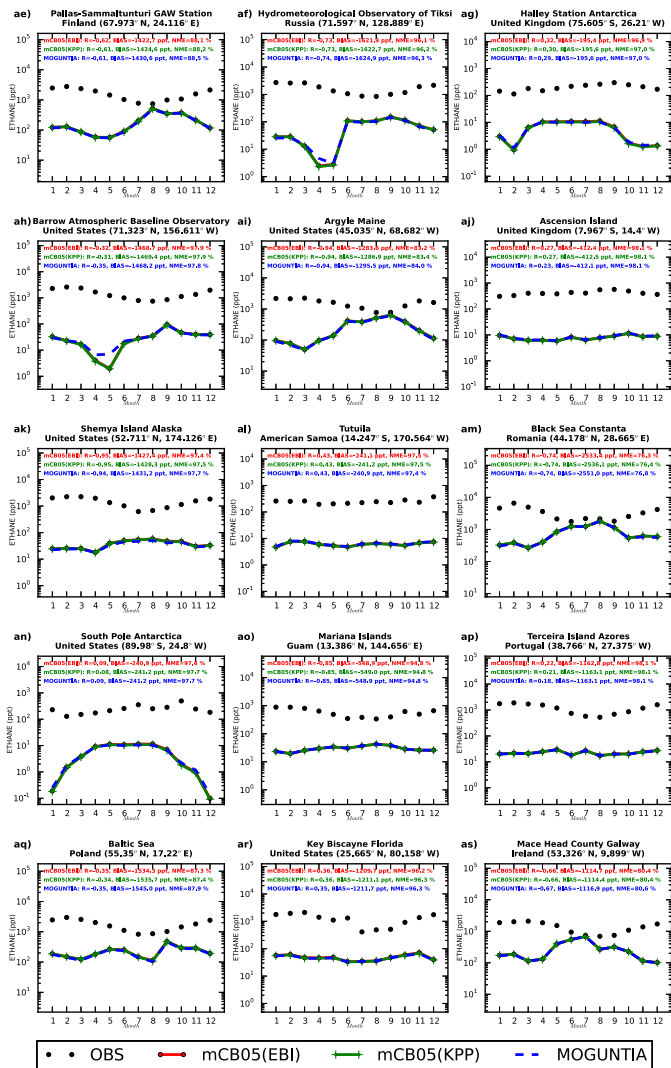


Figure S7: Monthly mean comparison of TM5-MP surface C_2H_6 (left column) and C_3H_8 (right column) using the base case emission scenario, doubling (2x) of the anthropogenic fossil fuel emissions, and quadrupling (4x) of the anthropogenic fossil fuel emissions of C_2H_6 and C_3H_8 against flask measurements (black dots) in ppt for the MOGUNTIA chemistry scheme (green line), using co-located model output for 2006 sampled at the measurement times. Shaded areas indicate the range of model results due to the different emission strengths. For this sensitivity analysis, the model runs in $3^\circ \times 2^\circ$ horizontal resolution in longitude by latitude, and 34 hybrid levels in the vertical.



Formatted: Right: -0.05 cm





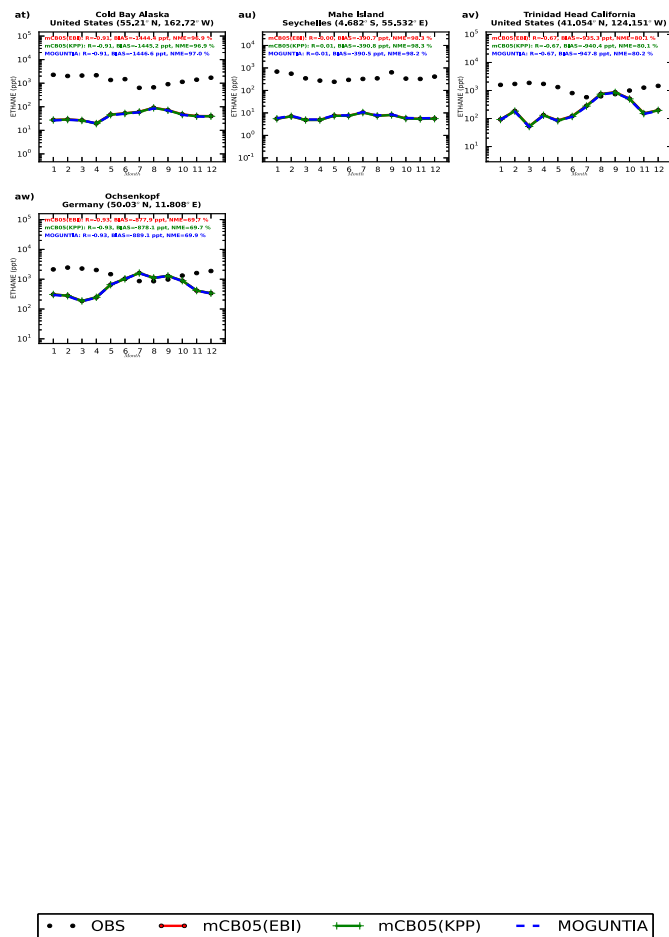
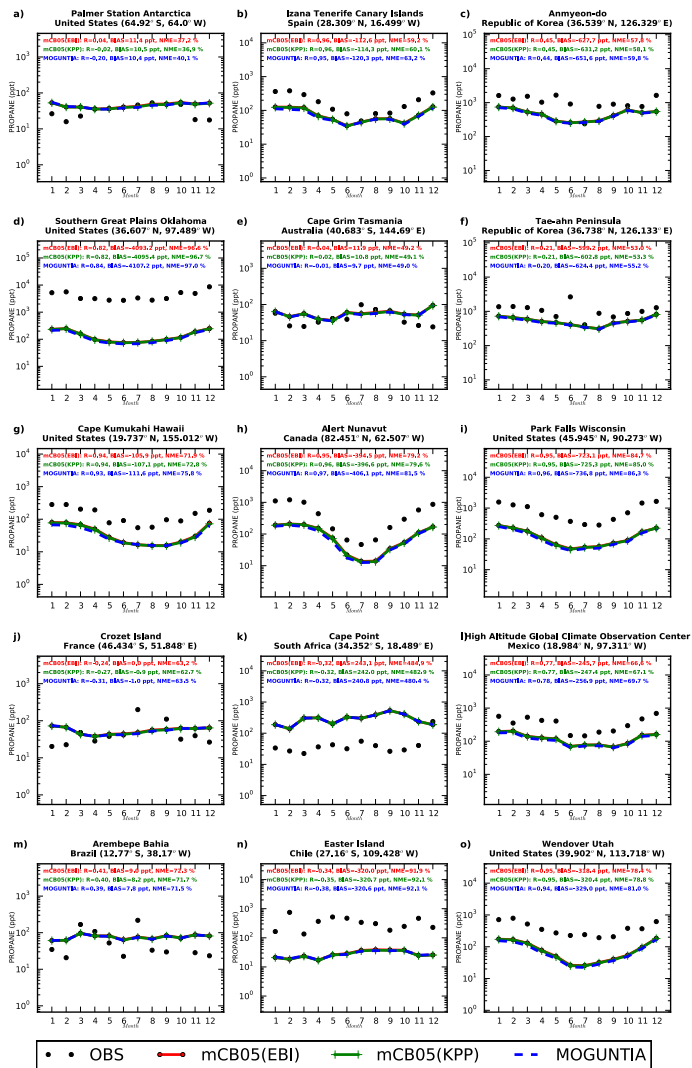
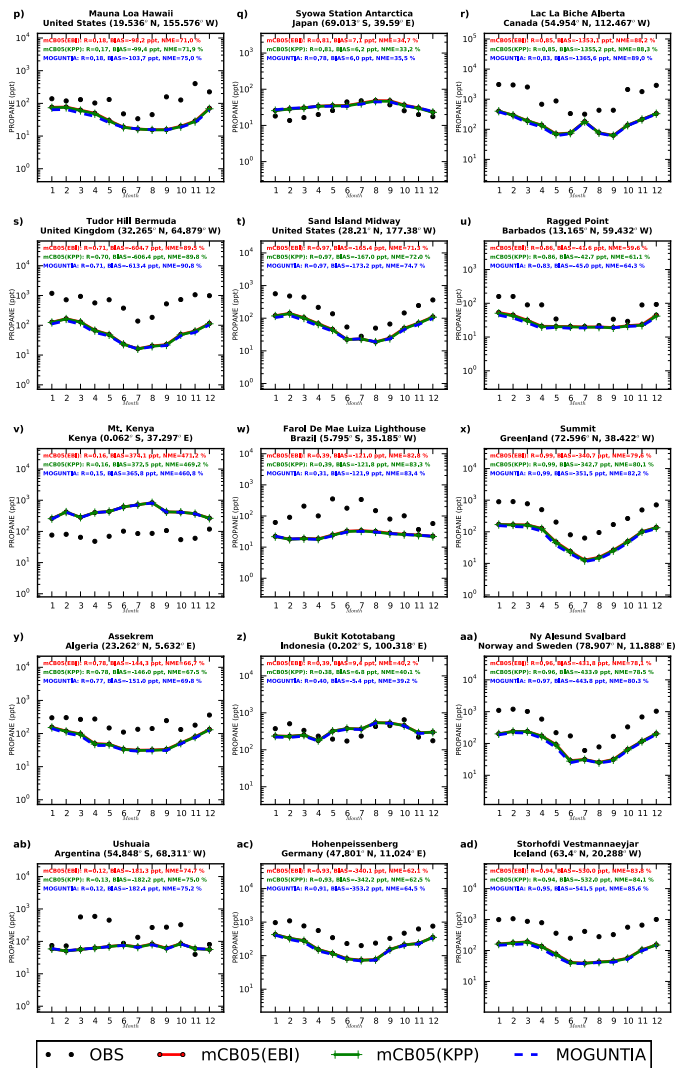
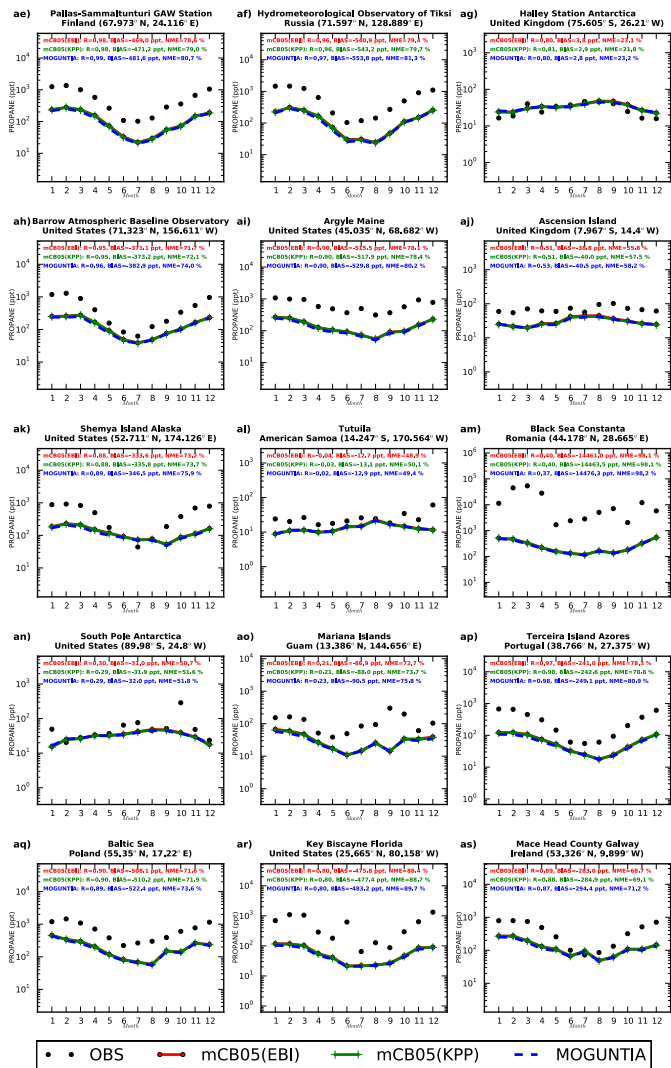


Figure S8: Comparison of monthly mean surface C_2H_6 flask measurements (black dots) in ppb with model results (red-line for mCB05(EBI), green-line for mCB05(KPP) and blue-line for MOGUNTIA) at various stations around the globe, as obtained from NOAA database, for the year 2006.

Deleted: 5







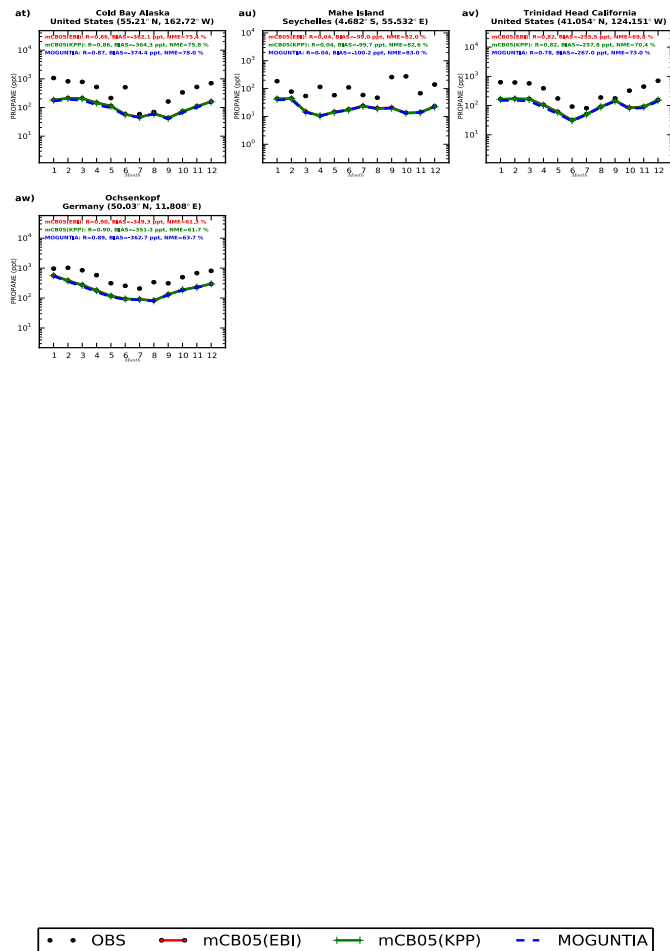
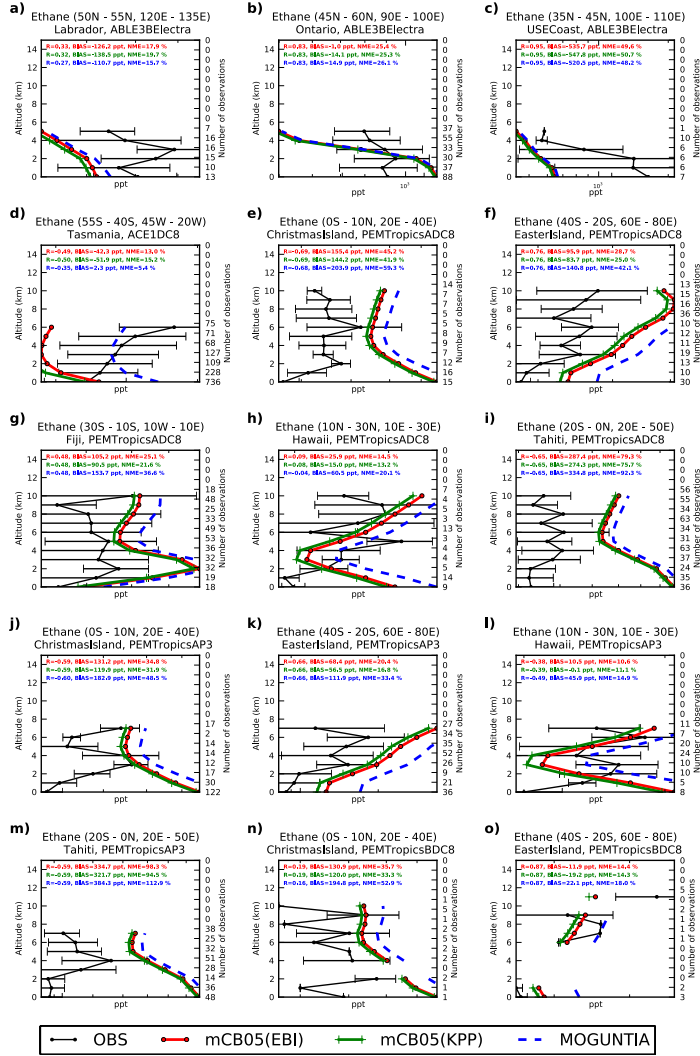
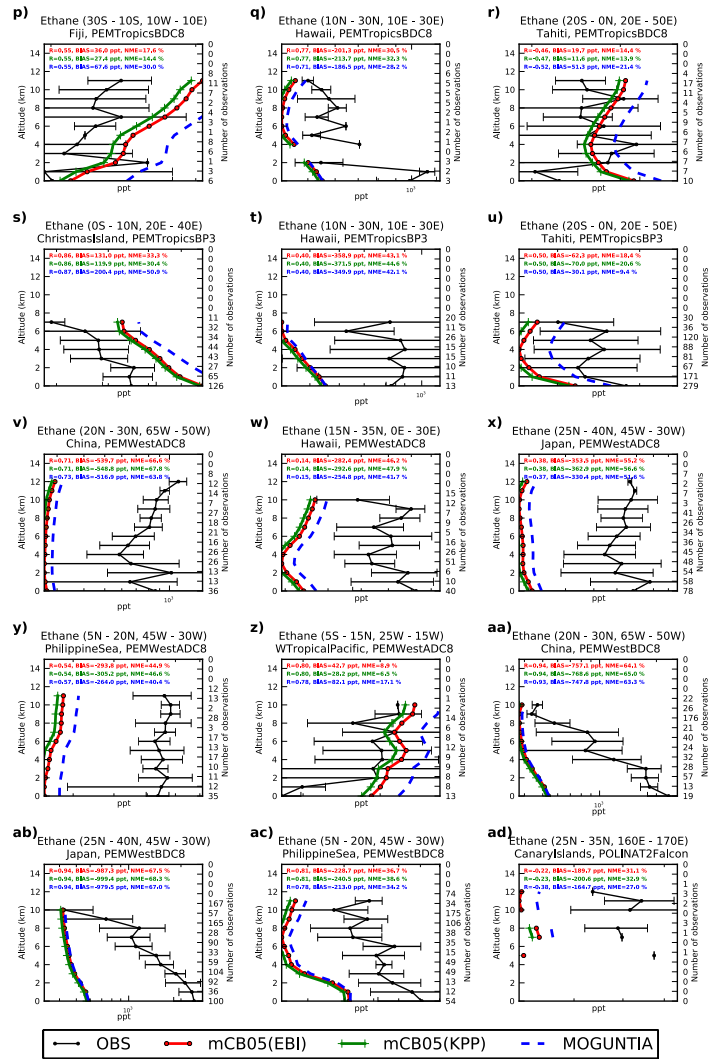


Figure S9: Comparison of monthly mean surface propane flask measurements (black dots) in ppb with model results (red-line for mCB05(EBI), green-line for mCB05(KPP) and blue-line for MOGUNTIA) at various stations around the globe, as obtained from NOAA database, for the year 2006.

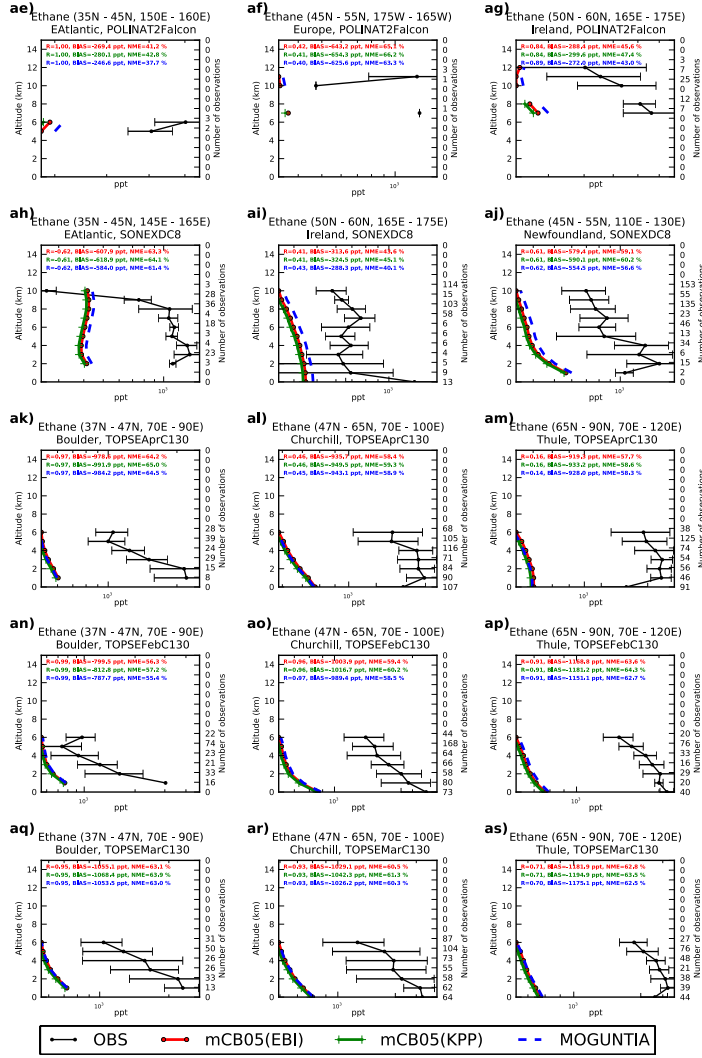
Deleted: 6

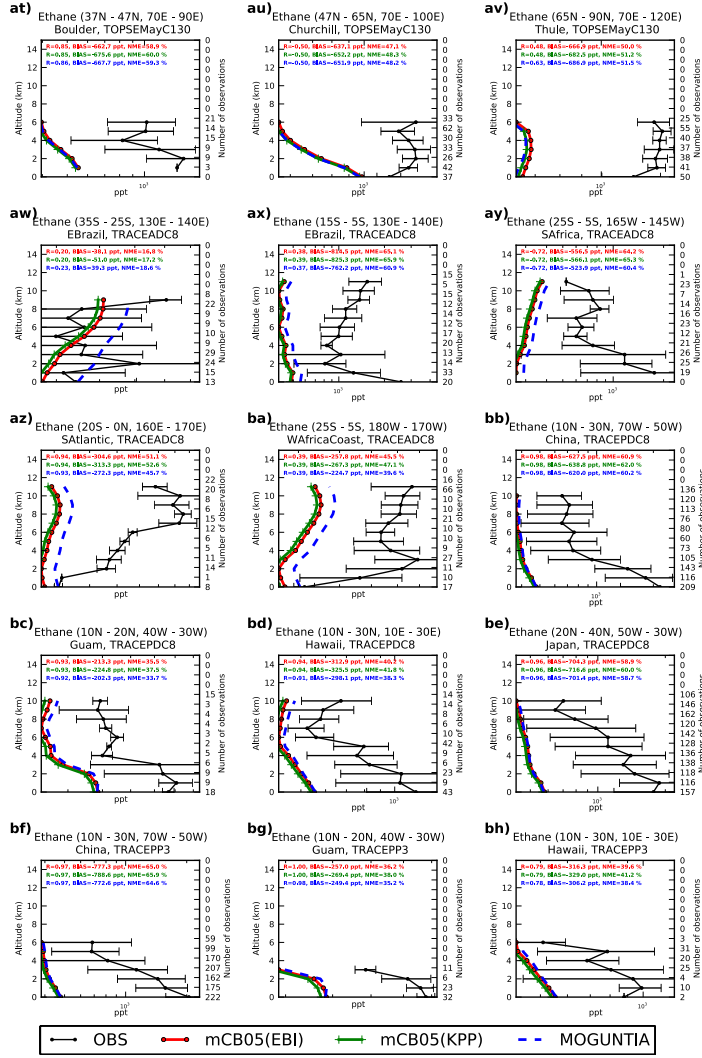
Formatted: Font: 10 pt, Not Bold





Formatted: Right: -0.05 cm, Line spacing: single





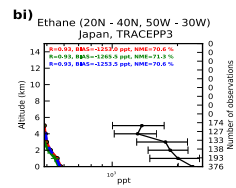
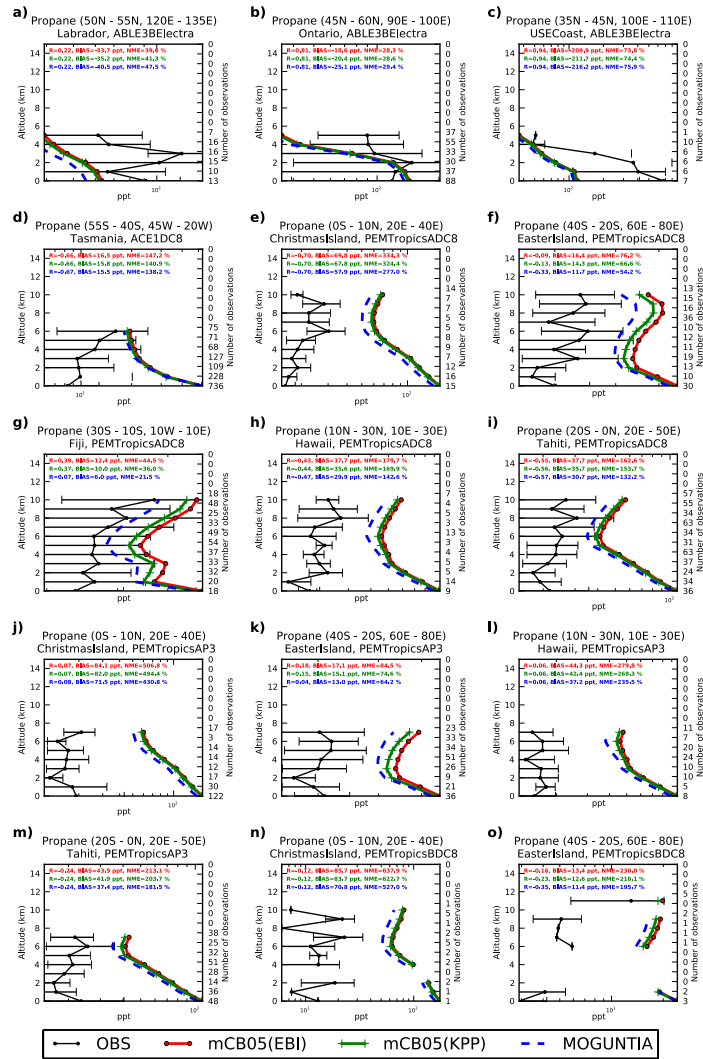


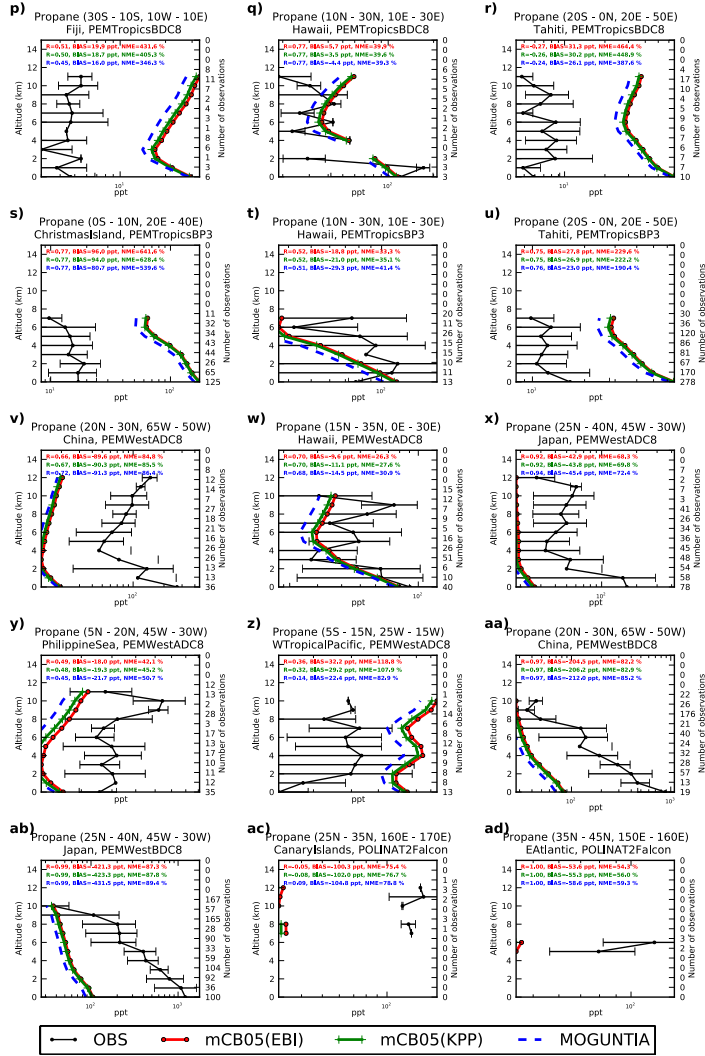
Figure S10: Comparison of TM5-MP vertical profiles (in km) of C_2H_6 against aircraft observations (black line) in ppt with model results (red-line for mCB05(EBI), green-line for mCB05(KPP) and blue-line for MOGUNTIA), using co-located model output for 2006 sampled at the measurement times; error bars indicate the standard deviation. The numbers on the right vertical axis indicate the number of available measurements.

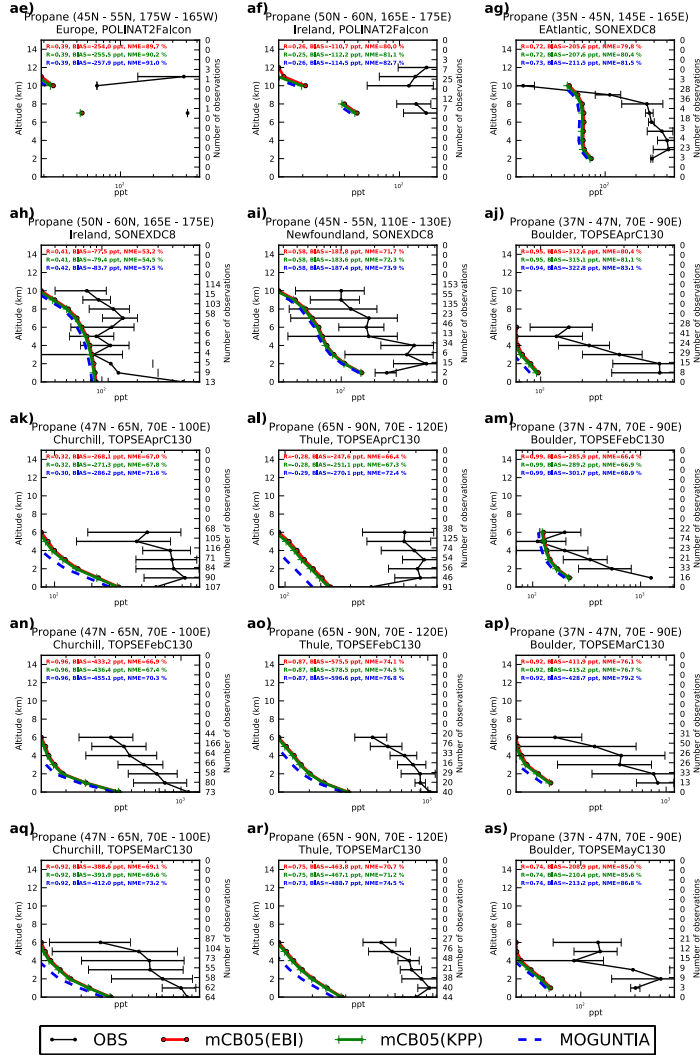
Formatted: Right: -0.05 cm

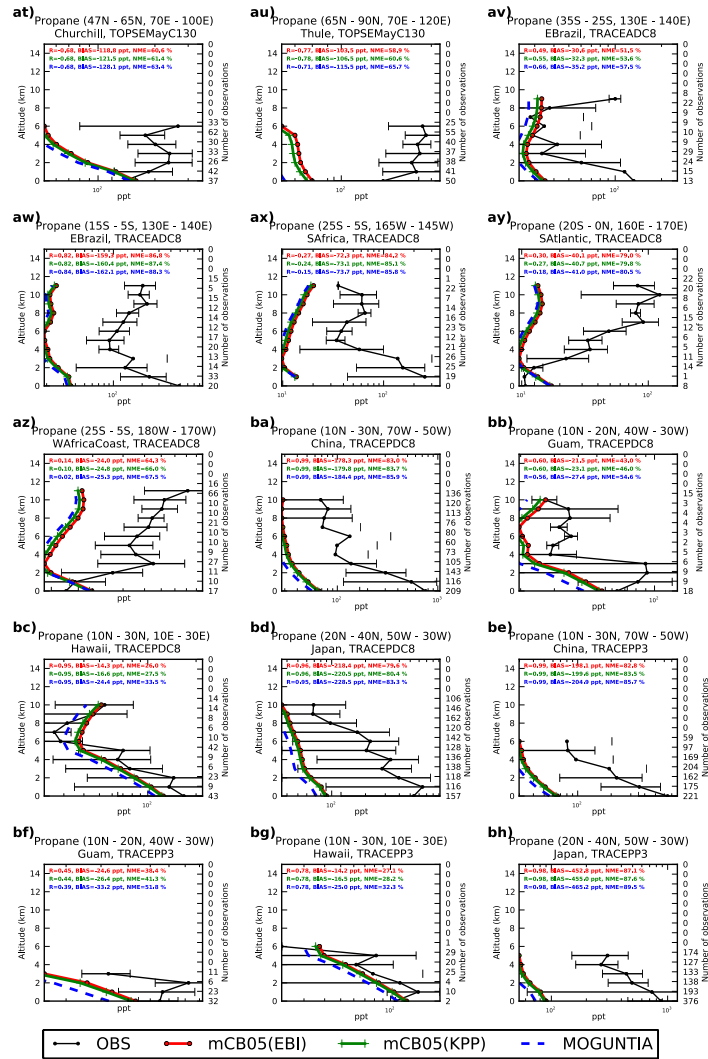
Deleted: 7



Formatted: Right: -0.05 cm, Line spacing: single







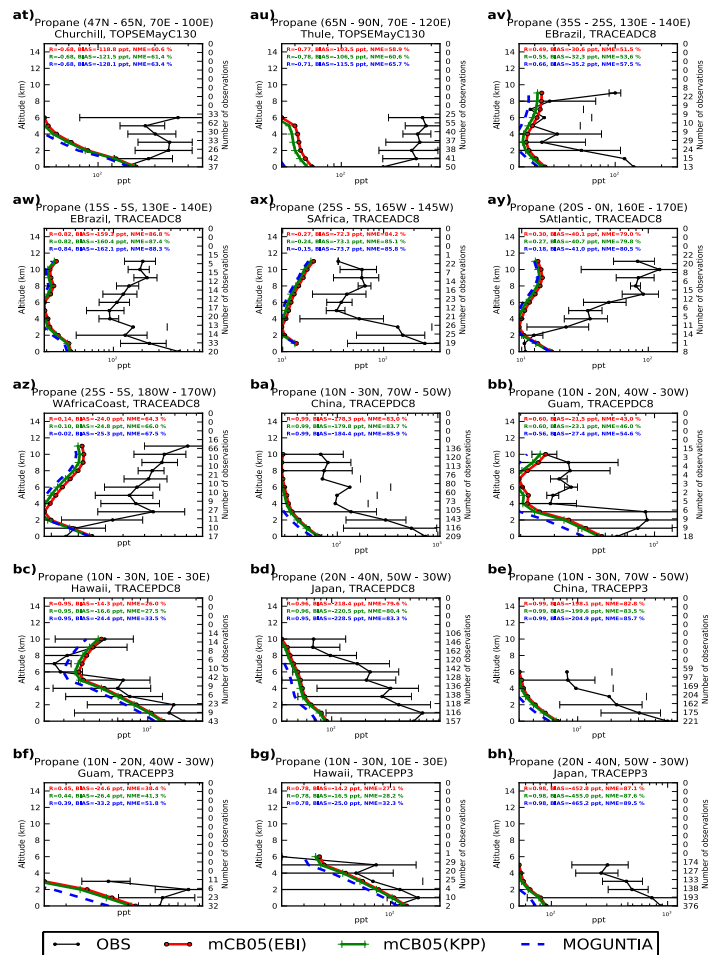
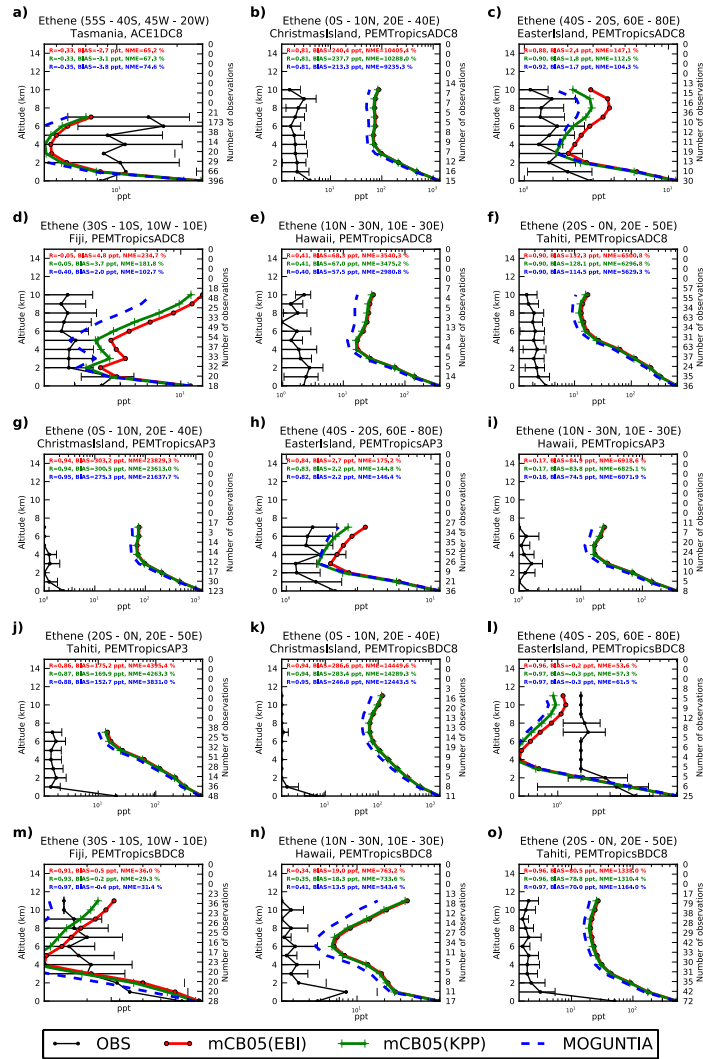


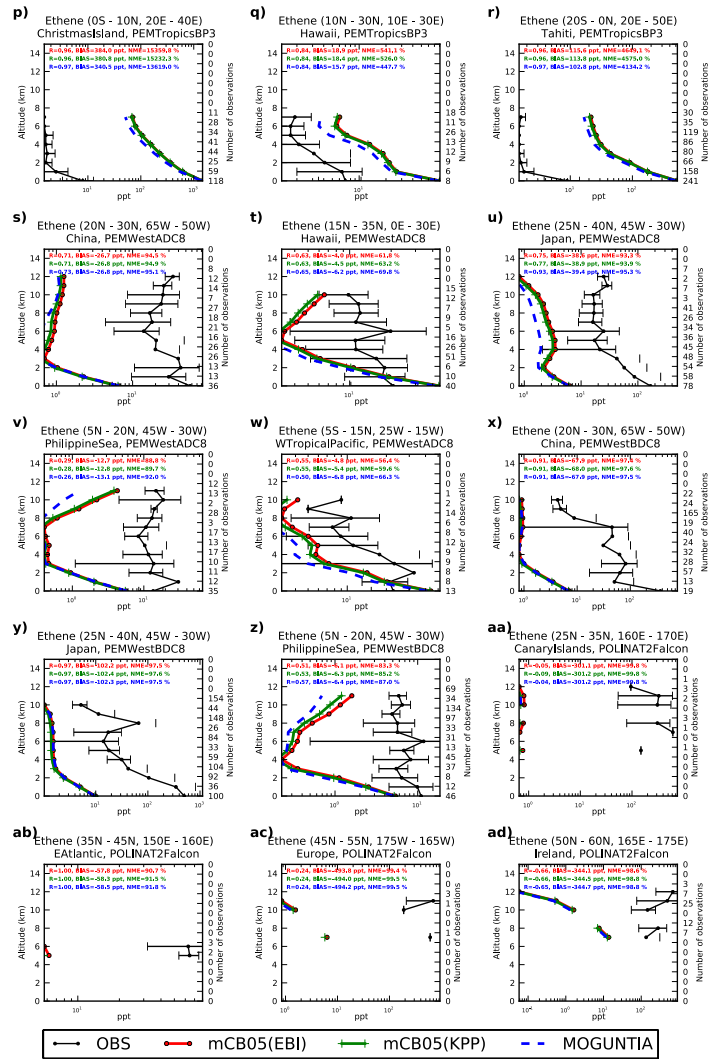
Figure S11: Comparison of TM5-MP vertical profiles (in km) of C_3H_8 against aircraft observations (black line) in ppt, with model results (red-line for mCB05(EBI), green-line for mCB05(KPP) and blue-line for MOGUNTIA), using co-located model output for 2006 sampled at the measurement times; error bars indicate the standard deviation. The numbers on the right vertical axis indicate the number of available measurements.

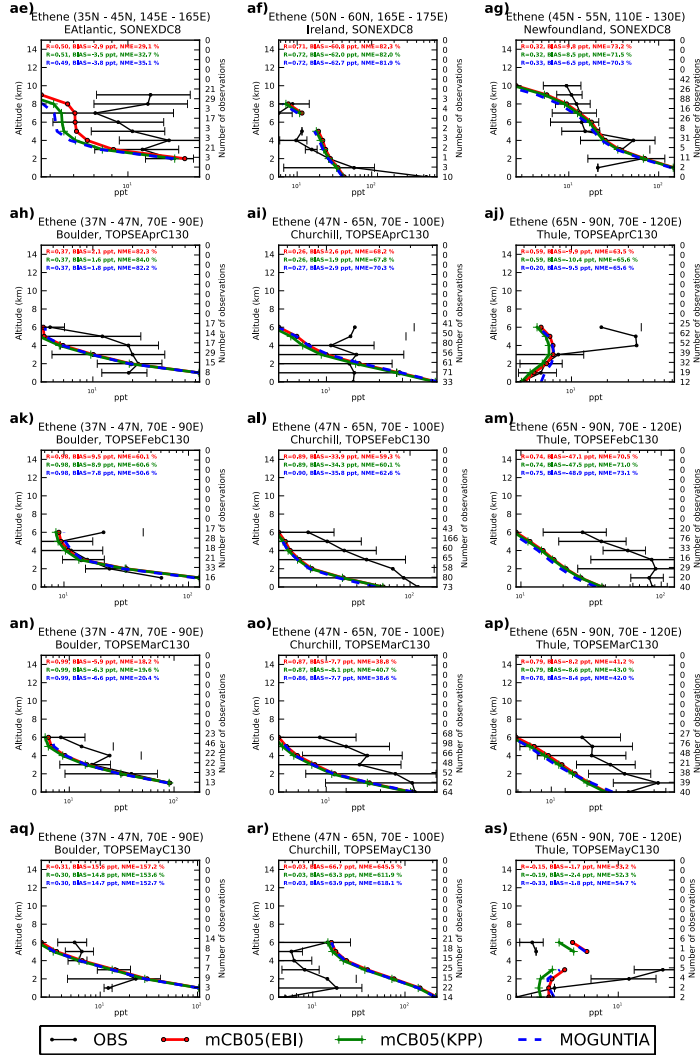
Formatted: Right: -0.05 cm

Deleted: 8



Formatted: Right: -0.05 cm, Line spacing: single





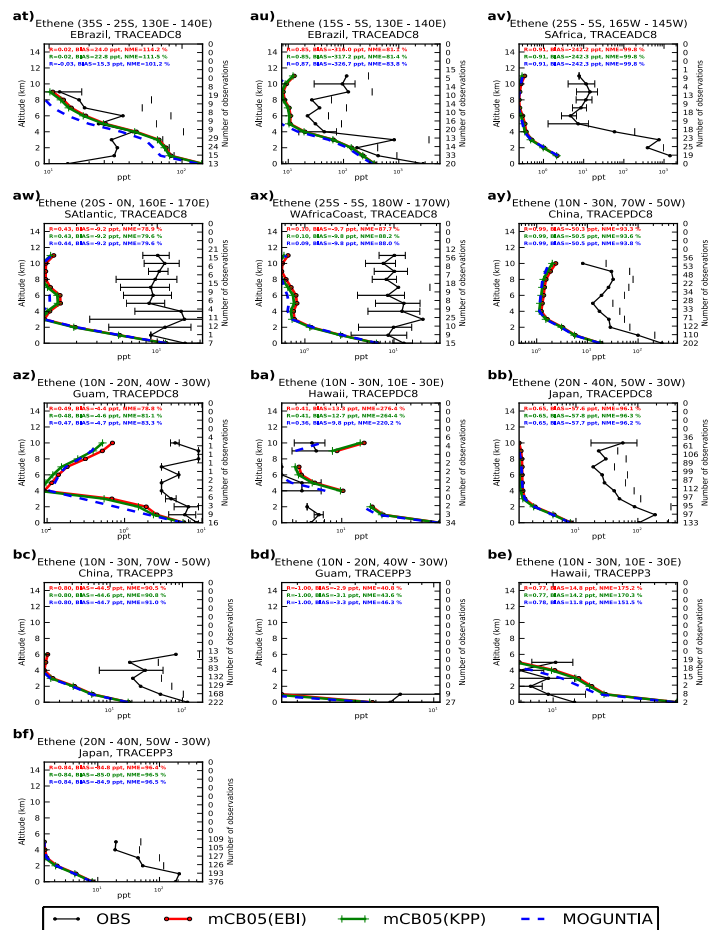
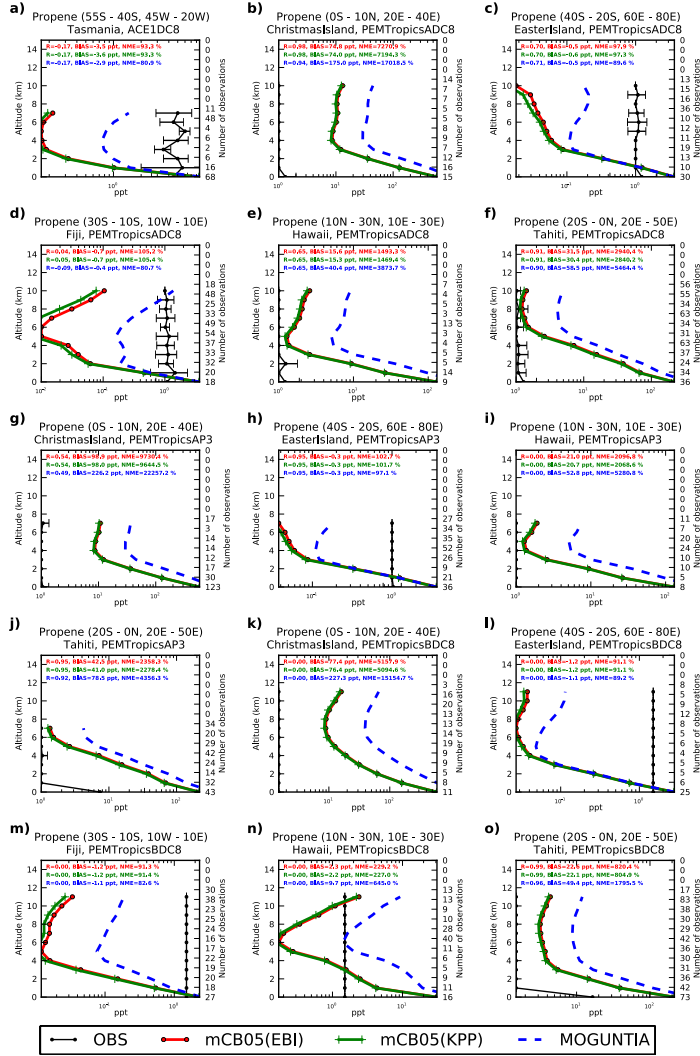


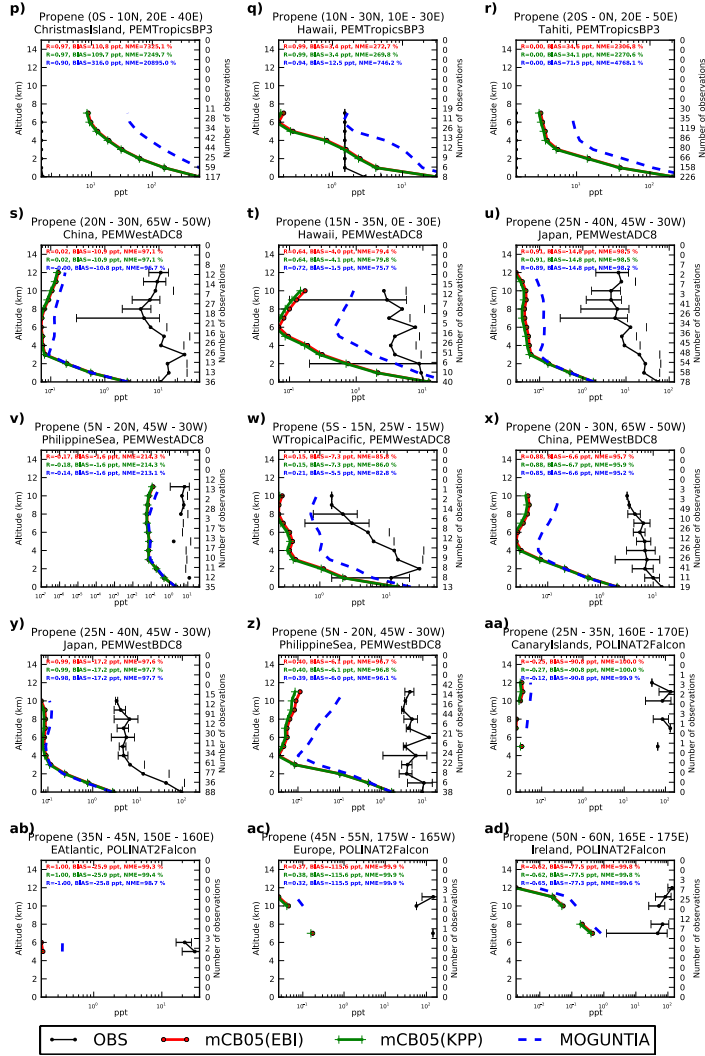
Figure S12: Comparison of TMS-MP vertical profiles (in km) of C₂H₄ against aircraft observations (black line) in ppt, with model results (red-line for mCB05(EBI), green-line for mCB05(KPP) and blue-line for MOGUNTIA), using co-located model output for 2006 sampled at the measurement times; error bars indicate the standard deviation. The numbers on the right vertical axis indicate the number of available measurements.

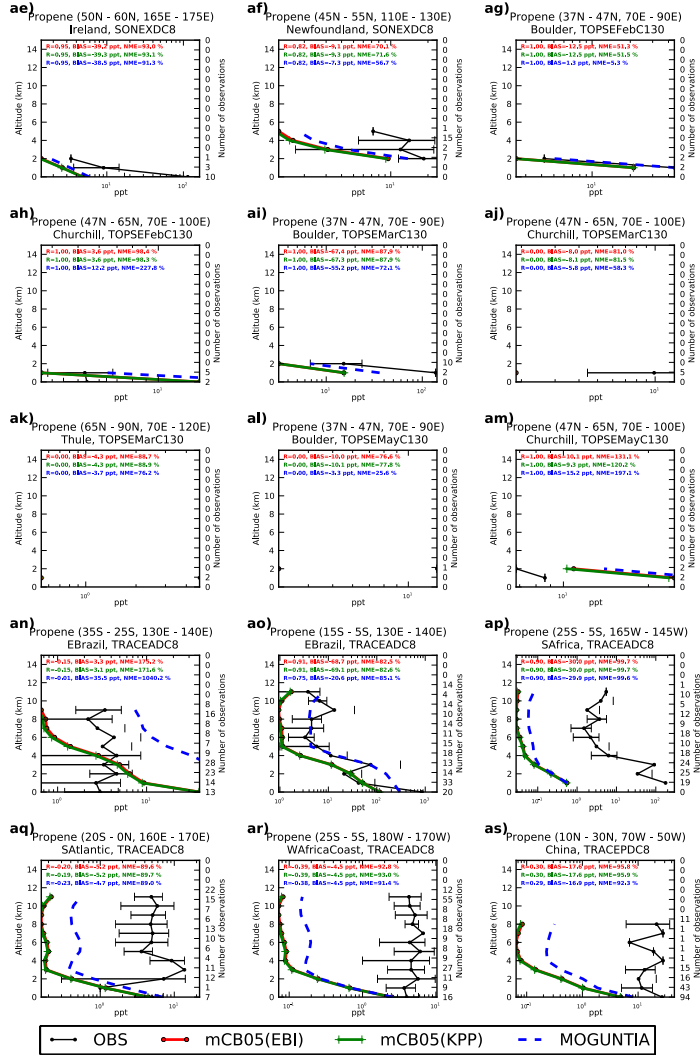
Formatted: Right: -0.05 cm

Deleted: 9



Formatted: Right: -0.05 cm, Line spacing: single





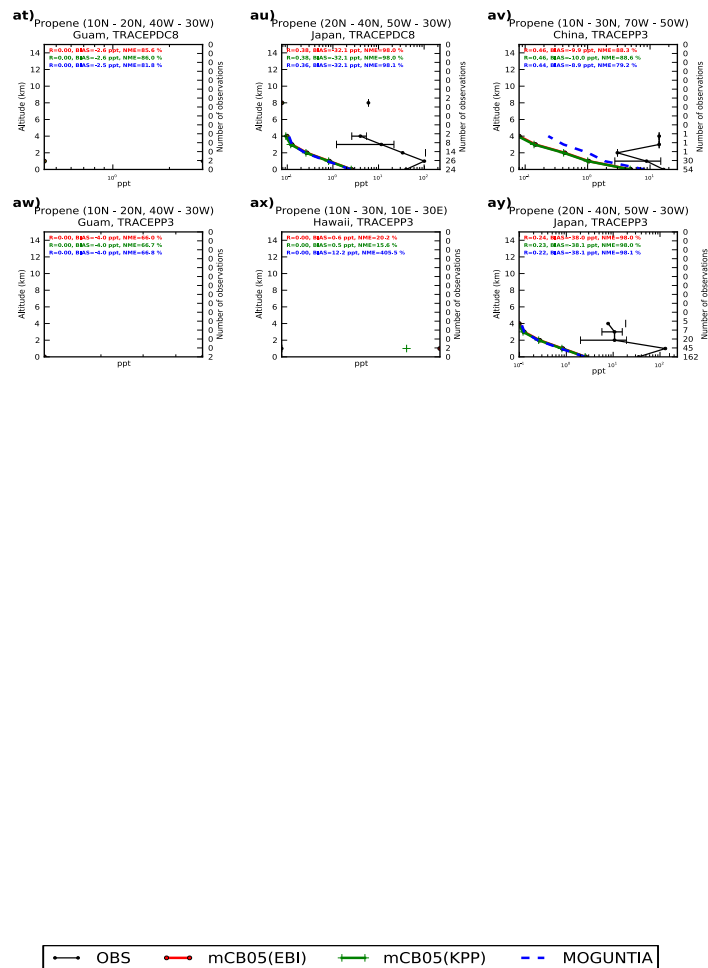


Figure S13: Comparison of TM5-MP vertical profiles (in km) of C_3H_6 against aircraft observations (black line) in ppt, with model results (red-line for mCB05(EBI), green-line for mCB05(KPP) and blue-line for MOGUNTIA), using co-located model output for 2006 sampled at the measurement times; error bars indicate the standard deviation. The numbers on the right vertical axis indicate the number of available measurements.

Formatted: Right: -0.05 cm

Deleted: 10

Supplementary References

Browne, E. C., Wooldridge, P. J., Min, K.-E. and Cohen, R. C.: On the role of monoterpene chemistry in the remote continental boundary layer, *Atmos. Chem. Phys.*, 14(3), 1225–1238, doi:10.5194/acp-14-1225-2014, 2014.

Ito, A., Sillman, S. and Penner, J. E.: Effects of additional nonmethane volatile organic compounds, organic nitrates, and direct emissions of oxygenated organic species on global tropospheric chemistry, *J. Geophys. Res.*, 112(D6), D06309, doi:10.1029/2005JD006556, 2007.

Sander, R.: Compilation of Henry's law constants (version 4.0) for water as solvent, *Atmos. Chem. Phys.*, 15(8), 4399–4981, doi:10.5194/acp-15-4399-2015, 2015.

Formatted: Right: -0.05 cm, Line spacing: single